

# Advances

## in Clinical and Experimental Medicine

MONTHLY ISSN 1899-5276 (PRINT) ISSN 2451-2680 (ONLINE)

[advances.umw.edu.pl](http://advances.umw.edu.pl)

2024, Vol. 33, No. 7 (July)

Impact Factor (IF) – 2.1  
Ministry of Science and Higher Education – 70 pts  
Index Copernicus (ICV) – 161.11 pts



WROCLAW  
MEDICAL UNIVERSITY

Advances  
in Clinical and Experimental  
Medicine



# Advances in Clinical and Experimental Medicine

ISSN 1899-5276 (PRINT)

ISSN 2451-2680 (ONLINE)

advances.umw.edu.pl

**MONTHLY 2024**  
**Vol. 33, No. 7**  
**(July)**

Advances in Clinical and Experimental Medicine (*Adv Clin Exp Med*) publishes high-quality original articles, research-in-progress, research letters and systematic reviews and meta-analyses of recognized scientists that deal with all clinical and experimental medicine.

## Editorial Office

ul. Marcinkowskiego 2–6  
50-368 Wrocław, Poland  
Tel.: +48 71 784 12 05  
E-mail: redakcja@umw.edu.pl

## Editor-in-Chief

Prof. Donata Kurpas

## Deputy Editor

Prof. Wojciech Kosmala

## Managing Editor

Marek Misiak, MA

## Statistical Editors

Wojciech Bombała, MSc

Łucja Janek, MSc

Anna Kopszak, MSc

Dr. Krzysztof Kujawa

Jakub Wronowicz, MSc

## Manuscript editing

Marek Misiak, MA

Paulina Piątkowska, MA

## Publisher

Wrocław Medical University  
Wybrzeże L. Pasteura 1  
50-367 Wrocław, Poland

Online edition is the original version  
of the journal

## Scientific Committee

Prof. Sandra Maria Barbalho

Prof. Antonio Cano

Prof. Chong Chen

Prof. Breno Diniz

Prof. Erwan Donal

Prof. Chris Fox

Prof. Yuko Hakamata

Prof. Carol Holland

Prof. Sabine Bährer-Kohler

Prof. Markku Kurkinen

Prof. Christos Lionis

Prof. Raimundo Mateos

Prof. Zbigniew W. Raś

Prof. Jerzy W. Rozenblit

Prof. Silvina Santana

Prof. Sajee Sattayut

Prof. James Sharman

Prof. Jamil Shibli

Prof. Michał J. Toborek

Prof. László Vécsei

Prof. Cristiana Vitale

Prof. Hao Zhang

## Section Editors

### Basic Sciences

Prof. Iwona Bil-Lula

Prof. Bartosz Kempisty

Dr. Wiesława Kranc

Dr. Anna Lebedeva

### Clinical Anatomy, Legal Medicine, Innovative Technologies

Prof. Rafael Boscolo-Berto

### Dentistry

Prof. Marzena Dominiak

Prof. Tomasz Gedrange

Prof. Jamil Shibli

### Laser Dentistry

Assoc. Prof. Kinga Grzech-Leśniak

### Dermatology

Prof. Jacek Szepietowski

### Emergency Medicine, Innovative Technologies

Prof. Jacek Smereka

### Gynecology and Obstetrics

Prof. Olimpia Sipak-Szmigiel

### Histology and Embryology

Dr. Mateusz Olbromski

### Internal Medicine

#### Angiology

Dr. Angelika Chachaj

#### Cardiology

Prof. Wojciech Kosmala

Dr. Daniel Morris

#### Endocrinology

Prof. Marek Bolanowski

#### Gastroenterology

Assoc. Prof. Katarzyna Neubauer

### Hematology

Prof. Andrzej Deptała  
Prof. Dariusz Wołowicz

### Nephrology and Transplantology

Prof. Mirosław Banasik  
Prof. Krzysztof Letachowicz

### Pulmonology

Prof. Anna Brzecka

### Microbiology

Prof. Marzenna Bartoszewicz  
Assoc. Prof. Adam Junka

### Molecular Biology

Dr. Monika Bielecka

Prof. Jolanta Saczko

### Neurology

Assoc. Prof. Magdalena Koszewicz  
Assoc. Prof. Anna Pokryszko-Dragan  
Dr. Masaru Tanaka

### Neuroscience

Dr. Simone Battaglia  
Dr. Francesco Di Gregorio

### Oncology

Prof. Andrzej Deptała  
Prof. Adam Maciejczyk

### Gynecological Oncology

Dr. Marcin Jędryka

### Ophthalmology

Dr. Małgorzata Gajdzis

### Orthopedics

Prof. Paweł Reichert

### Otolaryngology

Assoc. Prof. Tomasz Zatoński

### Pediatrics

### Pediatrics, Metabolic Pediatrics, Clinical Genetics, Neonatology, Rare Disorders

Prof. Robert Śmigiel

### Pediatric Nephrology

Prof. Katarzyna Kiliś-Pstrusińska

### Pediatric Oncology and Hematology

Assoc. Prof. Marek Ussowicz

### Pharmaceutical Sciences

Assoc. Prof. Marta Kepińska  
Prof. Adam Matkowski

### Pharmacoeconomics, Rheumatology

Dr. Sylwia Szafraniec-Buryło

### Psychiatry

Dr. Melike Küçükkarapınar  
Prof. Jerzy Leszek  
Assoc. Prof. Bartłomiej Stańczykiewicz

### Public Health

Prof. Monika Sawhney  
Prof. Izabella Uchmanowicz

### Qualitative Studies, Quality of Care

Prof. Ludmiła Marcinowicz

### Radiology

Prof. Marek Szaśniadek

### Rehabilitation

Dr. Elżbieta Rajkowska-Labon

### Surgery

Assoc. Prof. Mariusz Chabowski  
Assoc. Prof. Mirosław Kozłowski  
Prof. Renata Taboła

### Telemedicine, Geriatrics, Multimorbidity

Assoc. Prof. Maria Magdalena  
Bujnowska-Fedak

---

## Editorial Policy

Advances in Clinical and Experimental Medicine (Adv Clin Exp Med) is an independent multidisciplinary forum for exchange of scientific and clinical information, publishing original research and news encompassing all aspects of medicine, including molecular biology, biochemistry, genetics, biotechnology and other areas. During the review process, the Editorial Board conforms to the "Uniform Requirements for Manuscripts Submitted to Biomedical Journals: Writing and Editing for Biomedical Publication" approved by the International Committee of Medical Journal Editors ([www.ICMJE.org](http://www.ICMJE.org)). The journal publishes (in English only) original papers and reviews. Short works considered original, novel and significant are given priority. Experimental studies must include a statement that the experimental protocol and informed consent procedure were in compliance with the Helsinki Convention and were approved by an ethics committee.

For all subscription-related queries please contact our Editorial Office: [redakcja@umw.edu.pl](mailto:redakcja@umw.edu.pl)

For more information visit the journal's website: [advances.umw.edu.pl](http://advances.umw.edu.pl)

Pursuant to the ordinance of the Rector of Wrocław Medical University No. 37/XVI R/2024, from March 1, 2024, authors are required to pay a fee for each manuscript accepted for publication in the journal Advances in Clinical and Experimental Medicine. The fee amounts to 1600 EUR for all types of papers.

Advances in Clinical and Experimental Medicine has received financial support from the resources of Ministry of Science and Higher Education within the "Social Responsibility of Science – Support for Academic Publishing" project based on agreement No. RCN/SP/0584/2021.



Ministry of Education and Science  
Republic of Poland

Czasopismo Advances in Clinical and Experimental Medicine korzysta ze wsparcia finansowego ze środków Ministerstwa Edukacji i Nauki w ramach programu „Społeczna Odpowiedzialność Nauki – Rozwój Czasopism Naukowych” na podstawie umowy nr RCN/SP/0584/2021.



Ministerstwo  
Edukacji i Nauki

Indexed in: MEDLINE, Science Citation Index Expanded, Journal Citation Reports/Science Edition, Scopus, EMBASE/Excerpta Medica, Ulrich's™ International Periodicals Directory, Index Copernicus

Typographic design: Piotr Gil, Monika Kołęda

DTP: Wydawnictwo UMW

Cover: Monika Kołęda

Printing and binding: PRINT PROFIT Sp. z o.o., Koźmin 27, 59-900 Zgorzelec

## Contents

### Meta-analysis

- 661 Qing Song, Hang Yang, Xiaoliang Yang  
**Intravenous ketorolac versus metoclopramide in adult patients with migraine headaches: An updated systematic review and meta-analysis**
- 669 Zhuo Wang, Lihua Dong, Weiyan Shi, Ling Gao, Xin Jiang, Suyang Xue, Pengyu Chang  
**Postoperative therapy for local-advanced gastric cancer: A systematic review and meta-analysis**
- 679 Nianrong Mi, Mingyuan Liu, Chao Meng, Fangming Fu  
**Evaluation of the effects of vitamin D deficiency and cigarette smoking on insulin resistance in type 2 diabetes mellitus: A meta-analysis of randomized controlled trials**

### Original papers

- 691 Mehmet Ali Gul, Nezahat Kurt, Fatma Betul Ozgeris, Neslihan Yuce, Omer Faruk Kocak, Emine Parlak  
**C-terminal cross-linking telopeptide levels in COVID-19 patients: A prospective case-control study**
- 699 Ping Zhang, Qiong Zhou, Zhiyong Zeng  
**Combination of serum FOXR2 and transvaginal three-dimensional power Doppler ultrasonography in the diagnosis of uterine lesions**
- 709 Aneta Olszewska, Jacek Matys, Tomasz Gedrange, Elżbieta Paszyńska, Magdalena Maria Roszak, Agata Czajka-Jakubowska  
**Evaluation of photobiomodulation for postoperative discomfort following laser-assisted vital pulp therapy in immature teeth: A preliminary retrospective study**
- 717 Liyun Fang, Mao Zheng, Fengying He  
**Antioxidant, anti-inflammatory and antiseptic molecular actions of gedunin against lipopolysaccharide-induced sepsis in experimental rats**
- 729 Jing Xiao, Fang Wan, Lin Tian, Yao Li  
**Tumor suppressor miR-520a inhibits cell growth by negatively regulating PI3K/AKT signaling pathway in acute myeloid leukemia**
- 739 Xiaoxin Sui, Xiaowei Xi  
**MCT1 gene silencing enhances the immune effect of dendritic cells on cervical cancer cells**
- 751 Guiyan Mo, Xuan Long, Zan Hu, Yuling Tang, Zhiguo Zhou  
**Anoikis-related gene signatures can aid prognosis of lung adenocarcinoma**



# Intravenous ketorolac versus metoclopramide in adult patients with migraine headaches: An updated systematic review and meta-analysis

Qing Song<sup>1,A–C,E,F</sup>, Hang Yang<sup>2,C,D</sup>, Xiaoliang Yang<sup>3,D</sup>

<sup>1</sup> Department of Neurology, Tangshan Fengrun People's Hospital, China

<sup>2</sup> Tangshan Fengrun District Liujiaying Health Center, China

<sup>3</sup> Disinfection Supply Center, Tangshan Fengrun District People's Hospital, China

A – research concept and design; B – collection and/or assembly of data; C – data analysis and interpretation; D – writing the article; E – critical revision of the article; F – final approval of the article

Advances in Clinical and Experimental Medicine, ISSN 1899–5276 (print), ISSN 2451–2680 (online)

*Adv Clin Exp Med.* 2024;33(7):661–667

## Address for correspondence

Qing Song  
E-mail: songqingdr@sina.com

## Funding sources

None declared

## Conflict of interest

None declared

Received on April 11, 2023

Reviewed on August 10, 2023

Accepted on August 30, 2023

Published online on October 18, 2023

## Abstract

**Background.** Intravenous ketorolac and metoclopramide are common emergency treatments for adult patients with migraine headaches. The comparison between ketorolac and metoclopramide for migraine treatment is an intriguing issue for research and clinical practice.

**Objectives.** To provide an updated systematic review and meta-analysis of randomized clinical trials (RCTs) to help determine which treatment has better effects for migraine patients.

**Materials and methods.** Intravenous ketorolac and metoclopramide were compared to evaluate whether intravenous ketorolac is associated with significant benefits for pain intensity, short-term headache relief and sustained headache relief among adult patients with migraines. Adverse effects were also analyzed. Five studies with a total of 674 adult patients were included in the analysis, which focused on the outcomes of pain intensity, short-term headache relief, sustained headache relief, and adverse effects.

**Results.** The meta-analysis showed that the only modest but statistically significant difference was present in short-term headache relief when comparing intravenous ketorolac with intravenous metoclopramide. There were no significant differences between intravenous ketorolac and metoclopramide in terms of pain intensity, sustained headache relief or adverse effects.

**Conclusions.** The results suggest that there are no significant differences in most treatment effects (aside from short-term headache relief) and adverse effects when comparing intravenous ketorolac with intravenous metoclopramide. However, the paucity of literature on this topic might have limited the interpretation of the current results. Thus, more relevant studies are warranted.

**Key words:** meta-analysis, metoclopramide, migraine, intravenous, ketorolac

## Cite as

Song Q, Yang H, Yang X. Intravenous ketorolac versus metoclopramide in adult patients with migraine headaches: An updated systematic review and meta-analysis. *Adv Clin Exp Med.* 2024;33(7):661–667. doi:10.17219/acem/171697

## DOI

10.17219/acem/171697

## Copyright

Copyright by Author(s)

This is an article distributed under the terms of the Creative Commons Attribution 3.0 Unported (CC BY 3.0) (<https://creativecommons.org/licenses/by/3.0/>)

## Introduction

Migraine is a widespread neurological disease that may be debilitating, especially for young adults and women. Research has suggested that 1.04 billion people suffer from migraine headaches globally. Thus, attention from researchers and clinicians is warranted for this condition.<sup>1</sup> Various types of medications are available for treatment, including ibuprofen, triptans, ketorolac, and metoclopramide.<sup>2,3</sup> Ketorolac and metoclopramide are level B treatments for acute migraine attacks.<sup>3</sup> Ketorolac is a nonsteroidal anti-inflammatory drug that can inhibit the cyclooxygenase enzyme and reduce the production of prostaglandins, which can inhibit nociceptors at sites of inflammation<sup>4</sup> and reduce the severity of migraine-related pain.<sup>5</sup> Intravenous ketorolac administration is a common clinical strategy for acute migraine attacks.

Metoclopramide is another important choice for the treatment of acute migraine headaches, and a previous meta-analysis has suggested that intravenous metoclopramide should be the primary agent for treating acute cases.<sup>6</sup> In addition, a systematic review proposed that metoclopramide may be more effective than ketorolac in treating acute migraines.<sup>7</sup> However, there have been few meta-analyses focusing on comparisons between intravenous ketorolac and metoclopramide.

Comparative meta-analyses of these 2 agents have examined outcomes of pain intensity, ability to return to work or usual activities, the need for rescue medications, and the frequency of adverse events.<sup>8</sup> However, they have not examined other types of outcomes, such as relief from short-term headaches or sustained headaches, as well as individual subgroups of side effects, such as drowsiness and restlessness.

## Objectives

This meta-analysis was designed to evaluate updated literature regarding these unaddressed outcomes. Based on the available studies,<sup>8</sup> we hypothesized that intravenous ketorolac might be inferior to metoclopramide in terms of these outcomes in adult patients.

## Materials and methods

### Search strategy and information sources

A search for relevant prospective randomized clinical trials (RCTs) was conducted using Cochrane Central Register of Controlled Trials (CENTRAL), ScienceDirect, PubMed, Web of Science, and Embase. The following keywords have been used: “migraine”, “ketorolac”, “metoclopramide”, “pain”, “outcome”, “efficacy”, “versus”, “randomized”, “clinical”, “trials”, “controlled”, “therapy”, “treatment”, or “comparison”, “intravenous”, “headache”. The included studies were limited to those published

before October 2022. The inclusion criteria for the RCTs were as follows: 1) studies comparing ketorolac and metoclopramide treatment for adult patients with migraines; 2) RCTs with baseline data and post-treatment outcomes for pain intensity, relief of short-term headaches or sustained headaches, and side effects; 3) RCTs with detailed data on the outcomes regarding pain relief and adverse events; and 4) studies published in English.

### Assessment of evidence quality and data extraction

The Cochrane Handbook for Systematic Reviews of Interventions ([www.training.cochrane.org/handbook](http://www.training.cochrane.org/handbook)) was used as the basis for conducting the meta-analysis. The Preferred Reporting Items for Systematic Reviews and Meta-Analyses (PRISMA) guidelines<sup>9</sup> were used as a standard for reporting the process and results. The following data were extracted from the eligible RCTs regarding migraine patients treated with ketorolac and metoclopramide: pain intensity, the occurrence and rates of short-term headache relief and sustained headache relief, and the number of adverse events.

The abstracts were evaluated to screen studies, which were then independently assessed using the full text, tables and figures. The eligible studies included data on pain intensity, relief of short-term headaches or sustained headaches, and side effects. The risk of bias was evaluated according to the randomization process, deviations from intended interventions, missing outcome data, measurement methods, and selection of the reported results (Risk of Bias 2 (RoB 2), a revised Cochrane Risk of Bias tool for randomized trials (<https://www.riskofbias.info/welcome/rob-2-0-tool>)). A collaborative review was conducted by all the authors to achieve agreement ( $\kappa = 0.8$ ). The final results were also reviewed by all the authors.

### Meta-analysis and statistical analysis

We used the weighted mean difference to estimate numerical variables of pain intensity. Ketorolac and metoclopramide were compared to determine which medicine was better for relieving pain intensity. The overall effect size of post-treatment pain intensity was calculated as the weighted average of the inverse variance for study-specific estimates.

We generated pooled estimates of the relative risks (RRs) for short-term headache relief, sustained headache relief and adverse effects. The Cochrane Collaboration Review Manager Software Package (RevMan v. 5.4; Cochrane Collaboration, Nordic Cochrane Centre, Copenhagen, Denmark) was used. The weighted estimates of the average risks of the included studies were combined in a random-effects model. Ketorolac and metoclopramide treatments were compared to determine which treatment is more beneficial in terms of relief and side effects. The  $\chi^2$  test was used to assess the heterogeneity between RCTs.<sup>10</sup> The random-effects model was applied in the meta-analysis.



## Results

### Description of studies

The PRISMA selection process was followed to identify eligible studies (Fig. 1), and a qualitative analysis was performed on the final 5 eligible articles that were included in the analysis.<sup>11–15</sup> The characteristics of these studies are presented in Table 1. An assessment of the risk of bias is illustrated in Fig. 2.

### RR of short-term headache relief

Low heterogeneity was observed. The result for the overall effect was  $Z = 2.01$  ( $p = 0.04$ , Mantel–Haenszel method). A significant difference was observed in relative risk (RR) for short-term headache relief events between the intravenous ketorolac and metoclopramide treatments (Fig. 3). The funnel plot showed a symmetric distribution without significant publication bias (Fig. 4).

### Pain intensity

The difference in pain intensity between the group of patients that received ketorolac (196 subjects) and the group

that received metoclopramide (196 subjects) was 0.07 (95% confidence interval (95% CI):  $-0.40$ – $0.54$ , inverse variance method). This suggests that the effects of ketorolac and metoclopramide treatments on pain intensity were not significantly different (Fig. 5). The funnel plot showed a symmetric distribution without significant publication bias (Fig. 6).

### RR of sustained headache relief and adverse events

The RR of sustained headache relief was not statistically significant (test for overall effect:  $Z = 0.07$  ( $p = 0.94$ ), Mantel–Haenszel method). In addition, the RR of adverse events was not significant for ketorolac compared to metoclopramide (test for overall effect:  $Z = 1.15$  ( $p = 0.25$ ), Mantel–Haenszel method). The difference in drowsiness as an adverse event was not statistically significant (test for overall effect:  $Z = 0.84$  ( $p = 0.40$ ), Mantel–Haenszel method). Similarly, the dimensions of restlessness (test for overall effect:  $Z = 1.48$  ( $p = 0.14$ ), Mantel–Haenszel method) and high restlessness (test for overall effect:  $Z = 1.77$  ( $p = 0.08$ ), Mantel–Haenszel method) showed nonsignificant results. The forest plots, funnel plots and publication bias statistics in this section can be referred to in the supplementary data.

**Table 1.** Summary of randomized controlled trials (RCTs) for the effect of ketorolac compared to metoclopramide treatment on adult migraine patients

Study details (year of publication, study type, country)	Patients	Inclusion criteria	Intervention	Outcomes
Friedman et al., 2015 (single-center, USA) <sup>11</sup>	110 (15.5% male) patients in the ketorolac group compared to 108 (16.7% male) patients in the metoclopramide group (male age median: 35 years, female age median: 36 years)	acute migraine or acute probable migraine as defined by the International Headache Society (ICHD, 2 <sup>nd</sup> edition)	ketorolac (30 mg, intravenous) compared to metoclopramide (10 mg, intravenous)	1-hour headache relief sustained headache freedom adverse events
Friedman et al., 2014 (single-center, USA) <sup>12</sup>	110 (7% male; age median: 34 years) patients in the ketorolac group compared to 110 (8% male, age median: 34 years) patients in the metoclopramide group	acute migraine or acute probable migraine as defined by the International Headache Society (ICHD, 2 <sup>nd</sup> edition)	ketorolac (30 mg, intravenous) compared to metoclopramide (10 mg, intravenous)	pain intensity (1 h post-treatment) ability to return to work or usual activity sustained headache freedom within 24 h need for rescue medication frequency of adverse effects
Khazaei et al., 2019 (single-center, Iran) <sup>13</sup>	128 persons: 27 patients with aura (mean age $\pm$ SD, $37.81 \pm 9.27$ years), 101 patients without aura (mean age $\pm$ SD, $36.56 \pm 10.10$ years)	headaches examined by neurologists and meeting the International Headache Society criteria for migraine	ketorolac (30 mg, intravenous) compared to metoclopramide (10 mg, intravenous)	pain intensity 1 h post-treatment recurrence of headache post-treatment frequency of adverse effects
Klapper and Stanton, 1991 (single-center, USA) <sup>14</sup>	not mentioned	patients meeting the International Headache Society criteria for the diagnosis of migraine headache who called the Headache Center after failure of their customary abortive medication	ketorolac (60 mg, intravenous) compared to metoclopramide (5 mg, intravenous)	pain intensity at 1 h ability to return to work or usual activities need for rescue medication
Soltani et al., 2021 (single-center, Iran) <sup>15</sup>	mean $\pm$ SD for age was $34 \pm 8.54$ years; 57.4% of patients were female	migraine diagnosed based on the International Headache Society's ICHD-3 criteria	ketorolac (30 mg, intravenous) compared to metoclopramide (10 mg, intravenous)	pain scores adverse events (drowsiness at 1 h; restlessness during study)

SD – standard deviation; ICHD – International Classification of Headache Disorders.

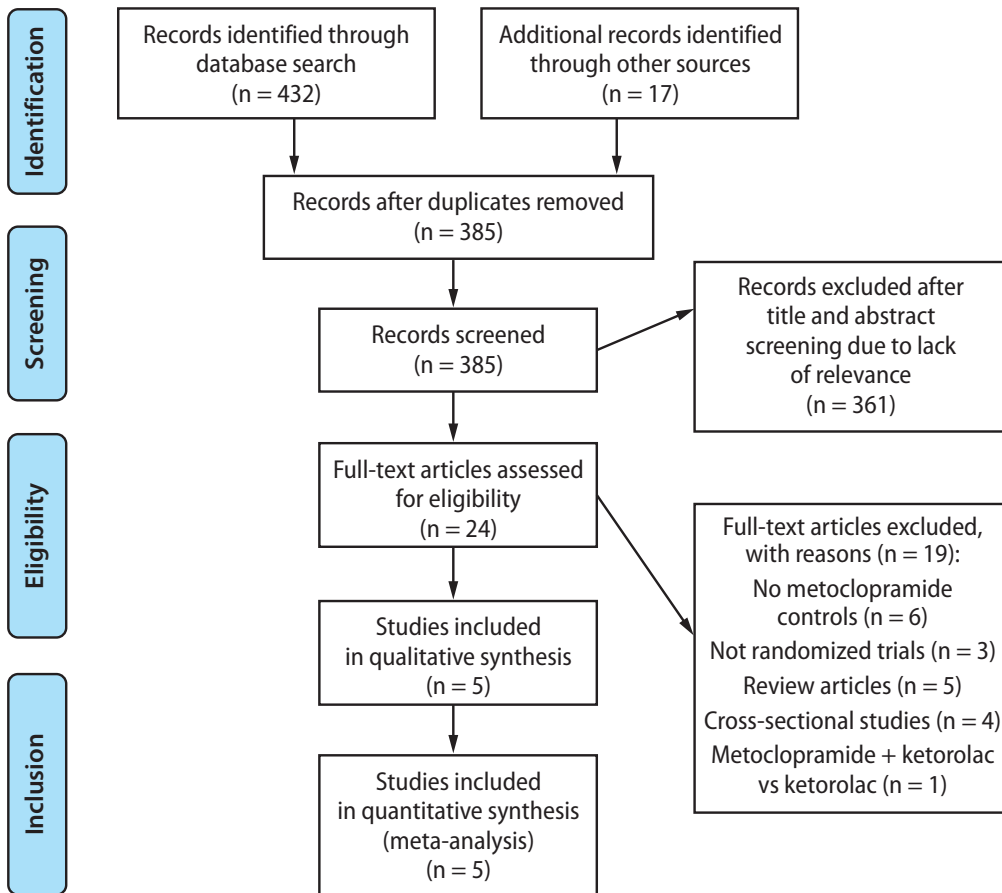


Fig. 1. Preferred Reporting Items for Systematic Reviews and Meta-Analyses (PRISMA) flowchart for the selection of enrolled randomized trials

Study	Risk of bias domains					Overall
	D1	D2	D3	D4	D5	
Friedman 2014	+	+	X	+	+	+
Friedman 2015	+	+	X	+	+	+
Khazaei 2019	X	-	-	+	+	-
Klapper 1991	X	X	X	-	-	X
Soltani 2021	+	+	+	+	-	+

Domains:  
 D1: Bias arising from the randomization process.  
 D2: Bias due to deviations from intended intervention.  
 D3: Bias due to missing outcome data.  
 D4: Bias in measurement of the outcome.  
 D5: Bias in selection of the reported result.

Judgement  
 X High  
 - Some concerns  
 + Low

Fig. 2. Assessment of the risk of bias (ROB v.2) of the included articles

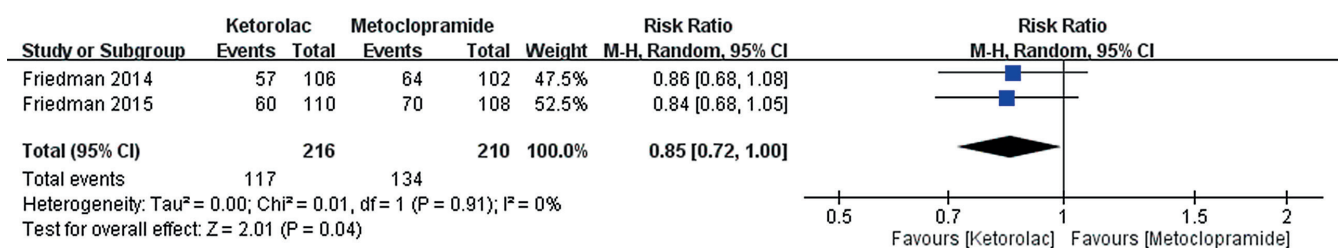
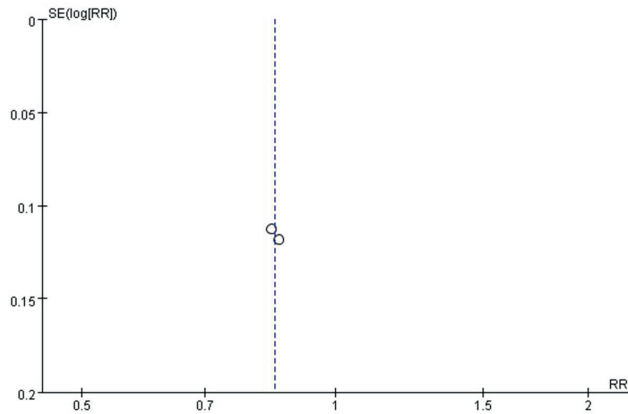


Fig. 3. Forest plot of relative risk (RR) for the meta-analysis results of short-term headache relief (ketorolac compared to metoclopramide). Intravenous ketorolac treatment showed a significant benefit of short-term headache relief events when compared with intravenous metoclopramide treatment (statistically significant, Mantel–Haenszel method)

95% CI – 95% confidence interval; df – degrees of freedom.



**Fig. 4.** Funnel plot of relative risk (RR) for the meta-analysis results of short-term headache relief (ketorolac compared to metoclopramide). The funnel plot showed a symmetric distribution of the included studies (fail-safe N calculation, observed significance level: 0.1521)

SE – standard error.

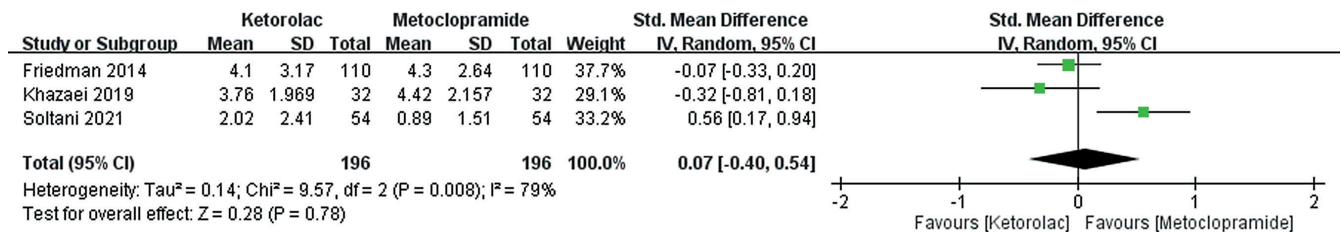


**Fig. 5.** Forest plot for the meta-analysis results of pain intensity (ketorolac compared to metoclopramide). The intravenous ketorolac and metoclopramide treatments showed no significant difference in pain intensity (inverse variance method)

95% CI – 95% confidence interval; df – degrees of freedom.

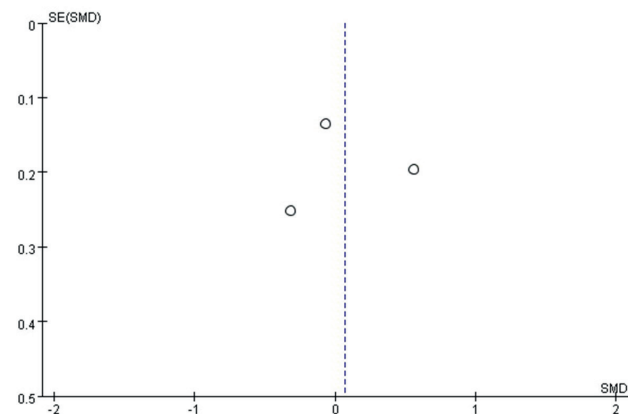


**Fig. 6.** Funnel plot for the meta-analysis results of pain intensity (ketorolac compared to metoclopramide). The funnel plot showed a symmetric distribution of the included studies (fail-safe N calculation, observed significance level: 0.5585)

SE – standard error; SMD – standardized mean difference.

## Discussion

Intravenous ketorolac and metoclopramide treatments were not significantly different with regard to most outcomes (pain intensity, sustained headache relief, adverse events, and side effects of drowsiness, restlessness, and

high restlessness). The only significantly different outcome was short-term headache relief. However, even though the results showed that intravenous ketorolac treatment was beneficial, the risk ratio of 0.85 suggests that it might be less effective for short-term headache relief. The 95% CI (0.72–1) indicates that the results might have the potential to be statistically nonsignificant.

In summary, the meta-analysis results demonstrated that intravenous ketorolac treatment had similar effects to intravenous metoclopramide treatment. In addition, the adverse events were not significantly different. The only potentially significant outcome of difference between the 2 treatments might be short-term headache relief events. However, due to the nondefinitive 95% CI values of the short-term headache relief results and the low number of included studies for these results, the research needs to be replicated in the future with more studies focusing on this outcome.

A previous systematic review of ketorolac for acute migraine attacks found that it might be as effective as meperidine and more effective than sumatriptan for the relief of acute migraine headaches. In addition, it was reported that ketorolac might not be as effective as metoclopramide.<sup>7</sup> The present meta-analysis showed that ketorolac and metoclopramide might not produce significant differences in pain intensity, sustained headache relief or adverse events. Therefore, this study could serve as an update of ketorolac’s characteristics in comparison with metoclopramide.

Ketorolac has been a standard option for migraine treatment and has been compared to other new medications.<sup>16–19</sup> Therefore, the effects of ketorolac treatment should not be undervalued, especially for pain intensity, sustained headache relief and adverse events. The only effect for which intravenous ketorolac might be inferior to intravenous metoclopramide is short-term headache relief.

The American Headache Society and the Canadian Headache Society recommended that clinicians prescribe metoclopramide for patients with acute migraines.<sup>20,21</sup> However, intravenous metoclopramide was not superior to intravenous ketorolac in terms of pain intensity, sustained headache relief and adverse events. Our meta-analysis results support those of another meta-analysis

on metoclopramide treatment for acute migraines, which suggests that metoclopramide is not associated with more significant adverse events than other kinds of medications.<sup>22</sup>

There is a lack of experimental evidence regarding the possible mechanism of the anti-migraine effects of metoclopramide, but underlying dopamine D2 antagonism and the related decrease in trigeminovascular activation might explain the treatment efficacy of metoclopramide for acute migraines.<sup>23</sup> Dopamine D2 antagonism may be related to extrapyramidal side effects, such as Parkinsonism and acute dystonia.<sup>24,25</sup> Thus, clinicians may consider the use of ketorolac for patients with migraines if they have concerns about the side effects of metoclopramide, such as extrapyramidal side effects.

For short-term headache relief, intravenous metoclopramide showed superior effects when compared to intravenous ketorolac. This is consistent with the recommendations made by the American Headache Society and the Canadian Headache Society. In our results, the highest dosage of intravenous metoclopramide was 10 mg, which corresponds with a study on the appropriate dose of metoclopramide.<sup>26</sup> Therefore, our research should be replicable in clinical practice when clinicians are treating acute migraines, considering different dimensions of outcomes, and determining their treatment goals.

## Limitations

Several limitations of our meta-analysis need to be mentioned. First, the included RCTs were limited in sample size. Therefore, large RCTs on this topic are warranted. Furthermore, the variable doses and types of ketorolac and metoclopramide treatments might have biased our results. However, in recent years, clinical practice regarding migraine treatment has still included ketorolac and metoclopramide. Thus, the present results might provide useful information for clinical practice.

Another issue is that the low numbers of included RCTs addressing several outcomes, such as short-term headache relief, might be a concern with regard to the significance of the results. In addition, the 95% CI of the only significant result might be another issue of concern. The lack of patient-level data and covariates might have led to bias. Not all included RCTs reported all the outcomes in a consistent style, and some of them reported results in a format that could not be used in the collection of data for our meta-analysis. The different definitions and severities of migraine headaches addressed in the included RCTs might have also influenced our results, and there was a lack of demographic data on the ketorolac and metoclopramide groups. Additionally, the different representations of the sexes of participants in some included RCTs might be a concern.

## Conclusions

This meta-analysis compared the effect of intravenous ketorolac with metoclopramide treatment on adult migraine patients. The results suggest that the differences in most treatment effects and adverse effects are not significant between the treatments, with the exception of short-term headache relief. However, few studies available on this topic might have been a limitation in the analysis. Thus, more studies are warranted to confirm the results.

## Supplementary data

The supplementary materials are available at <https://doi.org/10.5281/zenodo.8299830>. The package contains the following files:

Supplementary Fig. 1. The forest plot of RR for the meta-analysis results of sustained headache relief (ketorolac compared to metoclopramide, Mantel–Haenszel method).

Supplementary Fig. 2. The funnel plot of RR for the meta-analysis results of sustained headache relief (ketorolac compared to metoclopramide).

Supplementary Fig. 3. The forest plot of RR for the meta-analysis results of adverse events (ketorolac compared to metoclopramide).

Supplementary Fig. 4. The funnel plot of RR for the meta-analysis results of adverse events (ketorolac compared to metoclopramide).

Supplementary Fig. 5. The forest plot of RR for the meta-analysis results of drowsiness (ketorolac compared to metoclopramide).

Supplementary Fig. 6. The funnel plot of RR for the meta-analysis results of drowsiness (ketorolac compared to metoclopramide).

Supplementary Fig. 7. The forest plot of RR for the meta-analysis results of restlessness (ketorolac compared to metoclopramide).

Supplementary Fig. 8. The funnel plot of RR for the meta-analysis results of restlessness (ketorolac compared to metoclopramide).


Supplementary Fig. 9. The forest plot of RR for the meta-analysis results of high restlessness (ketorolac compared to metoclopramide).

Supplementary Fig. 10. The funnel plot of RR for the meta-analysis results of high restlessness (ketorolac compared to metoclopramide).

## ORCID iDs

Qing Song  <https://orcid.org/0000-0003-2098-8223>

Hang Yang  <https://orcid.org/0009-0005-0105-3395>

Xiaoliang Yang  <https://orcid.org/0009-0008-7242-0721>

## References

1. Stovner LJ, Nichols E, Steiner TJ, et al. Global, regional, and national burden of migraine and tension-type headache, 1990–2016: A systematic analysis for the Global Burden of Disease Study 2016. *Lancet Neurol.* 2018;17(11):954–976. doi:10.1016/S1474-4422(18)30322-3

2. Richer L, Billingham L, Linsdell MA, et al. Drugs for the acute treatment of migraine in children and adolescents. *Cochrane Database Syst Rev.* 2016;4(4):CD005220. doi:10.1002/14651858.CD005220.pub2
3. Marmura MJ, Silberstein SD, Schwedt TJ. The acute treatment of migraine in adults: The American Headache Society Evidence Assessment of Migraine Pharmacotherapies. *Headache.* 2015;55(1):3–20. doi:10.1111/head.12499
4. Vadivelu N, Gowda AM, Urman RD, et al. Ketorolac tromethamine: Routes and clinical implications. *Pain Pract.* 2015;15(2):175–193. doi:10.1111/papr.12198
5. Kelley NE, Tepper DE. Rescue therapy for acute migraine, part 3: Opioids, NSAIDs, steroids, and post-discharge medications. *Headache.* 2012; 52(3):467–482. doi:10.1111/j.1526-4610.2012.02097.x
6. Colman I, Brown MD, Innes GD, Grafstein E, Roberts TE, Rowe BH. Parenteral metoclopramide for acute migraine: Meta-analysis of randomised controlled trials. *BMJ.* 2004;329(7479):1369. doi:10.1136/bmj.38281.595718.7C
7. Taggart E, Doran S, Kokotillo A, Campbell S, Villa-Roel C, Rowe BH. Ketorolac in the treatment of acute migraine: A systematic review. *Headache.* 2013;53(2):277–287. doi:10.1111/head.12009
8. Nurathirah MN, Yazid MB, Norhayati MN, Baharuddin KA, Abu Bakar MA. Efficacy of ketorolac in the treatment of acute migraine attack: A systematic review and meta-analysis. *Acad Emerg Med.* 2022;29(9):1118–1131. doi:10.1111/acem.14457
9. Knobloch K, Yoon U, Vogt PM. Preferred reporting items for systematic reviews and meta-analyses (PRISMA) statement and publication bias. *J Craniomaxillofac Surg.* 2011;39(2):91–92. doi:10.1016/j.jcms.2010.11.001
10. Cumpston MS, McKenzie JE, Welch VA, Brennan SE. Strengthening systematic reviews in public health: Guidance in the *Cochrane Handbook for Systematic Reviews of Interventions*, 2<sup>nd</sup> edition. *J Public Health (Oxf).* 2022;44(4):e588–e592. doi:10.1093/pubmed/fdac036
11. Friedman BW, Cisewski DH, Holden L, Bijur PE, Gallagher EJ. Age but not sex is associated with efficacy and adverse events following administration of intravenous migraine medication: An analysis of a clinical trial database. *Headache.* 2015;55(10):1342–1355. doi:10.1111/head.12697
12. Friedman BW, Garber L, Yoon A, et al. Randomized trial of IV valproate vs metoclopramide vs ketorolac for acute migraine. *Neurology.* 2014;82(11):976–983. doi:10.1212/WNL.0000000000000223
13. Khazaei M, Hosseini Nejad Mir N, Yadranji Aghdam F, Taheri M, Ghafouri-Fard S. Effectiveness of intravenous dexamethasone, metoclopramide, ketorolac, and chlorpromazine for pain relief and prevention of recurrence in the migraine headache: A prospective double-blind randomized clinical trial. *Neurol Sci.* 2019;40(5):1029–1033. doi:10.1007/s10072-019-03766-x
14. Klapper JA, Stanton JS. Ketorolac versus DHE and metoclopramide in the treatment of migraine headaches. *Headache.* 1991;31(8):523–524. doi:10.1111/j.1526-4610.1991.hed3108523.x
15. Soltani KM, Motamed H, Eslami K, Majdinasab N, Kouti L. Randomised trial of IV metoclopramide vs IV ketorolac in treatment of acute primary headaches. *Am J Emerg Med.* 2021;50:376–380. doi:10.1016/j.ajem.2021.08.023
16. Engel ER, Cheng J. IM ketorolac vs diclofenac potassium powder for oral solution for the acute treatment of severe migraine: A randomized controlled trial. *Neurol Sci.* 2020;41(3):537–542. doi:10.1007/s10072-019-04157-y
17. Pfaffenrath V, Fenzl E, Bregman D, Färkkilä M. Intranasal ketorolac tromethamine (SPRIX®) containing 6% of lidocaine (ROX-828) for acute treatment of migraine: Safety and efficacy data from a phase II clinical trial. *Cephalalgia.* 2012;32(10):766–777. doi:10.1177/0333102412451359
18. Rao AS, Gelaye B, Kurth T, Dash PD, Nitchie H, Peterlin BL. A randomized trial of ketorolac vs sumatriptan vs placebo nasal spray (KSPN) for acute migraine. *Headache.* 2016;56(2):331–340. doi:10.1111/head.12767
19. Talebian MT, Mirbaha S, Davarinezhad-Moghadam E, Payandemehr P. Comparing the therapeutic effects of dexamethasone-metoclopramide with ketorolac in relieving headache in patients with acute migraine attacks presenting to the emergency department. *Adv J Emerg Med.* 2019;3(2):e17. doi:10.22114/ajem.v0i0.142
20. Orr SL, Friedman BW, Christie S, et al. Management of adults with acute migraine in the emergency department: The American Headache Society Evidence Assessment of Parenteral Pharmacotherapies. *Headache.* 2016;56(6):911–940. doi:10.1111/head.12835
21. Orr SL, Aubé M, Becker WJ, et al. Canadian Headache Society systematic review and recommendations on the treatment of migraine pain in emergency settings. *Cephalalgia.* 2015;35(3):271–284. doi:10.1177/0333102414535997
22. Ungrungseesopon N, Wongtanarasarin W. Pain reduction and adverse effects of intravenous metoclopramide for acute migraine attack: A systematic review and meta-analysis of randomized-controlled trials. *World J Methodol.* 2022;12(4):319–330. doi:10.5662/wjm.v12.i4.319
23. Doğanay Aydin H, Vuralli D, Akçali DT, Bolay H. Metoclopramide inhibits trigeminovascular activation: Evidence for effective acute attack treatment in migraine. *Turk J Med Sci.* 2017;47:343–347. doi:10.3906/sag-1601-195
24. Sykes DA, Moore H, Stott L, et al. Extrapyramidal side effects of antipsychotics are linked to their association kinetics at dopamine D2 receptors. *Nat Commun.* 2017;8(1):763. doi:10.1038/s41467-017-00716-z
25. Corripio I, Ferreira A, Portella MJ, et al. The role of striatal dopamine D2 receptors in the occurrence of extrapyramidal side effects: Iodine-123-iodobenzamide single photon emission computed tomography study. *Psychiatry Res Neuroimaging.* 2012;201(1):73–77. doi:10.1016/j.pscychresns.2011.02.004
26. Friedman BW, Mulvey L, Esses D, et al. Metoclopramide for acute migraine: A dose-finding randomized clinical trial. *Ann Emerg Med.* 2011;57(5):475–482.e1. doi:10.1016/j.annemergmed.2010.11.023



# Postoperative therapy for local-advanced gastric cancer: A systematic review and meta-analysis

Zhuo Wang<sup>1,B–D,F</sup>, Lihua Dong<sup>1,B,D,F</sup>, Weiyan Shi<sup>1,B,D,F</sup>, Ling Gao<sup>1,C,D,F</sup>, Xin Jiang<sup>1,C,D,F</sup>, Suyang Xue<sup>2,B,D,F</sup>, Pengyu Chang<sup>1,A,E,F</sup>

<sup>1</sup> Department of Radiation Oncology and Therapy, The First Hospital of Jilin University, Changchun, China

<sup>2</sup> Department of Interventional Therapy, The First Hospital of Jilin University, Changchun, China

A – research concept and design; B – collection and/or assembly of data; C – data analysis and interpretation; D – writing the article; E – critical revision of the article; F – final approval of the article

Advances in Clinical and Experimental Medicine, ISSN 1899–5276 (print), ISSN 2451–2680 (online)

*Adv Clin Exp Med.* 2024;33(7):669–678

## Address for correspondence

Pengyu Chang  
E-mail: radiojluedu@163.com

## Funding sources

The study was supported by the National Natural Science Foundation of China (grant No. 82272738)

## Conflict of interest

None declared

## Acknowledgements

We would like to thank Yao Yan for her biostatistics services.

Received on February 28, 2023

Reviewed on April 24, 2023

Accepted on August 28, 2023

Published online on December 12, 2023

## Abstract

**Background.** Adjuvant therapy after surgery is effective for the treatment of advanced gastric cancer (GC), but the regimens are not uniform, resulting in imbalanced benefits.

**Objectives.** To compare the overall survival (OS), relapse-free survival (RFS) and disease-free survival (DFS) of patients with local-advanced GC (LAGC) after surgery plus adjuvant therapy and with surgery alone based on meta-analysis.

**Materials and methods.** Literature search was performed among the articles published in the PubMed, Embase and Cochrane Library databases from January 2000 to December 2018. Study selection was conducted based on the following criteria: randomized clinical trials (RCTs) on surgery plus adjuvant therapy compared to surgery alone; studies compared OS and/or RFS/DFS; and cases medically confirmed with LAGC. Only articles in English were included.

**Results.** A total of 12 datasets from 11 randomized controlled trials (RCTs) involving 4606 patients were included in the meta-analysis. There was a significant improvement in OS of patients who underwent postoperative adjuvant therapy (HR 0.78; 95% CI: 0.72–0.84;  $p < 0.001$ ). In the subgroup analysis, it showed a higher improvement in OS patients who received adjuvant chemotherapy plus immunotherapy or radiotherapy (HR 0.72; 95% CI: 0.61–0.85;  $p < 0.001$ ).

**Conclusions.** Adjuvant therapy led to survival benefits in patients with LAGC.

**Key words:** chemotherapy, gastric cancer, radiotherapy, overall survival

## Cite as

Wang Z, Dong L, Shi W, et al. Postoperative therapy for local-advanced gastric cancer: A systematic review and meta-analysis. *Adv Clin Exp Med.* 2024;33(7):669–678. doi:10.17219/acem/171616

## DOI

10.17219/acem/171616

## Copyright

Copyright by Author(s)

This is an article distributed under the terms of the Creative Commons Attribution 3.0 Unported (CC BY 3.0) (<https://creativecommons.org/licenses/by/3.0/>)

## Background

Gastric cancer (GC) ranks as the 2<sup>nd</sup> leading cause of cancer-related mortality globally.<sup>1</sup> As revealed in GLOBOCAN 2012, the incidence of GC in East Asia populations is the highest.<sup>2</sup> Most patients are at an advanced stage at diagnosis, and surgery is their only chance of survival. In recent years, significant advances have been made in surgical techniques, and surgical concepts have been continuously updated. Although surgery for different extents of lymph node dissection, especially D2 lymphadenectomy, is well accepted as a standard for locally advanced GC (LAGC),<sup>3</sup> many patients still present local-regional recurrence and distant metastasis. On this basis, the efficacy of single radical surgery for LAGC is not sufficient.

In the past decades, there have been many explorations into the treatment of LAGC, including preoperative neoadjuvant radiotherapy, neoadjuvant chemotherapy, neoadjuvant chemoradiotherapy, and combined immunotherapy. These treatment options can reduce the stage of tumor regression and eliminate micrometastases before surgery, thereby improving the R0 resection rate and reducing intraoperative spread and the recurrence rate. These indeed prolong patient survival. Although these studies<sup>4–6</sup> have confirmed the efficacy and safety of neoadjuvant therapy in LAGC, there is still no treatment standard.

Postoperative chemotherapy has been considered an option for LAGC. Among these regimens, 5-fluorouracil (5-FU)-based chemotherapy combined with platinum and/or docetaxel is regarded as the standard.<sup>7</sup> In the previous meta-analysis, postoperative chemotherapy contributed to the extension of overall survival (OS) in LAGC after radical surgery.<sup>8</sup> In recent decades, several large-scale trials have continuously updated their data on treatment efficiency, such as CLASSIC<sup>9</sup> and ACTS-GC.<sup>10</sup> In recent years, with the development of radiation therapy and the gradual application of immunotherapy, many patients can benefit from radiotherapy and chemotherapy or combined immunotherapy. Meanwhile, other strategies (e.g., radiotherapy or immunotherapy) have been adopted for treating LAGC. However, the results of many studies are inconsistent, and there are disputes over therapeutic applications.

## Objectives

This study aimed to investigate the effects of postoperative treatment on the prognosis of LAGC patients, especially those receiving chemotherapy plus radiotherapy or immunotherapy. This meta-analysis was designed to compare the OS, relapse-free survival (RFS), and disease-free survival (DFS) of patients with LAGC after surgery plus adjuvant therapy and those with surgery alone.

## Materials and methods

### Study design

Based on the guidelines of meta-analysis of observational studies in epidemiology and Preferred Reporting Items for Systematic Reviews and Meta-Analyses (PRISMA), a protocol was designed by our team, including a search strategy, inclusion and exclusion criteria, primary and secondary outcomes, and statistical analysis. The study is consistent with the requirements of PRISMA and a measurement tool to assess systematic reviews (AMSTAR).

### Criteria of eligibility

Two authors (WZ and DLH) independently searched articles published in PubMed, Embase and Cochrane Library between January 2000 and December 2018. The terms utilized included “gastric carcinoma”, or “adenocarcinoma of the stomach”, or “gastric cancer”, or “stomach tumors” and “radiotherapy”, or “radiation therapy”, or “chemotherapy”, or “external irradiation therapy”, or “adjuvant chemotherapy”, or “external radiation therapy”. Only randomized controlled trials (RCTs) published in English were included in this meta-analysis. The eligible studies should have met the following criteria: 1) involving patients histologically confirmed with advanced GC; 2) RCTs reporting the comparison between adjuvant therapy after radical surgery or surgery alone; 3) Reporting the hazard ratio (HR) and the corresponding 95% confidence interval (95% CI) for OS and RFS/DFS.

### Data extraction

We extracted the following data from each eligible study: first author, study design, country, year of publication, patient age, number of patients (with/without postoperative adjuvant therapy), median survival, and HR of OS and/or RFS/DFS. In cases of missing data, we contacted the authors by e-mail to obtain the information. A comprehensive discussion was held among all investigators until reaching a consensus when there were any disputes on the data collection.

Hazard ratio was used to analyze the time-to-event data, including OS and RFS/DFS. The method by Tierney et al. was used to calculate the HR if it was not mentioned in the extracted articles.<sup>11</sup>

### Quality assessment

The risk of bias was evaluated using the domain-based Cochrane Collaboration’s tool as previously described.<sup>12</sup> Funnel plots were constructed to assess the risk of publication bias across the series for all outcome measures.



## Statistical analysis

The  $\chi^2$  test Q-statistics evaluated the heterogeneity, and the degree of heterogeneity was estimated with the  $I^2$  statistic. A random effects model was selected when  $p < 0.10$  or the  $I^2$  statistic was  $>50\%$ . Otherwise, a fixed-effects model was adopted. For the sensitivity analysis, we recalculated the pooled statistics after deleting the related study. Review Manager 5.3 (RevMan 5.3; Cochrane Collaboration, Copenhagen, Denmark) was used for the statistical analysis. A p-value of less than 0.05 was considered statistically significant.

## Results

### Characteristics of the eligible studies

Figure 1 shows the literature selection and screening flowchart, which resulted in 18 RCTs<sup>9,10,13–28</sup> enrolling 7,919 patients into the meta-analysis. The basic characteristics of these studies are summarized in Table 1. In brief, the studies were published from 2001 to 2018, and the sample sizes ranged from 137 to 1,059 people. Six studies used 3 datasets, which were updated using 3 RCTs, and only 3 studies were included. Four studies were excluded as the HR could not be extracted due to the absence of OS, PFS, or DFS.<sup>13–16</sup> Two datasets were selected from the 3-arm study.<sup>17</sup>

A total of 12 datasets were obtained from the RCTs comparing the OS of GC patients with or without postoperative therapy.<sup>9,10,17–24,27</sup> All RCTs had undergone peer-review between 2001 and 2014. Herein, 3 trials were from Japan, South Korea, and China, respectively, 2 from France,

4 from Italy, 1 from Poland, and 1 from the USA. A total of 4,606 patients were included in the analysis, among which 2319 received postoperative therapy, and 2,287 underwent radical surgery.

The disease-stage classification of LAGC patients was mainly performed based on the American Joint Committee on Cancer/Union for International Cancer Control (AJCC/UICC) tumor-node-metastasis (TNM) classification system, together with the classification system recommended by the Japanese Gastric Cancer Association (JGCA). Patients with at least a 70% lymph node-positive rate were recruited in 1 study.<sup>18</sup> In addition, patients with N<sup>+</sup> tumors with at least an 80% lymph node-positive rate were recruited in 7 studies.<sup>9,10,19–21,23,24</sup> Three trials recruited patients with N<sup>+</sup> tumors with a lymph node-positive rate of 100%.<sup>17,22,27</sup> Meanwhile, D2 lymphadenectomy was performed in 4 trials<sup>9,10,22,27</sup> and D1-plus and R0 resection was performed in 6 trials.<sup>9,10,18,21,22,27</sup>

### OS determination

All patients were followed up for more than 5 years. The OS rates were higher in most of adjuvant therapy groups than those of the surgery group in 5 of 11 trials<sup>9,10,17,22,24</sup> (Fig. 2A). We present the pooled OS data in Supplementary Fig. 1. In the study by Nitti et al.,<sup>21</sup> 2 datasets from the European Organization for Research and Treatment of Cancer (EORTC) trial and the International Collaborative Cancer Group (ICCG) were collected to be analyzed jointly. The OS rate in the adjuvant therapy group was higher than that in the surgery group in the EORTC trial.<sup>21</sup> However, in the ICCG trial, the OS rate of patients receiving adjuvant therapy was lower than that of surgery-only cases.<sup>21</sup>

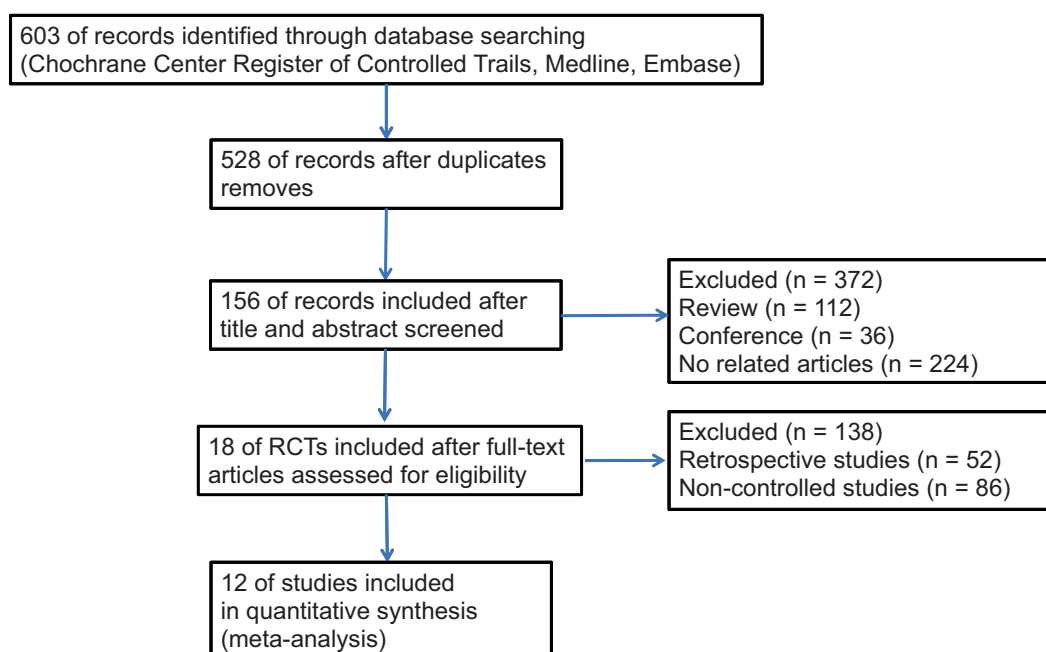


Fig. 1. Flow diagram of literature retrieval and screening

Table 1. The basic characteristics of included studies

Year	Study	Country	Age [years]	Phase	Surgery	AT+S	S	AT regimens
2002	Bajetta et al. (ITMO) <sup>27</sup>	Italy	≤70	III-IVM0	D2 (R0)	135	136	EAP
2004	Chipponi et al. (AURC) <sup>19</sup>	France	≤75	III-IVM0	D1/D2 (R0/R1)	93	103	LV+5FU+CDDP
2004	Popiela et al. (BCG+FAM) <sup>17</sup>	Poland	<70	III-IVM0	D1/D2(R0/R1)	51	52	BCG+FAM
2004	Popiela et al. (FAM) <sup>17</sup>	Poland	<70	III-IVM0	D1/D2(R0/R1)	53	52	FAM
2005	Bouché et al. (8801) <sup>20</sup>	France	31–83	II-IVM0	D0/D1/D2(R0)	127	133	5-FU+CDDP
2006	Nitti et al. (EORTC+ICCG) <sup>21</sup>	Italy	<71	IB-IVM0	D1+(R0)	194	203	FAMTX or FEMTX
2007	De Vita et al. (GOIM 9602 Study) <sup>18</sup>	Italy	<70	IB-IIIB	D1+ (R0)	112	113	ELFE
2007	Nakajima et al. (NCT00152243) <sup>22</sup>	Japan	20–75	III-IVM0	D2+ (R0)	93	95	UFT
2008	Di Costanzo et al. (GOIRC) <sup>23</sup>	Italy	<59	IB-IVM0	D1+	130	128	PELF
2011	Sasako et al. (ACTS-GC) <sup>10</sup>	Japan	20–80	II-IIIB	D2 (R0)	529	530	S-1
2012	Smalley et al. (Study 0116) <sup>24</sup>	USA	23–87	IB-IVM0	D0/D1/D2 (R0)	282	227	FU + LV + RT
2014	Noh et al. (CLASSIC) <sup>9</sup>	South Korea	≥18	II-IIIB	D2 (R0)	520	515	Cap+OXA

m – median; AT – adjuvant therapy; S – surgery; EAP – etoposide, adriamycin, cisplatin; BCG – bacille Calmette–Guérin; FAM – 5-FU, adriamycin, MMC; FAMTX – methotrexate, 5-FU, leucovorin, adriamycin; FEMTX – 5-FU, epirubicin, MTX, leucovorin; ELFE – epirubicin, leucovorin, 5-fluorouracil, etoposide; PELF – cisplatin, epirubicin, leucovorin, 5-fluorouracil; LV – leucovorin; Cap – capecitabine; OXA – oxaliplatin.

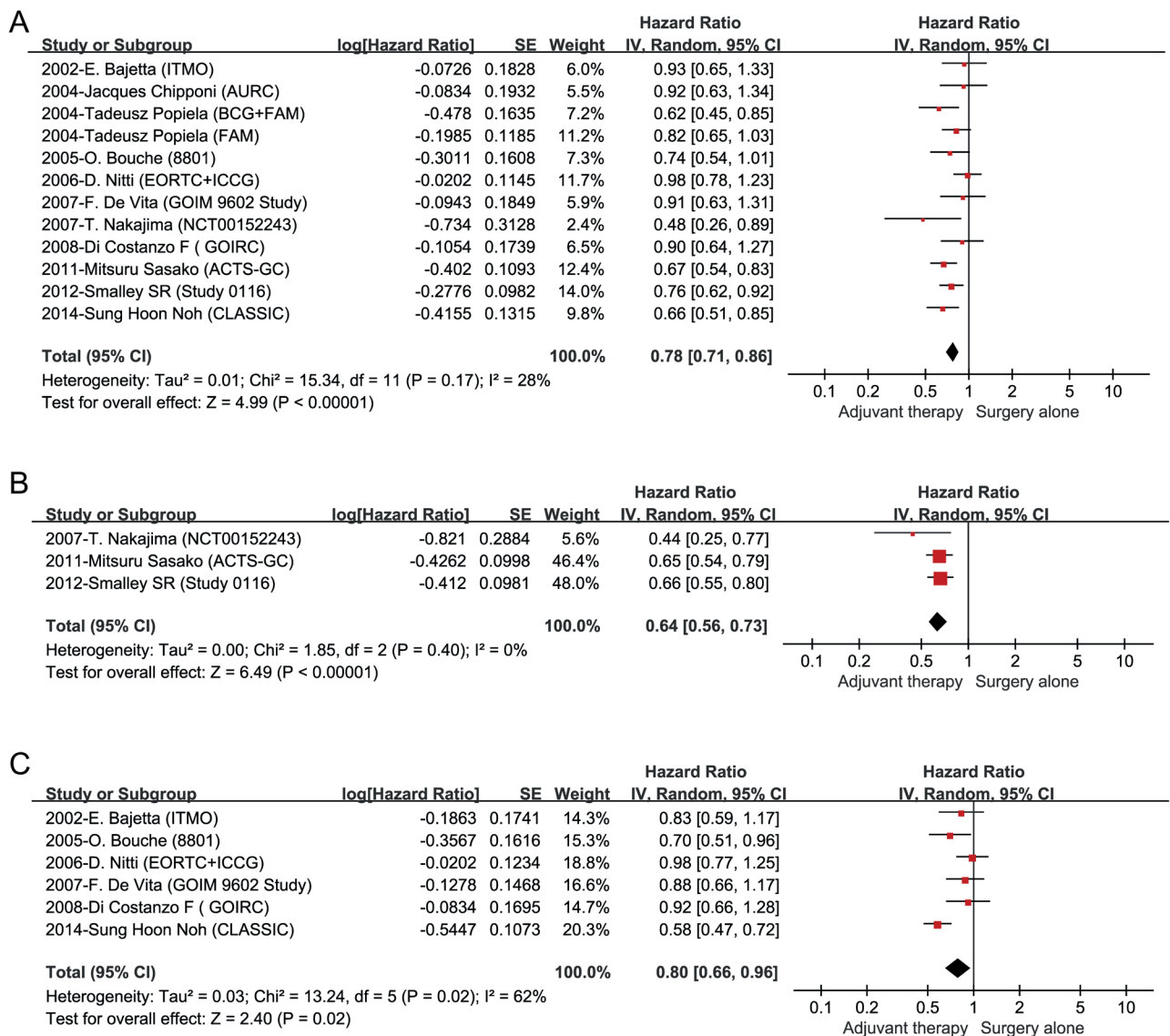


Fig. 2. A. Meta-analyses results for overall survival (OS); B. Relapse-free survival (RFS); C. Disease-free survival (DFS)

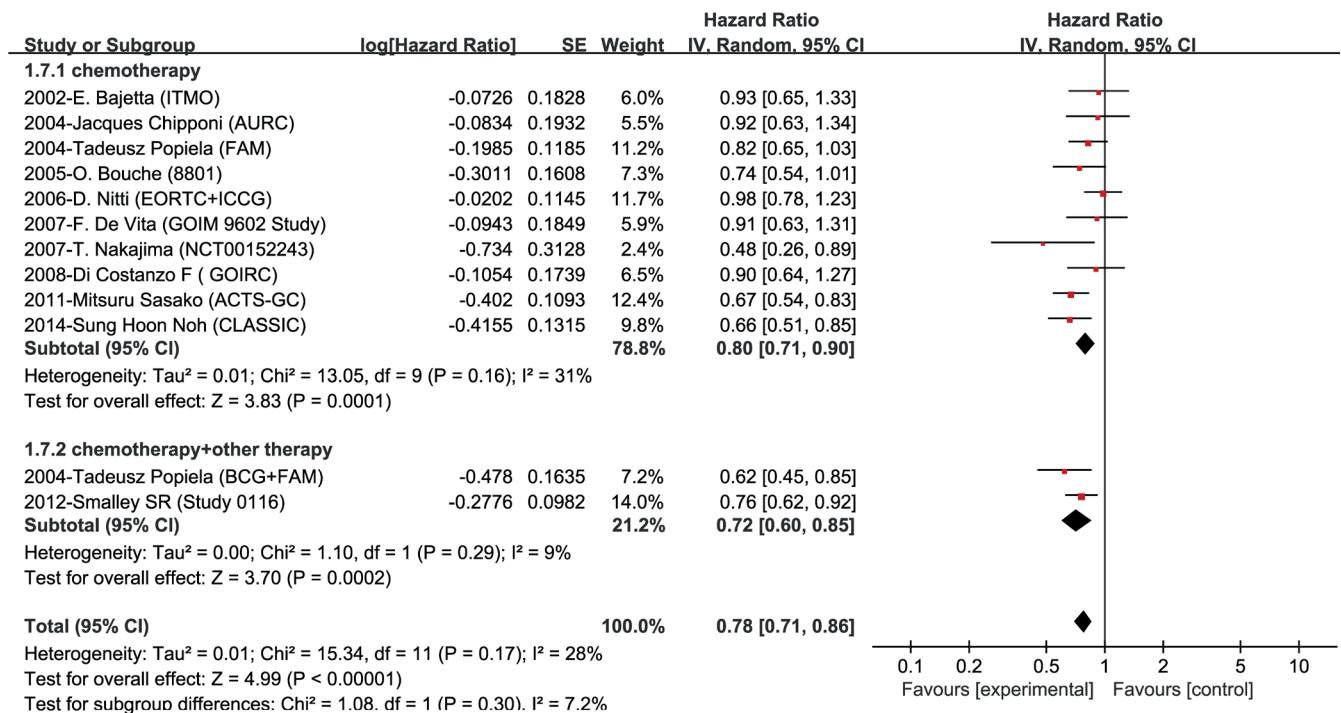


Fig. 3. Meta-analyses results for subgroup analysis of 5-year overall survival (OS)

## RFS

Three RCTs reported the RFS with no heterogeneity ( $p < 0.001$ ,  $I^2 = 0\%$ ).<sup>10,22,24</sup> Significant differences were observed between the patients receiving adjuvant therapy and those receiving just surgery (HR = 0.64; 95% CI: 0.56–0.73;  $I^2 = 0\%$ ; Fig. 2B). We present the pooled RFS data in Supplementary Fig. 2.

## DFS

Heterogeneity was observed in the DFS of 6 RCTs ( $p = 0.02$ ;  $I^2 = 62\%$ ).<sup>9,18,20,21,23,27</sup> On this basis, the random-effects model was used, which indicated significant differences in DFS between the patients receiving adjuvant therapy and those only receiving surgery (HR = 0.80; 95% CI: 0.66–0.96;  $p = 0.02$ ;  $I^2 = 62\%$ ). There was no heterogeneity for these studies after omitting 1 study<sup>9</sup> ( $I^2 = 0\%$ ; Fig. 2C). We present the pooled DFS data in Supplementary Fig. 3.

## Subgroup analysis

In addition to chemotherapy, we divided the 12 sets of data into 2 subgroups based on the combination of other adjuvant therapies (i.e., radiotherapy or immunotherapy). Subgroup analysis indicated that patients receiving postoperative chemotherapy plus radiotherapy or immunotherapy presented a significant increase in 5-year OS rate than those only receiving chemotherapy (HR = 0.72; 95% CI: 0.60–0.85;  $p < 0.001$ ; Fig. 3).

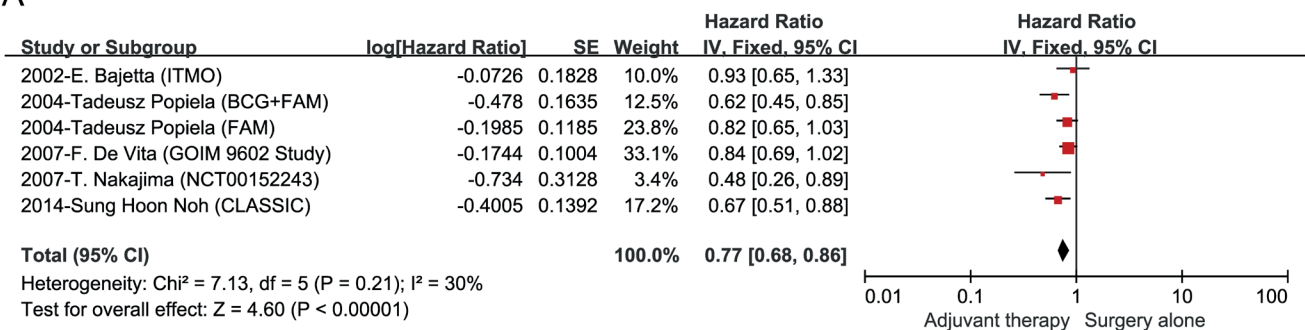
## Different postoperative adjuvant regimens may affect the prognosis

All patients enrolled in the RCTs received chemotherapy with different regimens, with all studies applying 5-FU except for 1 study<sup>9</sup> using capecitabine and oxaliplatin. Two studies involved the oral administration of fluorouracil agents, such as S-1 and tegafur–uracil (UFT).<sup>10,22</sup> The rest of the regimens were carried out by iv. infusion of 5-FU. Among the included studies, 1 involved immunotherapy using the bacille Calmette–Guérin (BCG),<sup>17</sup> and 1 involved radiotherapy.<sup>24</sup> The data supported that adjuvant chemotherapy combined with radiotherapy or immunotherapy contributed to the extension of OS (Fig. 3). The outcomes of OS for the patients with lymphatic metastasis are shown in Fig. 4.

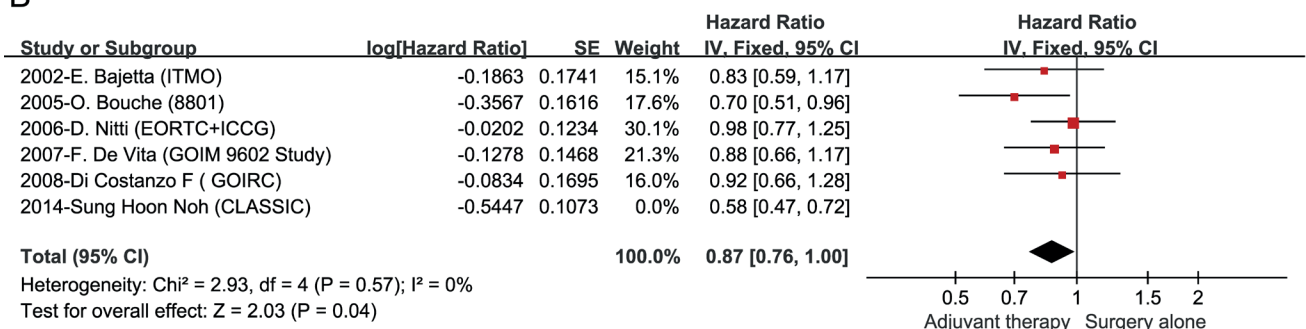
## Publication bias

As shown in Fig. 5, together with the Egger’s and Begg’s tests, the publication bias in these studies was low. Egger’s regression test determined the degree of asymmetry in the funnel plot by measuring the intercept of a standard normal regression that deviated from precision. The Begg’s rank correlation test explained the correlation between the rank of the effect size and its variance. A p-value of more than 0.05 demonstrated statistical difference with a low risk of publication bias. In this study, the p-values for the Begg’s test and Egger’s test in most of the groups were more than 0.05. However, p-value for the Begg’s test in the studies listed in Fig. 2B

A



B



C

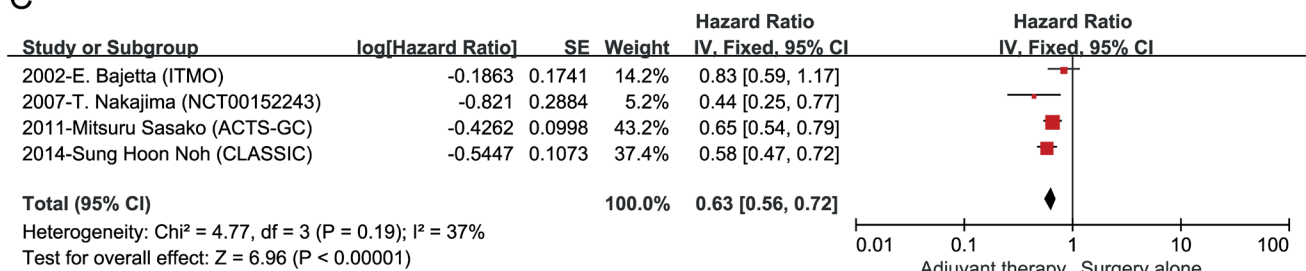
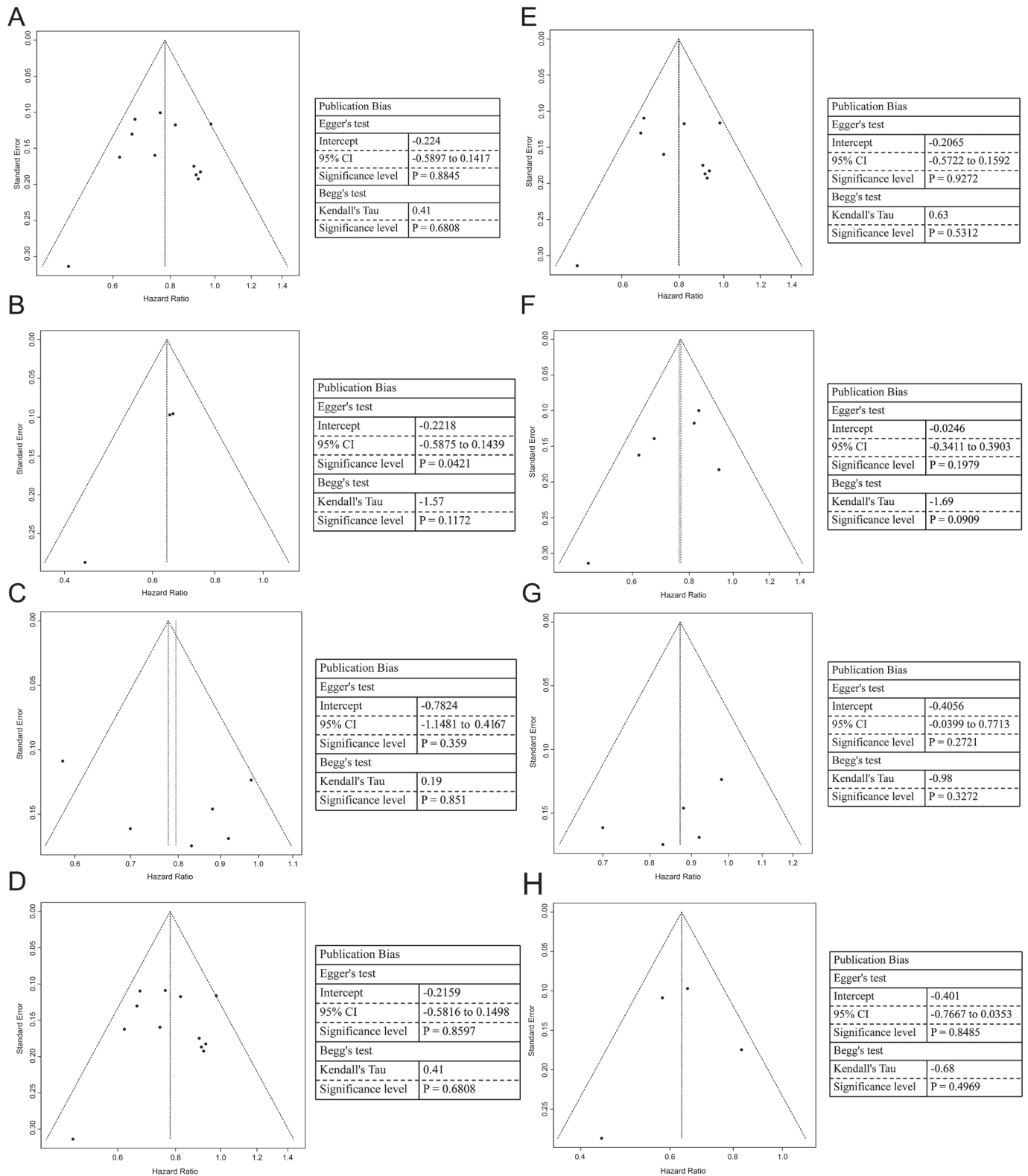


Fig. 4. A. Meta-analyses for the 5-year overall survival (OS) of patients with positive lymph nodes; B. Sensitivity analysis of disease-free survival (DFS) excluding the 2014 study by Noh et al.<sup>9</sup>; C. Meta-analyses for OS of patients receiving D2 gastrectomy showing no evidence of remaining tumor

was 0.1172, and p-value for the Egger's test was 0.0421 (Fig. 5B), which may be related to the minor trials in this group. The funnel plots of 12 trials listed in Fig. 2A were symmetric, and the p-values for the Begg's test and Egger's test were 0.885 and 0.680, respectively (Fig. 5A). Meanwhile, the p-values for the Begg's test and Egger's test for the studies listed in Fig. 2C were 0.851 and 0.359 (Fig. 5C), while those for the studies listed in Fig. 3 (chemotherapy and chemotherapy and other therapy) were 0.680 and 0.860 (Fig. 5D), respectively. The p-values for the Begg's test and Egger's test for chemotherapy of the study listed in Fig. 3 (chemotherapy only) were 0.531 and 0.927 (Fig. 5E), while those for the studies listed in Fig. 5A were 0.091 and 0.198 (Fig. 5F), those listed in Fig. 5B were 0.327 and 0.272 (Fig. 5G), and those listed in Fig. 5C were 0.497 and 0.858 (Fig. 5H), respectively. These data mostly indicated a low risk of publication bias.

## Discussion

The prognosis of LAGC patients is usually poor, and many present with recurrences or metastases. In recent years, immunotherapy has been reported to be effective in the treatment of multiple malignancies.<sup>29</sup> However, the efficacy of immunotherapy alone is limited. Indeed, many studies confirmed that chemotherapy or radiotherapy combined with immunotherapy after surgery is more effective for solid tumors.<sup>30–32</sup> This meta-analysis of 12 sets of data indicated that postoperative chemotherapy improved the prognosis of LAGC patients. Specifically, LAGC patients receiving adjuvant therapy showed an increase of about 22% in the 5-year OS rate compared to those only receiving radical surgery (Fig. 2A). Although there is a lack of statistical significance upon individual analysis, the OS data of 7 trials along with the DFS data from another 4 trials indicated that postoperative chemotherapy contributed



**Fig. 5.** Funnel plot for publication bias. A. The plot for the studies listed in Fig. 2A; B. The plot for the studies listed in Fig. 2B; C. The plot for the studies listed in Fig. 2C; D. The plot for the studies listed in Fig. 3 (chemotherapy and chemotherapy plus other therapy); E. The plot for the studies listed in Fig. 3 (chemotherapy only); F. The plot for the studies listed in Fig. 4A; G. The plot for the studies listed in Fig. 4B; H. The plot for the studies listed in Fig. 4C

to the survival of LAGC patients, though this is probably due to the small sample size enrolled in the trials. The survival benefits after postoperative chemotherapy were significant after pooling for the meta-analysis.

Six sets of data reported the OS outcomes for patients with lymphatic metastasis (Fig. 4A). The analysis of patients receiving postoperative chemotherapy showed increased OS by up to 23%. However, 3 trials supported

postoperative therapy with no statistically significant trends. Two RCTs mainly recruited patients with stage IIIA, IIIB, or IV (T4N1M0).<sup>17,27</sup> Likewise, in another study,<sup>18</sup> the ratio of patients with stage IIIA, IIIB, or IV (T4N1M0) exceeded 80% of all enrolled patients.

Nine studies considered RFS or DFS as their primary endpoint. Three RCTs compared the RFS of LAGC patients with and without postoperative chemotherapy,<sup>10,22,24</sup> which indicated the survival benefits of postoperative chemotherapy. The pooled HR was 0.64 (95% CI: 0.56–0.73) after combining all the HRs in the selected trials, which significantly favored postoperative chemotherapy ( $p < 0.001$ , Fig. 2B). Six RCTs compared the DFS of GC patients receiving postoperative treatment compared with those who received no postoperative treatment.<sup>9,18,20,21,23,27</sup> Almost all trials favored postoperative treatment except for 4 trials showing no statistical differences.<sup>18,21,23,27</sup> When considering the study of Noh et al.,<sup>9</sup> survival benefits were observed after postoperative therapy (HR = 0.80; 95% CI: 0.66–0.96;  $p = 0.02$ ) with high heterogeneity ( $I^2 = 62\%$ ; Fig. 2C). Upon removing the study, the survival benefits were significantly weaker (HR = 0.87; 95% CI: 0.76–1.0;  $p = 0.04$ ) with a low heterogeneity ( $I^2 = 0\%$ ; Fig. 4B). The high heterogeneity was mainly associated with higher weight and better survival benefits. In the study by Noh et al., 1,035 patients underwent curative D2 gastrectomy with no macroscopic or microscopic evidence of tumors. The radical surgical treatment produced a significant survival benefit, and the high heterogeneity might also be caused by the treatment design, including the chemotherapy regimen, the number of patients, and the surgeon's skills.

Four studies reported the outcomes of OS and RFS for patients who underwent D2 gastrectomy, with no evidence of remaining tumors noticed among these patients (Fig. 4C). The OS and RFS outcomes were consistent in the patients receiving combined therapy (OS: HR = 0.69; 95% CI: 0.58–0.83;  $p < 0.001$ ; RFS: HR = 0.63; 95% CI: 0.53–0.76;  $p < 0.001$ ). Patients enrolled in the Japanese trials showed higher postoperative survival rates than in trials carried out in Western Europe and the USA.<sup>8</sup> Three trials were carried out in Japan, and the results showed statistically significant trends to support postoperative therapy. There was no statistical significance in the study by Bajetta et al.,<sup>27</sup> which was probably due to the advanced stage of the eligible patients.

Several studies reported that 40–60% of GC patients undergoing radical surgery at stage II or III showed a loco-regional recurrence before postoperative therapy. Loco-regional failure often occurred in the anastomosis, followed by the stomach bed and undissected regional nodes. Radiotherapy could improve postoperative local control of GC, but there were some disputes on survival

in the data from randomized trials. D2 loco-regional node resection was the standard method, and postoperative radiotherapy (PORT) combined with chemotherapy was still controversial for treating LAGC.<sup>33</sup> In this meta-analysis, 2 studies confirmed that LAGC patients showed longer OS after PORT combined with chemotherapy. In 2018, a network meta-analysis confirmed that the 5-year OS rate and the 2-year PFS of patients receiving chemoradiotherapy were higher than those only receiving surgery (HR = 0.80 and 0.58, respectively).<sup>8</sup> However, the 5-year OS rate of patients who underwent PORT was poor, indicating that postoperative chemotherapy is important for advanced GC.

In this meta-analysis, there was a higher improvement in OS among patients receiving adjuvant chemotherapy plus immunotherapy or radiotherapy. Recently, malignant tumors have been confirmed to be immunogenic, and accumulating evidence demonstrates a potential link between cancer progression and anti-tumor immunity.<sup>34</sup> In 2018, a meta-analysis confirmed that chemotherapy combined with cytokine-induced killer cell (CIK)/dendritic cell-CIK (CIK/DC-CIK) therapy after surgery significantly increased OS rates (HR = 0.712; 95% CI: 0.594–0.854), DFS rates (HR = 0.66; 95% CI: 0.546–0.797), and T-lymphocyte responses in patients with GC.<sup>35</sup> In addition, a retrospective study reported a similar conclusion in epithelial ovarian cancer patients.<sup>34</sup> Another study confirmed that the immunotherapy group presented a higher 3-year OS rate and 5-year OS rate, respectively.<sup>29</sup> Meanwhile, patients receiving 3 or more cycles of immunotherapy showed a higher 5-year OS rate than those who received 2 cycles or less (82.10% compared to 69.90%;  $p = 0.035$ ).<sup>29</sup>

A study based on the National Cancer Database (NCDB) concluded that PORT conferred an additional OS advantage, which was higher than that of adjuvant chemotherapy alone for complete resection of N2 non-small cell lung cancer (NSCLC).<sup>36</sup> Similarly, another study reported that PORT was associated with improved OS in patients with incompletely resected stage II or III N0-2 NSCLC.<sup>37</sup> However, studies on PORT combined with immunotherapy are still limited for LAGC, and more clinical studies reporting the outcomes of LAGC are expected in the future.

## Limitations

Indeed, there are limitations in this meta-analysis. First, the study designs of the trials differed. For example, the chemotherapy regimens and cycles were not totally consistent. Second, we only focused on the influence of postoperative treatment rather than complications and adverse effects, which may exaggerate the benefits of postoperative treatment. Finally, we could not eliminate the potential publication bias.

## Conclusions

In conclusion, postoperative treatment plays a significant role in improving survival in patients with LAGC. We found that patients receiving adjuvant therapy after surgery showed a significant improvement in OS. Meanwhile, patients presented a higher improvement in OS after adjuvant chemotherapy plus immunotherapy or radiotherapy.

## Supplementary data

The Supplementary materials are available at <https://doi.org/10.5281/zenodo.8294045>. The package consists of the following files:

- Supplementary Fig. 1. Pooled data of OS including 11 RCTs.
- Supplementary Fig. 2. Pooled data of RFS including 3 RCTs.
- Supplementary Fig. 3. Pooled data of DFS including 6 RCTs.

## Data availability

The datasets generated and/or analyzed during the current study are available from the corresponding author on reasonable request.

## Consent for publication

Not applicable.

## ORCID iDs

Zhuo Wang  <https://orcid.org/0000-0001-8021-8146>  
 Lihua Dong  <https://orcid.org/0000-0002-9454-3596>  
 Weiyan Shi  <https://orcid.org/0009-0003-3290-678X>  
 Ling Gao  <https://orcid.org/0000-0001-5313-1395>  
 Xin Jiang  <https://orcid.org/0000-0002-4613-7438>  
 Suyang Xue  <https://orcid.org/0009-0002-8144-5070>  
 Pengyu Chang  <https://orcid.org/0000-0002-8916-3572>

## References

1. Wu DM, Wang S, Wen X, et al. Survival benefit of three different therapies in postoperative patients with advanced gastric cancer: A network meta-analysis. *Front Pharmacol*. 2018;9:929. doi:10.3389/fphar.2018.00929
2. Ng CJ, Teo CH, Abdullah N, Tan WP, Tan HM. Relationships between cancer pattern, country income and geographical region in Asia. *BMC Cancer*. 2015;15(1):613. doi:10.1186/s12885-015-1615-0
3. Mocellin S. The effect of lymph node dissection on the survival of patients with operable gastric carcinoma. *JAMA Oncol*. 2016;2(10):1363–1364. doi:10.1001/jamaoncol.2016.2044
4. Japanese Gastric Cancer Association. Japanese gastric cancer treatment guidelines 2014 (v. 4). *Gastric Cancer*. 2017;20(1):1–19. doi:10.1007/s10120-016-0622-4
5. Ychou M, Boige V, Pignon JP, et al. Perioperative chemotherapy compared with surgery alone for resectable gastroesophageal adenocarcinoma: An FNCLCC and FFCD multicenter phase III trial. *J Clin Oncol*. 2011;29(13):1715–1721. doi:10.1200/JCO.2010.33.0597
6. Cunningham D, Allum WH, Stenning SP, et al. Perioperative chemotherapy versus surgery alone for resectable gastroesophageal cancer. *N Engl J Med*. 2006;355(1):11–20. doi:10.1056/NEJMoa055531
7. Smyth EC, Verheij M, Allum W, Cunningham D, Cervantes A, Arnold D. Gastric cancer: ESMO Clinical Practice Guidelines for diagnosis, treatment and follow-up. *Ann Oncol*. 2016;27(Suppl 5):v38–v49. doi:10.1093/annonc/mdw350
8. Sun P, Xiang JB, Chen ZY. Meta-analysis of adjuvant chemotherapy after radical surgery for advanced gastric cancer. *Br J Surg*. 2009;96(1):26–33. doi:10.1002/bjs.6408
9. Noh SH, Park SR, Yang HK, et al. Adjuvant capecitabine plus oxaliplatin for gastric cancer after D2 gastrectomy (CLASSIC): 5-year follow-up of an open-label, randomized phase 3 trial. *Lancet Oncol*. 2014;15(12):1389–1396. doi:10.1016/S1470-2045(14)70473-5
10. Sasako M, Sakuramoto S, Katai H, et al. Five-year outcomes of a randomized phase III trial comparing adjuvant chemotherapy with S-1 versus surgery alone in stage II or III gastric cancer. *J Clin Oncol*. 2011;29(33):4387–4393. doi:10.1200/JCO.2011.36.5908
11. Tierney JF, Stewart LA, Ghersi D, Burdett S, Sydes MR. Practical methods for incorporating summary time-to-event data into meta-analysis. *Trials*. 2007;8(1):16. doi:10.1186/1745-6215-8-16
12. Higgins JPT, Thomas J, Chandler J, Cumpston M, Li T, Page MJ, Welch VA, eds. *Cochrane Handbook for Systematic Reviews of Interventions*. 2<sup>nd</sup> ed. Chichester, UK: Wiley & Sons; 2019. doi:10.1002/9781119536604
13. Neri B, Cini G, Andreoli F, et al. Randomized trial of adjuvant chemotherapy versus control after curative resection for gastric cancer: 5-year follow-up. *Br J Cancer*. 2001;84(7):878–880. doi:10.1054/bjoc.2000.1472
14. Nashimoto A, Nakajima T, Furukawa H, et al. Randomized trial of adjuvant chemotherapy with mitomycin, fluorouracil, and cytosine arabinoside followed by oral fluorouracil in serosa-negative gastric cancer: Japan Clinical Oncology Group 9206-1. *J Clin Oncol*. 2003;21(12):2282–2287. doi:10.1200/JCO.2003.06.103
15. The Gastric Cancer Surgical Study Group in the Japan Clinical Oncology Group; Miyashiro I, Furukawa H, et al. Randomized clinical trial of adjuvant chemotherapy with intraperitoneal and intravenous cisplatin followed by oral fluorouracil (UFT) in serosa-positive gastric cancer versus curative resection alone: Final results of the Japan Clinical Oncology Group trial JCOG9206-2. *Gastric Cancer*. 2011;14(3):212–218. doi:10.1007/s10120-011-0027-3
16. Mizutani T, Yamaguchi K, Mizusawa J, et al. A phase III trial to confirm modified S-1 adjuvant chemotherapy for pathological stage II/III vulnerable elderly gastric cancer patients who underwent gastric resection (JCOG1507, BIRDIE). *Jpn J Clin Oncol*. 2018;48(12):1101–1104. doi:10.1093/jjco/hyy152
17. Popiela T, Kulig J, Czupryna A, Szczepanik AM, Zembala M. Efficiency of adjuvant immunochemotherapy following curative resection in patients with locally advanced gastric cancer. *Gastric Cancer*. 2004;7(4):240–245. doi:10.1007/s10120-004-0299-y
18. De Vita F, Giuliani F, Orditura M, et al. Adjuvant chemotherapy with epirubicin, leucovorin, 5-fluorouracil and etoposide regimen in resected gastric cancer patients: A randomized phase III trial by the Gruppo Oncologico Italia Meridionale (GOIM 9602 Study). *Ann Oncol*. 2007;18(8):1354–1358. doi:10.1093/annonc/mdm128
19. Chipponi J, Huguier M, Pezet D, et al. Randomized trial of adjuvant chemotherapy after curative resection for gastric cancer. *Am J Surg*. 2004;187(3):440–445. doi:10.1016/j.amjsurg.2003.12.014
20. Bouché O, Ychou M, Burtin P, et al. Adjuvant chemotherapy with 5-fluorouracil and cisplatin compared with surgery alone for gastric cancer: 7-year results of the FFCD randomized phase III trial (8801). *Ann Oncol*. 2005;16(9):1488–1497. doi:10.1093/annonc/mdi270
21. Nitti D, Wils J, Dos Santos JG, et al. Randomized phase III trials of adjuvant FAMTX or FEMTX compared with surgery alone in resected gastric cancer: A combined analysis of the EORTC GI Group and the ICCG. *Ann Oncol*. 2006;17(2):262–269. doi:10.1093/annonc/mdj077
22. Nakajima T, Kinoshita T, Nashimoto A, et al. Randomized controlled trial of adjuvant uracil–tegafur versus surgery alone for serosa-negative, locally advanced gastric cancer. *Br J Surg*. 2007;94(12):1468–1476. doi:10.1002/bjs.5996
23. Di Costanzo F, Gasperoni S, Manzione L, et al. Adjuvant chemotherapy in completely resected gastric cancer: A randomized phase III trial conducted by GOIRC. *J Natl Cancer Inst*. 2008;100(6):388–398. doi:10.1093/jnci/djn054
24. Smalley SR, Benedetti JK, Haller DG, et al. Updated analysis of SWOG-directed intergroup study 0116: A phase III trial of adjuvant radiochemotherapy versus observation after curative gastric cancer resection. *J Clin Oncol*. 2012;30(19):2327–2333. doi:10.1200/JCO.2011.36.7136

25. Bang YJ, Kim YW, Yang HK, et al. Adjuvant capecitabine and oxaliplatin for gastric cancer after D2 gastrectomy (CLASSIC): A phase 3 open-label, randomized controlled trial. *Lancet*. 2012;379(9813):315–321. doi:10.1016/S0140-6736(11)61873-4
26. Sakuramoto S, Sasako M, Yamaguchi T, et al. Adjuvant chemotherapy for gastric cancer with S-1, an oral fluoropyrimidine. *N Engl J Med*. 2007;357(18):1810–1820. doi:10.1056/NEJMoa072252
27. Bajetta E, Buzzoni R, Mariani L, et al. Adjuvant chemotherapy in gastric cancer: 5-year results of a randomised study by the Italian Trials in Medical Oncology (ITMO) Group. *Ann Oncol*. 2002;13(2):299–307. doi:10.1093/annonc/mdf040
28. Macdonald JS, Smalley SR, Benedetti J, et al. Chemoradiotherapy after surgery compared with surgery alone for adenocarcinoma of the stomach or gastroesophageal junction. *N Engl J Med*. 2001;345:725–730. doi:10.1056/NEJMoa010187
29. Du XH, Liu HL, Li L, et al. Clinical significance of immunotherapy with combined three kinds of cells for operable colorectal cancer. *Tumor Biol*. 2015;36(7):5679–5685. doi:10.1007/s13277-015-3242-4
30. DeVita VT, Rosenberg SA. Two hundred years of cancer research. *N Engl J Med*. 2012;366(23):2207–2214. doi:10.1056/NEJMra1204479
31. Cheever MA, Higano CS. PROVENGE (Sipuleucel-T) in prostate cancer: The first FDA-approved therapeutic cancer vaccine. *Clin Cancer Res*. 2011;17(11):3520–3526. doi:10.1158/1078-0432.CCR-10-3126
32. Zhao H, Fan Y, Li H, et al. Immunotherapy with cytokine-induced killer cells as an adjuvant treatment for advanced gastric carcinoma: A retrospective study of 165 patients. *Cancer Biother Radiopharm*. 2013;28(4):303–309. doi:10.1089/cbr.2012.1306
33. Agolli L. Adjuvant radiochemotherapy for gastric cancer: Should we use prognostic factors to select patients? *World J Gastroenterol*. 2016;22(3):1131–1138. doi:10.3748/wjg.v22.i3.1131
34. Zhou Y, Chen CL, Jiang SW, et al. Retrospective analysis of the efficacy of adjuvant CIK cell therapy in epithelial ovarian cancer patients who received postoperative chemotherapy. *Oncoimmunology*. 2019;8(2):e1528411. doi:10.1080/2162402X.2018.1528411
35. Wang X, Tang S, Cui X, et al. Cytokine-induced killer cell/dendritic cell–cytokine-induced killer cell immunotherapy for the postoperative treatment of gastric cancer: A systematic review and meta-analysis. *Medicine (Baltimore)*. 2018;97(36):e12230. doi:10.1097/MD.00000000000012230
36. Robinson CG, Patel AP, Bradley JD, et al. Postoperative radiotherapy for pathologic N2 non-small-cell lung cancer treated with adjuvant chemotherapy: A review of the National Cancer Data Base. *J Clin Oncol*. 2015;33(8):870–876. doi:10.1200/JCO.2014.58.5380
37. Wang EH, Corso CD, Rutter CE, et al. Postoperative radiation therapy is associated with improved overall survival in incompletely resected stage II and III non-small-cell lung cancer. *J Clin Oncol*. 2015;33(25):2727–2734. doi:10.1200/JCO.2015.61.1517



# Evaluation of the effects of vitamin D deficiency and cigarette smoking on insulin resistance in type 2 diabetes mellitus: A meta-analysis of randomized controlled trials

Nianrong Mi<sup>1,A</sup>, Mingyuan Liu<sup>2,B</sup>, Chao Meng<sup>1,C</sup>, Fangming Fu<sup>1,D–F</sup>

<sup>1</sup> Department of Endocrinology, Central Hospital Affiliated to Shandong First Medical University, Jinan, China

<sup>2</sup> Department of Obstetrics, Jinan Maternity and Child Care Health Hospital, Shandong First Medical University, Jinan, China

A – research concept and design; B – collection and/or assembly of data; C – data analysis and interpretation;

D – writing the article; E – critical revision of the article; F – final approval of the article

Advances in Clinical and Experimental Medicine, ISSN 1899–5276 (print), ISSN 2451–2680 (online)

*Adv Clin Exp Med.* 2024;33(7):679–689

## Address for correspondence

Fangming Fu

E-mail: fufangming71@sina.com

## Funding sources

None declared

## Conflict of interest

None declared

Received on January 13, 2023

Reviewed on May 17, 2023

Accepted on August 22, 2023

Published online on October 30, 2023

## Abstract

There are contradictory findings regarding the effects of vitamin D supplementation and cigarette smoking on glucose metabolism in individuals with type 2 diabetes mellitus (T2DM). Consequently, this meta-analysis focused on the association between vitamin D interventions and smoking cessation on glycemic control in T2DM patients. This study adhered to the Preferred Reporting Items for Systematic Reviews and Meta-Analyses (PRISMA) guidelines. Cochrane Library, EMBASE and PubMed databases were used for a language-inclusive literature search until November 2022. The primary outcomes of this meta-analysis were changes in glycated hemoglobin (HbA1c) level, vitamin D concentration and body mass index (BMI) values. This meta-analysis included 14 randomized controlled trials (RCTs) with a total of 23,289 individuals with T2DM. Nine RCTs were related to vitamin D supplementation interventions, and 5 RCTs were related to smoking cessation interventions. The studies on vitamin D supplementation showed a substantial change in the intervention group, with a risk ratio (RR) of 0.72 (95% confidence interval (95% CI): 0.58, 0.88;  $p = 0.001$ ) and an odds ratio (OR) of 0.52 (95% CI: 0.34, 0.78;  $p = 0.002$ ); high heterogeneity was observed ( $I^2 \geq 95\%$ ). Similarly, the smoking cessation studies showed a substantial change in the intervention group, with a RR of 0.92 (95% CI: 0.86, 0.99;  $p = 0.04$ ) and an OR of 0.86 (95% CI: 0.74, 0.99;  $p = 0.04$ ); high heterogeneity was observed ( $I^2 = 87\%$ ). In conclusion, both vitamin D supplementation and smoking cessation are associated with moderate BMI decline and an improvement of insulin sensitivity in people with T2DM.

**Key words:** glycemic index, smoking, type 2 diabetes mellitus, vitamin D deficiency, homeostatic model assessment of insulin resistance (HOMA-IR)

## Cite as

Mi N, Liu M, Meng C, Fu F. Evaluation of the effects of vitamin D deficiency and cigarette smoking on insulin resistance in type 2 diabetes mellitus: A meta-analysis of randomized controlled trials. *Adv Clin Exp Med.* 2024;33(7):679–689. doi:10.17219/acem/171451

## DOI

10.17219/acem/171451

## Copyright

Copyright by Author(s)

This is an article distributed under the terms of the Creative Commons Attribution 3.0 Unported (CC BY 3.0) (<https://creativecommons.org/licenses/by/3.0/>)

## Introduction

Type 2 diabetes mellitus (T2DM) is a worldwide public health concern.<sup>1</sup> Globally, 597 million individuals were suffering from T2DM by the year 2021.<sup>2</sup> It is well documented that T2DM is a substantial risk factor for premature death and complications such as blindness, stroke, heart attack, amputation, and kidney failure.<sup>3,4</sup> Type 2 diabetes mellitus is a chronic metabolic condition characterized by relative insulin deficiency, insulin resistance and elevated blood glucose levels.<sup>5</sup> Vitamin D supplementation dramatically improves peripheral insulin sensitivity and beta-cell function in people with T2DM who were recently diagnosed or are at high risk of developing the disease, by directly promoting pancreatic insulin production. Vitamin D acts through nuclear vitamin D receptors, since a particular receptor for vitamin D was found in the human insulin gene promoters (between 761 and 732 base pairs), which allowed it to control insulin expression.<sup>6</sup> Considerable research has explored the relationship between circulating vitamin D concentrations and T2DM risk over the past few decades and has identified a high correlation between the two variables, but the results remain contradictory. For instance, Li et al.,<sup>7</sup> Hu et al.<sup>8</sup> and Łagowska et al.<sup>9</sup> reported in their systematic reviews and meta-analyses that vitamin D supplementation improves the insulin sensitivity of target cells (liver, skeletal muscle and adipose tissue) and, consequently, improves beta-cell function, glycated hemoglobin (HbA1c) level, insulin resistance, and homeostatic model assessment of insulin resistance (HOMA-IR) scores in T2DM patients. In contrast, Jamka et al.<sup>10</sup> and Al Thani et al.<sup>11</sup> showed that vitamin D supplementation had no effect on glucose tolerance or insulin sensitivity.

Similarly, many studies have demonstrated that cigarette smoking increases the risk of vascular problems in T2DM patients and diabetes incidence in the general population.<sup>12</sup> Smoking can influence glucose homeostasis by raising insulin resistance, lowering insulin production, or affecting pancreatic beta-cell function, and is linked to poor glycemic control in T2DM patients.<sup>13</sup> Cigarette smoking and nicotine exposure, for instance, reduce the efficiency of pancreatic cells, leading to elevated insulin resistance in T2DM patients, as documented in a review paper by Maddatu et al.<sup>14</sup> Contrary to this, Wang et al.<sup>15</sup> found that smoking is negatively associated with insulin resistance in T2DM, likely due to increased weight gain upon nicotine withdrawal.

Since the available randomized controlled trials (RCTs) showed contradictory results, the present meta-analysis of RCTs investigates the influence of vitamin D and smoking on insulin resistance in T2DM patients.

## Objectives

The aim of this meta-analysis was to assess the impact of vitamin D deficiency and cigarette smoking on insulin resistance in individuals with T2DM.

## Materials and methods

This meta-analysis was undertaken following the Preferred Reporting Items for Systematic Reviews and Meta-Analyses (PRISMA) guidelines.

### Data sources and literature search

An inclusive literature search was conducted without any restrictions on the year and language of publication using electronic databases, namely Cochrane Library, EMBASE and PubMed, up to November 2022. In addition, the bibliographies of relevant studies and meta-analyses were searched. The search strategy involved combinations of the following keywords: “type 2 diabetes mellitus”, “T2DM”, “insulin resistance”, “vitamin-D deficiency”, “vitamin-D supplementation”, “cigarette smoking”, “cessation of smoking”, “HbA1c”, “glycated hemoglobin”, “glycaemic index”, “meta-analysis”, and “systematic review”. Duplicate papers were deleted from the search results, followed by a title and abstract screening of the remaining articles. Finally, the full texts of the eligible studies were retrieved and reviewed, based on the inclusion and exclusion criteria.

### Study selection

The literature search was conducted separately by 2 authors. In the event of disputes, a consensus was obtained through discussion. The following conditions had to be met for a study to be eligible for the meta-analysis: (A) RCTs examining the effects of vitamin D deficiency on insulin resistance in T2DM; (B) RCTs examining the effects of cigarette smoking on insulin resistance in T2DM; and (C) studies evaluating the following outcomes: changes in vitamin D levels, HbA1c levels and body mass index (BMI) values. The exclusion criteria included clinical trials with a follow-up time of less than 1 month. Studies that were conducted on healthy volunteers or on those who suffered from type 1 diabetes mellitus were excluded from the study. Lastly, studies that compared factors other than vitamin D deficiency and cigarette smoking were not included in this meta-analysis.

### Data extraction

A computerized data extraction form was developed in Microsoft Excel (Microsoft Corp., Redmond, USA) and utilized for the purpose of documenting the essential information of the studies<sup>16–29</sup> selected for the meta-analysis. This included the first author's name, the year of publication, the intervention, the sample size in each group, the follow-up duration, and the study outcomes. Two different authors independently extracted the data, and their results were compared. In the case of divergent opinions, an agreement was obtained via discussion. Depending on the circumstances, a third author was also included.

## Quality assessment

The Cochrane Risk of Bias tool (Cochrane, London, UK) was applied in order to evaluate the methodological validity of each study that was incorporated into the meta-analysis. During the process of data extraction, selected articles were given a score, and RevMan v. 5.4.0<sup>30</sup> (Cochrane) was used to construct a quality evaluation graph.

## Data analysis

RevMan v. 5.4.0 and MedCalc software<sup>31</sup> were used throughout the procedure of data processing. The Mantel–Haenszel approach with the random-effects model<sup>29</sup> was utilized in order to calculate the pooled risk ratio (RR) and the 95% confidence interval (95% CI) for each of the 2 outcomes. A result was considered statistically significant if its p-value was less than 0.05.<sup>32,33</sup> The RCTs that did not have any outcome events recorded in the investigation groups were excluded from the analysis of a particular outcome event because they did not contribute to the RR. Forest plots<sup>34</sup> were used to visually represent the RRs and the 95% CIs. The I<sup>2</sup> statistics were used to assess the level of heterogeneity present in the results.<sup>35</sup>

## Results

### Literature search results

Figure 1 depicts the PRISMA chart for the study selection process. A total of 567 studies were retrieved through a comprehensive search of online databases. After eliminating duplicates, the abstracts and titles of 384 studies were screened. Only 120 studies qualified for full-text evaluation. Fourteen publications were ultimately included based on the PICOS criteria<sup>36</sup> presented in Table 1. The characteristics of all included trials are displayed in Table 2. The included studies evaluated the effectiveness of vitamin D supplementation and smoking cessation on glycemic index, HbA1c level and insulin sensitivity in individuals with T2DM. In all the included investigations, the median follow-up time ranged from 3 to 36 months.

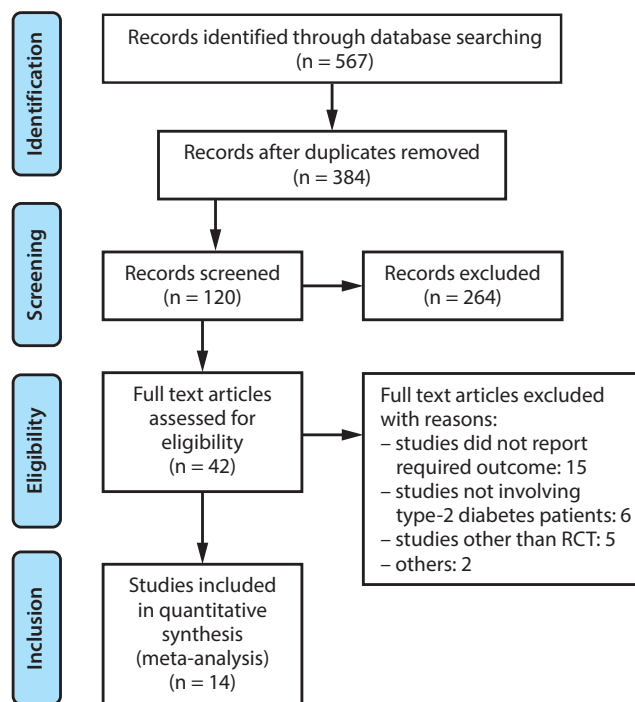


Fig. 1. Preferred Reporting Items for Systematic Reviews and Meta-Analyses (PRISMA) flowchart of study selection

RCT – randomized controlled trial.

### Risk of bias and publication bias

The quality of the included studies was assessed, as shown in Table 3. Figure 2 depicts a summary of the risk of bias, and Fig. 3 presents a risk of bias graph. Ten of the 14 included studies had a low risk of bias, whereas 3 studies had a moderate risk attributable to selective reporting or reporting bias. One study showed a high risk of performance bias. Figure 4A depicts the funnel plot for studies related to the effect of vitamin D supplementation, which indicates a low probability of publication bias, with a significant p-value of 0.394 (Begg’s test). Figure 4B depicts the funnel plot for studies related to the effect of cigarette smoking, which indicated a low probability of publication bias, with a significant p-value of 0.252 (Begg’s test).<sup>37</sup>

Table 1. PICOS search

PICOS criteria	Description
P (patient, problem, population)	people with T2DM
I (intervention)	the effect of vitamin D deficiency and cigarette smoking on people with T2DM
C (comparison, control or comparator)	vitamin D deficiency compared to vitamin D supplements smoking compared to smoking cessation
O (outcome (s))	the use of vitamin D supplements and smoking cessation have positive impacts on the glycemic index of people with T2DM
S (study type)	randomized controlled trials

T2DM – type 2 diabetes mellitus.

Author (Year)	Random sequence generation (selection bias)	Allocation concealment (selection bias)	Blinding of participants and personnel (performance bias)	Blinding of outcome assessment (detection bias)	Incomplete outcome data (attrition bias)	Selective reporting (reporting bias)	Other bias
Bunary et al 2017 [16]	+	+	+	+	+	+	+
Cho et al 2022 [25]	+	+	+	+	+	+	+
Cojic et al 2021 [17]	+	+	+	+	+	+	+
Gu et al 2022 [18]	+	+	+	+	+	+	+
Kawahara et al 2022 [19]	+	+	+	+	+	+	+
Kayaniyi et al 2010 [20]	+	+	+	+	+	+	+
Lemieux et al 2019 [21]	+	+	+	+	+	+	+
Molla et al 2020 [26]	+	+	+	+	+	+	+
Ohkuma et al 2015 [27]	+	+	+	+	+	+	+
Pittas et al 2020 [22]	+	+	+	+	+	+	+
Rad et al 2014 [23]	+	+	+	+	+	+	+
Sia et al 2022 [28]	+	+	+	+	+	+	+
Stadler et al 2014 [29]	+	+	+	+	+	+	+
Tahaee et al 2013 [24]	+	+	+	+	+	+	+

Fig. 2. Risk of bias summary

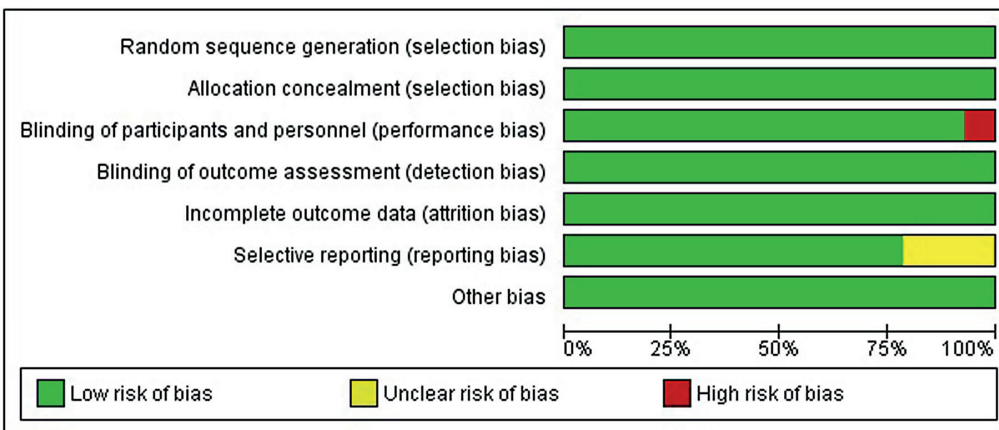


Fig. 3. Risk of bias graph

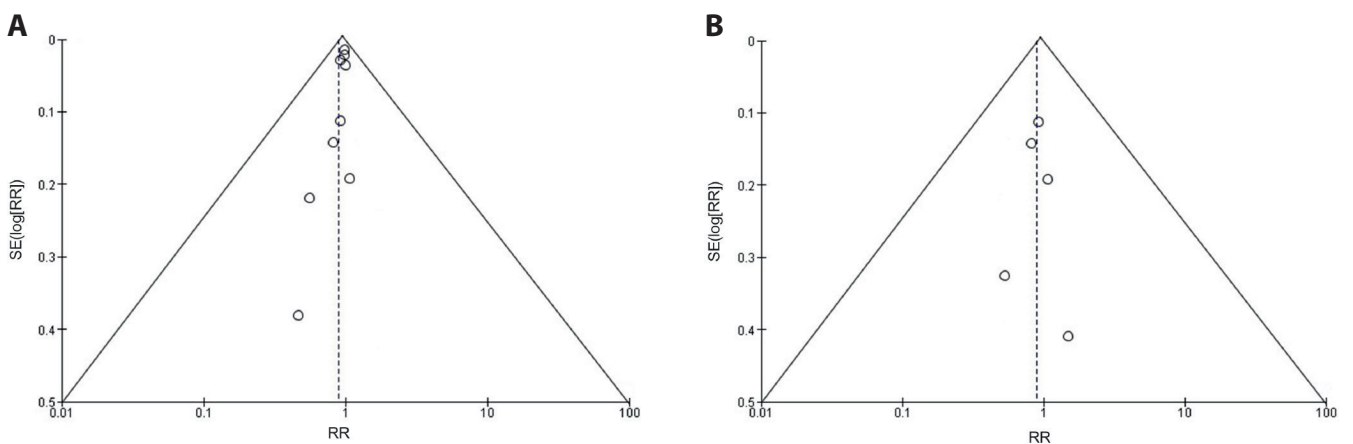


Fig. 4. A. Funnel plots for studies evaluating the effect of vitamin D supplementation on insulin resistance; B. Funnel plots for studies evaluating the effect of cigarette smoking on insulin resistance

RR – risk ratio; SE – standard error.

**Table 2.** Brief summary of the included studies evaluating the effect of vitamin D supplementation on type 2 diabetes mellitus (T2DM)

Study ID	Year	Journal of publication	Type of study	Follow-up	Intervention	Number of patients	Age of patients [years]	Gender M/F	Primary outcome	Conclusion
Buhary et al. <sup>16</sup>	2017	Journal of Clinical Medicine Research	randomized controlled trial	9 months	association of Hb1Ac levels with vitamin D supplementation	1000	20–65	397/603	BMI, change in vitamin D concentration, change in Hb1Ac level	There is a significant inverse association between serum 25(OH)D and HbA1c.
Cojic et al. <sup>17</sup>	2021	Frontiers in Endocrinology	randomized controlled trial	6 months	effect of vitamin D supplementation on patients with T2DM	130	50–70	94/36	BMI, change in vitamin D concentration, change in Hb1Ac level	Oral daily doses of vitamin D reduce the levels of HbA1c over a 6-month period.
Gu et al. <sup>18</sup>	2022	Journal of Clinical Laboratory Analysis	randomized controlled trial	3 months	effect of vitamin D supplementation on patients with T2DM	172	>18	102/70	BMI, change in vitamin D concentration, change in Hb1Ac level	Vitamin D supplementation has important beneficial effects in T2DM patients.
Kawahara et al. <sup>19</sup>	2022	The BMJ	randomized controlled trial	3 years	effect of vitamin D supplementation on glucose control and insulin resistance in patients with T2DM	1256	50–70	742/571	BMI, change in vitamin D concentration, change in Hb1Ac level	Vitamin D has potential beneficial effects in patients with insufficient insulin secretion.
Kayaniyl et al. <sup>20</sup>	2010	Diabetes Care	randomized controlled trial	2 years	association of vitamin D with insulin resistance in subjects with T2DM	712	40–60	462/498	BMI, change in vitamin D concentration, change in Hb1Ac level	Vitamin D has beneficial effects in patients with T2DM.
Lemieux et al. <sup>21</sup>	2019	European Journal of Endocrinology	randomized controlled trial	6 months	effect of vitamin D supplementation on insulin sensitivity and secretion	96	50–70	57/39	BMI, change in vitamin D concentration, change in Hb1Ac level	Vitamin D supplementation over a 6-month period significantly increased the peripheral insulin sensitivity and $\beta$ -cell function in T2DM patients.
Pittas et al. <sup>22</sup>	2020	New England Journal of Medicine	randomized controlled trial	2.5 years	effect of vitamin D supplementation on T2DM	2423	50–70	1337/1086	BMI, change in vitamin D concentration, change in Hb1Ac level	Vitamin D supplementation has important beneficial effects in T2DM patients.
Yousefi Rad et al. <sup>23</sup>	2014	Iranian Journal of Public Health	randomized controlled trial	2 months	effect of vitamin D supplementation on glucose control and insulin resistance in patients with T2DM	58	30–60	12/36	BMI, change in vitamin D concentration, change in Hb1Ac level	Vitamin D supplementation has beneficial effects on glucose homeostasis and can increase insulin sensitivity in T2DM patients.
Talaei et al. <sup>24</sup>	2013	Diabetology & Metabolic Syndrome	randomized controlled trial	2 months	effect of vitamin D supplementation on insulin resistance in patients with T2DM	100	30–70	30/70	BMI, change in vitamin D concentration, change in Hb1Ac level	Vitamin D supplementation could reduce insulin resistance in T2DM.
Cho et al. <sup>25</sup>	2022	Scientific Reports	randomized controlled trial	1 year	effect of short-term smoking on increasing the risk of insulin resistance	4043	19–70	2067/1976	change in HbA1c level, BMI	Smoking cessation may protect against insulin resistance.
Molla et al. <sup>26</sup>	2020	Canadian Journal of Diabetes	randomized controlled trial	6 months	effect of smoking on diabetes control in adults with T2DM	8278	>18	5036/3242	change in HbA1c level, BMI	Smoking prevention and cessation are beneficial for diabetes control.
Ohkuma et al. <sup>27</sup>	2015	PLOS One	randomized controlled trial	1 year	association of smoking and its cessation with insulin resistance in patients with T2DM	2490	>20	2490	change in HbA1c level, BMI	Smoking cessation has positive effects on glycemic control in patients with T2DM.
Sia et al. <sup>28</sup>	2022	Annals of Medicine	randomized controlled trial	1 year	association between smoking and glycemic control in men with T2DM	3044	>30	3044	change in HbA1c level, BMI	Smoking has unfavorable effects on glycemic control in men with T2DM.
Stadler et al. <sup>29</sup>	2014	European Journal of Endocrinology	randomized controlled trial	6 months	effect of smoking cessation on beta-cell function and insulin resistance in patients with T2DM	27	27–30	18/9	change in HbA1c level, BMI	Smoking cessation has positive outcomes on diabetes control.

HbA1c – glycated hemoglobin; BMI – body mass index.

## Efficacy outcomes

### Effect of vitamin D deficiency on insulin resistance

The 14 studies evaluated in this meta-analysis included a total of 23,289 individuals with T2DM. Among these, 9 studies provided information on the effect of vitamin D deficiency on insulin resistance in people with T2DM. Table 4 displays a detailed comparison of the intervention and control groups with respect to the main outcome, comparative BMI values, and changes in HbA1c and vitamin D levels due to vitamin D supplementation. The values presented in Fig. 5 show a substantial change in the intervention group, with a RR of 0.72 (95% CI: 0.58, 0.88;  $p = 0.001$ ), high heterogeneity value for risk ratio of 95%, an odds ratio (OR) of 0.52 (95% CI: 0.34, 0.78;  $p = 0.002$ ), and high heterogeneity value for odds ratio of 96%.

### Effect of smoking cessation on glycemic index

The remaining 5 studies provided information on the effect of cigarette smoking on glycemic index in people with T2DM. Table 5 displays a detailed comparison of the intervention and control groups with respect to the main outcomes, BMI of the control (non-smokers) and smoker

groups, and changes in HbA1c level due to smoking cessation. As in the case of vitamin D supplementation, the meta-analysis data show a substantial change in the intervention group, with a RR of 0.92 (95% CI: 0.86, 0.99;  $p = 0.04$ ) and an OR of 0.86 (95% CI: 0.74, 0.99;  $p = 0.04$ ); there was high heterogeneity of 87% (Fig. 6).

Risk ratio values and OR values lower than 1 indicate a high likelihood of the positive effect of vitamin D supplementation and smoking cessation on improving the glycemic index (HbA1c level) and insulin sensitivity in individuals with T2DM. High heterogeneity was detected among the pooled studies ( $I^2 > 85\%$ ).

Figure 7 presents a comparison of BMI for the control and vitamin D supplementation groups and the control (non-smoker) and smoker groups. Vitamin D supplementation reduces BMI values, while smoking increases BMI and obesity when compared to the control group.

## Discussion

In this meta-analysis designed to investigate the glycemic control outcomes in persons with T2DM, we discovered that vitamin D supplementation and smoking cessation decreased plasma HbA1c and insulin resistance.

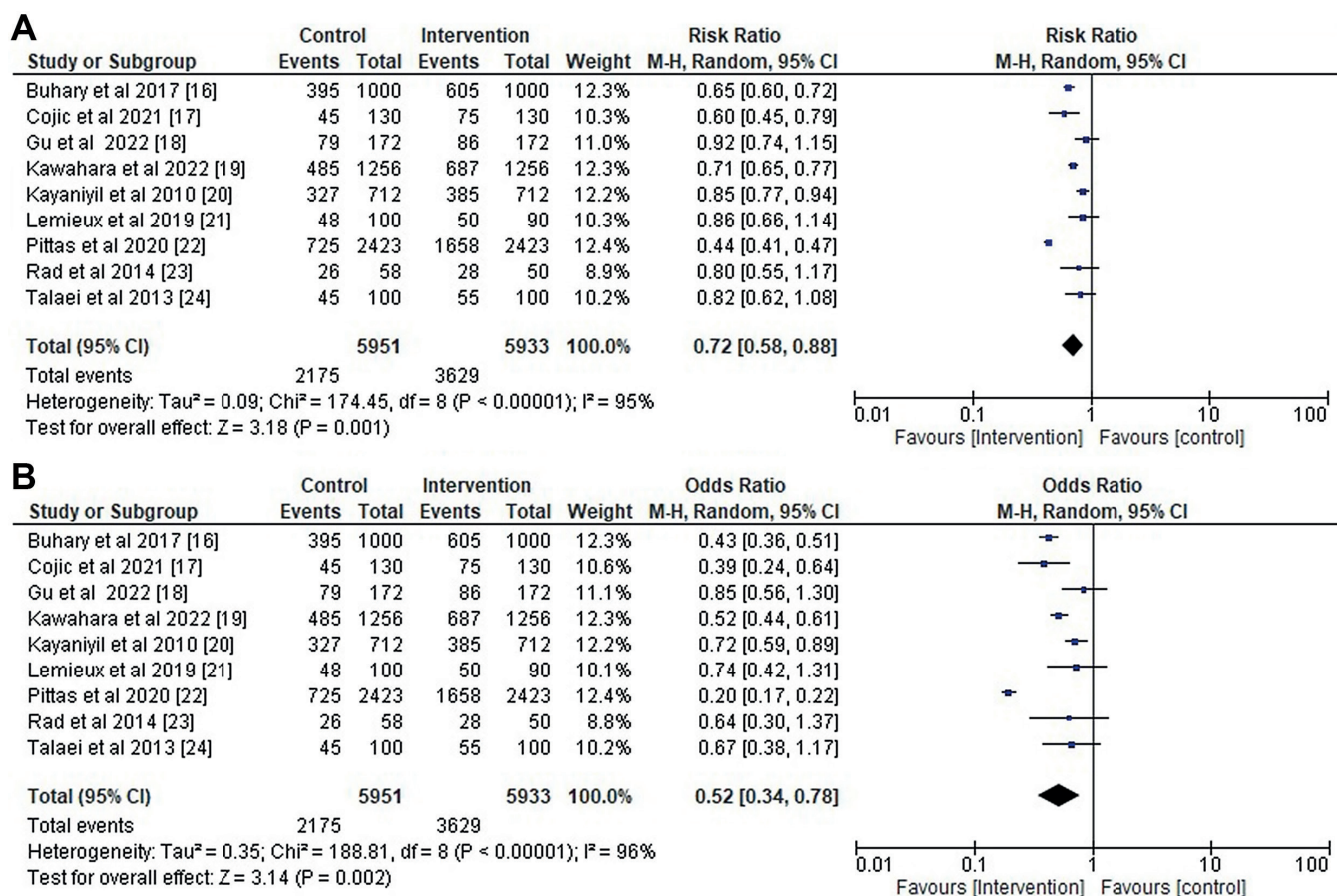


Fig. 5. Forest plot for the primary outcome. A. Risk ratio; B. Odds ratio of vitamin-D supplementation on insulin resistance

95% CI – 95% confidence interval; df – degrees of freedom.

**Table 3.** Risk assessment for the included studies

Study ID and year	Buhary et al. <sup>16</sup>	Cojic et al. <sup>17</sup>	Gu et al. <sup>18</sup>	Kawahara et al. <sup>19</sup>	Kayaniyl et al. <sup>20</sup>	Lemieux et al. <sup>21</sup>	Pittas et al. <sup>22</sup>	Yousefi Rad et al. <sup>23</sup>	Talaei et al. <sup>24</sup>	Cho et al. <sup>25</sup>	Molla et al. <sup>26</sup>	Ohkuma et al. <sup>27</sup>	Sia et al. <sup>28</sup>	Stadler et al. <sup>29</sup>
Did the study avoid inappropriate exclusions?	Y	Y	Y	Y	Y	Y	Y	Y	Y	Y	Y	Y	Y	Y
Did all patients receive the same reference standard?	Y	Y	Y	Y	Y	Y	Y	Y	Y	Y	Y	Y	Y	Y
Were all patients included in the analysis?	N	N	N	N	N	N	N	N	N	N	N	N	N	N
Was the sample frame appropriate to address the target population?	Y	Y	Y	Y	Y	Y	Y	Y	Y	Y	Y	Y	Y	Y
Were study participants sampled in an appropriate way?	Y	Y	Y	Y	Y	Y	Y	Y	Y	Y	Y	Y	Y	Y
Were the study subjects and the setting described in detail?	Y	Y	Y	Y	Y	Y	Y	Y	Y	Y	Y	Y	Y	Y
Were valid methods used for the identification of the condition?	Y	Y	Y	Y	Y	Y	Y	Y	Y	Y	Y	Y	Y	Y
Was the condition measured in a standard, reliable way for all participants?	Y	Y	Y	Y	Y	Y	Y	Y	Y	Y	Y	Y	Y	Y

**Table 4.** Primary outcomes of vitamin D supplementation in type 2 diabetes mellitus (T2DM)

Study ID	Effect of vitamin D deficiency	Dose of vitamin D3 supplementation	Duration of intervention	BMI [kg/m <sup>2</sup> ]		Change in vitamin D concentration in the intervention group			Change in Hb1Ac level in the intervention group		
				control group	intervention group	pre-treatment [ng/mL]	post-treatment [ng/mL]	p-value	pre-treatment (%)	post-treatment (%)	p-value
Buhary et al. <sup>16</sup>	affects insulin secretion and insulin sensitivity	4000 IU	9 months	32.65 ±5.6	25.79 ±4.7	40.09 ±23.13	80.5 ±29.77	0.0001	10.55 ±2.58	7.70 ±1.61	0.0001
Cojic et al. <sup>17</sup>	affects insulin action	3000 IU	6 months	30.13 ±4.6	29.79 ±5.0	48.79 ±31.63	92.24 ±20.25	0.0001	6.56 ±1.0	6.32 ±0.69	0.025
Gu et al. <sup>18</sup>	affects insulin secretion and insulin sensitivity	3000 IU	3 months	29.83 ±0.64	25.7 ±0.73	19.50 ±9.29	56.55 ±17.76	0.0001	7.0 ±0.23	6.44 ±0.24	0.0001
Kawahara et al. <sup>19</sup>	impaired glucose tolerance	4000 IU	3 years	24.5 ±1.8	24.1 ±2.7	21.0 ±6.2	47.7 ±22.2	0.0001	6.5 ±0.1	5.9 ±0.2	0.0001
Kayaniyl et al. <sup>20</sup>	affects insulin action	4000 IU	2 years	30.05 ±3.7	22.5 ±1.4	26.3 ±11.0	55.81 ±22.90	0.0001	7.14 ±0.1	6.1 ±0.2	0.0001
Lemieux et al. <sup>21</sup>	affects insulin secretion and insulin sensitivity	5000 IU	6 months	32.2 ±4.3	32.1 ±3.9	48.5 ±13.0	79.1 ±11.0	0.0001	6.94 ±0.2	5.6 ±0.1	0.0001
Pittas et al. <sup>22</sup>	impaired glucose tolerance	4000 IU	2.5 years	32.1 ±4.4	32.0 ±4.5	27.7 ±10.2	54.3 ±11.5	0.0001	6.85 ±0.1	5.9 ±0.2	0.0001
Yousefi Rad et al. <sup>23</sup>	affects insulin action	4000 IU	3 months	28.75 ±0.95	27.94 ±0.92	15.55 ±1.91	27.50 ±2.04	0.0001	7.29 ±0.22	6.76 ±0.18	0.0001
Talaei et al. <sup>24</sup>	affects insulin secretion and insulin sensitivity	5000 IU	2 months	31.3 ±4.3	30 ±2.8	43.03 ±19.28	58.52 ±22.22	0.0001	7.02 ±0.33	6.84 ±0.15	0.0001

HbA1c – glycated hemoglobin; BMI – body mass index.

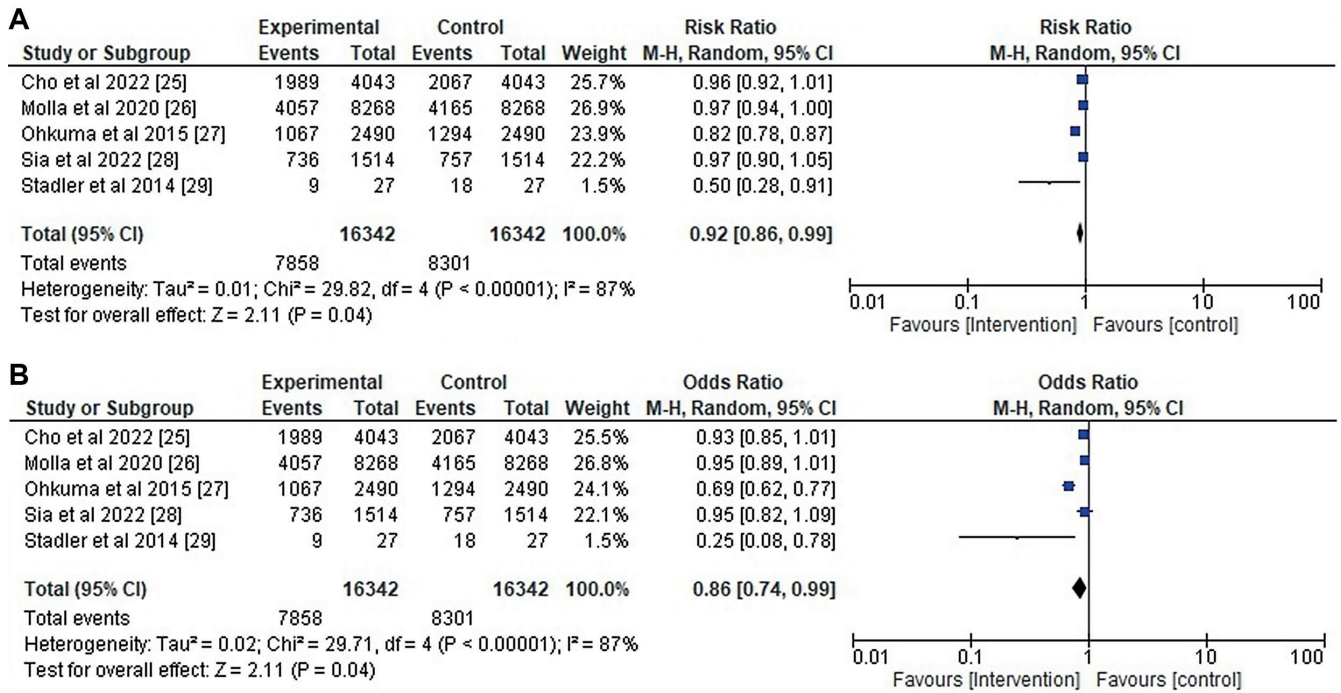


Fig. 6. Forest plot for the primary outcome. A. Risk ratio; B. Odds ratio of smoking effects on insulin resistance

95% CI – 95% confidence interval; df – degrees of freedom.

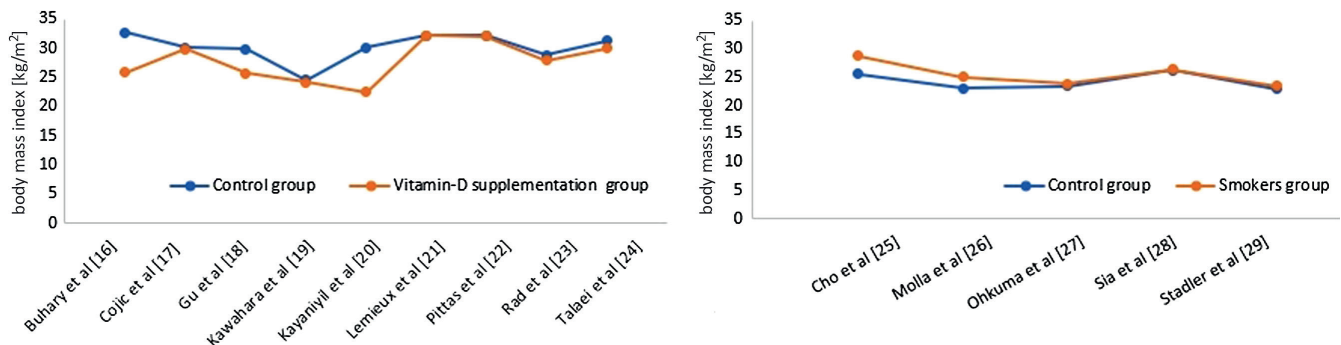


Fig. 7. Comparison of body mass index (BMI) in the control group with the intervention group

Table 5. Primary outcomes of cigarette smoking in type 2 diabetes mellitus (T2DM)

Study ID	Effect of cigarette smoking	Duration of intervention	BMI [kg/m <sup>2</sup> ]		Hb1Ac level		p-value
			control group	intervention group	control group (%)	intervention group (%)	
Cho et al. <sup>25</sup>	insulin resistance	1 year	25.6 ± 1.6	28.7 ± 2.5	6.21 ± 0.23	7.02 ± 0.17	0.0001
Molla et al. <sup>26</sup>	insulin resistance	6 months	23 ± 2.1	25 ± 1.5	8.39 ± 2.25	7.75 ± 3.43	0.0001
Ohkuma et al. <sup>27</sup>	insulin resistance	1 year	23.4 ± 3.4	23.8 ± 3.6	7.27 ± 0.04	7.47 ± 0.04	0.0001
Sia et al. <sup>28</sup>	insulin resistance	1 year	26.2 ± 4.2	26.3 ± 4.0	9.5 ± 2.8	9.0 ± 2.7	0.0001
Stadler et al. <sup>29</sup>	insulin resistance	6 months	22.9 ± 0.6	23.4 ± 0.8	4.9 ± 0.1	5.0 ± 0.1	0.0006

HbA1c – glycated hemoglobin; BMI – body mass index.

Additionally, we observed that vitamin D supplementation lowered BMI compared to the control group, which is consistent with the findings of other studies,<sup>38,39</sup> showing that vitamin D-deficient individuals have a higher BMI but experience a decrease in BMI after taking a reasonable

amount of vitamin D supplements. Similar to other studies<sup>40,41</sup> that demonstrated that smoking increases BMI and obesity, our research revealed that smoking raises BMI in comparison to the control group. Hemoglobin undergoes constant, gradual, non-enzymatic glycosylation due



to hyperglycemia.<sup>42</sup> The UK Prospective Diabetes Study established that HbA1c is the gold standard for assessing glycemic control in diabetes management.<sup>43</sup> George et al.<sup>44</sup> conducted a meta-analysis to assess the influence of vitamin D on glycemic management and insulin resistance. The authors reported a slight reduction in fasting blood glucose and insulin resistance, but no improvement in HbA1c levels. We found that vitamin D treatment decreased the elevated plasma HbA1c levels, indicating that vitamin D is advantageous for preventing or delaying the onset of diabetic complications. These disparate outcomes may be the result of our inclusion of a higher number of recent investigations. There was a substantial positive link between HOMA-IR and the development of T2DM. The HOMA-IR is an important factor in the onset of diabetes.<sup>45,46</sup> Insulin resistance is defined as a decreased sensitivity of insulin target tissues to insulin, and the majority of T2DM patients have mixed insulin resistance.<sup>47</sup> Frequently, blood glucose concentration and insulin secretion are indirect indicators of insulin sensitivity. In T2DM patients, the blood glucose has not been well managed, which triggered  $\beta$ -cells to produce even more insulin.<sup>48,49</sup> In the vitamin D treatment group, insulin and HOMA-IR values significantly decreased. Insulin secretion is a calcium-dependent mechanism. Vitamin D activates L-type calcium channels on islet beta cells, which modulate calcium levels, initiate insulin signaling and stimulate insulin release.<sup>50</sup> Vitamin D deficiency can be accompanied by a drop in plasma calcium concentration, which in turn induces a secondary increase in calcium levels, altering insulin signal transduction, interfering with insulin release and disturbing islet beta-cell function.<sup>51</sup> Therefore, the present study further validates these results and demonstrates that vitamin D supplementation improves insulin resistance in individuals with T2DM in the short term.

Smoking is associated with the early onset of microvascular disorders and may contribute to the pathogenesis of T2DM.<sup>52,53</sup> Both the transition from normal glycemia to impaired glucose tolerance and the increased risk of developing diabetes are predicted by smoking.<sup>54,55</sup> According to the studies by Akter et al.<sup>56</sup> and Campagna et al.,<sup>57</sup> smoking cessation can reduce the risk of macrovascular problems and significantly improve the glycemic index. This meta-analysis demonstrated a substantial association between smoking cessation and a drop in HbA1c level as well as an improvement in glycemic index, similar to the previous findings.

## Limitations

This study has a number of limitations. Even though it was completed with the recommended methodological rigor, its results are limited by the availability of only 14 RCTs with moderate to high heterogeneity. In addition, few long-term follow-up studies were included, and


the effects of vitamin D supplementation and smoking cessation on insulin secretion were not considered. Even if the heterogeneity of the literature was avoided, heterogeneity was still present due to the dose variability of vitamin D intake in the included studies and variable smoking cessation periods. In addition, the RR values were generally applied to establish the association between the two parameters, which may introduce bias when comparing the outcomes of RCTs of varied durations.


## Conclusions


In conclusion, both vitamin D supplementation and smoking cessation are associated with a moderate decline in BMI and an improvement in insulin sensitivity in people with T2DM.

### ORCID iDs

Nianrong Mi  <https://orcid.org/0009-0007-6947-3200>

Mingyuan Liu  <https://orcid.org/0000-0003-3499-89>

Chao Meng  <https://orcid.org/0009-0001-0352-63>

Fangming Fu  <https://orcid.org/0000-0003-1739-0327>

### References

1. Tinajero MG, Malik VS. An update on the epidemiology of type 2 diabetes. *Endocrinol Metab Clin North Am.* 2021;50(3):337–355. doi:10.1016/j.ecl.2021.05.013
2. Kotwas A, Karakiewicz B, Zabielska P, Wieder-Huszla S, Jurczak A. Epidemiological factors for type 2 diabetes mellitus: Evidence from the Global Burden of Disease. *Arch Public Health.* 2021;79(1):110. doi:10.1186/s13690-021-00632-1
3. Deshpande AD, Harris-Hayes M, Schootman M. Epidemiology of diabetes and diabetes-related complications. *Phys Ther.* 2008;88(11):1254–1264. doi:10.2522/ptj.20080020
4. Rossboth S, Lechleitner M, Oberaigner W. Risk factors for diabetic foot complications in type 2 diabetes: A systematic review. *Endocrinol Diab Metab.* 2021;4(1):e00175. doi:10.1002/edm2.175
5. Galicia-Garcia U, Benito-Vicente A, Jebari S, et al. Pathophysiology of type 2 diabetes mellitus. *Int J Mol Sci.* 2020;21(17):6275. doi:10.3390/ijms21176275
6. Yaribeygi H, Maleki M, Sathyapalan T, et al. The molecular mechanisms by which vitamin D improve glucose homeostasis: A mechanistic review. *Life Sci.* 2020;244:117305. doi:10.1016/j.lfs.2020.117305
7. Li X, Liu Y, Zheng Y, Wang P, Zhang Y. The effect of vitamin D supplementation on glycemic control in type 2 diabetes patients: A systematic review and meta-analysis. *Nutrients.* 2018;10(3):375. doi:10.3390/nu10030375
8. Hu Z, Chen J, Sun X, Wang L, Wang A. Efficacy of vitamin D supplementation on glycemic control in type 2 diabetes patients: A meta-analysis of interventional studies. *Medicine (Baltimore).* 2019;98(14):e14970. doi:10.1097/MD.00000000000014970
9. Łagowska K, Bajerska J, Jamka M. The role of vitamin D oral supplementation in insulin resistance in women with polycystic ovary syndrome: A systematic review and meta-analysis of randomized controlled trials. *Nutrients.* 2018;10(11):1637. doi:10.3390/nu10111637
10. Jamka M, Woźniewicz M, Jeszka J, Mardas M, Bogdański P, Stelmach-Mardas M. The effect of vitamin D supplementation on insulin and glucose metabolism in overweight and obese individuals: Systematic review with meta-analysis. *Sci Rep.* 2015;5(1):16142. doi:10.1038/srep16142
11. Al Thani M, Sadoun E, Sofroniou A, et al. The effect of vitamin D supplementation on the glycemic control of pre-diabetic Qatari patients in a randomized control trial. *BMC Nutr.* 2019;5(1):46. doi:10.1186/s40795-019-0311-x
12. Xie X tao, Liu Q, Wu J, Wakui M. Impact of cigarette smoking in type 2 diabetes development. *Acta Pharmacol Sin.* 2009;30(6):784–787. doi:10.1038/aps.2009.49

13. Oba S, Suzuki E, Yamamoto M, Horikawa Y, Nagata C, Takeda J. Active and passive exposure to tobacco smoke in relation to insulin sensitivity and pancreatic  $\beta$ -cell function in Japanese subjects. *Diabetes Metab.* 2015;41(2):160–167. doi:10.1016/j.diabet.2014.09.002
14. Maddatu J, Anderson-Baucum E, Evans-Molina C. Smoking and the risk of type 2 diabetes. *Transl Res.* 2017;184:101–107. doi:10.1016/j.trsl.2017.02.004
15. Wang S, Chen J, Wang Y, et al. Cigarette smoking is negatively associated with the prevalence of type 2 diabetes in middle-aged men with normal weight but positively associated with stroke in men. *J Diabetes Res.* 2019;2019:1853018. doi:10.1155/2019/1853018
16. Buhary BM, Almohareb O, Aljohani N, et al. Association of glycosylated hemoglobin levels with vitamin D status. *J Clin Med Res.* 2017;9(12):1013–1018. doi:10.14740/jocmr3227w
17. Cojic M, Kocic R, Klisic A, Kocic G. The effects of vitamin D supplementation on metabolic and oxidative stress markers in patients with type 2 diabetes: A 6-month follow up randomized controlled study. *Front Endocrinol (Lausanne).* 2021;12:610893. doi:10.3389/fendo.2021.610893
18. Gu J, Wu Y, Huang W, et al. Effect of vitamin D on oxidative stress and serum inflammatory factors in the patients with type 2 diabetes. *Clin Lab Anal.* 2022;36(5):e24430. doi:10.1002/jcla.24430
19. Kawahara T, Suzuki G, Mizuno S, et al. Effect of active vitamin D treatment on development of type 2 diabetes: DPVD randomised controlled trial in Japanese population. *BMJ.* 2022;377:e066222. doi:10.1136/bmj-2021-066222
20. Kayaniyl S, Vieth R, Retnakaran R, et al. Association of vitamin D with insulin resistance and  $\beta$ -cell dysfunction in subjects at risk for type 2 diabetes. *Diabetes Care.* 2010;33(6):1379–1381. doi:10.2337/dc09-2321
21. Lemieux P, Weisnagel SJ, Caron AZ, et al. Effects of 6-month vitamin D supplementation on insulin sensitivity and secretion: A randomised, placebo-controlled trial. *Eur J Endocrinol.* 2019;181(3):287–299. doi:10.1530/EJE-19-0156
22. Pittas AG, Jorde R, Kawahara T, Dawson-Hughes B. Vitamin D supplementation for prevention of type 2 diabetes mellitus: To D or not to D? *J Clin Endocrinol Metab.* 2020;105(12):3721–3733. doi:10.1210/clinem/dgaa594
23. Yousefi Rad E, Djalali M, Koohdani F, et al. The effects of vitamin D supplementation on glucose control and insulin resistance in patients with diabetes type 2: A randomized clinical trial study. *Iran J Public Health.* 2014;43(12):1651–1656. PMID:26171357.
24. Talaei A, Mohamadi M, Adgi Z. The effect of vitamin D on insulin resistance in patients with type 2 diabetes. *Diabetol Metab Syndr.* 2013;5(1):8. doi:10.1186/1758-5996-5-8
25. Cho SH, Jeong SH, Shin J, Park S, Jang S. Short-term smoking increases the risk of insulin resistance. *Sci Rep.* 2022;12(1):3550. doi:10.1038/s41598-022-07626-1
26. Molla GJ, Ismail-Beigi F, Larijani B, et al. Smoking and diabetes control in adults with type 1 and type 2 diabetes: A nationwide study from the 2018 National Program for Prevention and Control of Diabetes of Iran. *Can J Diabetes.* 2020;44(3):246–252. doi:10.1016/j.cjcd.2019.07.002
27. Ohkuma T, Iwase M, Fujii H, et al. Dose- and time-dependent association of smoking and its cessation with glycemic control and insulin resistance in male patients with type 2 diabetes mellitus: The Fukuoka Diabetes Registry. *PLoS One.* 2015;10(3):e0122023. doi:10.1371/journal.pone.0122023
28. Sia HK, Kor CT, Tu ST, Liao PY, Wang JY. Association between smoking and glycemic control in men with newly diagnosed type 2 diabetes: A retrospective matched cohort study. *Ann Med.* 2022;54(1):1385–1394. doi:10.1080/07853890.2022.2075559
29. Stadler M, Tomann L, Storka A, et al. Effects of smoking cessation on  $\beta$ -cell function, insulin sensitivity, body weight, and appetite. *Eur J Endocrinol.* 2014;170(2):219–227. doi:10.1530/EJE-13-0590
30. Schmidt L, Shokraneh F, Steinhausen K, Adams CE. Introducing RAPTOR: RevMan Parsing Tool for Reviewers. *Syst Rev.* 2019;8(1):151. doi:10.1186/s13643-019-1070-0
31. Elovic A, Pourmand A. MDCalc medical calculator app review. *J Digit Imaging.* 2019;32(5):682–684. doi:10.1007/s10278-019-00218-y
32. Dettori JR, Norvell DC, Chapman JR. Fixed-effect vs random-effects models for meta-analysis: 3 points to consider. *Global Spine J.* 2022;12(7):1624–1626. doi:10.1177/21925682221110527
33. Henmi M, Copas JB, Eguchi S. Confidence intervals and p-values for meta-analysis with publication bias. *Biometrics.* 2007;63(2):475–482. doi:10.1111/j.1541-0420.2006.00705.x
34. Huedo-Medina TB, Sánchez-Meca J, Marín-Martínez F, Botella J. Assessing heterogeneity in meta-analysis: Q statistic or I<sup>2</sup> index? *Psychol Methods.* 2006;11(2):193–206. doi:10.1037/1082-989X.11.2.193
35. Saaqi M, Ashraf B. Modifying “PICO” question into “PICOS” model for more robust and reproducible presentation of the methodology employed in a scientific study. *World J Plast Surg.* 2017;6(3):390–392. PMID:29218294; PMCID:PMC5714990
36. Amir-Behghadami M, Janati A. Population, Intervention, Comparison, Outcomes and Study (PICOS) design as a framework to formulate eligibility criteria in systematic reviews. *Emerg Med J.* 2020;37(6):387. doi:10.1136/emered-2020-209567
37. Simmonds M. Quantifying the risk of error when interpreting funnel plots. *Syst Rev.* 2015;4(1):24. doi:10.1186/s13643-015-0004-8
38. Wamberg L, Pedersen SB, Rejnmark L, Richelsen B. Causes of vitamin D deficiency and effect of vitamin D supplementation on metabolic complications in obesity: A review. *Curr Obes Rep.* 2015;4(4):429–440. doi:10.1007/s13679-015-0176-5
39. De Oliveira LF, De Azevedo LG, Da Mota Santana J, De Sales LPC, Pereira-Santos M. Obesity and overweight decreases the effect of vitamin D supplementation in adults: Systematic review and meta-analysis of randomized controlled trials. *Rev Endocr Metab Disord.* 2020;21(1):67–76. doi:10.1007/s11154-019-09527-7
40. Harris KK, Zopey M, Friedman TC. Metabolic effects of smoking cessation. *Nat Rev Endocrinol.* 2016;12(5):299–308. doi:10.1038/nrendo.2016.32
41. Yu W, Gao C, Zhao X, et al. Four-way decomposition of effect of cigarette smoking and body mass index on serum lipid profiles. *PLoS One.* 2022;17(8):e0270486. doi:10.1371/journal.pone.0270486
42. Kennedy L, Lyons TJ. Non-enzymatic glycosylation. *Br Med Bull.* 1989;45(1):174–190. doi:10.1093/oxfordjournals.bmb.a072310
43. UK Prospective Diabetes Study (UKPDS). VIII. Study design, progress and performance. *Diabetologia.* 1991;34(12):877–890. PMID:1778353.
44. George PS, Pearson ER, Witham MD. Effect of vitamin D supplementation on glycaemic control and insulin resistance: A systematic review and meta-analysis. *Diabet Med.* 2012;29(8):e142–e150. doi:10.1111/j.1464-5491.2012.03672.x
45. Carrillo-Larco RM, Miranda JJ, Gilman RH, et al. The HOMA-IR performance to identify new diabetes cases by degree of urbanization and altitude in Peru: The CRONICAS Cohort Study. *J Diabetes Res.* 2018;2018:7434918. doi:10.1155/2018/7434918
46. Tokodai K, Amada N, Haga I, Takayama T, Nakamura A, Kashiwade T. Insulin resistance as a risk factor for new-onset diabetes after kidney transplantation. *Transplant Proc.* 2014;46(2):537–539. doi:10.1016/j.transproceed.2013.10.060
47. Ronald Kahn C. Insulin resistance, insulin insensitivity, and insulin unresponsiveness: A necessary distinction. *Metabolism.* 1978;27(12):1893–1902. doi:10.1016/S0026-0495(78)80007-9
48. Miyazaki Y, Akasaka H, Ohnishi T, Saitoh S, DeFronzo RA, Shimamoto K. Differences in insulin action and secretion, plasma lipids and blood pressure levels between impaired fasting glucose and impaired glucose tolerance in Japanese subjects. *Hypertens Res.* 2008;31(7):1357–1363. doi:10.1291/hypres.31.1357
49. Aoyama-Sasabe S, Fukushima M, Xin X, et al. Insulin secretory defect and insulin resistance in isolated impaired fasting glucose and isolated impaired glucose tolerance. *J Diabetes Res.* 2016;2016:1298601. doi:10.1155/2016/1298601
50. Klec C, Ziomek G, Pichler M, Malli R, Graier WF. Calcium signaling in  $\beta$ -cell physiology and pathology: A revisit. *Int J Mol Sci.* 2019;20(24):6110. doi:10.3390/ijms20246110
51. Charoenngam N, Holick MF. Immunologic effects of vitamin D on human health and disease. *Nutrients.* 2020;12(7):2097. doi:10.3390/nu12072097
52. Palladino R, Tabak AG, Khunti K, et al. Association between pre-diabetes and microvascular and macrovascular disease in newly diagnosed type 2 diabetes. *BMJ Open Diab Res Care.* 2020;8(1):e001061. doi:10.1136/bmjdr-2019-001061
53. Zhu P, Pan XF, Sheng L, Chen H, Pan A. Cigarette smoking, diabetes, and diabetes complications: Call for urgent action. *Curr Diab Rep.* 2017;17(9):78. doi:10.1007/s11892-017-0903-2

54. Petersen JL, McGuire DK. Impaired glucose tolerance and impaired fasting glucose: A review of diagnosis, clinical implications and management. *Diab Vasc Dis Res.* 2005;2(1):9–15. doi:10.3132/dvdr.2005.007
55. Unwin N, Shaw J, Zimmet P, Alberti KGMM. Impaired glucose tolerance and impaired fasting glycaemia: The current status on definition and intervention. *Diabet Med.* 2002;19(9):708–723. doi:10.1046/j.1464-5491.2002.00835.x
56. Akter S, Goto A, Mizoue T. Smoking and the risk of type 2 diabetes in Japan: A systematic review and meta-analysis. *J Epidemiol.* 2017;27(12):553–561. doi:10.1016/j.je.2016.12.017
57. Campagna D, Alamo A, Di Pino A, et al. Smoking and diabetes: Dangerous liaisons and confusing relationships. *Diabetol Metab Syndr.* 2019;11(1):85. doi:10.1186/s13098-019-0482-2



# C-terminal cross-linking telopeptide levels in COVID-19 patients: A prospective case-control study

Mehmet Ali Gul<sup>1,A,C,D</sup>, Nezahat Kurt<sup>2,C</sup>, Fatma Betul Ozgeris<sup>3,B</sup>, Neslihan Yuce<sup>4,C</sup>, Omer Faruk Kocak<sup>5,C</sup>, Emine Parlak<sup>6,B,C</sup>

<sup>1</sup> Department of Medical Biochemistry, Faculty of Medicine, Amasya University, Turkey

<sup>2</sup> Department of Medical Biochemistry, Faculty of Medicine, Erzincan Binali Yildirim University, Turkey

<sup>3</sup> Department of Nutrition and Dietetics, Faculty of Healthy Sciences, Ataturk University, Erzurum, Turkey

<sup>4</sup> Department of Medical Biochemistry, Faculty of Medicine, Ataturk University, Erzurum, Turkey

<sup>5</sup> Department of Chemical Technology, Erzurum Vocational Training College, Ataturk University, Turkey

<sup>6</sup> Department of Infectious Diseases and Clinical Microbiology, Faculty of Medicine, Ataturk University, Erzurum, Turkey

A – research concept and design; B – collection and/or assembly of data; C – data analysis and interpretation;

D – writing the article; E – critical revision of the article; F – final approval of the article

Advances in Clinical and Experimental Medicine, ISSN 1899–5276 (print), ISSN 2451–2680 (online)

*Adv Clin Exp Med.* 2024;33(7):691–698

## Address for correspondence

Mehmet Ali Gul

E-mail: mehmetali999@hotmail.com

## Funding sources

None declared

## Conflict of interest

None declared

Received on November 1, 2022

Reviewed on August 23, 2023

Accepted on February 22, 2024

Published online on March 21, 2024

## Cite as

Gul MA, Kurt N, Ozgeris FB, Yuce N, Kocak OF, Parlak E. C-terminal cross-linking telopeptide levels in COVID-19 patients: A prospective case-control study. *Adv Clin Exp Med.* 2024;33(7):691–698. doi:10.17219/acem/185254

## DOI

10.17219/acem/185254

## Copyright

Copyright by Author(s)

This is an article distributed under the terms of the Creative Commons Attribution 3.0 Unported (CC BY 3.0) (<https://creativecommons.org/licenses/by/3.0/>)

## Abstract

**Background.** Coronavirus disease 19 (COVID-19) is a viral infection mediated by coronavirus-2 that causes severe acute respiratory syndrome (SARS-CoV-2). The disease may affect biochemical parameters and electrolytes. C-terminal cross-linking telopeptide (CTX-I) is released during mature bone resorption and is a biomarker for predicting bone resorption.

**Objectives.** As the pandemic progressed, understanding the effects of COVID-19 disease remained critical. Inflammatory responses triggered by the virus can result in a bone metabolism regulation imbalance. As such, this study aimed to analyze serum levels of CTX-I, calcium (Ca), phosphorus (P), magnesium (Mg), C-reactive protein (CRP), and alkaline phosphatase (ALP) in COVID-19 patients to investigate the relationship between bone resorption and the disease.

**Materials and methods.** The study included 56 individuals with COVID-19 (divided into mild, moderate and severe subgroups depending on disease severity) and 25 healthy adults as a control group. Serum CTX-I concentrations were measured with enzyme-linked immunosorbent assay (ELISA). In addition, CRP, Ca, Mg, P, and ALP levels were measured using an automated clinical chemistry analyzer.

**Results.** Serum CTX-I levels were significantly higher in COVID-19 patients than in the control group ( $p < 0.05$ ). Furthermore, a positive weak relationship was detected between CRP and CTX-I ( $r = 0.303$ ,  $p < 0.05$ ).

**Conclusions.** Increased serum CTX-I levels in the patient group caused COVID-19-driven bone degradation, though serum CTX-I levels did not differ according to disease severity.

**Key words:** bone, COVID-19, CTX-I

## Background

Coronavirus disease 19 (COVID-19), caused by severe acute respiratory syndrome coronavirus-2 (SARS-CoV-2) infection, was first detected in December 2019 in Wuhan, China, and spread rapidly over almost the entire globe.<sup>1,2</sup> Coronaviridae is a family of single-stranded ribonucleic acid (RNA) viruses, including SARS-CoV-2, that affect many animals, while other coronaviruses could infect humans.<sup>3</sup> Subjective clinical findings are considered more reliable with the concomitant biomarkers, which provide measurable data during the progression of biological processes.<sup>4</sup> With the rapid spread of COVID-19 and increased mortality in extreme cases, a better understanding of clinical features, determining its effects on metabolism and finding accurate laboratory markers are required to elucidate the disease process. Indeed, its influence on metabolism is not fully known, and there is a need for studies on the effects of COVID-19 on various human organs and tissues, such as muscle and bone.

The bone organic matrix comprises around 90–98% collagen I, which is proteolytically degraded by osteoclasts during bone turnover, releasing small C-terminal cross-linking telopeptide (CTX-I) peptide fragments.<sup>5–7</sup> Serum CTX-I levels correlate with histomorphometric measurements of bone resorption.<sup>8</sup> Although different biomarkers are available for measuring the metabolic products of bone resorption, serum CTX-I stands out for its high correlation with bone turnover rate and its immediate response to changes in bone metabolism, making it a sensitive marker of bone resorption.<sup>5,9</sup>

## Objectives

Studies show that inflammation and bone metabolism are associated with various biological and clinical mechanisms and suggest measuring bone metabolism markers, such as CTX-I, in COVID-19 patients.<sup>10</sup> To investigate the effect of COVID-19 on bone, the current study examined the impact of COVID-19 on serum levels of the bone resorption marker CTX-I.

## Materials and methods

### Patients

This prospective observational research, conducted in June and July 2020, included 56 patients diagnosed with COVID-19 and 25 individuals with no health problems. The Clinical Research Ethics Committee of Ataturk University (Erzurum, Turkey) approved this research prior to experiments (approval No. B.30.2.ATA 0.01.00/369).

All participants provided written informed consent, and the study conformed to the principles outlined in the Declaration of Helsinki.

Participants provided nasopharyngeal and oropharyngeal samples for real-time polymerase chain reaction (PCR) COVID-19 detection, with those testing positive stratified to the COVID-19 group and those testing negative to the control group. Those diagnosed with COVID-19 ( $n = 56$ ) were divided into mild, moderate and severe subgroups based on disease severity, with 25 healthy individuals used as a control group. Power analysis was performed before determining sample size. Subgroups included a non-complicated group (NCG), with mild fever and cough present/no and no radiological pulmonary findings, a moderate group (MG) with fever-cough, radiological uni/bilateral lung involvement and oxygen saturation  $SpO_2 > 93\%$ , and a severe group (SG) displaying lung radiological imaging with uni/bilateral involvement and  $SpO_2 < 93\%$ . Exclusion criteria encompassed being aged less than 18 years, the presence of diseases affecting bone metabolism, undergoing chemotherapy or immunosuppressive drug treatment, and using calcium, magnesium or calcitriol supplements. The MG and SG included some patients with hypertension, diabetes mellitus and chronic obstructive pulmonary disease (COPD).

### Blood sampling

Participants provided fasting blood on the first day of hospital admission, with venous blood drawn using a 10 mL syringe and transferred to gel-containing vacutainers. After 30 min, samples were centrifuged at  $1,500 \times g$  for 10 min, and serum was stored at  $-80^\circ\text{C}$  until the day of measurement.

### Measurement and data collection

Serum CTX-I concentrations were analyzed using a human-specific CTX-I sandwich enzyme-linked immunosorbent assay (ELISA) (cat. No. CSB-E11224h; Cusabio Technology, Wuhan, USA). The kit detection range was 0.625–40 ng/mL, with an intra-assay coefficient of variance (CV%)  $< 8\%$ , inter-assay precision CV% of  $< 10\%$  and sensitivity of 0.156 ng/mL. The ELISA measurements used serum samples (100  $\mu\text{L}$ ) according to the manufacturer's instructions, with samples analyzed using an XS PowerWave multi-plate spectrophotometer (Agilent Technologies, Santa Clara, USA). Other biochemical parameters were measured using compatible kits and detected on a cobas 8000 modular analyzer (Roche Diagnostics, Basel, Switzerland), with C-reactive protein (CRP) immunoturbidimetrically detected in the e801 module, and calcium (Ca), magnesium (Mg), phosphorus (P), and alkaline phosphatase (ALP) in the c502 module. These results were obtained from existing patient files. Analysis was carried out at the Faculty of Medicine of Ataturk University.

## Statistical analyses

Data analysis employed IBM SPSS 20.0 (IBM Corp., Armonk, USA). Shapiro–Wilk tests evaluated numerical data distribution, and F test/Brown–Forsythe tests confirmed the homogeneity of variances. Normally distributed data were calculated as mean ± standard deviation (SD). Student’s t-test was used to compare 2 groups and analysis of variance (ANOVA) 3 groups. Data with a non-normal distribution were calculated as median and interquartile range (Me (IQR)), with Mann–Whitney U tests used for paired group comparisons and Kruskal–Wallis post hoc with Dunn’s test used for 3 group comparisons. Spearman’s correlation coefficient was employed to evaluate the monotonic component in the relationship between the data. A  $p < 0.05$  was considered significant, and  $p < 0.001$  very significant. Supplementary tables (<https://doi.org/10.5281/zenodo.10719329>) provide confirmation of parametric test assumptions and related data for the control group, COVID-19 patient group and COVID-19 subgroups (NCG, MG and SG).

## Results

Table 1 shows the clinical and demographic characteristics of COVID-19 patients. While 30 of the 56 COVID-19 patients were female and 26 were male, the control group contained 11 women and 14 men. There was no statistical difference between group mean age ( $p > 0.05$ ).

Serum CTX-I levels were higher in COVID-19 patients than in the control group ( $p < 0.001$ ), as were CRP levels ( $p < 0.001$ ). On the other hand, serum Ca, Mg, P, ALP, creatinine, and blood urea nitrogen (BUN) levels were similar in both groups ( $p > 0.05$ ). Table 2,3 show the biochemical tests measured in both groups, while Fig. 1A–H provides box-whisker graphics of the group comparison.

When the COVID-19 subgroups were compared and evaluated, the highest serum CTX-I levels were found in the NCG, but this difference was not significant ( $p > 0.05$ ). While CRP was significantly higher in the SG compared to the other groups ( $p < 0.05$ ), no difference was observed between other parameters ( $p > 0.05$ ). Table 4,5 show the COVID-19 subgroup’s serum biochemical tests, and Fig. 2A–H presents box-whisker graphics of the group comparisons.

Spearman’s correlation analysis indicated a positive weak monotonic correlation between CTX-I and CRP in all

**Table 1.** Demographic data of all participants

Variables	COVID-19				Control (n = 25)
	non-complicated group (n = 19)	moderate severe group (n = 25)	severe group (n = 12)	total COVID-19 (n = 56)	
Age [years], mean ±SD	40.5 ±15.9	52.6 ±18.0	58.7 ±13.3	49.9 ±17.8	48.2 ±13.3
Sex (female/male), mean ±SD	6/12	14/11	4/9	30/26	11/14

mean ±SD – mean ± standard deviation.

**Table 2.** Biochemical parameters of the coronavirus disease 19 (COVID-19) and control groups

Variables	COVID-19 mean ±SD (n = 56)	Control mean ±SD (n = 25)	F	Sig.	t	df	Mean difference	Standard error difference	95% CI of the difference		p-value
									lower	upper	
Ca [mg/dL]	8.9 ±0.4	9.1 ±0.4	0.331	0.567	-1.788	79	-0.1833	0.1025	-0.3874	0.0208	0.780
Mg [mg/dL]	2 ±0.2	2.1 ±0.2	2.644	0.108	-1.674	79	-0.07424	0.04434	-0.16250	2.644	0.980
P [mg/dL]	3.2 ±0.6	3.1 ±0.4	10.554	0.002	0.205	79	0.0282	0.1378	-0.2461	0.3026	0.838

Ca – calcium; Mg – magnesium; P – phosphorus; mean ±SD – mean ± standard deviation; df – degrees of freedom; 95% CI – 95% confidence interval. The t-test was used for Ca, Mg, and P.

**Table 3.** Biochemical parameters of the coronavirus disease 19 (COVID-19) and control groups

Variables	COVID-19 Me (IQR) (n = 56)	Control Me (IQR) (n = 25)	Mann–Whitney U	Wilcoxon W	Z	p-value
CTX-I [ng/mL]	3.81 (2.18)	2.94 (0.76)	239.00	564.000	-4.714	0.001*
ALP [U/L]	79.5 (32)	99 (58)	501.50	2097.500	-2.032	0.095
CRE [mg/dL]	0.8 (0.3)	0.8 (0.2)	420	612.000	-0.59	0.552
CRP [mg/L]	5.5 (28.3)	3.0 (2)	204.00	529.000	-5.094	0.001*
BUN [mg/dL]	14.9 (5.4)	15 (8.1)	643.5	968.5	-0.578	0.563

CTX-I – C-terminal cross-linking telopeptide; ALP – alkaline phosphatase; BUN – blood urea nitrogen; CRP – C-reactive protein; CRE – creatinine; Me (IQR) – median (interquartile range); \*statistically significant. Mann–Whitney U test used for CTX-I, ALP, BUN, CRE, and CRP.

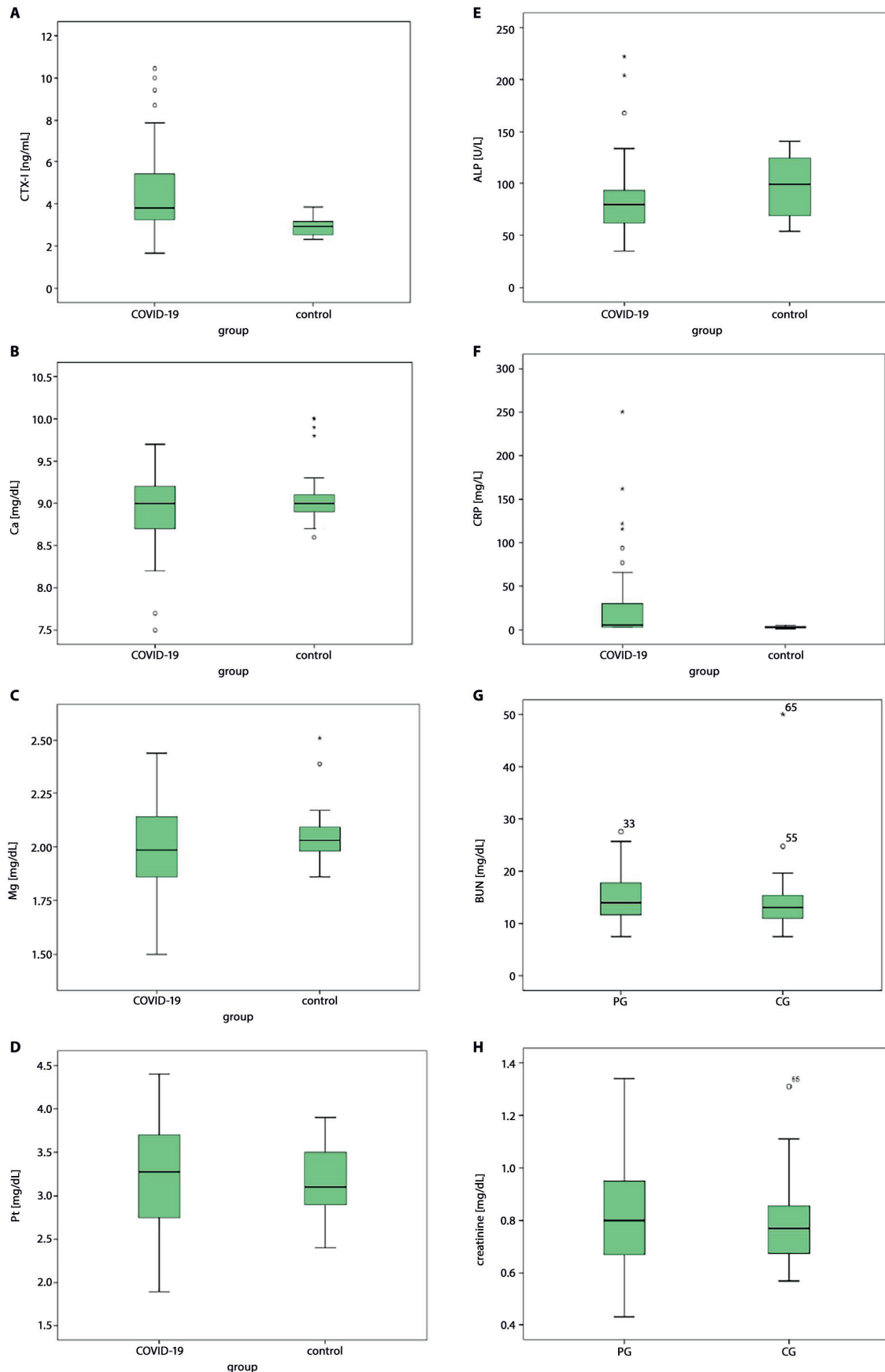


**Fig.1.** A. Comparison of serum CTX-I in COVID-19 and control groups; B. Comparison of serum Ca in COVID-19 and control groups ( $p > 0.05$ ); C. Comparison of serum Mg in COVID-19 and control groups ( $p > 0.05$ ); D. Comparison of serum P in COVID-19 and control groups ( $p > 0.005$ ); E. Comparison of serum ALP in COVID-19 and control groups ( $p > 0.05$ ); F. Comparison of serum CRP in COVID-19 and control groups ( $p > 0.05$ ); G. Comparison of serum BUN in COVID-19 and control groups ( $p > 0.05$ ); H. Comparison of serum CRE in COVID-19 and control groups ( $p > 0.005$ ). COVID-19 group  $n = 56$  and control group  $n = 25$ . The lowest and last stem ends show the minimum and maximum values. The bottom and top edges of the box indicate the IQR, and the line in the middle of the box indicates the median. A t-test was used for Ca, Mg and P, and a Mann–Whitney U test was used for CTX-I, ALP, BUN, CRE, and CRP

ALP – alkaline phosphatase; Ca – calcium; COVID-19 – coronavirus disease 19; CRE – creatine; CRP – C-reactive protein; CTX-I – C-terminal cross-linking telopeptide; BUN – blood urea nitrogen; IQR – interquartile range; Mg – magnesium; P – phosphorus.



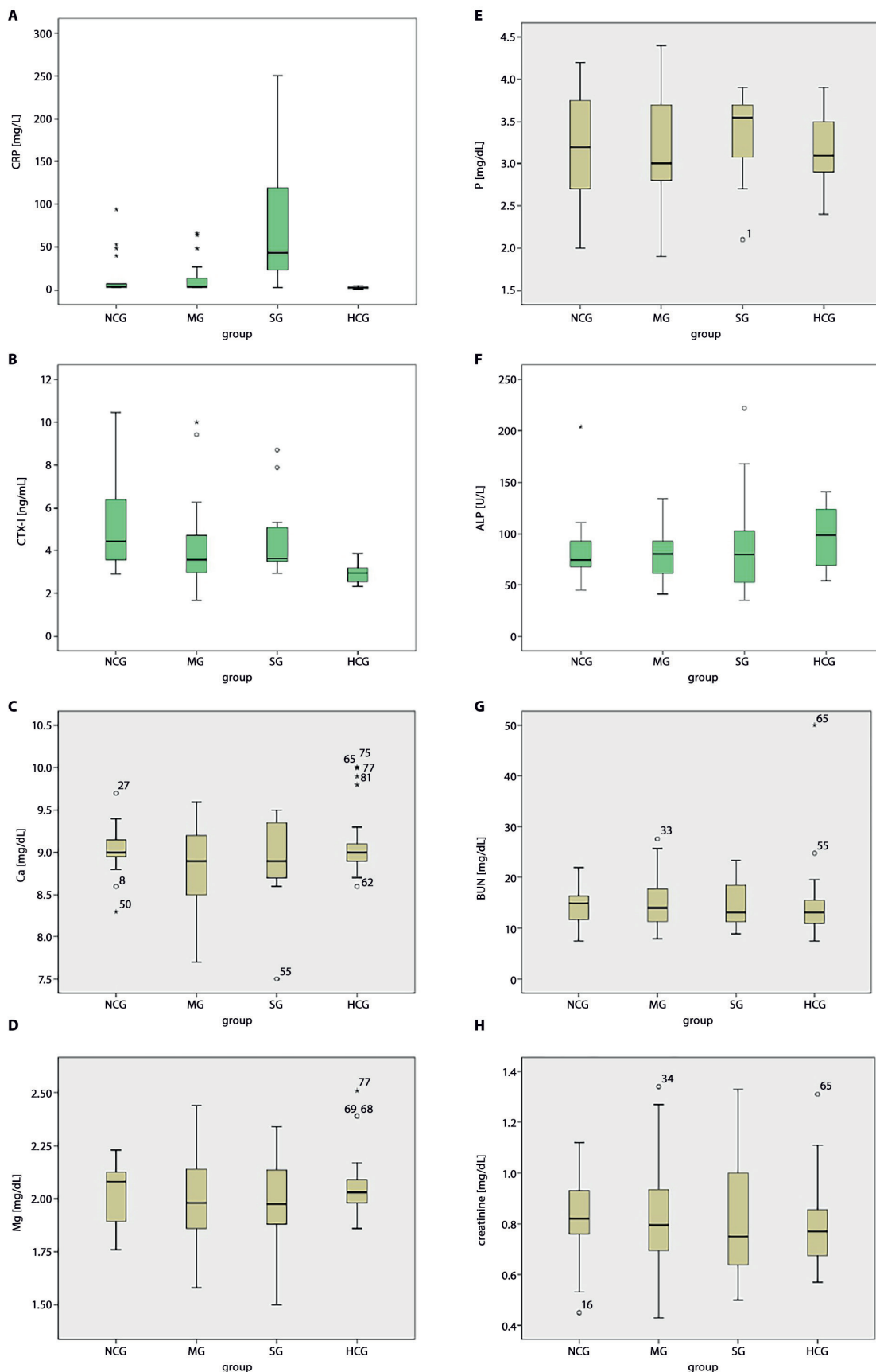


**Fig. 2.** A. Comparison of serum CRP of all groups ( $p < 0.200$  for COVID-19 subgroups). B. Comparison of serum CTX-I of all groups ( $p > 0.005$  for COVID-19 subgroups). C. Comparison of serum Ca of all groups ( $p > 0.005$  for COVID-19 subgroups). D. Comparison of serum Mg of all groups ( $p > 0.005$  for COVID-19 subgroups). E. Comparison of serum P of all groups ( $p > 0.005$  for COVID-19 subgroups). F. Comparison of serum ALP of all groups ( $p > 0.005$  for COVID-19 subgroups). G. Comparison of serum BUN of all groups ( $p > 0.005$  for COVID-19 subgroups). H. Comparison of serum CRE of all groups ( $p > 0.005$  for COVID-19 subgroups). Non-complicated group  $n = 19$ , moderate severe group  $n = 25$ , severe group  $n = 12$ , and control group  $n = 25$ . The lowest and last stem ends show the minimum and maximum values. The bottom and top edges of the box indicate the IQR, and the line in the middle of the box indicates the median. ANOVA was used for CA, Mg and P, and a Kruskal–Wallis test was used for CTX-I, ALP, CRE, BUN, and CRP

ALP – alkaline phosphatase; ANOVA – analysis of variance; Ca – calcium; COVID-19 – coronavirus disease 19; CRE – creatine; CRP – C-reactive protein; CTX-I – C-terminal cross-linking telopeptide; BUN – blood urea nitrogen; IQR – interquartile range; Mg – magnesium; P – phosphorus.

**Table 4.** Biochemical parameters of the coronavirus disease 19 (COVID-19) subgroups

Variables	Non-complicated group mean $\pm$ SD (n = 19)	Moderate severe group mean $\pm$ SD (n = 25)	Severe group mean $\pm$ SD (n = 12)	Sum of squares	df	Mean square	F	p-value
Ca [mg/dL]	9.0 $\pm$ 0.3	8.8 $\pm$ 0.5	8.9 $\pm$ 0.5	0.40	2	0.20	1.05	0.358
Mg [mg/dL]	2 $\pm$ 0.1	1.9 $\pm$ 0.2	1.9 $\pm$ 0.2	0.02	2	0.01	0.22	0.799
P [mg/dL]	3.14 $\pm$ 0.7	3.11 $\pm$ 0.6	3.34 $\pm$ 0.53	0.45	2	0.23	0.54	0.586

Ca – calcium; Mg – magnesium; P – phosphorus; mean  $\pm$ SD – mean  $\pm$  standard deviation; df – degrees of freedom. The analysis of variance (ANOVA) was used for Ca, Mg and P.

**Table 5.** Biochemical parameters of the coronavirus disease 19 subgroups

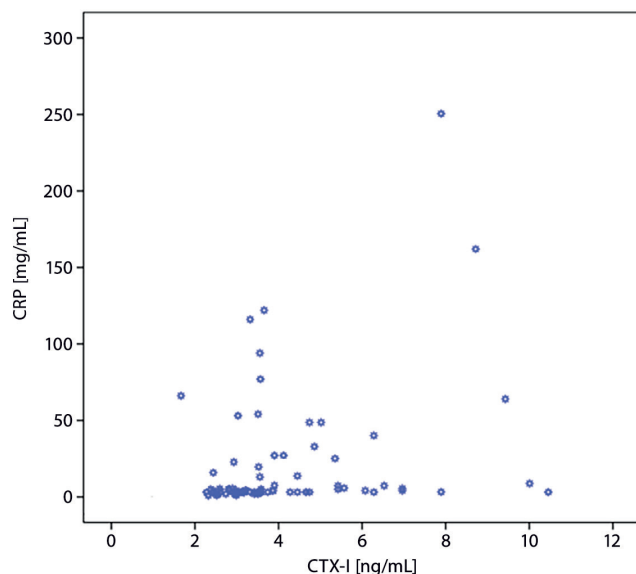
Variables	Non-complicated group Me (IQR) (n = 19)	Moderate severe group Me (IQR) (n = 25)	Severe group Me (IQR) (n = 12)	$\chi^2$	df	p-value
CTX-I [ng/mL]	4.45 (2.97)	3.56 (2.09)	3.6 (1.73)	3.21	2	0.200
ALP [U/L]	74 (29)	80 (33)	79.5 (61)	0.14	2	0.933
CRE [mg/dL]	0.82 (0.27)	0.80 (0.26)	0.75 (0.39)	0.183	2	0.991
CRP [mg/L]	4.2 (4.4)	4.1 (11.7)	43.5 (92)	13.68	2	0.001*
BUN [mg/dL]	14.9 (4.7)	14.5 (8.3)	13.1 (7.9)	0.302	2	0.860

CTX-I – C-terminal cross-linking telopeptide; ALP – alkaline phosphatase; CRP – C-reactive protein; CRE – creatinine; BUN – blood urea nitrogen; Me (IQR) – median; df – degrees of freedom; \*statistically significant. Kruskal–Wallis test used for CTX-I, ALP, CRE, BUN, and CRP.

**Table 6.** Spearman's correlation analyses between CTX-I and other tests

Parameter	CRP	Ca	Mg	P	ALP	BUN	CRE	
CTX-I	r-value	0.303*	-0.104	0.201	-0.083	-0.020	0.023	-0.025
	p-value	0.006	0.357	0.073	0.460	0.858	0.841	0.827

CTX-I – C-terminal cross-linking telopeptide; Ca – calcium; Mg – magnesium; P – phosphorus; ALP – alkaline phosphatase; BUN – blood urea nitrogen; CRP – C-reactive protein; CRE – creatinin; \*statistically significant.

**Fig. 3.** Relationship between C-reactive protein (CRP) and C-terminal cross-linking telopeptide-I (CTX-I) for all participants

participants ( $r = 0.303$ ,  $p < 0.05$ ). Table 6 shows the analysis of the monotonic component of the relationship between CTX-I and other tests, and Fig. 3 shows the relationship between CTX-I and CRP

## Discussion

To the best of our knowledge, this is the first study reporting on serum CTX-I levels in patients with COVID-19. The findings demonstrated that serum CTX-I levels were statistically higher in the COVID-19 patient group than in the healthy controls. However, there were no differences between COVID-19 patients divided into subgroups according to disease severity (mild, moderate and severe).

Many studies on diverse viruses have sought to characterize their roles in bone metabolism,<sup>10</sup> with those on bone metabolism in SARS-CoV-2 indicating that much more research is required on the risk of fracture in patients recovering from SARS-CoV-2 infection.<sup>10</sup> Although not all features of COVID-19 are fully understood, pathological studies on the lungs, liver and heart have shown the potential negative effects of COVID-19 on certain tissues.<sup>11</sup> In this regard, bone-forming capacity is prone to worsen due to the progression of underlying diseases resulting from SARS-CoV-2 infection.<sup>12</sup>

Serum CTX-I levels increase following proteolysis of type I collagen, the main component of the bone extracellular organic matrix, during mature bone resorption. Therefore, CTX-I levels decrease in patients with suppressed bone resorption.<sup>9,13</sup> Most research on viruses

and CTX-I shows that virus infection causes increased CTX-I levels. Huang et al.<sup>14</sup> showed that the dengue virus caused a temporary inflammatory reaction in bone tissue and increased osteolytic activity to release CTX-I. Research on human immunodeficiency virus (HIV) and hepatitis C virus (HCV) infections showed that HIV was related to increased bone resorption and formation, and increases in CTX-I, whereas HCV infection was not associated with CTX-I.<sup>15</sup> Increased bone resorption has been shown in the pathogenesis of bone loss, which was evaluated by measuring CTX-I in hemophiliacs and correlations with HIV infection.<sup>16</sup>

A study on biochemical markers of bone metabolism in SARS conducted in Hong Kong showed significant bone resorption, as indicated by a significant increase in serum CTX-I from certain days after fever onset.<sup>17</sup> Patients with chronic hepatitis C (CHC) and osteoporosis or osteopenia had higher serum CTX-I levels, which may mean that bone loss in the early stages of CHC is not due to reduced bone synthesis but secondary to increased bone resorption.<sup>18</sup> Furthermore, animal studies on SARS-CoV-2 demonstrate a significant reduction in several bone parameters.<sup>19</sup>

Tao et al. hypothesized that angiotensin-converting enzyme 2 (ACE2) deficiency caused by SARS-CoV2 invasion may result in bone matrix reduction and that COVID-19 can cause anaphase bone loss and earlier muscle disorder by targeting ACE2 in the bone marrow microenvironment.<sup>12</sup> The current study supports this hypothesis by showing higher CTX-I levels in patients with COVID-19 than in the healthy controls.

Magnesium has many biological functions, especially in bone, with 60% of the total body content found in bone.<sup>20</sup> A recent meta-analysis showed an association between unstable Mg homeostasis and COVID-19, and suggested incorporating Mg into the ionogram and supplementing it externally.<sup>21</sup> In parallel, a lower Mg level was observed in the COVID-19 group in our study, but this decrease was not significant. In addition, moderate and severe patients had lower Mg than non-complicated patients, though this difference was not significant. A retrospective study by Pal et al.<sup>22</sup> found widespread hypocalcemia in mildly severe COVID-19 patients and attributed it to the disease, though they did not clarify its pathophysiological mechanism.

In a study of 420 COVID-19 patients and 165 healthy controls, serum Ca was lower in the COVID-19 patients. Although the current study found a slight discrepancy in Ca levels, it was not considered significant.

Alkaline phosphatase is a bone-building enzyme with several isoforms. Although studies on bone-specific ALP (B-ALP) in COVID-19 are limited to only a few case reports,<sup>23,24</sup> a study showing elevated total ALP in COVID-19 patients suggested it was primarily due to liver damage. In the current study, serum ALP values were similar in both groups and although it increased with COVID-19 severity, this difference was not significant.

Since CTX-I excretion takes place in the kidneys, the CTX-I level may be high in the plasma due to impaired renal function. However, kidney function tests of serum creatinine and BUN showed no differences between the healthy group and COVID-19 patients, indicating that the high CTX-I level was of COVID-19 origin. The CRP serum level, which is a positive acute phase reactant, increases during infection,<sup>25</sup> with many reports showing increased CRP in COVID-19 patients.<sup>26,27</sup> Our findings showed an increase in CRP levels in COVID-19 patients, which is compatible with current research results. In addition, a positive weak relationship was found between CTX-I and CRP.

## Limitations

Study limitations include the absence of B-ALP and radiological images to support bone resorption. While this study includes critical clinical laboratory parameter results, the small sample size could be a limitation, particularly within the COVID-19 subgroups. Another limitation is the lack of parathyroid hormone (PTH) and calcitriol measurement since they play a role in bone metabolism.

## Conclusions

The study showed that COVID-19 patients had increased serum CTX-I levels, a reference marker for bone resorption, though there were no differences based on disease severity. Our data may be foundational to clinical studies investigating bone metabolism in COVID-19.

## Supplementary data

The Supplementary materials are available at <https://doi.org/10.5281/zenodo.10719329>. The package includes the following files:

Supplementary Table 1. Verification of parametric test assumption for control.

Supplementary Table 2. Verification of parametric test assumption for COVID-19 patient group.

Supplementary Table 3. Verification of parametric test assumption for NCG COVID-19 subgroup.

Supplementary Table 4. Verification of parametric test assumption for MG COVID-19 subgroup.

Supplementary Table 5. Verification of parametric test assumption for SG COVID-19 subgroup.

Supplementary Table 6. Tests of homogeneity.

## Data availability

The datasets generated and/or analyzed during the current study are available from the corresponding author on reasonable request.

## Consent for publication

Not applicable.

## ORCID IDs

Mehmet Ali Gul  <https://orcid.org/0000-0002-5849-0116>

Nezahat Kurt  <https://orcid.org/0000-0002-1685-5332>

## References

- Ren LL, Wang YM, Wu ZQ, et al. Identification of a novel coronavirus causing severe pneumonia in human: A descriptive study. *Chin Med J (Engl)*. 2020;133(9):1015–1024. doi:10.1097/CM9.0000000000000722
- Khan IH, Zahra SA, Zaim S, Harky A. At the heart of COVID-19. *J Card Surg*. 2020;35(6):1287–1294. doi:10.1111/jocs.14596
- Le Bert N, Tan AT, Kunasegaran K, et al. SARS-CoV-2-specific T cell immunity in cases of COVID-19 and SARS, and uninfected controls. *Nature*. 2020;584(7821):457–462. doi:10.1038/s41586-020-2550-z
- Kermali M, Khalsa RK, Pillai K, Ismail Z, Harky A. The role of biomarkers in diagnosis of COVID-19 A systematic review. *Life Sci*. 2020;254:117788. doi:10.1016/j.lfs.2020.117788
- Marx RE, Cillo JE, Ulloa JJ. Oral bisphosphonate-induced osteonecrosis: Risk factors, prediction of risk using serum CTX testing, prevention, and treatment. *J Oral Maxillofac Surg*. 2007;65(12):2397–2410. doi:10.1016/j.joms.2007.08.003
- Lazarovici TS, Mesilaty-Gross S, Vered I, et al. Serologic bone markers for predicting development of osteonecrosis of the jaw in patients receiving bisphosphonates. *J Oral Maxillofac Surg*. 2010;68(9):2241–2247. doi:10.1016/j.joms.2010.05.043
- Seibel MJ. Biochemical markers of bone turnover. Part I: Biochemistry and variability. *Clin Biochem Rev*. 2005;26(4):97–122. PMID:16648882. PMCID:PMC1320175.
- Chavassieux P, Portero-Muzy N, Roux JP, Garnero P, Chapurlat R. Are biochemical markers of bone turnover representative of bone histomorphometry in 370 postmenopausal women? *J Clin Endocrinol Metab*. 2015;100(12):4662–4668. doi:10.1210/jc.2015-2957
- Chubb SAP. Measurement of C-terminal telopeptide of type I collagen (CTX) in serum. *Clin Biochem*. 2012;45(12):928–935. doi:10.1016/j.clinbiochem.2012.03.035
- Salvio G, Gianfelice C, Firmani F, Lunetti S, Balercia G, Giacchetti G. Bone metabolism in SARS-CoV-2 disease: Possible osteoimmunology and gender implications. *Clinic Rev Bone Miner Metab*. 2020;18(4):51–57. doi:10.1007/s12018-020-09274-3
- Xu Z, Shi L, Wang Y, et al. Pathological findings of COVID-19 associated with acute respiratory distress syndrome. *Lancet Respir Med*. 2020;8(4):420–422. doi:10.1016/S2213-2600(20)30076-X
- Tao H, Bai J, Zhang W, et al. Bone biology and COVID-19 infection: Is ACE2 a potential influence factor? *Med Hypotheses*. 2020;144:110178. doi:10.1016/j.mehy.2020.110178
- Lee CYS, Suzuki JB. CTX biochemical marker of bone metabolism: Is it a reliable predictor of bisphosphonate-associated osteonecrosis of the jaws after surgery? Part I: Biological concepts with a review of the literature. *Implant Dent*. 2009;18(6):492–500. doi:10.1097/ID.0b013e3181c6837c
- Huang YL, Chen ST, Liu RS, et al. CLEC5A is critical for dengue virus-induced osteoclast activation and bone homeostasis. *J Mol Med*. 2016;94(9):1025–1037. doi:10.1007/s00109-016-1409-0
- Bedimo R, Cutrell J, Zhang S, et al. Mechanisms of bone disease in HIV and hepatitis C virus: Impact of bone turnover, tenofovir exposure, sex steroids and severity of liver disease. *AIDS*. 2016;30(4):601–608. doi:10.1097/QAD.0000000000000952
- Katsarou O, Terpos E, Chatzismalis P, et al. Increased bone resorption is implicated in the pathogenesis of bone loss in hemophiliacs: Correlations with hemophilic arthropathy and HIV infection. *Ann Hematol*. 2010;89(1):67–74. doi:10.1007/s00277-009-0759-x
- Chan MHM, Chan PKS, Griffith JF, et al. Steroid-induced osteonecrosis in severe acute respiratory syndrome: A retrospective analysis of biochemical markers of bone metabolism and corticosteroid therapy. *Pathology*. 2006;38(3):229–235. doi:10.1080/00313020600696231
- Lin JC, Hsieh TY, Wu CC, et al. Association between chronic hepatitis C virus infection and bone mineral density. *Calcif Tissue Int*. 2012;91(6):423–429. doi:10.1007/s00223-012-9653-y
- Awosanya OD, Dalloul CE, Blosser RJ, et al. Osteoclast-mediated bone loss observed in a COVID-19 mouse model. *Bone*. 2022;154:116227. doi:10.1016/j.bone.2021.116227
- De Baaij JHF, Hoenderop JGJ, Bindels RJM. Magnesium in man: Implications for health and disease. *Phys Rev*. 2015;95(1):1–46. doi:10.1152/physrev.00012.2014
- Trapani V, Rosanoff A, Baniyadi S, et al. The relevance of magnesium homeostasis in COVID-19. *Eur J Nutr*. 2022;61(2):625–636. doi:10.1007/s00394-021-02704-y
- Pal R, Ram S, Zohmangaihi D, et al. High prevalence of hypocalcemia in non-severe COVID-19 patients: A retrospective case-control study. *Front Med (Lausanne)*. 2021;7:590805. doi:10.3389/fmed.2020.590805
- Erat T, Atar M, Kontbay T. Transient benign hyperphosphatemia due to COVID-19: The first case report. *J Pediatr Endocrinol Metab*. 2021;34(3):385–387. doi:10.1515/jpem-2020-0503
- Ploegmakers DJM, Zielman-Blokhuis AM, van Duijnhoven HJR, de Rooy JJJ, Geurts ACH, Nonnekens J. Heterotopic ossifications after COVID-19 pneumonia [in Dutch]. *Ned Tijdschr Geneesk*. 2020;164:D5357. PMID:33331722.
- Pepys MB, Hirschfield GM. C-reactive protein: A critical update. *J Clin Invest*. 2003;111(12):1805–1812. doi:10.1172/JCI200318921
- Liu F, Li L, Xu M, et al. Prognostic value of interleukin-6, C-reactive protein, and procalcitonin in patients with COVID-19. *J Clin Virol*. 2020;127:104370. doi:10.1016/j.jcv.2020.104370
- Lagunas-Rangel FA. Neutrophil-to-lymphocyte ratio and lymphocyte-to-C-reactive protein ratio in patients with severe coronavirus disease 2019 (COVID-19): A meta-analysis. *J Med Virol*. 2020;92(10):1733–1734. doi:10.1002/jmv.25819

# Combination of serum FOXR2 and transvaginal three-dimensional power Doppler ultrasonography in the diagnosis of uterine lesions

Ping Zhang<sup>A,D,F</sup>, Qiong Zhou<sup>B,C</sup>, Zhiyong Zeng<sup>E,F</sup>

Department of Ultrasound, Hunan Provincial People's Hospital (The First Hospital Affiliated with Hunan Normal University), Changsha, China

A – research concept and design; B – collection and/or assembly of data; C – data analysis and interpretation; D – writing the article; E – critical revision of the article; F – final approval of the article

Advances in Clinical and Experimental Medicine, ISSN 1899–5276 (print), ISSN 2451–2680 (online)

*Adv Clin Exp Med.* 2024;33(7):699–708

## Address for correspondence

Zhiyong Zeng  
E-mail: zhiyongzeng2022@163.com

## Funding sources

None declared

## Conflict of interest

None declared

Received on March 1, 2023  
Reviewed on June 23, 2023  
Accepted on August 18, 2023

Published online on October 13, 2023

## Abstract

**Background.** Cervical carcinoma and endometrial carcinoma are the most common gynecologic cancers worldwide. Forkhead-box R2 (FOXR2) plays an important role in the progression of various malignant tumors. However, the effects of FOXR2 on the development of uterine lesions remain unclear.

**Objectives.** This prospective observational study aimed to investigate the diagnostic performance of FOXR2 and transvaginal three-dimensional power Doppler ultrasonography (3D-PDU) for malignant uterine lesions.

**Materials and methods.** This study included 404 uterine lesion patients and 200 healthy individuals who visited the hospital for a physical examination from April 2014 to May 2016. All patients received FOXR2 detection and 3D-PDU examination at admission. The demographic data and clinical data, including age, body mass index (BMI), and the International Federation of Gynecology and Obstetrics (FIGO) stage, were collected. All the patients were followed up for 5 years. The overall survival (OS) was analyzed using Kaplan–Meier (K–M) curve analysis. The diagnostic value of FOXR2 and 3D-PDU was evaluated using receiver operating characteristic (ROC) curves.

**Results.** Serum levels of FOXR2 mRNA were upregulated in patients with malignant uterine lesions. Patients with high expression of FOXR2 showed a higher expression of the cancer biomarkers CA125, CA199, CEA, and SCCA. It was also found that FOXR2 expression was associated with the clinical outcomes of patients with malignant uterine lesions. Moreover, higher expression of FOXR2 predicted a poor prognosis. The combined use of FOXR2 and 3D-PDU showed favorable potential for the diagnosis of malignant uterine lesions, especially for cervical carcinoma and endometrial carcinoma.

**Conclusions.** The combination of serum FOXR2 and transvaginal 3D-PDU has a potential in the diagnosis of uterine lesions.

**Key words:** diagnosis, FOXR2, 3D-PDU, uterine lesions

## Cite as

Zhang P, Zhou Q, Zeng Z. Combination of serum FOXR2 and transvaginal three-dimensional power Doppler ultrasonography in the diagnosis of uterine lesions. *Adv Clin Exp Med.* 2024;33(7):699–708. doi:10.17219/acem/171382

## DOI

10.17219/acem/171382

## Copyright

Copyright by Author(s)

This is an article distributed under the terms of the Creative Commons Attribution 3.0 Unported (CC BY 3.0) (<https://creativecommons.org/licenses/by/3.0/>)

## Background

Cervical carcinoma and endometrial carcinoma are the most common gynecologic cancers in developed countries, ranking 2<sup>nd</sup> and 4<sup>th</sup>, respectively, in malignant tumors of the female reproductive system.<sup>1-4</sup> In the last decade, the incidence and mortality rates of malignant gynecologic cancers have been increasing year by year.<sup>5-7</sup> As reported, the 5-year survival for cervical carcinoma patients with high tumor stage is no more than 60%.<sup>8</sup> Although huge progress has been made in the treatment, such as radiotherapy and chemotherapy, the long-term survival for patients with tumor metastasis is still not satisfactory.<sup>9-11</sup> Therefore, finding a novel diagnostic method is important.

Three-dimensional power Doppler ultrasonography (3D-PDU) is a new imaging technique widely used in gynecology, especially in gynecologic oncology.<sup>12-14</sup> The 3D-PDU exhibits a similar diagnostic performance as magnetic resonance imaging (MRI) in predicting deep myometrial invasion and cervical involvement for endometrial cancer staging.<sup>15-17</sup> Zhang et al. found that combined applications of 3D-PDU and MRI showed a better effect on the staging diagnosis of endometrial cancer with hepatitis B virus infections than a single examination using 3D-PDU or MRI.<sup>18</sup> Several biomarkers are proven to be associated with the diagnosis of endometrial carcinoma and cervical carcinoma, including CA125, CA15-3, CA19-9, CEA, and SCCA.<sup>19-21</sup> Among these biomarkers, forkhead-box R2 (FOXR2) is involved in gynecologic oncology. A previous study revealed the upregulation of FOXR2 in the tissues of patients with ovarian cancer, suggesting an obvious association of the biomarker with the prevalence of ovarian cancer.<sup>22</sup> Another study demonstrated that FOXR2 accelerated tumor metastasis and the growth of ovarian cancer cells by stimulating angiogenesis and activating the Hedgehog signaling pathway.<sup>23</sup> However, the evidence shows that FOXR2 serves as a tumor promoter in different cancers, such as human colorectal cancer,<sup>24</sup> lung cancer<sup>25</sup> and thyroid cancer.<sup>26</sup> The clinical significance of FOXR2 in uterine lesions needs further investigation.

## Objectives

We conducted an observational study to investigate the association between the expression of FOXR2 and the prognosis of uterine lesion patients, and analyze the diagnostic performance of combined applications of FOXR2 and 3D-PDU for uterine lesions.

## Materials and methods

### Participants and samples

Our prospective observational study included 404 uterine lesion patients who reported to Hunan Provincial People's Hospital (The First Hospital Affiliated with Hunan Normal University), Changsha, China, for treatment between April 2014 and May 2016. All patients were diagnosed with uterine lesions through histological analysis. The inclusion criteria were as follows: 1) no history of severe drug allergy; 2) no serious cardiovascular diseases, including uncontrolled hypertension, coronary heart disease, angina pectoris, heart failure, or myocardial infarction; and 3) patients without dyspnea or severe pulmonary insufficiency. The following patients were excluded: 1) patients who received chemotherapy or radiotherapy before the study; 2) patients who underwent a traumatic operation before examination, such as hysteroscopy and diagnostic curettage; and 3) patients with other cancers. The tumor stage was evaluated according to the International Federation of Gynecology and Obstetrics (FIGO) criteria.<sup>27</sup> Additional 200 healthy female patients who visited the hospital for physical examinations during the same period were enrolled in our study as controls. Blood samples were collected from all participants. The tumor tissues of all patients were obtained and immediately stored at  $-80^{\circ}\text{C}$  for the following analysis. Fasting peripheral venous blood samples (5 mL) were collected from all patients within 24 h of admission and stored at  $-80^{\circ}\text{C}$  for the following experiments. This study obtained the approval from the Ethics Committee of the Hunan Provincial People's Hospital (The First Hospital Affiliated with Hunan Normal University, approval No. HuNPPH-20150058). Written informed consent was provided by all participants. The study conformed to the principles outlined in the Declaration of Helsinki.

### Calculation of sample size

The following formulas (Equation 1,2) were implemented:

$$N_{\text{SEN}} = \frac{Z_{1-\alpha/2}^2 \text{SEN}(1 - \text{SEN})}{d_{\text{SEN}}^2 P} \quad (1)$$

$$N_{\text{SPE}} = \frac{Z_{1-\alpha/2}^2 \text{SPE}(1 - \text{SPE})}{d_{\text{SPE}}^2 P} \quad (2)$$

Minimal sample size ( $N$ ) =  $\max(N_{\text{SEN}}, N_{\text{SPE}})$ , where  $\alpha$  stands for the test level,  $d$  indicates the tolerance error,  $Z$  represents the  $Z$  score,  $Z_{1-\alpha/2}$  indicates that the sample follows a standard normal distribution,  $Z_{1-\alpha/2}$  is identified as 1.96, SEN stands for sensitivity, SPE indicates specificity, and  $P$  represents the prevalence of disease.

The mean SEN value was 0.828 and the SPE level was 0.834, according to previous studies. The p-value was 0.456 for the prevalence of malignant uterine lesions, and 0.544 for the prevalence of benign lesions. Thus,  $\alpha = 0.05$ ,  $Z_{1-\alpha/2} = 1.96$ ,  $d = 0.1$ ,  $N_{SEN} = 120$ ,  $N_{SPE} = 98$ , and minimal sample size ( $N$ ) = 120.

## Reverse transcription-quantitative polymerase chain reaction

Total RNAs were extracted from serum samples using Trizol reagent (Tiangen Biotech, Beijing, China). The RNA concentrations were detected using a NanoDrop spectrophotometer (Thermo Fisher Scientific, Waltham, USA). Subsequently, reverse transcription of RNA was conducted using a PrimeScript RT reagent Kit (Takara, Shiga, Japan), and the target genes were quantified using ABI PRISM7300 Sequence Detection System (Applied Biosystems, Waltham, USA) with the SYBR Premix ExTaq (Thermo Fisher Scientific). The following primers were used: F 5'-ACTGGGTCTCATGATGGTGG-3' and R 5'-CTCCATCCAGGAGGTGATCT-3' for FOXR2 and F 5'-TAGACTTCGAGCAGGAGATG-3' and R 5'-ACTCATCGTACTCCTGCTTG-3' for  $\beta$ -actin. The  $\beta$ -actin was utilized as an internal control, and the relative expression of FOXR2 mRNA was calculated using the  $2^{-\Delta\Delta Ct}$  method.

## Transvaginal three-dimensional power Doppler ultrasonography (3D-PDU)

The vaginal volume probe with the power Doppler mode (Voluson E8; GE Healthcare, Chicago, USA) was used to examine the uteri of all patients. The sampling volume was placed on the color central blood flow, adjusted to about 5 mm from the edge of the tumor. Subsequently, the piezoelectric chip of the probe was rotated automatically at a 90° angle to scan the whole lesion. A complete three-dimensional power Doppler image was obtained. The thickness, shape, echo, and integrity of the endometrial contour, the location, number, size, shape, boundary, echo, and surface of lesions, as well as the relationship between basement and endometrium, were evaluated. The Virtual Organ Computer-aided Analysis (VOCAL) software (GE Healthcare) for the 3D power Doppler histogram analysis with computer algorithms was used to analyze the indices of blood flow and vascularization, including the vascularization index (VI), flow index (FI) and vascularization flow index (VFI).

## Data collection and follow-up

Demographic data of all patients, including age, body mass index (BMI) and tumor stage, were collected. Serum levels of cancer-related biomarkers, including serum CA15-3, CA125, CA19-9, CEA, and SCCA, were

determined using chemiluminescence immunoassay, as reported in a previous study.<sup>28</sup> All patients were followed up for 5 years from admission to death or the last follow-up.

## Statistical analyses

First, the Kolmogorov–Smirnov analysis was used to confirm whether the data were normally distributed. The normally distributed data were expressed as mean  $\pm$  standard deviation ( $M \pm SD$ ), and non-normally distributed data were presented as median with range. The heterogeneity of variance was analyzed using Levene's test. For normally distributed data (data expressed as  $M \pm SD$ ), the comparison between 2 groups was conducted using Student's t-test, while the non-normally distributed data (data expressed as median with range) were compared using the Mann–Whitney U test. The rates were compared with the  $\chi^2$  test. A receiver operating characteristic (ROC) curve was used to analyze the diagnostic value. A Kaplan–Meier (K–M) curve with a log-rank test were used to examine the survival time. A p-value  $< 0.05$  was considered statistically significant. All calculations were made using SPSS 18.0 (SPSS Inc., Chicago, USA) and GraphPad v. 6.0 (GraphPad Software, San Diego, USA) software.

## Results

### Basic clinical characteristics of all patients

This prospective observational study included 204 cases of malignant uterine lesions, 200 cases of benign lesions and 200 healthy controls. All participants were consecutively enrolled. Compared to the benign lesion group, the malignant lesion group had higher serum levels of CA15-3, CA125, CA19-9, CEA, and SCCA, and a higher ratio of positive human papillomavirus (HPV). No significant difference was found for age and BMI between the malignant lesion group and the benign lesion group, as well as between the uterine lesion group and the healthy group (Table 1).

### Serum levels of FOXR2 were elevated in malignant uterine lesion patients

Subsequently, the expression of FOXR2 in serum samples and tissue samples was determined. As shown in Fig. 1A, the serum FOXR2 expression was notably upregulated in all uterine lesion patients, including benign lesion patients, compared to healthy controls ( $p < 0.001$ ). The FOXR2 expression in tissue samples was increased in all malignant uterine lesion patients, endometrial carcinoma patients and cervical carcinoma patients compared to benign uterine lesion patients (Fig. 1B,  $p < 0.001$ ). These findings illustrate that FOXR2 expression is upregulated in patients with malignant uterine lesions.

Table 1. Basic clinical characteristics of all patients

Variables	All patients (n = 404)	Malignant lesions (n = 204)	Benign lesions (n = 200)	Healthy (n = 200)	Test value (t, U or $\chi^2$ )	p-value*
Age [years] <sup>a</sup>	53.46 ± 5.05	53.38 ± 5.24	53.55 ± 4.85	53.10 ± 4.63	-0.343	0.732
BMI [kg/m <sup>2</sup> ] <sup>a</sup>	21.20 ± 5.00	21.05 ± 4.85	21.34 ± 5.17	21.31 ± 5.28	-0.608	0.544
CA153 [U/mL] <sup>b</sup>	39.91 (32.25, 49.32)	49.13 (45.62, 54.77)	32.21 (30.37, 34.28)	22.09 (20.82, 23.49)	41	<0.001
CA125 [U/mL] <sup>b</sup>	50.85 (30.53, 68.30)	68.26 (59.76, 77.53)	30.38 (25.27, 35.88)	22.69 (19.16, 27.14)	0	<0.001
CEA [ng/mL] <sup>b</sup>	7.46 (5.06, 11.96)	11.81 (9.89, 15.39)	5.05 (4.74, 5.29)	2.49 (2.34, 2.64)	0	<0.001
CA199 [U/mL] <sup>b</sup>	47.79 (39.70, 69.88)	69.61 (59.94, 78.78)	39.69 (37.54, 41.92)	17.44 (13.60, 21.15)	66	<0.001
SCCA [ $\mu$ g/L] <sup>b</sup>	1.51 (1.28, 3.06)	3.04 (1.62, 4.32)	1.31 (1.18, 1.46)	1.02 (0.89, 1.13)	3292	<0.001
Positive HPV, n (%) <sup>c</sup>	147 (36.39)	120 (58.82)	27 (13.50)	14 (7.00)	44.487	<0.001

\* comparison for all variables was conducted between the malignant lesion and benign lesion groups; <sup>a</sup> comparison for normally distributed data (data expressed as mean ± standard deviation (M ± SD)) was conducted using Student's t-test; <sup>b</sup> non-normally distributed data (data expressed as median with range) were compared using the Mann-Whitney U test; <sup>c</sup>  $\chi^2$  test was used for the comparison of rates. Positive human papillomavirus (HPV): at least 1 HPV subtype was positive.

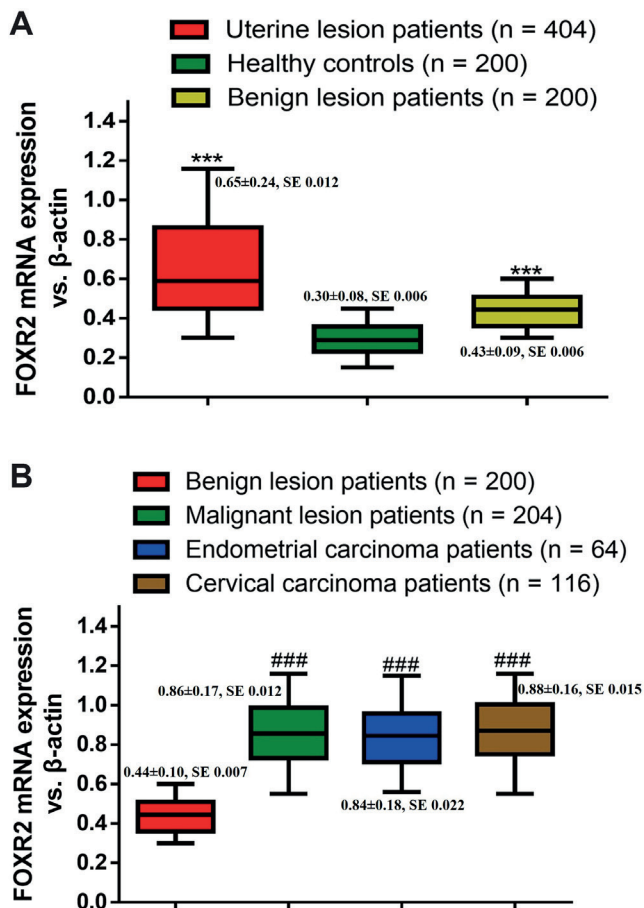


Fig. 1. Forkhead-box R2 (FOXR2) levels in serum and tissue samples were elevated in malignant uterine lesion patients. A. Detection of serum levels of FOXR2 in all uterine lesion patients ( $0.65 \pm 0.24$ ), healthy controls ( $0.30 \pm 0.08$ ) and benign lesion patients ( $0.43 \pm 0.09$ ) using quantitative reverse transcription polymerase chain reaction (RT-qPCR) assay. The comparison was made between the uterine lesion patients and healthy group ( $p < 0.001$ , 95% CI:  $-0.382$ – $-0.328$ ), and between the benign lesion patients and healthy group ( $p < 0.001$ , 95% CI:  $-0.161$ – $-0.128$ ) using Student's t-test; B. Determination of the mRNA expression of FOXR2 in tissue samples of all malignant lesion patients ( $0.86 \pm 0.17$ ), endometrial carcinoma patients ( $0.84 \pm 0.18$ ), cervical carcinoma patients ( $0.88 \pm 0.16$ ), and benign lesion patients ( $0.44 \pm 0.10$ ) using RT-qPCR assay. The comparison was made between the benign lesion and malignant lesion groups ( $p < 0.001$ , 95% CI:  $0.392$ – $0.444$ ), between the benign lesion and endometrial carcinoma patients ( $p < 0.001$ , 95% CI:  $-0.450$ – $-0.358$ ), and between the benign lesion and cervical carcinoma groups ( $p < 0.001$ , 95% CI:  $-0.471$ – $-0.407$ ) using Student's t-test

\*\*\* $p < 0.001$  compared to healthy controls; ### $p < 0.001$  compared to benign lesion patients; SE – standard error; 95% CI – 95% confidence interval.

## Serum FOXR2 was associated with cancer-related biomarkers and clinical outcomes of malignant uterine lesion patients

To further investigate the role of FOXR2 in uterine lesions, all malignant uterine lesion patients were divided into 2 groups, namely a high FOXR2 expression group and a low FOXR2 expression group, according to the median value of FOXR2 mRNA ( $0.855$  compared to  $\beta$ -actin). Basic characteristics, including levels of tumor markers and the rate

of positive HPV, were detected. As shown in Table 2, serum levels of CA15-3, CA125, CA19-9, CEA, and SCCA were significantly higher in the high FOXR2 group than in the low FOXR2 group for all malignant lesion patients and cervical carcinoma patients (all  $p < 0.001$ ). However, endometrial carcinoma patients with high/low FOXR2 expression showed no significant difference in SCCA expression. Additionally, the ratio of positive HPV ( $p < 0.001$  for all comparisons), advanced FIGO stage ( $p < 0.001$  for malignant lesions and cervical carcinoma,  $\chi^2 = 11.746$  and  $p = 0.001$  for endometrial carcinoma), lymph node metastasis (LNM) ( $p < 0.001$  for malignant lesions and cervical carcinoma,  $\chi^2 = 8.749$  and  $p = 0.003$  for endometrial carcinoma), and distant metastasis ( $p < 0.001$  for malignant lesions and cervical carcinoma,  $\chi^2 = 8.749$  and  $p = 0.003$  for endometrial carcinoma) were notably higher in patients with high expression of FOXR2. We further identified the early diagnostic value of FOXR2 for malignant lesions. As shown in Table 3, the ratio of patients with high FOXR2 expression increased along with the FIGO stage in all malignant lesion patients. The K–M curve analysis showed that patients with



**Table 2.** Basic characteristics of all uterine lesion patients

Variables	Malignant lesions (n = 204)				Endometrial carcinoma (n = 64)				Cervical carcinoma (n = 116)			
	high FOXR2 (n = 102)	low FOXR2 (n = 102)	t, U or $\chi^2$	p-value	high FOXR2 (n = 31)	low FOXR2 (n = 33)	t, U or $\chi^2$	p-value	high FOXR2 (n = 63)	low FOXR2 (n = 53)	t, U or $\chi^2$	p-value*
Age [years] <sup>a</sup>	53.26 ±5.00	53.50 ±5.50	-0.330	0.741	52.96 ±5.03	53.26 ±5.22	-0.233	0.817	52.96 ±4.85	54.00 ±5.90	-1.042	0.300
BMI [kg/m <sup>2</sup> ] <sup>a</sup>	20.94 ±5.30	21.16 ±4.38	-0.323	0.747	20.66 ±6.21	21.26 ±4.32	-0.448	0.656	20.91 ±5.07	21.20 ±4.58	-0.323	0.747
CA153 [U/mL] <sup>b</sup>	54.71 (50.80, 58.74)	46.19 (43.84, 48.46)	1019	<0.001	53.90 (49.37, 58.84)	48.97 (46.28, 53.52)	217	<0.001	54.68 (51.27, 58.33)	46.69 (43.88, 48.42)	264	<0.001
CA125 [U/mL] <sup>b</sup>	76.02 (68.14, 83.34)	59.79 (56.44, 68.52)	1345	<0.001	76.11 (71.50, 84.90)	73.50 (66.03, 79.30)	293	<0.001	77.54 (70.23, 83.64)	59.39 (55.66, 65.44)	197	<0.001
CEA [ng/mL] <sup>b</sup>	15.39 (13.82, 16.94)	9.96 (9.26, 10.87)	168	<0.001	14.40 (13.60, 15.92)	10.41 (9.91, 14.11)	20	<0.001	15.40 (13.80, 17.09)	9.81 (8.94, 11.06)	46	<0.001
CA199 [U/mL] <sup>b</sup>	78.69 (73.96, 82.70)	59.94 (55.96, 64.56)	322	<0.001	77.95 (74.73, 82.26)	60.66 (58.33, 63.08)	8	<0.001	78.89 (74.81, 84.37)	62.21 (55.93, 67.60)	165	<0.001
SCCA [ $\mu$ g/L] <sup>b</sup>	4.03 (1.63, 5.21)	2.60 (1.58, 3.25)	3142	<0.001	1.50 (1.39, 1.61)	1.51 (1.42, 1.61)	481	0.682	5.01 (4.26, 5.48)	3.12 (2.57, 3.55)	200	<0.001
Positive HPV, n (%) <sup>c</sup>	89 (87.25)	31 (30.39)	66.924	<0.001	24 (77.42)	11 (27.27)	50.411	<0.001	59 (93.65)	17 (32.08)	81.193	<0.001
FIGO stage $\geq$ III, n (%) <sup>c</sup>	49 (48.04)	19 (18.63)	19.461	<0.001	10 (32.26)	4 (12.12)	11.746	0.001	33 (52.38)	12 (22.64)	18.871	<0.001
LNM, n (%) <sup>c</sup>	43 (42.16)	17 (16.67)	15.647	<0.001	9 (29.03)	4 (12.12)	8.749	0.003	30 (47.62)	10 (18.87)	18.622	<0.001
Distant metastasis, n (%) <sup>c</sup>	38 (37.25)	15 (14.71)	13.047	<0.001	9 (29.03)	4 (12.12)	8.749	0.003	27 (42.85)	9 (16.98)	15.961	<0.001
Mortality, n (%) <sup>c</sup>	50 (49.02)	17 (16.67)	23.723	<0.001	11 (35.48)	3 (9.09)	20.106	<0.001	35 (55.56)	12 (22.64)	22.756	<0.001

FOXR2 – forkhead-box R2; FIGO – the International Federation of Gynecology and Obstetrics; LNM – lymph node metastasis; \*comparison for all variables was made between the high/low FOXR2 expression groups; <sup>a</sup> comparison for normally distributed data (data expressed as mean ± standard deviation (M ±SD)) was conducted using Student’s t-test; <sup>b</sup> non-normally distributed data (data expressed as median with range) were compared using the Mann–Whitney U test; <sup>c</sup>  $\chi^2$  test was used for the comparison of rates. Positive human papillomavirus (HPV): at least 1 HPV subtype was positive.

**Table 3.** Forkhead-box R2 (FOXR2) expression in all uterine lesion patients with different International Federation of Gynecology and Obstetrics (FIGO) stages

Indices		FIGO stage			
		I (n = 68)	II (n = 68)	III (n = 36)	IV (n = 32)
Malignant lesions	high FOXR2	20 (29.41)	33 (48.53)	24 (69.44)	25 (78.13)
	low FOXR2	48 (70.59)	35 (51.47)	12 (33.33)	7 (21.87)
Endometrial carcinoma	high FOXR2	9 (13.24)	12 (17.65)	4 (11.11)	6 (18.75)
	low FOXR2	18 (26.47)	11 (16.18)	3 (8.33)	1 (3.13)
Cervical carcinoma	high FOXR2	12 (17.65)	18 (26.47)	18 (50.00)	15 (46.88)
	low FOXR2	27 (39.71)	14 (20.59)	8 (22.22)	4 (12.50)

high FOXR2 had a shorter 5-year survival time compared to those with low FOXR2 in all malignant lesion patients (Fig. 2A,  $p < 0.001$ ), endometrial carcinoma patients (Fig. 2B,  $\chi^2 = 6.235$  and  $p = 0.0125$ ) and cervical carcinoma patients (Fig. 2C,  $p < 0.001$ ). These findings suggested that higher FOXR2 expression predicted poor clinical outcomes and prognosis for patients with malignant lesions.

### Diagnostic value of serum FOXR2 in benign/malignant uterine lesions

Next, a ROC curve analysis was performed to analyze the diagnostic value of FOXR2 in malignant uterine lesions. The cutoff value of FOXR2 mRNA for malignant uterine lesions was 0.545 compared to  $\beta$ -actin, with

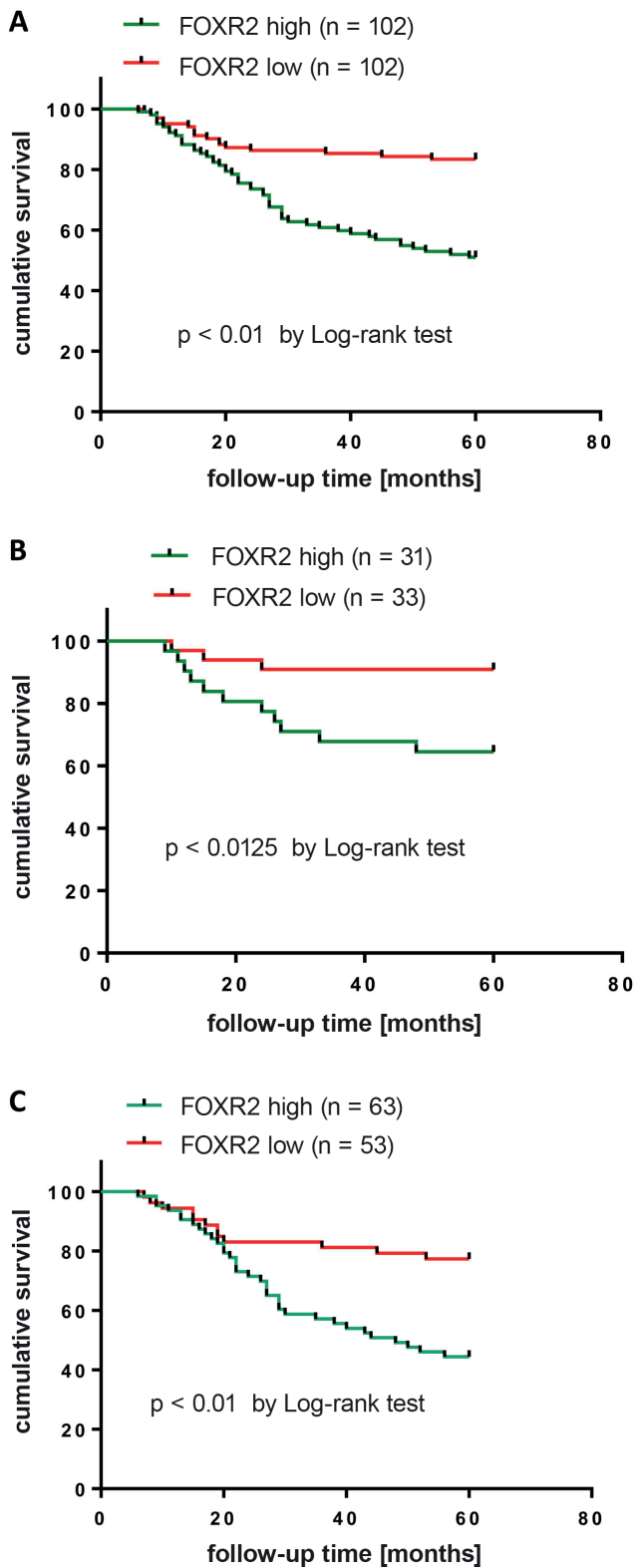


Fig. 2. Kaplan–Meier (K–M) curves of 5-year survival time for malignant lesion patients with high/low expression of forkhead-box R2 (FOXR2). A. K–M curves with log-rank test for all malignant lesion patients; B. K–M curves with log-rank test for endometrial carcinoma patients; C. K–M curves with log-rank test for cervical carcinoma patients

an area under the ROC curve (AUC) of 0.996, sensitivity of 100% and specificity of 87.0% ( $p < 0.001$ , 95% confidence interval (95% CI): 0.992–0.999, Fig. 3A). The cutoff

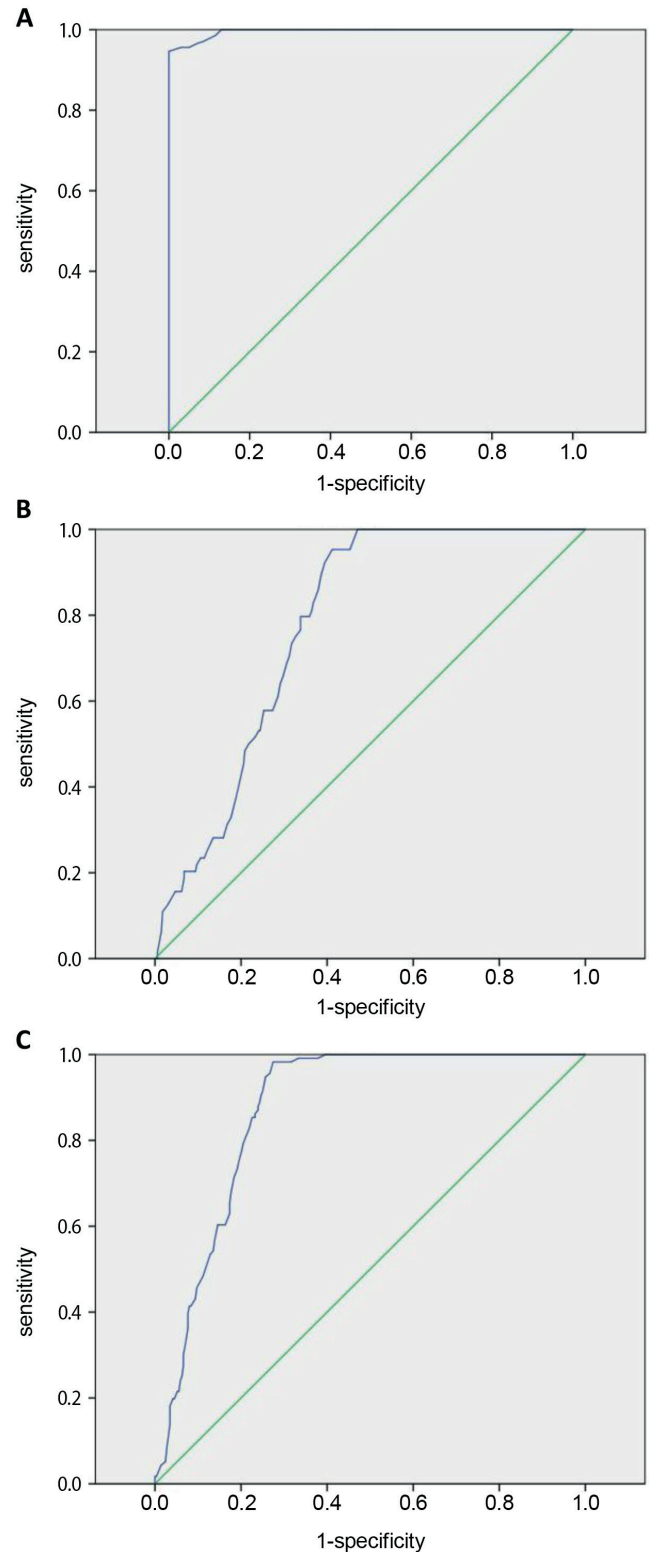


Fig. 3. Receiver operating characteristic (ROC) curves for forkhead-box R2 (FOXR2) levels in the diagnosis of benign uterine lesions and malignant uterine lesions. A. ROC curves for FOXR2 in the diagnosis of benign uterine lesions and malignant uterine lesions; B. ROC curves for FOXR2 in the diagnosis of endometrial carcinoma; C. ROC curves for FOXR2 in the diagnosis of cervical carcinoma

value of FOXR2 for the diagnosis of endometrial carcinoma was 0.645 compared to  $\beta$ -actin, with an AUC of 0.776, sensitivity of 81.3% and specificity of 63.5%

**Table 4.** Combination of serum forkhead-box R2 (FOXR2) and transvaginal three-dimensional power Doppler ultrasonography (3D-PDU) in the diagnosis of malignant uterine lesions

Indices	Methods	True positive	False positive	True negative	False negative	Sensitivity (%)	Specificity (%)	Accuracy (%)
Malignant uterine lesions	histological	204	0	200	0	100	100	100
	FOXR2	204	26	200	0	100	88.50	93.95
	3D-PDU	201	7	193	3	98.53	96.50	97.52
	FOXR2/3D-PDU	202	5	190	7	96.65	97.44	97.03
Endometrial carcinoma	histological	64	0	340	0	100	100	100
	FOXR2	52	106	234	12	81.25	68.82	70.79
	3D-PDU	62	8	332	2	96.88	97.65	97.52
	FOXR2/3D-PDU	51	6	334	13	79.69	98.24	95.30
Cervical carcinoma	histological	116	0	288	0	100	100	100
	FOXR2	114	79	209	2	98.28	72.56	79.95
	3D-PDU	115	6	282	1	99.14	97.92	98.27
	FOXR2/3D-PDU	110	85	203	5	95.65	70.49	77.67

sensitivity = true positive/(true positive+false negative) × 100%; specificity = true negative/(true negative+false positive) × 100%; accuracy = (true positive+true negative)/(true positive+false negative+false positive+true negative) × 100%.

( $p < 0.001$ , 95% CI: 0.730–0.823, Fig. 3B). The cutoff value for FOXR2 in the diagnosis of cervical carcinoma was 0.605 compared to  $\beta$ -actin, with an AUC of 0.871, sensitivity of 98.3% and specificity of 75.3% ( $p < 0.001$ , 95% CI: 0.838–0.905, Fig. 3C). These findings suggested that serum FOXR2 levels might serve as a potential diagnostic marker for malignant uterine lesions. Furthermore, FOXR2 showed satisfactory diagnostic value for endometrial carcinoma and cervical carcinoma.

### Combination of serum FOXR2 and transvaginal 3D-PDU in the diagnosis of malignant uterine lesions

Finally, the combined application of serum FOXR2 and transvaginal 3D-PDU in the diagnosis of malignant uterine lesions was analyzed. All patients received a transvaginal 3D-PDU examination at admission. A cutoff value of 0.545 for FOXR2 mRNA was considered diagnostic for malignant uterine lesions, as was a FOXR2 mRNA of 0.645 for endometrial carcinoma and FOXR2 mRNA of 0.605 for cervical carcinoma. As shown in Table 4, the application of FOXR2 combined with 3D-PDU exhibited satisfactory potential in the diagnosis of malignant uterine lesions, with a sensitivity of 96.65%, specificity of 97.44% and accuracy of 97.03%. Moreover, the application of FOXR2 combined with 3D-PDU showed a sensitivity of 79.69%, specificity of 99.17% and accuracy of 98.27% in the diagnosis of endometrial carcinoma, and a sensitivity of 95.65%, specificity of 70.49% and accuracy of 77.67% in the diagnosis of cervical carcinoma. The above results illustrated that FOXR2 combined with transvaginal 3D-PDU might be useful in the diagnosis of malignant uterine lesions, including endometrial carcinoma and cervical carcinoma.

## Discussion

Although the diagnostic methods for uterine lesions have developed in the last few decades, the early diagnosis of malignant uterine lesions still requires improvement.<sup>29–31</sup> Reportedly, the 5-year survival rate for malignant uterine lesion patients with a high tumor stage is no more than 50%.<sup>32–34</sup> Thus, finding early diagnostic methods and potentially novel biomarkers for malignant lesions of the uterus is of extreme importance. Our study illustrated that FOXR2 was increased in patients with malignant uterine lesions, and a higher FOXR2 expression was associated with a poorer prognosis and shorter 5-year survival time. Moreover, FOXR2, as well as the combined application of FOXR2 and transvaginal 3D-PDU, might be a potential method for the diagnosis of malignant uterine lesions.

Emerging evidence states that FOXR2 is a tumor promoter responsible for the development of different cancers, such as liver cancer,<sup>35</sup> lung cancer<sup>36</sup> or prostate cancer, among others.<sup>37</sup> As reported, FOXR2 was upregulated in breast cancer tissue and was remarkably associated with tumor size and LNM status, indicating that FOXR2 is an independent prognostic factor for breast cancer patients.<sup>38</sup> Lu et al. found that FOXR2 promoted proliferation, invasion and epithelial–mesenchymal transition (EMT) of human colorectal cancer cells.<sup>24</sup> Nevertheless, limited studies have illustrated the role of FOXR2 in tumors of the female reproductive system. A previous study revealed that FOXR2 expression was elevated in endometrial adenocarcinoma (EAC), and an increased FOXR2 expression was related to a poor prognosis in EAC patients.<sup>39</sup> The FOXR2 was also increased in epithelial ovarian adenocarcinoma tissue, and notable correlations between FOXR2 mRNA expression and EMT-related biomarkers were identified in ovarian

adenocarcinoma patients with a high-grade cancer stage.<sup>22</sup> In addition, another study found a greater upregulation of FOXR2 in paclitaxel (PTX)-resistant ovarian cancer tissues compared to PTX-sensitive ovarian cancer tissues.<sup>40</sup> However, the role of FOXR2 has not been well investigated in uterine diseases, especially in endometrial carcinoma and cervical carcinoma. In the present study, we demonstrated that FOXR2 was upregulated in malignant uterine lesion patients and was closely associated with levels of cancer-related biomarkers, namely CA125, CA19-9, CEA, and SCCA. At the same time, the high expression of FOXR2 predicted poorer clinical outcomes and prognosis for patients with malignant uterine lesions.

The most recent study suggests that fluorodeoxyglucose (FDG) positron emission tomography/computed tomography (PET/CT) imaging is recommended for the assessment of various malignancies, such as lung cancer,<sup>41</sup> hypopharyngeal squamous cell carcinoma<sup>42</sup> and breast cancer.<sup>43</sup> The FDG PET/CT also exhibits good diagnostic performance in endometrial carcinoma<sup>44</sup> and cervical cancer.<sup>45</sup> Numerous studies report on the application of 3D-PDU in various diseases. Data show that the sensitivity of 3D-PDU is higher than that of digital rectal examination, grey-scale ultrasonography and power Doppler ultrasonography, but its specificity is lower.<sup>46</sup> The 3D-PDU has been widely used in the diagnosis of benign and malignant uterine lesions. A previous study revealed that 3D-PDU exhibited higher sensitivity and specificity for detecting local recurrence or persistence in cervical carcinoma compared to serum markers (SSCA, CEA and CA125).<sup>47</sup> Other research suggested that 3D-PDU imaging showed a potential in monitoring early therapeutic responses to concurrent chemo-radiotherapy (CCRT) in patients with cervical cancer.<sup>48</sup> Belitsos et al. found the indicators of 3D-PDU to be positively correlated with cervical volume except for other pathological characteristics in cervical cancer patients.<sup>49</sup> Furthermore, compared to early-stage ovarian tumors, the levels of vascular indicators of 3D-PDU were higher in patients with advanced-stage and metastatic ovarian cancers.<sup>50</sup> The combination of the Mainz ultrasound scoring system with 3D-PDU enhanced its sensitivity and specificity in identifying benign and malignant pelvic tumors.<sup>51</sup> Various biomarkers have been used in the diagnosis of malignant tumors, such as SSCA,<sup>52</sup> CEA<sup>53</sup> and CA125.<sup>54</sup> However, the combination of biomarkers with 3D-PDU in the diagnosis of malignant uterine lesions was rarely addressed. The present study illustrated that the combination of serum FOXR2 and transvaginal 3D-PDU exhibited a potential in the diagnosis of malignant uterine lesions, especially for endometrial carcinoma and cervical carcinoma.

## Limitations

This study has some limitations. First, the samples were collected from a single center. Second, the molecular mechanism of FOXR2 in uterine lesions was not

investigated. Third, the diagnostic value of 3D-PDU was not fully addressed. Further studies are needed to solve the above issues.

## Conclusions


In summary, the present study illustrated that serum FOXR2 levels were upregulated in patients with malignant uterine lesions. The FOXR2 was associated with cancer-related biomarkers CA125, CA19-9, CEA, and SCCA. A higher expression of FOXR2 predicted poorer clinical outcomes and shorter 5-year survival times. Both FOXR2 and the combination of FOXR2 with transvaginal 3D-PDU showed potential in the early diagnosis of malignant uterine lesions, especially for endometrial carcinoma and cervical carcinoma. This observational study might provide novel research targets and new diagnostic methods for uterine lesions.


## Data availability

All data that support the findings of the study can be obtained from the corresponding author upon reasonable request.

## ORCID iDs

Ping Zhang  <https://orcid.org/0009-0000-1000-1822>

Qiong Zhou  <https://orcid.org/0009-0009-3671-1633>

Zhiyong Zeng  <https://orcid.org/0009-0006-3913-6337>

## References

- Kroesen M, Mulder HT, Van Holthe JML, et al. Confirmation of thermal dose as a predictor of local control in cervical carcinoma patients treated with state-of-the-art radiation therapy and hyperthermia. *Radiother Oncol.* 2019;140:150–158. doi:10.1016/j.radonc.2019.06.021
- Dou Y, Kawaler EA, Cui Zhou D, et al. Proteogenomic characterization of endometrial carcinoma. *Cell.* 2020;180(4):729–748.e26. doi:10.1016/j.cell.2020.01.026
- Varma KR, Dabbs DJ. Cervical carcinoma with divergent neuroendocrine and gastrointestinal differentiation. *Int J Gynecol Pathol.* 2018; 37(5):488–491. doi:10.1097/PGP.0000000000000438
- Concin N, Matias-Guiu X, Vergote I, et al. ESGO/ESTRO/ESP guidelines for the management of patients with endometrial carcinoma. *Int J Gynecol Cancer.* 2021;31(1):12–39. doi:10.1136/ijgc-2020-002230
- Wang Z, Wang J, Fan J, et al. Risk factors for cervical intraepithelial neoplasia and cervical cancer in Chinese women: Large study in Jiexiu, Shanxi province, China. *J Cancer.* 2017;8(6):924–932. doi:10.7150/jca.17416
- Brüggmann D, Ouassou K, Klingelhöfer D, Bohlmann MK, Jaque J, Groneberg DA. Endometrial cancer: Mapping the global landscape of research. *J Transl Med.* 2020;18(1):386. doi:10.1186/s12967-020-02554-y
- Taylan E, Oktay K. Fertility preservation in gynecologic cancers. *Gynecol Oncol.* 2019;155(3):522–529. doi:10.1016/j.ygyno.2019.09.012
- Cheng H, Wang W, Zhang Y, et al. Expression levels and clinical significance of hepsin and HMGB1 proteins in cervical carcinoma. *Oncol Lett.* 2017;14(1):159–164. doi:10.3892/ol.2017.6116
- Papathemelis T, Scharl S, Kronberger K, et al. Survival benefit of pelvic and paraaortic lymphadenectomy in high-grade endometrial carcinoma: A retrospective population-based cohort analysis. *J Cancer Res Clin Oncol.* 2017;143(12):2555–2562. doi:10.1007/s00432-017-2508-1
- Plotti F, Terranova C, Luvero D, et al. Diet and chemotherapy: The effects of fasting and ketogenic diet on cancer treatment. *Chemotherapy.* 2020;65(3–4):77–84. doi:10.1159/000510839

11. Mauricio D, Zeybek B, Tymon-Rosario J, Harold J, Santin AD. Immunotherapy in cervical cancer. *Curr Oncol Rep*. 2021;23(6):61. doi:10.1007/s11912-021-01052-8
12. El-Sharkawy M, El-Mazny A, Ramadan W, et al. Three-dimensional ultrasonography and power Doppler for discrimination between benign and malignant endometrium in premenopausal women with abnormal uterine bleeding. *BMC Womens Health*. 2016;16(1):18. doi:10.1186/s12905-016-0297-3
13. Zhou J, Xiong Y, Ren Y, Zhang Y, Li X, Yan Y. Three-dimensional power Doppler ultrasonography indicates that increased placental blood perfusion during the third trimester is associated with the risk of macrosomia at birth. *J Clin Ultrasound*. 2021;49(1):12–19. doi:10.1002/jcu.22912
14. Schiffer VMMM, Pellaers D, Hoenen JLJM, Van Kuijk SMJ, Spaanderman MEA, Al-Nasiry S. Feasibility of three dimensional power Doppler ultrasonography methods to assess placental perfusion. *Eur J Obstet Gynecol Reprod Biol*. 2020;254:321–328. doi:10.1016/j.ejogrb.2020.08.006
15. Yang T, Tian S, Li Y, et al. Magnetic resonance imaging (MRI) and three-dimensional transvaginal ultrasonography scanning for preoperative assessment of high risk in women with endometrial cancer. *Med Sci Monit*. 2019;25:2024–2031. doi:10.12659/MSM.915276
16. Zhang Y, Chen J, Zhen Z, Xu XY. Antidiastole value of three-dimensional ultrasonography and power Doppler between uterine parenchyma lumps and endometrial cancer: A retrospective study. *Curr Med Sci*. 2019;39(5):816–819. doi:10.1007/s11596-019-2110-7
17. Pandey H, Guruvare S, Kadavigere R, Rao CR. Utility of three dimensional (3-D) ultrasound and power Doppler in identification of high risk endometrial cancer at a tertiary care hospital in southern India: A preliminary study. *Taiwan J Obstet Gynecol*. 2018;57(4):522–527. doi:10.1016/j.tjog.2018.06.007
18. Zhang T, Qi J, Zhang C. The effect of three-dimensional ultrasound and magnetic resonance imaging in the staging diagnosis of endometrial cancer with hepatitis B virus infection and construction of mathematical model. *Results Phys*. 2021;25:104307. doi:10.1016/j.rinp.2021.104307
19. Liu SY, Ahsan Bilal M, Zhu JH, Li SM. Diagnostic value of serum human epididymis protein 4 in esophageal squamous cell carcinoma. *World J Gastrointest Oncol*. 2020;12(10):1167–1176. doi:10.4251/wjgo.v12.i10.1167
20. Lin D, Zhao L, Zhu Y, et al. Combination IETA ultrasonographic characteristics simple scoring method with tumor biomarkers effectively improves the differentiation ability of benign and malignant lesions in endometrium and uterine cavity. *Front Oncol*. 2021;11:605847. doi:10.3389/fonc.2021.605847
21. Li X, Cheng Y, Dong Y, et al. An elevated preoperative serum calcium level is a significant predictor for positive peritoneal cytology in endometrial carcinoma. *Chin J Cancer Res*. 2019;31(6):965–973. doi:10.21147/j.issn.1000-9604.2019.06.12
22. Asadollahi S, Mazaheri MN, Karimi-Zarchi M, Fesahat F, Farzaneh M. The relationship of *FOXR2* gene expression profile with epithelial-mesenchymal transition related markers in epithelial ovarian cancer. *Klin Onkol*. 2020;33(3):201–207. PMID:32683876.
23. Li B, Huang W, Cao N, Lou G. Forkhead-box R2 promotes metastasis and growth by stimulating angiogenesis and activating hedgehog signaling pathway in ovarian cancer. *J Cell Biochem*. 2018;119(9):7780–7789. doi:10.1002/jcb.27148
24. Lu SQ, Qiu Y, Dai WJ, Zhang XY. *FOXR2* promotes the proliferation, invasion, and epithelial-mesenchymal transition in human colorectal cancer cells. *Oncol Res*. 2017;25(5):681–689. doi:10.3727/096504016X14771034190471
25. Wang XH, Cui YX, Wang ZM, Liu J. Down-regulation of *FOXR2* inhibits non-small cell lung cancer cell proliferation and invasion through the Wnt/ $\beta$ -catenin signaling pathway. *Biochem Biophys Res Commun*. 2018;500(2):229–235. doi:10.1016/j.bbrc.2018.04.046
26. Liao C, Zheng C, Wang L. Down-regulation of *FOXR2* inhibits hypoxia-driven ROS-induced migration and invasion of thyroid cancer cells via regulation of the hedgehog pathway. *Clin Exp Pharmacol Physiol*. 2020;47(6):1076–1082. doi:10.1111/1440-1681.13286
27. FIGO Committee on Gynecologic Oncology. FIGO staging for carcinoma of the vulva, cervix, and corpus uteri. *Int J Gynaecol Obstet*. 2014;125(2):97–98. doi:10.1016/j.ijgo.2014.02.003
28. Wei X, Su J, Yang K, et al. Elevations of serum cancer biomarkers correlate with severity of COVID-19. *J Med Virol*. 2020;92(10):2036–2041. doi:10.1002/jmv.25957
29. Ueno Y, Forghani B, Forghani R, et al. Endometrial carcinoma: MR imaging-based texture model for preoperative risk stratification. A preliminary analysis. *Radiology*. 2017;284(3):748–757. doi:10.1148/radiol.2017161950
30. Devine C, Gardner C, Sagebiel T, Bhosale P. Magnetic resonance imaging in the diagnosis, staging, and surveillance of cervical carcinoma. *Semin Ultrasound CT MRI*. 2015;36(4):361–368. doi:10.1053/j.sult.2015.05.004
31. Koh WJ, Abu-Rustum NR, Bean S, et al. Cervical Cancer, Version 3. 2019, NCCN Clinical Practice Guidelines in Oncology. *J Natl Compr Canc Netw*. 2019;17(1):64–84. doi:10.6004/jnccn.2019.0001
32. Harsh KK, Kapoor A, Paramanandhan M, et al. Induction chemotherapy followed by concurrent chemoradiation in the management of different stages of cervical carcinoma: 5-year retrospective study. *J Obstet Gynecol India*. 2016;66(5):372–378. doi:10.1007/s13224-015-0699-4
33. Matei D, Filiaci V, Randall ME, et al. Adjuvant chemotherapy plus radiation for locally advanced endometrial cancer. *N Engl J Med*. 2019;380(24):2317–2326. doi:10.1056/NEJMoa1813181
34. Banerjee S, Moore KN, Colombo N, et al. Maintenance olaparib for patients with newly diagnosed advanced ovarian cancer and a BRCA mutation (SOLO1/GOG 3004): 5-year follow-up of a randomised, double-blind, placebo-controlled, phase 3 trial. *Lancet Oncol*. 2021;22(12):1721–1731. doi:10.1016/S1470-2045(21)00531-3
35. Wang X, He B, Gao Y, Li Y. *FOXR2* contributes to cell proliferation and malignancy in human hepatocellular carcinoma. *Tumor Biol*. 2016;37(8):10459–10467. doi:10.1007/s13277-016-4923-3
36. Tian X, Zhang L, Jiao Y, Chen J, Shan Y, Yang W. *CircABC10* promotes nonsmall cell lung cancer cell proliferation and migration by regulating the miR-1252/*FOXR2* axis. *J Cell Biochem*. 2019;120(3):3765–3772. doi:10.1002/jcb.27657
37. Xu W, Chang J, Liu G, Du X, Li X. Knockdown of *FOXR2* suppresses the tumorigenesis, growth and metastasis of prostate cancer. *Biomed Pharmacother*. 2017;87:471–475. doi:10.1016/j.biopha.2016.12.120
38. Song H, He W, Huang X, Zhang H, Huang T. High expression of *FOXR2* in breast cancer correlates with poor prognosis. *Tumor Biol*. 2016;37(5):5991–5997. doi:10.1007/s13277-015-4437-4
39. Deng X, Hou C, Liang Z, Wang H, Zhu L, Xu H. miR-202 suppresses cell proliferation by targeting *FOXR2* in endometrial adenocarcinoma. *Dis Markers*. 2017;2017:2827435. doi:10.1155/2017/2827435
40. Zhang S, Cheng J, Quan C, et al. *circCELSR1* (hsa\_circ\_0063809) contributes to paclitaxel resistance of ovarian cancer cells by regulating *FOXR2* expression via miR-1252. *Mol Ther Nucleic Acids*. 2020;19:718–730. doi:10.1016/j.omtn.2019.12.005
41. Huang B, Sollee J, Luo YH, et al. Prediction of lung malignancy progression and survival with machine learning based on pre-treatment FDG-PET/CT. *EBioMedicine*. 2022;82:104127. doi:10.1016/j.ebiom.2022.104127
42. Suzuki S, Toyoma S, Abe T, et al. 18F-FDG-PET/CT can be used to predict distant metastasis in hypopharyngeal squamous cell carcinoma. *J Otolaryngol Head Neck Surg*. 2022;51(1):13. doi:10.1186/s40463-022-00568-8
43. Paydari K, Seraj SM, Zadeh MZ, et al. The evolving role of FDG-PET/CT in the diagnosis, staging, and treatment of breast cancer. *Mol Imaging Biol*. 2019;21(1):1–10. doi:10.1007/s11307-018-1181-3
44. Albano D, Zizioli V, Odicino F, Giubbini R, Bertagna F. Clinical and prognostic value of 18F-FDG PET/CT in recurrent endometrial carcinoma [in Spanish]. *Rev Esp Med Nucl Imag Mol (Engl Ed)*. 2019;38(2):87–93. doi:10.1016/j.remn.2018.09.005
45. Lawal IO, Ololade KO, Popoola GO, et al. 18F-FDG-PET/CT imaging of uterine cervical cancer recurrence in women with and without HIV infection. *Q J Nucl Med Mol Imaging*. 2022;66(1):52–60. doi:10.23736/S1824-4785.19.03156-X
46. Unal D, Sedelaar JPM, Aarnink RG, et al. Three-dimensional contrast-enhanced power Doppler ultrasonography and conventional examination methods: The value of diagnostic predictors of prostate cancer. *BJU Int*. 2007;86(1):58–64. doi:10.1046/j.1464-410x.2000.00719.x
47. Huang YF, Cheng YM, Wu YP, et al. Three-dimensional power Doppler ultrasound in cervical carcinoma: Monitoring treatment response to radiotherapy. *Ultrasound Obstet Gynecol*. 2013;42(1):84–92. doi:10.1002/uog.11223

48. Xu Y, Zhu L, Ru T, et al. Three-dimensional power Doppler ultrasound in the early assessment of response to concurrent chemo-radiotherapy for advanced cervical cancer. *Acta Radiol.* 2017;58(9):1147–1154. doi:10.1177/0284185116684677
49. Belitsos P, Papoutsis D, Rodolakis A, Mesogitis S, Antsaklis A. Three-dimensional power Doppler ultrasound for the study of cervical cancer and precancerous lesions. *Ultrasound Obstet Gynecol.* 2012;40(5): 576–581. doi:10.1002/uog.11134
50. Alcázar JL. Tumor angiogenesis assessed by three-dimensional power Doppler ultrasound in early, advanced and metastatic ovarian cancer: A preliminary study. *Ultrasound Obstet Gynecol.* 2006;28(3): 325–329. doi:10.1002/uog.3804
51. Li KT, Jiang ZH, Tian JW, Liu YJ, Ren M. The value of Mainz ultrasound scoring system combined with 3D-power Doppler ultrasound in differentiating benign and malignant pelvic masses. *Chin J Ultrasonography.* 2018;1:53–57. <https://rs.yiigle.com/cmaid/1028613>. Accessed April 1, 2023.
52. Fu S, Niu Y, Zhang X, Zhang JR, Liu ZP, Wang RT. Squamous cell carcinoma antigen, platelet distribution width, and prealbumin collectively as a marker of squamous cell cervical carcinoma. *Cancer Biomark.* 2018;21(2):317–321. doi:10.3233/CBM-170442
53. Chmura A, Wojcieszek A, Mrochem J, et al. Usefulness of the SCC, CEA, CYFRA 21.1, and CRP markers for the diagnosis and monitoring of cervical squamous cell carcinoma [in Polish]. *Ginekol Pol.* 2009;80(5): 361–366. [https://journals.viamedica.pl/ginekologia\\_polska/article/download/46612/33399](https://journals.viamedica.pl/ginekologia_polska/article/download/46612/33399). Accessed April 10, 2009.
54. Tsai CC, Liu YS, Huang EY, et al. Value of preoperative serum CA125 in early-stage adenocarcinoma of the uterine cervix without pelvic lymph node metastasis. *Gynecol Oncol.* 2006;100(3):591–595. doi:10.1016/j.ygyno.2005.09.049

# Evaluation of photobiomodulation for postoperative discomfort following laser-assisted vital pulp therapy in immature teeth: A preliminary retrospective study

Aneta Olszewska<sup>1,A–D</sup>, Jacek Matys<sup>2,C,D</sup>, Tomasz Gedrange<sup>2,E</sup>,  
Elżbieta Paszyńska<sup>3,C,E</sup>, Magdalena Maria Roszak<sup>4,C</sup>, Agata Czajka-Jakubowska<sup>1,E,F</sup>

<sup>1</sup> Department of Orthodontics and Temporomandibular Disorders, Poznan University of Medical Sciences, Poland

<sup>2</sup> Department of Dental Surgery, Wrocław Medical University, Poland

<sup>3</sup> Department of Integrated Dentistry, Community Dentistry Section, Poznań, Poland

<sup>4</sup> Department of Computer Science and Statistics, Poznan University of Medical Sciences, Poland

A – research concept and design; B – collection and/or assembly of data; C – data analysis and interpretation;

D – writing the article; E – critical revision of the article; F – final approval of the article

Advances in Clinical and Experimental Medicine, ISSN 1899–5276 (print), ISSN 2451–2680 (online)

Adv Clin Exp Med. 2024;33(7):709–716

## Address for correspondence

Jacek Matys

E-mail: jacek.matys@wp.pl

## Funding sources

None declared

## Conflict of interest

None declared

Received on June 13, 2023

Reviewed on August 13, 2023

Accepted on September 4, 2023

Published online on October 18, 2023

## Cite as

Olszewska A, Matys J, Gedrange T, Paszyńska E, Roszak MM, Czajka-Jakubowska A. Evaluation of photobiomodulation for postoperative discomfort following laser-assisted vital pulp therapy in immature teeth: A preliminary retrospective study. *Adv Clin Exp Med*. 2024;33(7):709–716.

doi:10.17219/acem/171812

doi:10.17219/acem/171812

## DOI

10.17219/acem/171812

## Copyright

Copyright by Author(s)

This is an article distributed under the terms of the Creative Commons Attribution 3.0 Unported (CC BY 3.0) (<https://creativecommons.org/licenses/by/3.0/>)

## Abstract

**Background.** Minimally invasive endodontics is recommended for young, immature teeth to preserve healthy pulp and dentin tissue.

**Objectives.** The aim of the study was to examine the cold sensitivity of immature teeth that received photobiomodulation (PBM) after vital pulp therapy (VPT).

**Materials and methods.** The study followed the STROBE guidelines and included 123 healthy patients aged 8–13. The immature teeth (incisors, premolars and molars) that qualified for VPT received the bio-ceramic material – Biodentine. In this experiment, teeth were treated immediately and at 24 h post-VPT with a 635-nm diode laser using a power of 100 mW, a power density of 200 mW/cm<sup>2</sup> and a total energy of 4 J (PBM group, n = 43), while those not treated were the control group (n = 43). The tooth sensitivity to cold was measured using a visual analogue scale (VAS) before and at 6 h, 1 day, 7, 30, and 90 days after treatment. The predictor variable was PBM skills regarding the ability to decrease cold sensitivity after VPT. The primary endpoint was the time to reverse hypersensitivity to cold, and the secondary endpoint was the occurrence of possible side effects. The Mann–Whitney U test, Friedman test along with Dunn's post hoc test, and the  $\chi^2$  test were used to investigate tooth sensitivity.

**Results.** Eighty-six immature permanent teeth of 86 children were included in the study. It was shown that the difference was significant for sensitivity to a cold stimulus between the groups at 6 h, 24 h, 7 days, and 30 days, but no difference was found preoperatively and at 90 days (6 h, 24 h, 7 days, and 30 days,  $p < 0.001$ , and 90 days,  $p = 0.079$ ). However, patients in both groups reported a decrease in discomfort provoked by cold stimuli throughout the follow-up period.

**Conclusions.** Photobiomodulation decreased postoperative sensitivity and was more acceptable for patients. Further randomized clinical studies with placebo-controlled groups are needed.

**Key words:** dental pulp capping, calcium hydroxide (CH), dental pulp test, photobiomodulation therapy

## Background

Young permanent teeth are teeth that have erupted and are present in the oral cavity but have not fully matured in morphology and structure, and have not established an occlusal relationship with their antagonists. The anatomical characteristics of these immature teeth include short clinical crowns, wide pulp cavities, thin hard tissues, short roots, and trumpet-shaped apical foramina. During the first 3–5 years after the eruption, the root formation process continues, and factors such as caries, developmental deformities and trauma can cause pulp lesions or even necrosis.<sup>1</sup> The bacteria and toxins from necrotic pulp tissue can spread to the surrounding tissues, resulting in shortening of the root or even tooth loss.<sup>2</sup> Since the apical orifice in immature teeth is wide and open, conventional root canal treatment (RCT) may not effectively control bacterial infections. In addition, due to the thin root canal wall and poor resistance, these teeth are prone to fracture even under physiological forces.<sup>3</sup>

Vital pulp therapy (VPT) is expanding its indications with the advancement of biomimetic oral materials and modern equipment, coupled with the deepening of basic oral research.<sup>4</sup> The current trend in dentistry is minimally invasive treatment, especially in endodontics for young, immature teeth, with an emphasis on preserving healthy dentin and pulp tissue at every stage of clinical intervention, from diagnosis to preparation. While there is local inflammation and bacterial infections in cases of irreversible pulpitis, histological and micro-biological studies reveal that the entire pulp need not be removed as the inflammation and bacteria are generally confined to the local pulp tissue near the lesions.<sup>5</sup> Pulp tissue a few millimeters away from the infected tissue and necrotic pulp is typically free of inflammation and bacteria.<sup>6</sup> Furthermore, current research has shed light on the ability of dental pulp tissue to prevent bacterial penetration into the dentin by producing reactive or reparative dentin.<sup>7</sup> The traditional approach to the complete removal of the pulp (RCT) once it is infected is being challenged by these new findings. Pulp tissue has the opportunity to self-repair by isolating itself from bacteria and toxins, and it is recommended to preserve it, especially in young permanent teeth where the healing potential is relatively high.<sup>8</sup>

The primary objective of VPT is to prevent pulpitis by stimulating the production of reparative dentin or a calcium bridge, which ensures the continued functioning of the affected teeth. The ultimate aim is to preserve pulp vitality and retain the affected teeth in the long run. The commonly used methods for VPT are pulpotomy and pulp capping. According to a recent study by Wu et al.,<sup>9</sup> pulpitis-derived stem cells exhibit comparable proliferative capacity and multidirectional differentiation potential as dental pulp-derived stem cells, suggesting that it is possible to adequately preserve pulp in irreversible pulpitis without completely removing it. Vital pulp therapy for

young permanent teeth includes indirect pulp capping (IPC), direct pulp capping (DPC), partial pulpotomy, and total pulpotomy. Among these techniques, IPC and DPC are more effective at preserving the entire pulp and enhancing tooth development, while partial pulpotomy and total pulpotomy are partial pulp preservation methods. The application of VPT methods varies, depending on the age group.<sup>10</sup>

After VPT, patients most often complain of hypersensitivity to cold.<sup>10</sup> As pain is very subjective, it is difficult to calibrate the sensations registered by patients, especially in the case of young patients, who usually exaggerate pain. Nowadays, there is no recommended effective method to overcome this complication and to help patients deal with postoperative discomfort.<sup>10,11</sup> Several studies have proposed photobiomodulation (PBM) as an effective new attempt of pain control in medicine and dentistry that is well accepted by patients due to its high success rate.<sup>11,12</sup>

Photobiomodulation was formerly known and described in the literature as low-level laser therapy (LLLT). After it had been reported that the use of not only coherent monochrome light sources, such as lasers, but also non-coherent light sources such as light emitting diodes (LEDs) was effective and led to similar biomodulation processes, the therapy received a new name in practice.<sup>13</sup> Numerous effects of PBM have been identified in the literature, including improved cell regeneration and tissue formation by promoting the proliferation of stem cells, enhanced microcirculation and capillary development, as well as the production of analgesic and anti-inflammatory effects.<sup>12,14</sup>

Thus, PBM has been used in dentistry following VPT due to its well-documented anti-inflammatory, regenerative and analgesic properties.<sup>11</sup> Additionally, it has been reported that laser irradiation has a stimulatory effect on the dental pulp cells, odontoblasts. In fact, they release tertiary dentin, which is an important process in dentin bridge formation at the pulp exposure site.<sup>15</sup>

## Objectives

The objective of this study was to clinically evaluate the effectiveness of PBM using a 635-nm diode laser in reducing postoperative sensitivity and pain following VPT in the immature teeth of young patients. Additionally, in both groups, the clinical success rates of VPT were analyzed.

## Materials and methods

### Study design

The study was conducted as a retrospective analysis and was granted the approval by the Local Ethics Committee of Wrocław Medical University's Faculty of Dentistry



(approval No. KB235/2021). All the participants and their parents provided informed consent in compliance with the Declaration of Helsinki.

## Setting

The analysis included the results of PBM following VPT in children aged 8–13 years who received the treatment at the Department of Pediatric Dentistry of Poznan University of Medical Sciences, from October 2021 to October 2022, who had relevant clinical data from available patients' records and met the inclusion criteria of the study. Data were collected from January 2023 to February 2023.

## Participants

A total of 123 patients were selected for this study from the pool of children referred for routine treatment. Then, we identified a group of 86 children who fulfilled all the inclusion criteria for the study.

## Variables

The data available for this study included the patient's age and gender, treated tooth, and discomfort level measured with the visual analogue scale (VAS). The treatment was performed by a single operator and aimed to standardize the groups based on the number of clinical cases (i.e., age, gender and tooth).

The inclusion criteria for the study included patients aged 8–13 years with immature mandibular and maxillary permanent incisors, premolars, and molars that did not have any periodontal problems (i.e., probing depth was no more than 3 mm). All patients receiving 980-nm diode laser-assisted VPT with or without PBM were included. Pulpal exposure of 0.5–1.0 mm, occurring only on the occlusal side of premolars and molars, was also a requirement. In addition, patients had to be generally healthy, not requiring analgesics or antibiotics in the past 2 weeks, and not taking immunosuppressive drugs or requiring antibiotic prophylaxis. To participate in the study, all parents of the participants were required to sign a declaration of informed consent, based on the age of the patients. The patients' data had to be accurately recorded and complete. Patients were excluded from the study if they required a second anesthetic, had undergone previous treatment and restoration, had severe tooth pain or pain that could not be localized, had taken pain medication prior to their visit, had problems with cooperation, or lacked data during follow-up.

Vital pulp therapy included cases with clinically vital (in cold test) and asymptomatic pulp, where mechanical exposure occurred during the preparation of caries in teeth isolated with a rubber dam. Indications for VPT were pulp exposure with controlled bleeding and the possibility

of direct contact of vital pulp tissue with capping material, Biodentine, with adequate coronal seal due to the final restoration at the same visit.

In total, out of 123 teeth, only 86 teeth from 86 individuals were further examined and included in the study (43 children who received PBM after pulp therapy (PBM group) and 43 patients who did not receive PBM after the procedure (control group)).

## Data sources

All data included in the study were collected from the patient's dental records, examinations and radiographs.

## Study size

The patients were chosen as participants of the study according to the inclusion criteria. No other criteria were used for the selection of the participants. The study size of 123 teeth included all VPT cases treated from October 2021 to October 2022 at the Department of Pediatric Dentistry.

## Clinical procedures

Before the clinical examination, medical and dental anamnesis were obtained from both the parents and participants. The baseline preoperative pain level (VAS) and preoperative radiographs were recorded after stimulation with a cold thermal test. Cold spray (Coltene/Wahledent Inc., Mahwah, USA) was applied to a regular microbrush applicator ( $\varnothing$  2.00 mm) and held on the healthy enamel for 5 s. Assuming pain produced by cold stimulation, a short-lived, sharp pain that subsides when the test is over (5 s) is considered normal for the pulp and reversible pulpitis, and was an inclusion criterion for the study.

If the pain was pronounced or exaggerated and lingered for more than 10 s after the removal of the microbrush tip, it was considered irreversible pulpitis and the patient was excluded from the study. Local anesthesia (4% articaine and epinephrine 1:200,000; Citocartin; Molteni Dental, Milan, Italy) and rubber dam isolation were used. The procedure was performed using  $\times 6.4$  magnification loupes (Exam Vision, Samsø, Denmark) and included the laser protocol. The cavity was prepared, and any carious tissue was removed using a sterile bur (Meisinger, Neuss, Germany). In cases where pulpal exposure occurred due to the removal of caries, a sterile saline-soaked cotton pellet was placed in the cavity for 2 min to control the bleeding. If the bleeding from the exposed pulp continued for more than 5 min, the patient was deemed to have irreversible inflammation of the pulp tissue and a pulpotomy or RCT was considered, resulting in the patient being excluded from the study based on the results.

## Laser procedures

After 2 min, if bleeding control was successful, a 980-nm diode laser (SmartM PRO; Lasotronix, Piaseczno, Poland) was used for coagulation and cavity decontamination, as shown in Table 1.

The decontamination of the cavity was performed with a non-activated 400- $\mu\text{m}$  fiber, in the defocused mode, with a 1-millimeter tip-to-target distance and a circular movement of 2 mm/s.

The coagulation protocol included the irradiation time of 2 s and a tip-to-target distance of 1 mm. The procedure was repeated until the denaturation effect was achieved on the exposed pulp. When the hemorrhage was controlled, Biodentine (Septodont, Saint-Maur-des-Fossés, France), mixed according to the manufacturer's instructions, was placed on the area of pulp exposure. After 20 min, a Single Bond Universal (3M, Maplewood, USA) and dual-cure composite PREDICTA BULK Bioactive (Parkell, Edgewood, USA) were placed as a final restoration. Control radiographs were taken at the end of the visit.

**Table 1.** 980-nm diode laser parameters for pulp coagulation and decontamination of the cavity

Parameters	Laser protocol	
	coagulation	cavity decontamination
Fiber	400 $\mu\text{m}$	400 $\mu\text{m}$
	activated	non-activated
Power	0.4–0.5 W	1 W
Mode	defocused	defocused
Tip-to-target distance	1 mm	1 mm
Emission	continuous (t = 2 s)	gate pulsed emission (10 ms $t_{\text{on}}$ , 20 ms $t_{\text{off}}$ )

## PBM procedure

A 635-nm diode laser (SmartM PRO; Lasotronix) was used for PBM irradiation under the parameters described in Table 2. After VPT, the first session of laser irradiation was performed at the apex area from the buccal and lingual side using a contact technique. The second session of PBM was conducted 24 h after treatment (Table 2).

To prevent any harm during laser application, safety glasses were provided to both the clinicians and patients. A control group was also established by selecting non-irradiated patients.

## Follow-up

The effectiveness of PBM was assessed at various follow-up points after VPT, including 6 h, 24 h, 7 days, 30 days, and 90 days. Postoperative sensitivity was evaluated using a thermal test (cold spray) and recorded using VAS, which features

**Table 2.** The 635-nm diode laser protocol (photobiomodulation (PBM))

Parameters		PBM protocol
Power	100 mW	first session: immediately after procedure; second session: 24 h after procedure
Applicator diameter	8 mm	
Beam spot size at target	0.5 $\text{cm}^2$	
Irradiance at target	200 $\text{mW}/\text{cm}^2$	
Exposure duration	20 s	
Radiant exposure	4 $\text{J}/\text{cm}^2$	
Radiant energy	2 J	
Number of points (buccal and lingual gingivae over the apex)	2 (0.5 $\text{cm}^2$ per point)	
Irradiated area	1 $\text{cm}^2$	
Application technique	contact	
Number and frequency of treatment sessions	2	
Total radiant energy	4 J	
Operating mode	continuous	

a 10-cm scale with no pain representing the value of 0 and unbearable pain representing the value of 10. Patients and parents were instructed to record pain intensity at home for 6 h, specifically for tooth sensitivity caused by cold beverages. At the 24-hour and 7-day follow-ups, pain levels were evaluated using VAS. Additionally, the PBM group underwent a second session after 24 h. Clinical and radiographic examinations were conducted at 1 and 3 months post-VPT. The treatment success was defined as the absence of clinical symptoms and complete radiographic development of the apical area, while failure was indicated by inflammatory signs, periapical lesions, pulp necrosis, and uncontrollable pain, necessitating a referral for RCT.

## Statistical analyses

The analysis of the statistical data was conducted using 2 software programs: Statistica® v. 13.5.0 (TIBCO Software Inc., Palo Alto, USA) and PQStat 1.8.0.414 (PQStat software, Poznań, Poland). The results were compared before and after PBM with regard to the evaluation time and grouping. The Mann–Whitney U test was used for comparing 2 independent groups, while Friedman test with Dunn's post hoc test was employed for comparing more than 2 paired groups. Categorical data were analyzed using the  $\chi^2$  test. Statistical significance was considered for  $p < 0.05$ .

## Quantitative variables

Quantitative variables were analyzed and compared in terms of mean  $\pm$  standard deviation ( $M \pm SD$ ), median, minimum and maximum values, interquartile range (IQR), absolute numbers, and/or percentages as per suitability.

## Results

The study was performed at the Department of Pediatric Dentistry of Poznan Medical University, Poland, between October 2021 and October 2022. From a pool of 123 cases, as documented in VPT records, only 86 directly capped immature permanent teeth met all the inclusion criteria. The PBM group and the control group included 43 teeth each, according to the study protocol. The baseline characteristics of the subjects revealed no differences in age, gender and tooth location between the PBM and control groups. The patient distribution is presented in Table 3.

**Table 3.** The baseline characteristics of the study participants included in both the photobiomodulation (PBM) and control groups

Characteristics of the study groups		PBM (n = 43)	Control (n = 43)
Age [years] (mean)		10	10
Gender, n (%)	female	22 (51.2)	27 (62.8)
	male	21 (48.8)	16 (37.2)
Tooth location, n (%)	maxilla	27 (62.8)	23 (53.48)
	mandible	16 (37.2)	20 (24.6)
Tooth type, n (%)	incisors	20 (46.5)	21 (48.8)
	premolars	10 (23.25)	8 (18.6)
	molars	13 (30.2)	14 (32.5)

## Thermal sensitivity assessment (VAS)

In this study, the Friedman test with Dunn’s post hoc test and the  $\chi^2$  tests were used to investigate the discomfort duration (sensitivity to cold) in the PBM and control groups. After conducting thermal tests at the 3 postoperative follow-up periods, lower pain scores were observed in the PBM group compared to the control group (Fig. 1A,B).

The difference in sensitivity to a cold stimulus was significant between the groups at 6 h, 24 h, 7 days, and

30 days, but no difference was found preoperatively and at 90 days ( $p_{6h,24h,7\ days,30\ days} < 0.001$  and  $p_{90days} = 0.079$ ). A significantly greater decrease in VAS scores was observed in the PBM group than in the control group, while both groups showed a reduction in discomfort throughout the follow-up period, as shown in Fig. 1A,B.

## VPT success rate

The success rate analysis showed a success rate of 93.02% in the PBM group (40/43) and of 81.4% (35/43) in the control group. The overall success rate of VPT in our study was 87.2% (75/86). This showed a recorded failure of VPT in 11 cases in total. Three cases failed in the PBM group and 8 in the control group. No statistically significant difference was observed in success rates between the groups ( $p = 0.10646$ , Table 4). The radiological treatment success is presented in Fig. 2.

**Table 4.** Clinical and radiological assessment of vital pulp therapy (VPT) success rate

Group	Success (%)	Failure (%)
PBM	40 (93.02)	3 (7)
Control	35 (81.40)	8 (18.6)
p-value (Pearson’s $\chi^2$ )	0.10646	

PBM – photobiomodulation.

## Discussion

Based on our study, it has been found that PBM following the VPT procedure could be an effective approach to increase not only the comfort of patients with postoperative pain but also the success rate of the treatment itself. Prolonged sensitivity to cold might be a false indication for RCT, especially when misdiagnosed in young patients, who often exaggerate sensations or have a problem with their evaluation. The findings revealed a decrease in pain

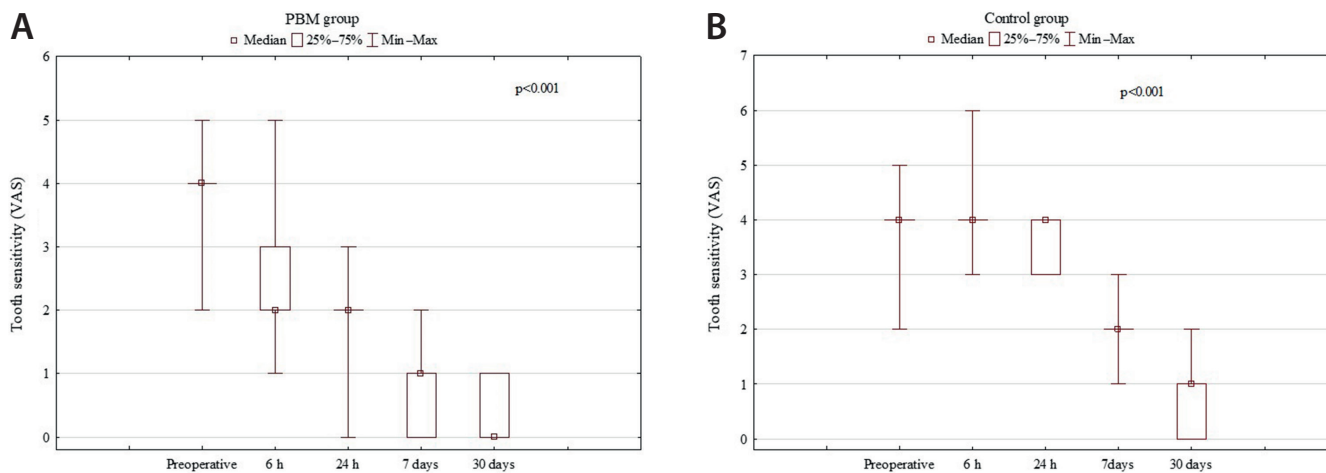


**Fig. 1.** The evaluation of tooth sensitivity (visual analogue scale (VAS)) within the photobiomodulation (PBM) group (A) and control group (B) was conducted intragroup, before treatment (preoperative) and at 4 different examination periods after treatment ( $p < 0.001$ )

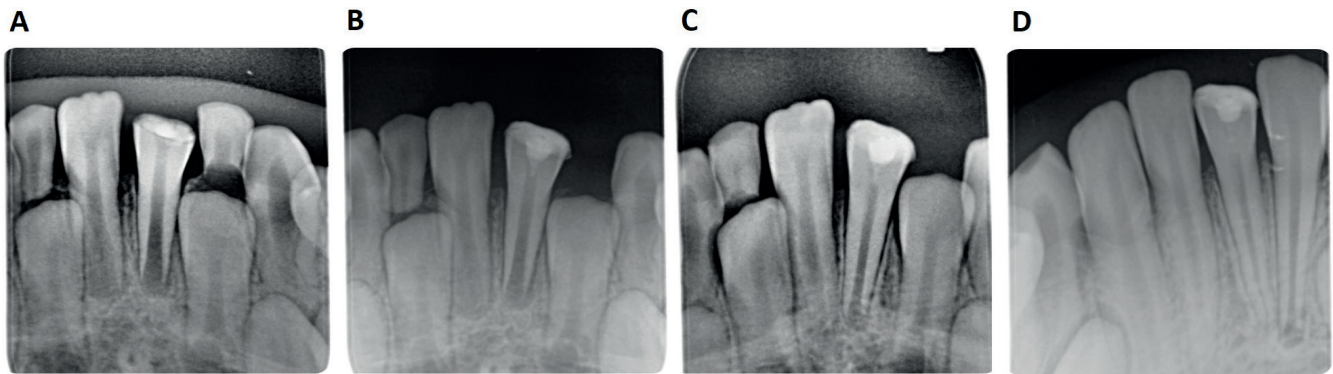


Fig. 2. A. Radiological assessment of vital pulp therapy (VPT) success; B. First appointment; C. Healing after 30 days; D. Healing after 30 days

levels on the VAS during the 3 postoperative follow-up periods among the PBM group, compared to the control group. Specifically, a notable reduction in pain scores was observed in the PBM group on day 7. Additionally, when comparing the discomfort relief between the preoperative period and each follow-up period, the PBM group demonstrated a considerably higher level of pain relief than the control group (primary endpoint), with no reported complications.

Several studies have demonstrated that sensitivity to cold is a frequent complication following the VPT procedure.<sup>16,17</sup> The varied levels of pain and discomfort experienced by patients, particularly young ones, are unpleasant. Prolonged pain and difficulties in objectively evaluating such sensations have been deemed treatment failures. Despite the significance of the issue,<sup>15–18</sup> a definitive strategy for addressing postoperative pain and sensitivity has yet to be identified. Currently, PBM is being utilized as an additional technique in VPT to address postoperative sensitivity and improve the success rate of treatment. It has been proven that PBM, a non-invasive approach to the biomodulation of the dental pulp, utilizes low-level energy lasers. Though it does not provide total anesthesia (complete insensitivity to sensation), similar to infiltrative local anesthesia, it alters the behavior of neuronal cell membranes, temporarily impeding the Na-K pump, thereby interrupting impulse transmission and leading to a painkilling effect.<sup>19</sup>

Broadly, there are 2 recommended techniques for using lasers in VPT. The first one involves the direct application of the laser on the exposed pulp to promote coagulation and decontamination. The 2<sup>nd</sup> method involves using low-power lasers to arouse systemic responses from tissues.<sup>19</sup> Several studies have used various laser wavelengths with different parameters for irradiating exposed pulp tissue using the first technique, and have reported higher success rates than for the other method. For instance, a carbon dioxide laser (10,600 nm) was employed as a supplement to DPC in a study conducted by Moritz et al.<sup>20</sup> The use of 635-nm and 980-nm diode lasers in VPT offers several benefits that contribute to better results in the laser-treated group. These benefits include efficient decontamination due to the laser's ability to penetrate deeply

into the dentin and scatter significantly. The hemostatic effect is achieved through the laser's absorption by hemoglobin and melanin. Additionally, the biostimulation effect of the laser results in reduced inflammation and pain, increased cell proliferation and migration, dentinogenesis and cytodifferentiation of odontoblast-like cells, as well as the synthesis of the dentin extracellular matrix leading to the formation of reparative dentin.<sup>21,22</sup> The success rates of laser treatment were reportedly higher than those of calcium hydroxide alone, as noted in the Santucci's study.<sup>21</sup> In a study by Olivi et al., different power parameters and durations of Er:YAG lasers as an adjunct to DPC did not show any significant difference in success rates compared to other studies.<sup>22</sup> Moosavi et al. conducted a study to evaluate the effectiveness of PBM in reducing postoperative sensitivity in patients with class V cavities.<sup>12</sup> Their findings showed that patients who received PBM had significantly lower pain scores on days 1, 14 and 30, compared to those in the placebo group. Our study showed an overall success rate of 87.2% for VPT, with a success rate of 93.2% in the PBM group and 86.1% in the control group. However, there were no significant differences in the treatment success between the 2 groups. There are limited studies on postoperative pain following VPT stimulated by cold, with variations in factors such as pulp capping material, irradiation parameters and tooth type, making it difficult to compare the results.

Despite using a different laser application technique, our study showed a significant decrease in pain levels in the PBM group on day 7, similar to the findings of the previous study.<sup>23</sup> While pain levels in the PBM group significantly decreased at all 3 follow-up points, there was no significant difference in the control group. However, treatment outcomes may vary based on factors such as laser wavelength and power settings, with some studies recommending lasers with a wavelength of 700–1070 nm and 250–500 mW power, and emphasizing the importance of the proper application technique.<sup>23–25</sup> In our study, we applied the laser at the buccal and lingual gingiva over the apex, using an 8-millimeter probe to prevent potential tissue damage. Unlike other studies, we applied the laser

to the periapical area for pulp tissue biostimulation, without intervening in the filling. The aim was to determine PBM's ability to decrease postoperative sensitivity to cold after VPT in immature teeth, where tissue formation requires the presence of vital pulp and irradiation influences microcirculation in the periapical area by eliminating toxins and improving blood supply to the pulp.

Research has shown that the type of pulp capping material can affect the outcome of VPT.<sup>26,27</sup> While calcium hydroxide (CH) was previously the standard for DPC, it has become less popular due to its lack of sealing ability, degradation over time and inefficient biocompatibility. Recent studies have demonstrated better clinical outcomes with the use of mineral trioxide aggregates (MTA) or Biodentine in VPT.<sup>26,28</sup> For this reason, Biodentine was chosen as the pulp capping material for this study. While CH had a 13% success rate in the several studies published in recent 10 years, DPC with MTA showed an 80% success rate after 2 years of follow-up.<sup>28</sup> However, some researchers have reported similar outcomes for CH and MTA.<sup>29,30</sup> Nowadays, MTA is the preferred standard capping material for DPC due to its favorable properties, such as increased transcription factor levels and better biocompatibility.<sup>31,32</sup> TheraCal and Biodentine may also be used as alternative materials for indirect pulp therapy (IPT) in young permanent teeth, with a success rate of approx. 95.83% based on radiographic and clinical results.<sup>33</sup> A recent study by Sharma et al. showed that combining laser treatment with the use of Biodentine has an additional effect on the formation of tertiary dentin.<sup>34</sup> By penetrating dentinal tubules, the antibacterial laser can accelerate the formation of dentin bridges in deep caries lesions and improve the success rate of the procedure. In our study, Biodentine was used as the standard material for all VPT procedures due to its superior properties and higher success rate compared to CH in the long term.<sup>35,36</sup> Additionally, the PBM group showed a significantly greater decrease in hypersensitivity than the control group on the first 3 evaluation time points, with no reported side effects after VPT.

## Limitations

This research presents a new alternative to alleviate postoperative hypersensitivity after VPT. Photobiomodulation is a secure, non-invasive and uncomplicated approach to decrease pain and discomfort following VPT. To establish PBM as an adjuvant therapy and minimize discomfort during pulp capping procedures, extended follow-up periods and laser applications with diverse parameters must be examined. Patient age is also a critical factor to consider. Researchers have suggested that DPC is more efficient in patients under 40 years of age.<sup>36,37</sup> Thus, we focused on individuals aged 8–13 years with immature young permanent teeth indicating unfinished root development. Notably, there are no existing data


on this topic in the literature, making a direct comparison of our findings challenging. Due to the retrospective nature of this study, no sample size calculations were performed, and all appropriate patients who underwent laser application, VPT, or VPT alone during the specified study period were included. A significant limitation of our study is the non-randomized distribution of samples and the lack of evaluation of various wavelengths and capping materials. Moreover, our retrospective study had no placebo-controlled group, and the subjects, irradiation operators and examiners who performed the assessment and analyses were not blinded. The irradiated parameters were not calibrated or validated before each application, which could also affect the results.


## Conclusions


The study revealed significantly lower tooth sensitivity to cold stimulus for PBM application measured after 6 h and 1, 7, and 30 days. The results obtained after 3 months were insignificant. The present study introduced PBM as a reliable, secure and non-invasive technique to improve patient comfort by minimizing pain and discomfort after VPT procedures, especially in the initial postoperative period, the most important for diagnostic concerns. However, as this was a preliminary study, further randomized clinical studies with placebo-controlled groups are essential to explore PBM with various wavelengths and different capping materials.


## ORCID iDs

Aneta Olszewska  <https://orcid.org/0000-0003-1286-6779>

Jacek Matys  <https://orcid.org/0000-0002-3801-0218>

Tomasz Gedrange  <https://orcid.org/0000-0002-3551-6467>

Elżbieta Paszyńska  <https://orcid.org/0000-0001-7135-6264>

Magdalena Maria Roszak  <https://orcid.org/0000-0001-6495-6771>

Agata Czajka-Jakubowska  <https://orcid.org/0000-0002-1692-2910>

## References

- Guan X, Zhou Y, Yang Q, et al. Vital pulp therapy in permanent teeth with irreversible pulpitis caused by caries: A prospective cohort study. *J Pers Med*. 2021;11(11):1125. doi:10.3390/jpm11111125
- Cerqueira-Neto ACCL, Prado MC, Pereira AC, et al. Clinical and radiographic outcomes of regenerative endodontic procedures in traumatized immature permanent teeth: Interappointment dressing or single-visit? *J Endod*. 2021;47(10):1598–1608. doi:10.1016/j.joen.2021.07.013
- Ok E, Altunsoy M, Tanriver M, Capar ID, Kalkan A, Gok T. Fracture resistance of simulated immature teeth after apexification with calcium silicate-based materials. *Eur J Dent*. 2016;10(02):188–192. doi:10.4103/1305-7456.178301
- Gutmann J. Minimally invasive dentistry (endodontics). *J Conserv Dent*. 2013;16(4):282. doi:10.4103/0972-0707.114342
- Ricucci D, Loghin S, Siqueira JF. Correlation between clinical and histologic pulp diagnoses. *J Endod*. 2014;40(12):1932–1939. doi:10.1016/j.joen.2014.08.010
- Hahn C, Liewehr F. Update on the adaptive immune responses of the dental pulp. *J Endod*. 2007;33(7):773–781. doi:10.1016/j.joen.2007.01.002
- Farges JC, Alliot-Licht B, Renard E, et al. Dental pulp defence and repair mechanisms in dental caries. *Mediators Inflamm*. 2015;2015:230251. doi:10.1155/2015/230251

8. Asgary S, Ahmadyar M. Vital pulp therapy using calcium-enriched mixture: An evidence-based review. *J Conserv Dent*. 2013;16(2):92. doi:10.4103/0972-0707.108173
9. Wu Y, Zhou C, Tong X, Li S, Liu J. Histochemical localization of putative stem cells in irreversible pulpitis. *Oral Dis*. 2022;28(4):1207–1214. doi:10.1111/odi.13850
10. Krastl G, Weiger R, Ebeleseder K, Galler K. Present status and future directions: Endodontic management of traumatic injuries to permanent teeth. *Int Endodontic J*. 2022;55(Suppl 4):1003–1019. doi:10.1111/iej.13672
11. Seraj B, Ghadimi S, Hakimiha N, Kharazifard MJ, Hosseini Z. Assessment of photobiomodulation therapy by an 810-nm diode laser on the reversal of soft tissue local anesthesia in pediatric dentistry: A preliminary randomized clinical trial. *Lasers Med Sci*. 2020;35(2):465–471. doi:10.1007/s10103-019-02850-0
12. Moosavi H, Maleknejad F, Sharifi M, Ahrari F. A randomized clinical trial of the effect of low-level laser therapy before composite placement on postoperative sensitivity in class V restorations. *Lasers Med Sci*. 2015;30(4):1245–1249. doi:10.1007/s10103-014-1565-9
13. Hamblin MR. Photobiomodulation or low-level laser therapy. *J Biophotonics*. 2016;9(11–12):1122–1124. doi:10.1002/jbio.201670113
14. Chen Y, Chen XL, Zou XL, Chen SZ, Zou J, Wang Y. Efficacy of low-level laser therapy in pain management after root canal treatment or retreatment: A systematic review. *Lasers Med Sci*. 2019;34(7):1305–1316. doi:10.1007/s10103-019-02793-6
15. Islam A, Özverel CS, Yilmaz HG. Comparative evaluation of low-level laser therapy on proliferation of long-term cryopreserved human dental pulp cells isolated from deciduous and permanent teeth. *Lasers Med Sci*. 2021;36(2):421–427. doi:10.1007/s10103-020-03090-3
16. Yilmaz Y, Keles S, Mete A. Temperature changes in the pulpal chamber and the sealing performance of various methods of direct pulp capping of primary teeth. *Eur J Paediatr Dent*. 2013;14(2):95–100. PMID:23758456.
17. Yazdanfar I, Gutknecht N, Franzen R. Effects of diode laser on direct pulp capping treatment: A pilot study. *Lasers Med Sci*. 2015;30(4):1237–1243. doi:10.1007/s10103-014-1574-8
18. Zhang B, Yang BB, Gao ZY, Li L, An H. Efficiency of diode laser-assisted methods in direct pulp capping of carious teeth [in Chinese]. *Shanghai Kou Qiang Yi Xue*. 2020;29(5):554–556. PMID:33543227.
19. Javed F, Kellesarian SV, Abduljabbar T, et al. Role of laser irradiation in direct pulp capping procedures: A systematic review and meta-analysis. *Lasers Med Sci*. 2017;32(2):439–448. doi:10.1007/s10103-016-2077-6
20. Moritz A, Schoop U, Goharkhay K, Sperr W. Advantages of a pulsed CO<sub>2</sub> laser in direct pulp capping: A long-term in vivo study. *Lasers Surg Med*. 1998;22(5):288–293. doi:10.1002/(sici)1096-9101(1998)22:5<288::aid-lsm5>3.0.co;2-l.
21. Santucci PJ. Dycal versus Nd:YAG laser and Vitrebond for direct pulp capping in permanent teeth. *J Clin Laser Med Surg*. 1999;17(2):69–75. doi:10.1089/clm.1999.17.69
22. Olivi G, Genovese MD, Maturo P, Docimo R. Pulp capping: Advantages of using laser technology. *Eur J Paediatr Dent*. 2007;8(2):89–95. PMID:17571933.
23. Yazdanfar I, Barekattain M, Zare Jahromi M. Combination effects of diode laser and resin-modified tricalcium silicate on direct pulp capping treatment of caries exposures in permanent teeth: A randomized clinical trial. *Lasers Med Sci*. 2020;35(8):1849–1855. doi:10.1007/s10103-020-03052-9
24. Migliorati C, Hewson I, Lalla RV, et al; for the Mucositis Study Group of the Multinational Association of Supportive Care in Cancer/International Society of Oral Oncology (MASCC/ISOO). Systematic review of laser and other light therapy for the management of oral mucositis in cancer patients. *Support Care Cancer*. 2013;21(1):333–341. doi:10.1007/s00520-012-1605-6
25. Heidari M, Fekrazad R, Sobouti F, et al. Evaluating the effect of photobiomodulation with a 940-nm diode laser on post-operative pain in periodontal flap surgery. *Lasers Med Sci*. 2018;33(8):1639–1645. doi:10.1007/s10103-018-2492-y
26. Barthel C, Rosenkranz B, Leuenberg A, Roulet J. Pulp capping of carious exposures: Treatment outcome after 5 and 10 years. A retrospective study. *J Endod*. 2000;26(9):525–528. doi:10.1097/00004770-200009000-00010
27. Nammour S, El Mobadder M, Namour M, et al. Success rate of direct pulp capping with conventional procedures using Ca (OH)<sub>2</sub> and bioactive tricalcium silicate paste vs. laser-assisted procedures (diode 980 nm, CO<sub>2</sub>, and Er: YAG). *Photonics*. 2023;10(7):834. doi:10.3390/photonics10070834
28. Hilton TJ, Ferracane JL, Mancl L, et al. Comparison of CaOH with MTA for direct pulp capping: A PBRN randomized clinical trial. *J Dent Res*. 2013;92(7 Suppl):S16–S22. doi:10.1177/0022034513484336
29. Iwamoto CE, Adachi E, Pameijer CH, Barnes D, Romberg EE, Jefferies S. Clinical and histological evaluation of white ProRoot MTA in direct pulp capping. *Am J Dent*. 2006;19(2):85–90. PMID:16764130.
30. Tuna D, Ölmez A. Clinical long-term evaluation of MTA as a direct pulp capping material in primary teeth. *Int Endod J*. 2008;41(4):273–278. doi:10.1111/j.1365-2591.2007.01339.x
31. Youssef AR, Emara R, Taher MM, et al. Effects of mineral trioxide aggregate, calcium hydroxide, biodentine and Emdogain on osteogenesis, odontogenesis, angiogenesis and cell viability of dental pulp stem cells. *BMC Oral Health*. 2019;19(1):133. doi:10.1186/s12903-019-0827-0
32. Tabari M, Seyed Mjidi M, Hamzeh M, Ghoreishi S. Biocompatibility of mineral trioxide aggregate mixed with different accelerators: An animal study. *J Dent (Shiraz)*. 2019;21(1):48–55. doi:10.30476/dentjods.2019.77826.0
33. Rahman B, Goswami M. Comparative evaluation of indirect pulp therapy in young permanent teeth using biodentine and theracal: A randomized clinical trial. *J Clin Pediatr Dent*. 2021;45(3):158–164. doi:10.17796/1053-4625-45.3.3
34. Sharma N, Malik N, Garg Y, Singh H, Garg K, Bagaria A. Comparative evaluation of effect of lasers and biodentine in dentine regeneration: A clinical study. *J Contemp Dent Pract*. 2019;20(4):434–443. PMID:31308273.
35. Eskandarinezhad M, Ghodrati M, Pournaghi Azar F, et al. Effect of incorporating hydroxyapatite and zinc oxide nanoparticles on the compressive strength of white mineral trioxide aggregate. *J Dent (Shiraz)*. 2020;21(4):300–306. doi:10.30476/dentjods.2020.82963.1034
36. Dammaschke T, Leidinger J, Schäfer E. Long-term evaluation of direct pulp capping: Treatment outcomes over an average period of 6.1 years. *Clin Oral Invest*. 2010;14(5):559–567. doi:10.1007/s00784-009-0326-9
37. Lipski M, Nowicka A, Kot K, et al. Factors affecting the outcomes of direct pulp capping using Biodentine. *Clin Oral Invest*. 2018;22(5):2021–2029. doi:10.1007/s00784-017-2296-7

# Antioxidant, anti-inflammatory and antiseptic molecular actions of gedunin against lipopolysaccharide-induced sepsis in experimental rats

Liyun Fang<sup>1,A,D,F</sup>, Mao Zheng<sup>2,B</sup>, Fengying He<sup>2,C,F</sup>

<sup>1</sup> Department of Pediatrics, The Affiliated Hospital of Northwest University, Xi'an No.3 Hospital, China

<sup>2</sup> Department of Emergency, Xi'an Children's Hospital (Xi'an Jiaotong University Affiliated Children's Hospital), China

A – research concept and design; B – collection and/or assembly of data; C – data analysis and interpretation;

D – writing the article; E – critical revision of the article; F – final approval of the article

Advances in Clinical and Experimental Medicine, ISSN 1899–5276 (print), ISSN 2451–2680 (online)

Adv Clin Exp Med. 2024;33(7):717–728

## Address for correspondence

Fengying He

E-mail: oupula123@sina.com

## Funding sources

None declared

## Conflict of interest

None declared

Received on September 17, 2022

Reviewed on September 27, 2022

Accepted on August 24, 2023

Published online on October 19, 2023

## Cite as

Fang L, Zheng M, He F. Antioxidant, anti-inflammatory and antiseptic molecular actions of gedunin against lipopolysaccharide-induced sepsis in experimental rats.

Adv Clin Exp Med. 2024;33(7):717–728.

doi:10.17219/acem/171537

## DOI

10.17219/acem/171537

## Copyright

Copyright by Author(s)

This is an article distributed under the terms of the Creative Commons Attribution 3.0 Unported (CC BY 3.0) (<https://creativecommons.org/licenses/by/3.0/>)

## Abstract

**Background.** Sepsis is a life-threatening organ dysfunction without effective therapeutic options. Lipopolysaccharide (LPS), a bacterial endotoxin, is known to induce sepsis. It is associated with oxidative stress, inflammation and multiple organ failure. Gedunin (GN) is a tetranortriterpenoid isolated from the *Meliaceae* family. Gedunin possesses numerous pharmacological properties, including antibacterial, anti-inflammatory, antiallergic, and anticancer activities. However, the molecular anti-inflammatory mechanism of GN in sepsis has not been established.

**Objectives.** The aim of the study was to explore the antioxidant and anti-inflammatory molecular actions underlying the antiseptic activity of GN in an LPS-induced rat model.

**Materials and methods.** Rats were randomized into 4 sets: group 1 (control) was given 1 mL of dimethyl sulfoxide (DMSO) by gavage, group 2 rats were treated with LPS (100 µg/kg body weight (BW), intraperitoneally (ip.)), group 3 rats were given LPS (100 µg/kg BW, ip.)+GN (50 mg/kg BW in DMSO), and rats in the group 4 were given GN (50 mg/kg BW in DMSO) alone. We studied hepatic markers, inflammatory cytokines and antioxidants using specific biochemical kits and analyzed their statistical significance. Histopathology of liver, lungs and kidney tissues was also explored. The mRNA levels and conducted protein investigations were performed using real-time quantitative reverse transcription polymerase chain reaction (qRT-PCR) and western blot, respectively.

**Results.** Our findings revealed that GN significantly ( $p < 0.05$ ) inhibited oxidative stress, lipid peroxides, toxic markers, pro-inflammatory cytokines, and histological changes, thereby preventing multi-organ impairment. Additionally, GN attenuated the HMGβ1/NLRP3/NF-κB signaling pathway and prevented the degradation of Iκβa.

**Conclusions.** Gedunin is a promising natural antiseptic agent for LPS-induced sepsis in rats.

**Key words:** oxidative stress, sepsis, lipopolysaccharide, gedunin, HMGβ1/NLRP3/NF-κB pathway

## Background

Sepsis is triggered by microorganisms or microbial toxins, such as lipopolysaccharide (LPS). Lipopolysaccharide, an endotoxin of Gram-negative bacteria, causes a systemic inflammatory response syndrome (SIRS).<sup>1,2</sup> In the USA, 700,000 sepsis cases with more than 200,000 deaths occur annually and the condition contributes to 10% of deaths.<sup>3</sup> Sepsis is the invasion of microbes or endotoxins into cells and body fluids and it activates the inflammatory pathways.<sup>4</sup> The healing process is initiated by an inflammatory response. However, high doses of endotoxin cause imbalances in reactive oxygen species (ROS), inflammatory cytokines and homeostasis, which lead to organ dysfunction.<sup>5</sup> Lipopolysaccharide triggers the discharge of strong pro-inflammatory intermediaries, causing cardiac disorders, multiple organ disorders, tremors, and death.<sup>6,7</sup> Sepsis induces a drop in general vascular function, leading to multiple organ failure.<sup>8</sup> Almost half of the patients with septic shock develop acute renal failure (ARF) and require dialysis.<sup>9</sup> Sepsis leads to hemodynamic fluctuations such as hypotension, drop in renal blood flow, and local renal ischemia causing ARF.<sup>10</sup> Moreover, the condition causes tissue impairment, multiple organ dysfunction, acute lung disease, septic shock, and death.<sup>11,12</sup> Due to its critical nature, sepsis attracts the attention of clinicians and researchers. Thus, both in-vitro and in-vivo experiments are being conducted to find new antiseptic agents.<sup>13</sup>

An endotoxin, LPS, has been used to prompt sepsis in the experimental rat model.<sup>14</sup> Lipopolysaccharide activates the inflammatory cascade by stimulating macrophage and monocyte cell membrane receptors. This triggers nuclear factor kappa B (NF- $\kappa$ B) signaling pathways, which in turn stimulate the discharge of cytokines, pro-inflammatory intermediaries and ROS from leukocytes, plasma and blood cells.<sup>15</sup> The key cytokines, namely interleukin (IL)-1 $\beta$ , tumor necrosis factor alpha (TNF- $\alpha$ ) and IL-6, are significant controllers in the inflammatory reaction during sepsis. The TNF- $\alpha$  is a primary mediator of septic shock. It is released instantly after infection and causes the pathological progression of septic shock. In reaction to cytokines, ROS are produced from neutrophils and phagocytic cells, which trigger oxidative stress.<sup>16</sup> The free radicals produce malondialdehyde (MDA) and impair biomolecules. This leads to various chronic illnesses, namely osteoporosis, atherosclerosis, cancer, and arthritis.<sup>15,17</sup> Unrestrained inflammation and extreme oxidative stress are the prominent signs of sepsis that culminate in multiple organ failures and mortality.<sup>18</sup> Due to an excess of free radicals, oxidative stress is rummaged by antioxidant guard systems, including catalase (CAT), superoxide dismutase (SOD) and glutathione peroxidase (GSH-Px).<sup>19</sup> Hence, sepsis can be treated with antibiotics, antioxidants, corticosteroids, and anti-inflammatory mediators.

Oxidative stress is crucial in sepsis-associated transience and multi-organ impairment.<sup>16,18</sup> Many researchers have been attentive to anti-cytokines, drug targets and antioxidants to control the pathophysiology of sepsis-prompted acute lung injury (ALI).<sup>13,19</sup> The high mobility group box (HMG $\beta$ 1) protein plays a vital part in the development and evolution of sepsis-prompted lung damage.<sup>20</sup> The HMG $\beta$ 1 is stimulated by immune cells, such as macrophages, dendritic cells and mononuclear cells, and induced by inflammatory cytokines and endotoxins.<sup>21</sup> Hence, the restraint of HMG $\beta$ 1 discharge mitigates SIRS and sepsis-induced organ injury.<sup>22</sup> A previous study on the activation of inflammatory caspases and processing of pro-IL- $\beta$  also highlighted the key role of NOD-like receptor protein 3 (NLRP3) inflammasomes in inflammation.<sup>23</sup> Increased NLRP3 expression causes the secretion of pro-inflammatory cytokines, immune cell gathering, and augmented stimulation of the adaptive immune reaction.<sup>23,24</sup> Hou et al.<sup>25</sup> described that NLRP3 facilitated the increased secretion of HMG $\beta$ 1 in lung injury. Thus, drugs targeting the inhibition of HMG $\beta$ 1 and NLRP3 have a possible role in the treatment of sepsis and associated lung failure. Potent antioxidant and anti-inflammatory activities might reduce the severity of sepsis. Isik et al.<sup>26</sup> demonstrated that sentinel lymph node biopsy (SLNB) is the accepted approach to stage the clinically negative axilla, and the incidence of lymphedema (LE) after SLNB is about 5%. Furthermore, the authors hypothesized that patients undergoing axillary excision of >5 lymph nodes (LNs) were at an increased risk of developing LE.

Gedunin (GN) is the main tetranortriterpenoid sequestered from the neem tree. Gedunin is identified to restrain the stress-prompted chaperone heat shock protein, Hsp90.<sup>27</sup> Blocking Hsp90 produces a multi-directed beneficial method since Hsp90 proteins are associated with numerous transcription factors and kinases, particularly NF- $\kappa$ B.<sup>28</sup> The Hsp90 regulators diminish inflammation in various experimental models, such as atherosclerosis, uveitis and lung inflammation.<sup>29,30</sup> Gedunin can restrain prostate gland, ovary and colon cancer cell proliferation.<sup>31,32</sup> It also subdues articular inflammation in a zymosan-induced acute articular inflammation model.<sup>33</sup> Gedunin affixes to MD-2, damages TLR4/MD-2/CD14 pathways, and reduces LPS-stimulated inflammatory reactions in macrophages in silico and surface plasmon resonance studies.<sup>34</sup> However, the anti-inflammatory, antioxidant and in-vivo antiseptic efficacy of GN in LPS-induced sepsis has not yet been evaluated.

## Objectives

Hence, the current research explores the molecular actions underlying the antioxidant, anti-inflammatory and antiseptic activity of GN in the LPS-induced rat model.



## Materials and methods

### Chemicals

Gedunin, LPS, dimethyl sulfoxide (DMSO), antibodies, antibiotics, and all the biochemicals were obtained from Gibco (Carlsbad, USA). The antibodies for western blot analysis were acquired from Santa Cruz Biotechnology (Santa Cruz, USA).

### Trial animals

A total of 40 Wistar albino male rats weighing 225–250 g were obtained from Xi'an Yifengda Biotechnology Co., Ltd (Xi'an, China). Rats were housed in aseptic polypropylene cages under fixed laboratory circumstances. The animals were nourished with a regular pellet diet ad libitum. Rats were adapted for 7 days before the experiments. The trial was approved by the of Xi'an Zhongkai Animal Experiments Medical Research Ethics Committee (approval No. 4894).

### Experimental design

The animals were randomized into 4 sets of 10 rats each. Group 1 was the control group and was given 1 mL of DMSO for 10 days by gavage. The rats in the group 2 were given a single dosage of LPS (100 µg/kg body weight (BW), intraperitoneally (ip.)). Group 3 rats were administered LPS (100 µg/kg b.w., i.p.)+GN (50 mg/kg b.w. in DMSO). The rats in the group 4 were treated with GN (50 mg/kg b.w. in DMSO) alone. A single intraperitoneal dose of LPS was injected, and 1 mL of GN was given daily for 10 days by alimentation. After the experiment, all animals were anesthetized and euthanized by cervical dislocation.

### Sample preparation

The blood of the rats was drawn through cardiac puncture and centrifuged at 4,000 rpm. The serum was separated and preserved at –80°C. The residual serum was recollected at 4°C to estimate hepatic markers. Tissues (liver, kidney and lung) were dissected and divided into 2 parts. One portion was kept at –80°C for antioxidant assessments. The second part of the tissues was fixed in 10% formalin for histopathological assessment.<sup>35</sup>

### Biochemical assessments

For biochemical analyses, tissues of the rats' liver, kidney and lung were washed with deionized ice-cold water. One gram of tissue sample was treated with phosphate-buffered saline (PBS, pH: 7.2, 1:9 ratio) and was homogenized. Afterward, the homogenate was centrifuged for 1 h, and the supernatant was analyzed. Malondialdehyde, CAT, SOD, and GSH-Px were determined by the kits acquired

from Elabscience (Wuhan, China). Cytokine levels were quantified by enzyme-linked immunosorbent assay (ELISA) kit (Cayman Chemical, Ann Arbor, USA) as per the manufacturer's protocol. Toxicity markers (aspartate aminotransferase (AST) and alanine transaminase (ALT)) were assayed using kits delivered by Cayman Chemical, according to the manufacturer's instruction.

### Histopathological analysis

Liver, kidney and lung tissues were preserved with formaldehyde (10%), fixed in paraffin blocks, cut into slices, and stained with hematoxylin and eosin (H&E). Successively, stained tissues were identified for histological changes and inflammation under a light microscope (model CX33; Olympus Corp., Tokyo, Japan).

### Determination of mRNA levels by qRT-PCR

The total RNA of lung tissue was sequestered using TRIzol<sup>®</sup> reagent (Abcam, Waltham, USA), according to the manufacturer's protocol. The isolated RNA was converted to cDNA through reverse transcription by using a high-capacity cDNA Reverse Transcription Kit (Beyotime Biotechnology). FastStart SYBR Green Master Mix (Abcam) was used to explore the cDNAs. The band intensity was scrutinized with 1.5% agarose gel electrophoresis. Finally, the band intensity was measured by Image J v. 1.48 software (National Institutes of Health, Bethesda, USA). The fold variations were calculated using the  $2^{-\Delta\Delta Ct}$  formula. The used real-time quantitative reverse transcription polymerase chain reaction (qRT-PCR) primer sequences are as follows (Table 1):

Table 1. Primer list

Gene	Primer sequences
<i>HMGB1</i>	F: 5'-TTGTGCAAACTTGCCGGGAGGA-3' R: 5'-ACTTCTCCTTCAGCTTGGCAGC-3'
<i>NLRP3</i>	F: 5'-GGAGGAGGAGGAAGAGGAGATA-3' R: 5'-AGGACTGAGAAGATGCCACTAC-3'
<i>NF-κB</i>	F: 5'-GATCACACAGGCCGGACAAT-3' R: 5'-CTCGGCTACACTCAGATCG-3';
<i>IL-1β</i>	F: 5'-CCTGTGTGATGAAAGACGGC-3' R: 5'-TATGTCCCACCATGTGCTGT-3'
<i>TNF-α</i>	F: 5'-AGCCACGTCGTAGCAAACCAACAA-3; R: 5'-AACACCCATTCCCTTAC-AGAGCAAT-3'
<i>β-actin</i>	F: 5'-CCACCATGTATCCAGGCATT-3' R: 5'-AGGGGTGAAAACGCAGCTCA-3'

### Western blotting analysis

Hepatic tissue was dissected 12 h after the induction of sepsis.<sup>33</sup> The tissues were cleaned twice with PBS and lysed with a cold lysis buffer consisting of 0.01% protease inhibitor. Then, these were preserved on ice for half an hour. The lysate was cold (4°C) and centrifuged for 10 min at 13,000 rpm, and the resulting solution was

passed through sodium dodecyl-sulfate polyacrylamide gel electrophoresis (SDS-PAGE) (10%) and shifted electrophoretically to the polyvinylidene difluoride (PVDF) film. Then, 5% of fat-free milk was used to block the membrane. Next, it was conserved with the primary antibodies, namely IRAK-1 (sc-5288), TRAF-6 (sc-8409), I $\kappa$ B $\alpha$  (sc-1643), MyD88 (sc-74532), and  $\beta$ -actin (sc-69879), followed by horseradish peroxidase-conjugated secondary antibodies (1:500 dilution). The  $\beta$ -actin was utilized as a reference. The membrane was reviewed using enhanced chemiluminescence (ECL) (Millipore, Burlington, USA).

## Statistical analysis

All statistical analyses were conducted using GraphPad Prism v. 8.0.1 (GraphPad Software, San Diego, USA) and SPSS v. 25 (IBM Corp., Armonk, USA) software.

The measurement data were reported as median and quartiles. The normality of the distribution was tested using the Kolmogorov–Smirnov test. All parameters had normal distribution for which we used a nonparametric test due to small sample sizes. The comparison among groups was performed using the nonparametric Kruskal–Wallis test, followed by Dunn’s test to compare variables among the groups. When the test standard had a value of  $p < 0.05$ , the difference was considered statistically significant.

## Results

All variables had a normal distribution. Table 2 demonstrates the results of compared variables among the groups.

**Table 2.** Comparison of the study groups

Variables	Group 1 (control) (n = 6)	Group 2 (n = 6)	Group 3 (n = 6)	Group 4 (n = 6)	p-value*
AST_Serum	108.26 (98.47–117.95)	204.4 (185.91–222.69)	140.47 (127.76–153.04)	109.15 (99.28–118.92)	<0.001
ALT_Serum	58.38 (53.10–63.60)	96.85 (88.09–105.51)	70.96 (64.55–77.31)	59.04 (53.70–64.32)	<0.001
IL-1 $\beta$ _Serum	255.23 (232–278)	597 (543–650)	418 (380–455)	262 (238–285)	<0.001
IL-10_Serum	105 (95–114)	243 (221–264)	160 (145–174)	102 (93–111)	<0.001
TNF- $\alpha$ _Serum	50 (45–54)	310 (282–338)	171 (155–186)	55 (50–59)	<0.001
IL-6_Serum	1570 (1428–1711)	3682 (3348–4011)	2521 (2293–2747)	1555 (1415–1695)	<0.001
MDA_Liver	0.51 (0.41–0.56)	0.77 (0.70–0.84)	0.54 (0.49–0.59)	0.47 (0.43–0.51)	0.001
SOD_Liver	0.19 (0.17–0.21)	0.09 (0.08–0.1)	0.16 (0.15–0.17)	0.18 (0.16–0.20)	<0.001
GSH-Px_Liver	95 (86–103)	52 (47–56)	72 (65–78)	95 (86–103)	<0.001
CAT_Liver	1.2 (1.09–1.31)	0.93 (0.85–1.01)	1.07 (0.97–1.17)	1.19 (1.08–1.30)	0.001
MDA_Kidney	0.60 (0.55–0.65)	0.75 (0.68–0.82)	0.62 (0.56–0.68)	0.52 (0.47–0.57)	0.001
SOD_Kidney	0.19 (0.17–0.21)	0.11 (0.10–0.12)	0.15 (0.14–0.16)	0.18 (0.16–0.20)	<0.001
GSH-Px_Kidney	87 (79–95)	56 (51–61)	80 (73–87)	85 (77–92)	0.002
CAT_Kidney	0.56 (0.51–0.61)	0.32 (0.29–0.35)	0.52 (0.47–0.57)	0.55 (0.50–0.60)	0.003
MDA_Lung	0.73 (0.66–0.80)	1.19 (1.08–1.30)	0.87 (0.79–0.95)	0.71 (0.65–0.77)	<0.001
SOD_Lung	0.17 (0.15–0.19)	0.08 (0.07–0.09)	0.13 (0.12–0.14)	0.16 (0.15–0.17)	<0.001
GSH-Px_Lung	57 (52–62)	25 (23–27)	42 (39–46)	56 (51–61)	<0.001
CAT_Lung	0.70 (0.64–0.76)	0.28 (0.25–0.31)	0.48 (0.44–0.52)	0.69 (0.63–0.75)	<0.001
HMG $\beta$ 1_Lung	1 (0.91–1.09)	3.6 (3.28–3.92)	2.59 (2.36–2.82)	1.48 (1.35–1.61)	<0.001
NLRP3_Lung	1 (0.91–1.09)	7.21 (6.56–7.86)	4.14 (3.77–4.51)	1.75 (1.59–1.91)	<0.001
NF- $\kappa$ B_Lung	1 (0.91–1.09)	6.43 (5.85–7.01)	3.50 (3.19–3.82)	2.37 (2.16–2.58)	<0.001
IL-1 $\beta$ _Lung	1 (0.91–1.09)	8.90 (8.10–9.70)	3.86 (3.51–4.21)	1.95 (1.77–2.13)	<0.001
TNF- $\alpha$ _Lung	1 (0.91–1.09)	1.20 (1.09–1.31)	1.01 (0.92–1.10)	0.95 (0.86–1.04)	0.005
IRAK-1_Lung	1 (0.91–1.09)	1.64 (1.49–1.79)	1.29 (1.17–1.41)	0.95 (0.86–1.04)	<0.001
TRAF6_Lung	1 (0.91–1.09)	1.53 (1.39–1.67)	1.22 (1.11–1.33)	1.08 (0.98–1.18)	<0.001
I $\kappa$ B $\alpha$ _Lung	1 (0.91–1.09)	0.28 (0.25–0.31)	0.60 (0.55–0.65)	0.95 (0.86–1.04)	<0.001
MyD88_Lung	1 (0.91–1.09)	1.16 (1.06–1.26)	1 (0.91–1.09)	0.82 (0.75–0.89)	0.001

AST – aspartate aminotransferase; ALT – alanine transaminase; IL – interleukin, TNF- $\alpha$  – tumor necrosis factor alpha; MDA – malondialdehyde; SOD – superoxide dismutase; GSH-Px – glutathione peroxidase; CAT – catalase; NLRP3 – NOD-like receptor protein 3; HMG $\beta$ 1 – high mobility group box protein 1; NF- $\kappa$ B – nuclear factor kappa B; \*p-value was generated from Kruskal–Wallis test. Data were presented as median (Q1 and Q3). There was a significant difference among all groups in Dunn’s test.

## GN reduces hepatic toxicity enzyme markers

Hepatic toxicity serum enzymes (AST and ALT) were significantly elevated ( $p < 0.05$ ) in LPS-treated septic rats compared to controls (Fig. 1A,B). The hepatic enzyme levels were reduced in the LPS-treated GN group. Normal marker enzyme levels were detected in the GN alone-treated rats and control rats. Hence, GN may be effective in reducing liver damage.

## GN alleviates pro-inflammatory cytokine levels

The serum cytokines, namely IL-6, IL-10, IL-1 $\beta$ , and TNF- $\alpha$ , were significantly elevated ( $p < 0.05$ ) in LPS-induced sepsis animals (Fig. 2A–D). The cytokine levels declined in the GN+LPS-prompted septic rats. Cytokine levels in control rats and GN alone-treated rats were similar.

## Effect of GN on MDA and antioxidant enzymes in hepatic tissue

Malondialdehyde levels in liver tissue were significantly higher ( $p < 0.05$ ), and antioxidant enzyme (SOD, CAT and GSH-Px) levels were lower in the LPS-induced sepsis animals compared to the control rats (Fig. 3A–D). The GN+LPS-treated rats had significantly decreased ( $p < 0.05$ ) MDA levels and increased antioxidant enzymes compared to the LPS alone-treated rats. The GN alone-treated rats had similar results to the control rats.

## Effect of GN on MDA and antioxidant enzymes in kidney tissue

Malondialdehyde levels were significantly increased in kidney tissues ( $p < 0.05$ ), and antioxidant enzyme (SOD, CAT and GSH-Px) levels were alleviated

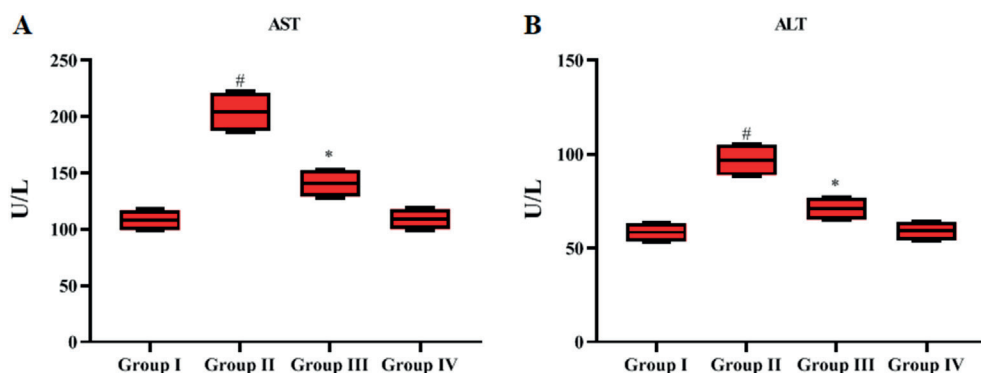


**Fig. 1.** Gedunin (GN) alleviates hepatic toxicity marker enzymes. Aspartate aminotransferase (AST) (A) and alanine transaminase (ALT) (B) in the serum of a lipopolysaccharide (LPS)-induced septic rat model. The data were generated from the nonparametric Kruskal–Wallis and Dunn’s post-hoc tests

group I – the control group; group II – LPS-treated rats; group III – LPS+GN-treated rats; group IV – GN alone-treated rats; # $p < 0.01$  compared to group II; \* $p < 0.05$  compared to group III.

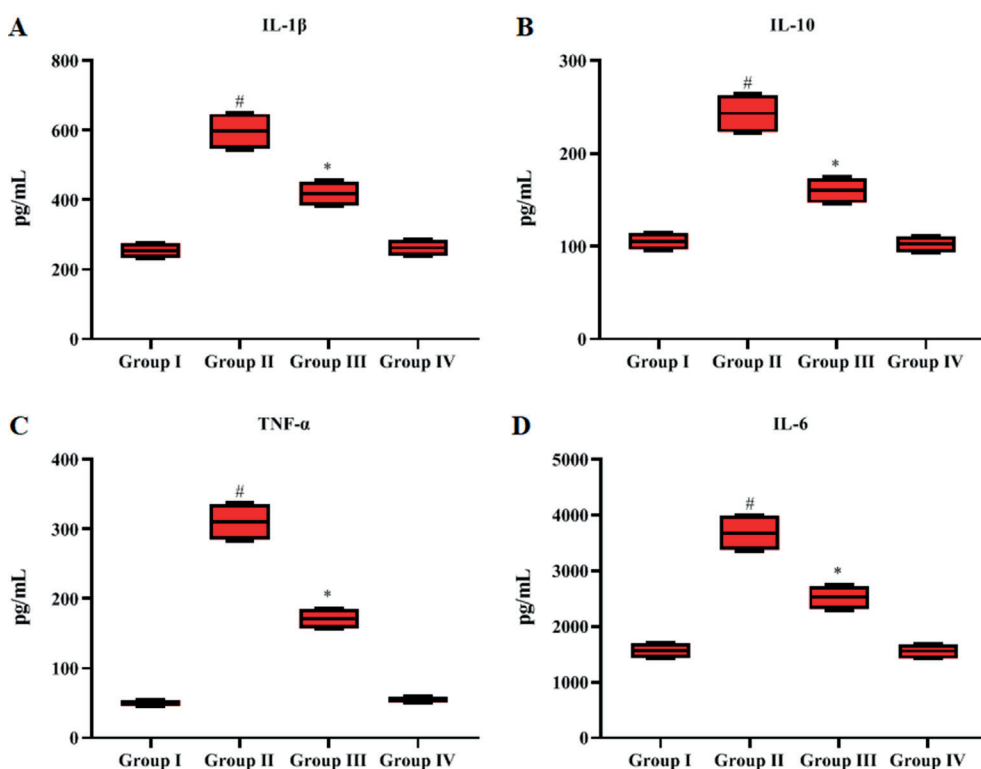


**Fig. 2.** Gedunin (GN) lessens pro-inflammatory cytokines. Interleukin-1 beta (IL-1 $\beta$ ) (A), interleukin-10 (IL-10) (B), tumor necrosis factor-alpha (TNF- $\alpha$ ) (C), and interleukin-6 (IL-6) (D) levels in the serum of the lipopolysaccharide (LPS)-prompted septic rat model. The data were generated from the nonparametric Kruskal–Wallis and Dunn’s post-hoc tests

group I – the control group; group II – LPS-treated rats; group III – LPS+GN-treated rats; group IV – GN alone-treated rats; # $p < 0.01$  compared to group II; \* $p < 0.05$  compared to group III.

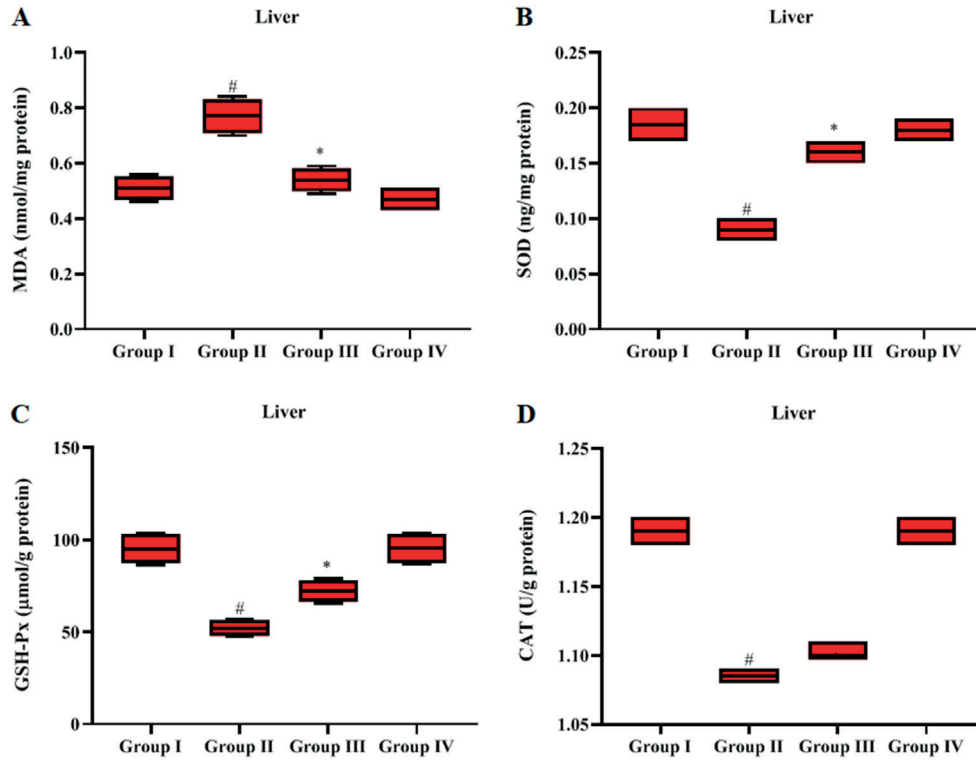


**Fig. 3.** Influence of gedunin (GN) on malondialdehyde (MDA) (A), superoxide dismutase (SOD) (B), glutathione peroxidase (GSH-Px) (C), and catalase (CAT) (D) activity in hepatic tissues in the lipopolysaccharide (LPS)-induced septic rat model. The data were generated from the nonparametric Kruskal–Wallis and Dunn’s post-hoc tests

group I – the control group; group II – LPS-treated rats; group III – LPS+GN-treated rats; group IV – GN alone-treated rats; <sup>#</sup> $p < 0.01$  compared to group II; <sup>\*</sup> $p < 0.05$  compared to group III.

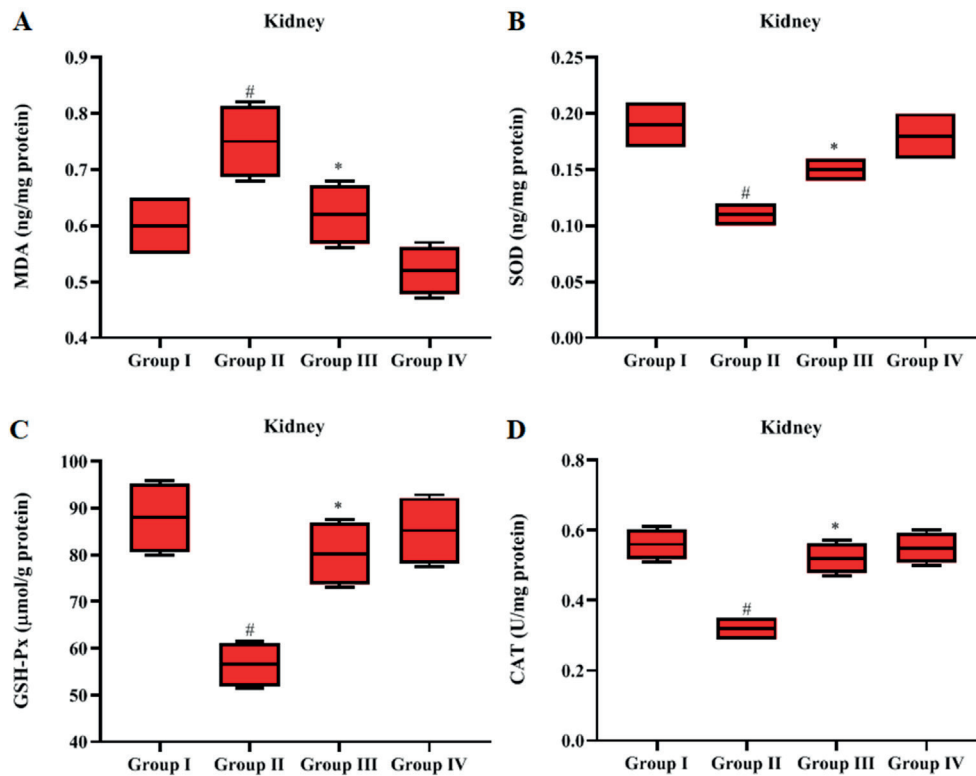


**Fig. 4.** Influence of gedunin (GN) on malondialdehyde (MDA) (A), superoxide dismutase (SOD) (B), glutathione peroxidase (GSH-Px) (C), and catalase (CAT) (D) activity in kidney tissues in a lipopolysaccharide (LPS)-induced septic rat model. The data were generated from the nonparametric Kruskal–Wallis and Dunn’s post-hoc tests

group I – the control group; group II – LPS-treated rats; group III – LPS+GN-treated rats; group IV – GN alone-treated rats; <sup>#</sup> $p < 0.01$  compared to group II; <sup>\*</sup> $p < 0.05$  compared to group III.

in the LPS-induced septic rats compared to the controls (Fig. 4A–D). The GN+LPS-treated rats had significantly reduced ( $p < 0.05$ ) MDA levels and enhanced antioxidant enzymes in comparison to the LPS alone-treated rats. The GN alone-treated rats displayed similar results as controls.

### Effect of GN on MDA and antioxidant enzymes in lung tissue

Malondialdehyde levels in lung tissues were significantly increased ( $p < 0.05$ ), and antioxidant enzyme (SOD, CAT and GSH-Px) levels were reduced in the LPS-induced

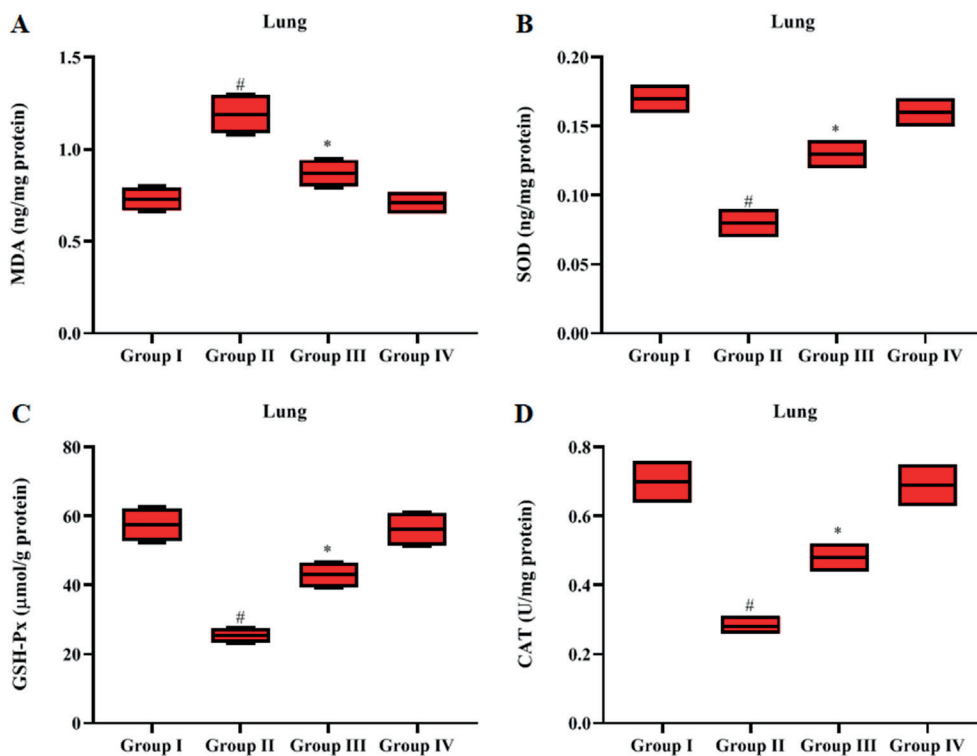


**Fig. 5.** Influence of gedunin (GN) on malondialdehyde (MDA) (A), superoxide dismutase (SOD) (B), glutathione peroxidase (GSH-Px) (C), and catalase (CAT) (D) activity in lung tissues in a lipopolysaccharide (LPS)-induced septic rat model. The data were generated from the nonparametric Kruskal–Wallis and Dunn’s post-hoc tests

group I – the control group; group II – LPS-treated rats; group III – LPS+GN-treated rats; group IV – GN alone-treated rats; #  $p < 0.01$  compared to group II; \*  $p < 0.05$  compared to group III.

septic rats in contrast to the control rats (Fig. 5A–D). The GN+LPS-treated rats had significantly reduced ( $p < 0.05$ ) MDA levels and augmented antioxidant enzymes as compared to the LPS alone-treated rats. The GN alone-treated rats presented similar results as controls.

### Effect of GN on histopathological analysis of liver, kidney and lung tissues

Figures 6A–C exhibit the histopathological examination of the liver, kidneys and lungs in control and experimental rats. Histopathological damages and lesions were absent in the hepatic, kidney and lung tissues of control and GN alone-treated rats. Lipopolysaccharide caused severe inflammation and damage to hepatic tissues, as well as inter-alveolar septum condensing, hyperemia, and severe inflammation in the peri-bronchiolar and peri-vascular regions of the lungs. Moreover, it induced modest assembly of the hyaline cylinder in the lumen of renal tubules, mild relapse of tubular epithelium, and serious interstitial vessel hyperemia in renal tissues. The GN-treated septic rats demonstrated mild renal tubule lumens and extinct deterioration in the tubular hyperemia in comparison to the LPS-prompted septic rats. Only mild inflammation of hepatic tissue was present in the GN-supplemented septic rats. The GN group presented with condensed interstitial thickening and inflammation in the lungs in contrast to the LPS-stimulated sepsis animals.

### GN alleviates mRNA expression of inflammatory mediators in lung tissues of LPS-induced septic rats

To assess whether GN (50 mg/kg BW) mitigated inflammation in lung tissues of septic rats, the HMG $\beta$ 1, NF- $\kappa$ B, NLRP3, TNF- $\alpha$ , and IL-1 $\beta$  mRNA levels were evaluated (Fig. 7A–E). The levels of HMG $\beta$ 1, NF- $\kappa$ B, NLRP3, TNF- $\alpha$ , and IL-1 $\beta$  mRNA were significantly enhanced ( $p < 0.05$ ) in the LPS-induced septic rats as compared to the control group. The administration of GN significantly attenuated ( $p < 0.05$ ) these inflammatory mediators in contrast to the LPS-prompted septic rats (Fig. 7).

### GN attenuates the protein expression of IRAK-1, TRAF-6, MYD88, and I $\kappa$ B $\alpha$ in hepatic tissues of LPS-induced septic rats

In the western blot analysis, we found that the protein levels of IRAK-1, TRAF-6 and MYD88 were augmented, whereas I $\kappa$ B $\alpha$  levels declined in the hepatic tissues of LPS-prompted sepsis animals (Fig. 8A–E). It was observed that GN reduced IRAK-1, TRAF-6 and MyD88 levels, and enhanced I $\kappa$ B $\alpha$  protein levels in hepatic tissues. The stimulation of NF- $\kappa$ B is regulated by I $\kappa$ B $\alpha$  proteins, and they inhibit NF- $\kappa$ B triggering. The I $\kappa$ B $\alpha$  expression was suppressed in LPS-induced septic rats. Gedunin inhibited the degradation of I $\kappa$ B $\alpha$ .

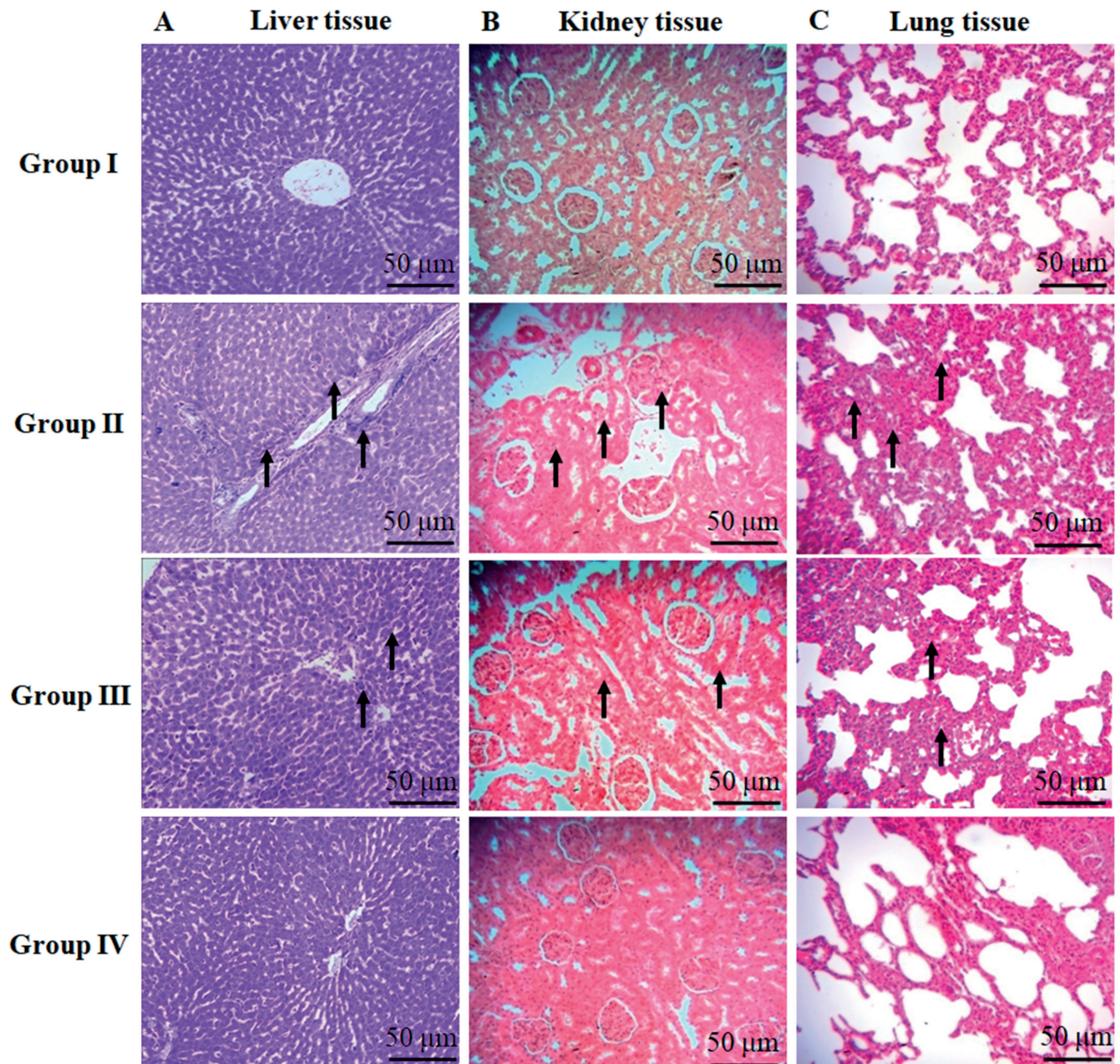


**Fig. 6.** A. Effect of gedunin (GN) on the histopathology of hepatic tissues in the lipopolysaccharide (LPS)-induced septic rat model. Control rats revealed normal histology of hepatic tissues. The hepatic tissues of LPS-induced septic rats displayed severe inflammation and hepatic impairments. The LPS+GN-treated rats exhibited only mild inflammation of liver tissues. Normal liver histology was detected in the GN-alone treated group (stained with hematoxylin and eosin (H&E), magnification (×40), scale bar = 50 µm); B. Effect of GN on the histopathology of kidney tissues in the LPS-prompted septic rat model. Control rats represented normal histology of kidney tissues. The LPS-induced renal tissue revealed a modest gathering of hyaline cylinders in the lumen, minor relapses of tubular epithelium, and serious interstitial vessel hyperemia. The LPS+GN-treated septic rats had mild renal tubule lumens and extinct degeneration in the tubular hyperemia. Normal renal histology can be viewed in the GN alone-treated group (stained with H&E, magnification (×40), scale bar = 50 µm); C. Influence of GN on the histopathology of lung tissues in the LPS-prompted septic rat model. Control rats showed normal histology of lung tissues. The LPS-induced lung tissue represents interalveolar septum condensing, hyperemia, severe inflammation in the peri-bronchiolar and peri-vascular region, and moderate inflammation of the interalveolar septum. The lung tissues of the LPS+GN-treated rats revealed condensed interstitial thickening and inflammation, noticing only mild inflammation. Normal lung histology can be viewed in the GN alone-treated group (stained with H&E, magnification (×40), scale bar = 50 µm)

group I – the control group; group II – LPS-treated rats; group III – LPS+GN-treated rats; group IV – GN alone-treated rats.

## Discussion

Septic shock is one of the stages of SIRS, which subsequently causes multiple organ failure. An endotoxin, LPS, is a powerful stimulator that activates macrophages

or monocytes in order to produce assorted pro-inflammatory cytokines.<sup>1,2</sup> The LPS-prompted septic rat model behaves like a human disease.<sup>13,14</sup> Sepsis causes uneven immune reactions, oxidative stress and mitochondrial disorders.<sup>11,12</sup> Meanwhile, an immune reaction in sepsis

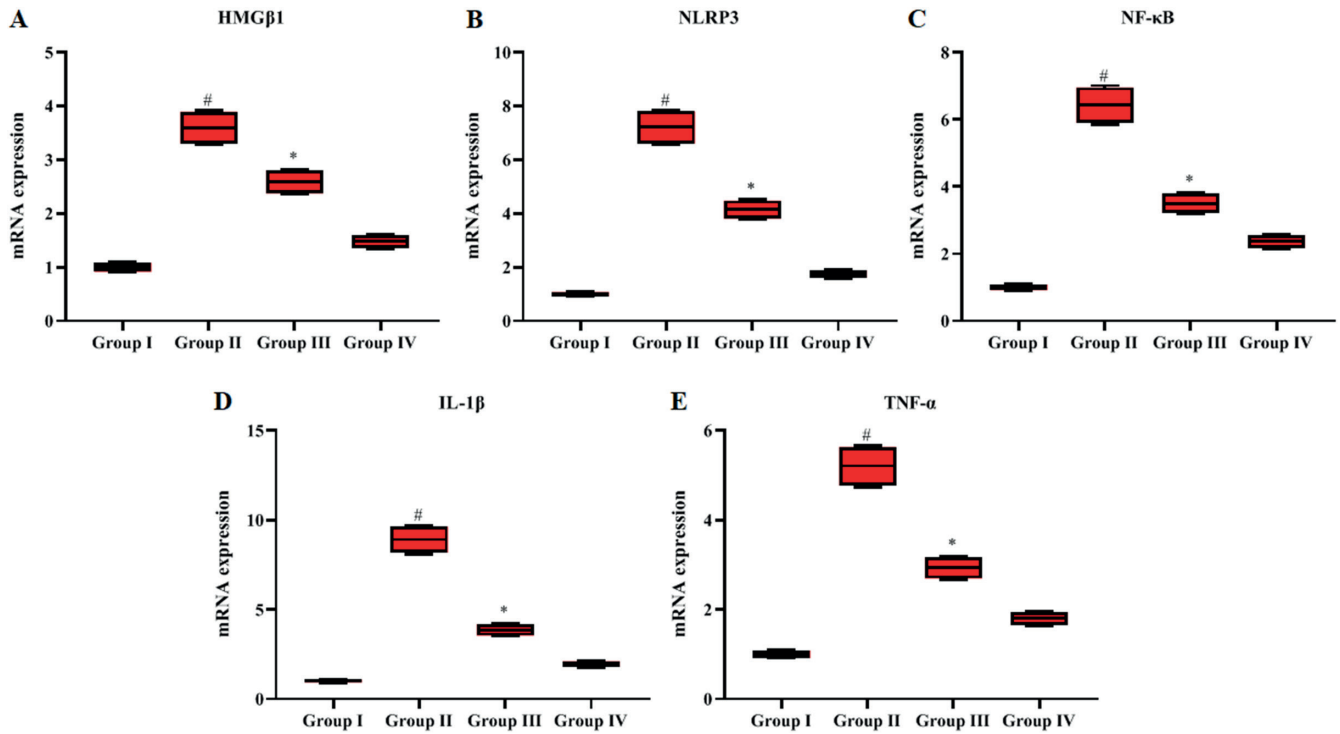


Fig. 7. Influence of gedunin (GN) on mRNA levels in lung tissues in the LPS-prompted septic rat model. The mRNA expression levels of high-mobility group box 1 (HMGβ1) (A), nucleotide-binding domain (NOD)-like receptor protein 3 (NLRP3) (B), nuclear factor kappa B (NF-κB) (C), interleukin-1β (IL-1β) (D), and tumor necrosis factor alpha (TNF-α) (E) were measured using real-time quantitative reverse transcription polymerase chain reaction (qRT-PCR). The data were generated from the nonparametric Kruskal–Wallis and Dunn’s post-hoc tests

group I – the control group; group II – LPS-treated rats; group III – LPS+GN-treated rats; group IV – GN alone-treated rats; #p < 0.01 compared to group I; \*p < 0.05 compared to group III.

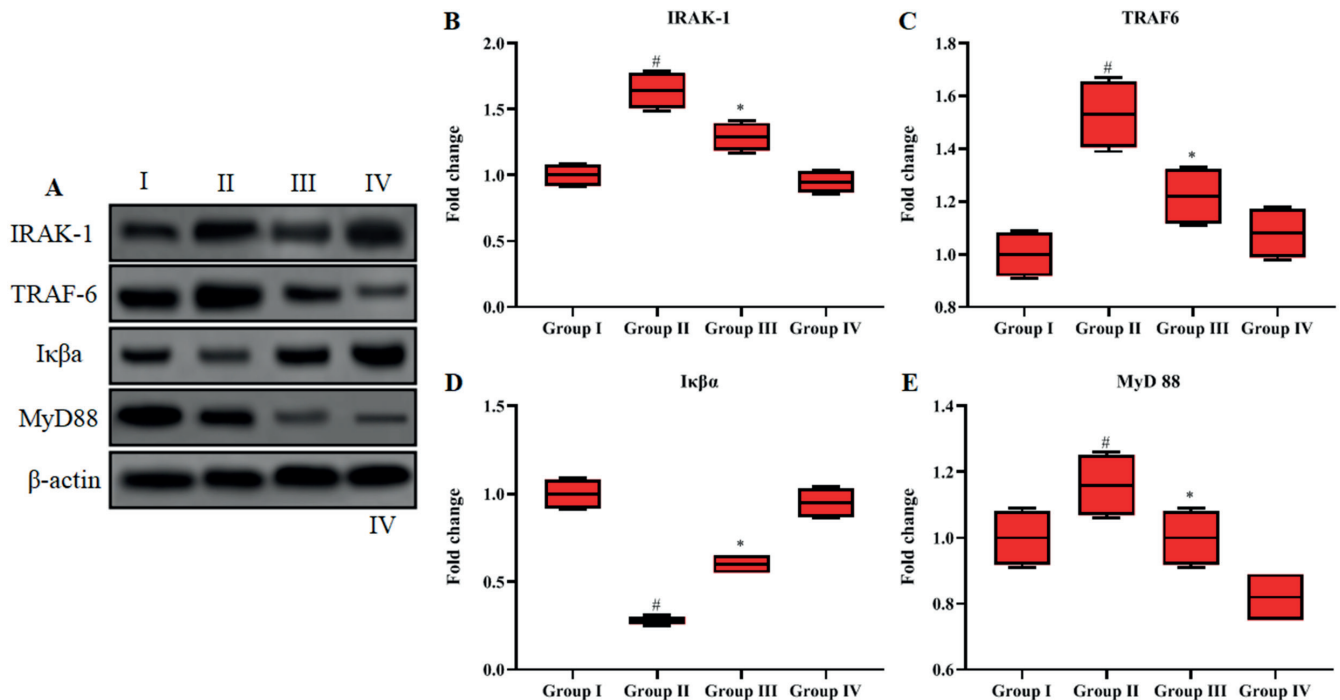


Fig. 8. A. This representative photograph shows the comparative protein expression in western blots. The band intensities were quantified by densitometry and normalized to the respective β-actin loading controls. Related protein expression of interleukin-1 receptor-associated kinase 1 (IRAK-1) (B), tumor necrosis factor receptor-associated factor 6 (TRAF-6) (C), inhibitory protein κBa (Iκβa) (D), and myeloid differentiation primary response 88 (MyD88) (E) were assessed with western blots. The data were generated from the nonparametric Kruskal–Wallis and Dunn’s post-hoc tests

group I – the control group; group II – LPS-treated rats; group III – LPS+GN-treated rats; group IV – GN alone-treated rats; #p < 0.01 compared to group I; \*p < 0.05 compared to group III.

is an exceptionally complex single antimicrobial remedy that appears to be enough to increase survival. Antioxidants play a defensive role in sepsis-associated inflammation and oxidative stress.<sup>13,19</sup> The efficacy of medications in sepsis treatment via LPS-triggered cytokines and stimulated signals has been reported.<sup>13,14,33,34</sup> Thus, we aimed to evaluate the anti-inflammatory and antioxidant effects of GN on an LPS-induced rat model. Gedunin significantly reduced cytokines, chemokines and pro-inflammatory mediators, and enhanced the antioxidant activities in our LPS-prompted septic rat model. Numerous studies have previously proposed that GN exerts anti-inflammatory and antioxidant activities in lung inflammation, acute articular inflammation and LPS-induced inflammation models.<sup>30,33,34</sup>

The generation of increased free radicals leads to oxidative damage. Extreme oxidative stress is a unique feature of LPS. Sustained vascular inflammation and oxidative stress due to LPS stimulation are distinctive features in sepsis.<sup>18</sup> The antioxidant resistance is due to a variety of antioxidants: CAT, SOD and GSH-Px. Our study shows that LPS modifies the antioxidant enzymes and thiobarbituric acid reactive substances (TBARS), and GN treatment prevents oxidative stress. Increased TBARS formation and reduced antioxidant levels confirm LPS-induced lipid peroxidation. Gedunin treatment inhibited this peroxidation. This result is in agreement with previous studies which reported that GN, neem leaf and bark extract reversed elevated MDA levels and enhanced the antioxidant status.<sup>36,37</sup> Hence, GN could reduce oxidative stress and exert protection against free radicals generated by LPS-induced sepsis in rat models.

Numerous studies have indicated that inflammatory cytokines, particularly TNF- $\alpha$ , play a vital role in LPS-prompted sepsis and endotoxin shock.<sup>16</sup> Tumor necrosis factor alpha, a pleiotropic cytokine, is responsible for multiple physiological functions and is released by various immune cells due to LPS triggers.<sup>38</sup> The ELISA tests identified LPS serum cytokines in rats. Lipopolysaccharide enhanced the levels of inflammatory cytokines (TNF- $\alpha$ , IL-10, IL-1 $\beta$ , and IL-6) and GN reduced them. These results establish that GN can constrain the secretion of inflammatory cytokines and block inflammatory reactions. Previous reports have also suggested that GN reduces inflammatory cytokines and inflammatory mediators in experimental animals.<sup>33,34</sup> The HMGB1 functions as an extracellular signal molecule and has a role at the molecular level in inflammation, cell diversity, relocation, and metastasis.<sup>39</sup> In an earlier study, an increase in HMGB1 led to a subsequent increase in TNF- $\alpha$ , which resulted in the release of IL-6, reflecting co-activation between early inflammatory cytokines and HMGB1.<sup>40</sup> The HMGB1 acts as a controller or modulator in the organ responses to sepsis. In the current trial, HMGB1 was significantly augmented in the LPS-induced septic rats, and significantly reduced in the GN-treated

animals. Thus, GN prevents the inflammatory reaction of sepsis in the lungs by attenuating HMGB1 and thus protects against lung damage. To the best of our knowledge, the action of GN on HMGB1 has not been previously explored. Our study is the first one to reveal the impact of GN on HMGB1.

Recently, it has been discovered that HMGB1 amplifies TLR-facilitated activation of NF- $\kappa$ B.<sup>41</sup> Nuclear factor kappa B plays a crucial role in controlling the gene transcription of pro-inflammatory cytokines.<sup>42</sup> Preceding trials have explored the pathways of NF- $\kappa$ B stimulation and signal transduction in the pathophysiology of sepsis. The NF- $\kappa$ B, a transcription element, prompts an upsurge of cytokines (IL-6 and TNF- $\alpha$ ) to initiate inflammation and apoptosis.<sup>43,44</sup> The multi-protein signaling complexes, such as inflammasomes, promote the stimulation of caspases and IL-1 $\beta$ . The NLRP3 is a renowned inflammasome that is associated with autoimmune disorders. It is also a key target for anti-inflammatory treatments.<sup>45</sup> Control of HMGB1 improves inflammation and sepsis-promoted lung damage by restraining NLRP3 through the NF- $\kappa$ B pathways.<sup>46</sup> Our findings demonstrate that GN causes anti-inflammatory action in septic lungs by subduing NF- $\kappa$ B activation, which results in reduced levels of HMGB1, NLRP3 and pro-inflammatory cytokines. Thus, due to its anti-inflammatory and antioxidant properties, GN protects against lung impairment.

Sepsis causes hyper-expression of inflammatory moderator systems to produce cytokines. The NF- $\kappa$ B stimulation is key to those principal systems.<sup>47</sup> The suppression of NF- $\kappa$ B reduces acute inflammatory changes and organ impairment in sepsis. In the current research, we proposed that GN could mitigate hepatic phosphorylated NF- $\kappa$ Bp65. Earlier reports found that MRP-8 openly interrelates with TLR-4/MD-2 and persuades NF- $\kappa$ B stimulation.<sup>48</sup> The MRP8 promotes MyD88 intracellular translocation and the initiation of IRAK-1 and NF- $\kappa$ B that subsequently upregulates TNF- $\alpha$  expression.<sup>48</sup> Our study documents that GN diminishes MyD88, IRAK-1 and NF- $\kappa$ Bp65 adaptor protein expressions. Hence, the protective effect of GN could be mediated by the suppression of other inflammatory molecules involved in the NF- $\kappa$ B pathway. Nevertheless, further investigations over a longer period of time should assess if there are any side effects associated with GN treatment before human use.

## Limitations

The current study showed that GN significantly reduced cytokines, chemokines and pro-inflammatory mediators, and enhanced the antioxidant activities in the LPS-prompted septic rat model. However, one should note that except for IL-6, none has found its way from bench to bedside. Interestingly, GN is the promising candidate to control the sepsis, but further clinical research is needed.



## Conclusions

In summary, this study demonstrates for the first time that GN could mitigate ROS in organs (liver, kidneys and lungs), and it could reduce pro-cytokines, lessen hepatic toxicity, reduce tissue damage, and enhance antioxidant activity in the LPS-induced septic rat model. We also discovered that GN treatment alleviated the MyD88, IRAK-1, TRAF-6, and NF- $\kappa$ B protein levels and subdued I $\kappa$ B $\alpha$  degradation in the LPS-induced septic rat model through its anti-inflammatory effects. While these results may be due to the powerful antioxidant properties of GN, they may also be caused by the repression of the intensified inflammation cascade. This suppression prevents serious impairment by attenuating HMGB1, NF- $\kappa$ B and NLRP3 levels and averts a cytokine storm. Our findings imply that GN is a potential remedy for sepsis due to its anti-inflammatory and antioxidant properties. Further research is required to confirm the antiseptic activity of GN on various signaling pathways in an in vivo model.

## Supplementary data

The supplementary materials are available at <https://doi.org/10.5281/zenodo.8297655>. The package contains the following files:

Supplementary Table 1. Results of normality test as presented in Fig. 1.

Supplementary Table 2. Results of normality test as presented in Fig. 2.

Supplementary Table 3. Results of normality test as presented in Fig. 3.

Supplementary Table 4. Results of normality test as presented in Fig. 4.

Supplementary Table 5. Results of normality test as presented in Fig. 5.

Supplementary Table 6. Results of normality test as presented in Fig. 7.

Supplementary Table 7. Results of normality test as presented in Fig. 8.

Supplementary Fig. 1. Results of the Kruskal–Wallis test as presented in Fig. 1.

Supplementary Fig. 2. Results of the Kruskal–Wallis test as presented in Fig. 2.

Supplementary Fig. 3. Results of the Kruskal–Wallis test as presented in Fig. 3.

Supplementary Fig. 4. Results of the Kruskal–Wallis test as presented in Fig. 4.

Supplementary Fig. 5. Results of the Kruskal–Wallis test as presented in Fig. 5.

Supplementary Fig. 6. Results of the Kruskal–Wallis test as presented in Fig. 7.

Supplementary Fig. 7. Results of the Kruskal–Wallis test as presented in Fig. 8.

## ORCID iDs

Liyun Fang  <https://orcid.org/0000-0002-2387-4953>

Mao Zheng  <https://orcid.org/0000-0003-1971-3118>

Fengying He  <https://orcid.org/0000-0001-5392-781X>

## References

- Xu J, Lu C, Liu Z, Zhang P, Guo H, Wang T. Schizandrin B protects LPS-induced sepsis via TLR4/NF- $\kappa$ B/MyD88 signaling pathway. *Am J Transl Res*. 2018;10(4):1155–1163. PMID:29736208.
- Alamili M, Bendtzen K, Lykkesfeldt J, Rosenberg J, Gøgenur I. Effect of melatonin on human nighttime endotoxaemia: Randomized, double-blinded, cross-over study. *In Vivo*. 2014;28(6):1057–1063. PMID:25398799.
- Schrier RW, Wang W. Acute renal failure and sepsis. *N Engl J Med*. 2004;351(2):159–169. doi:10.1056/NEJMra032401
- Thimmulappa RK. Nrf2 is a critical regulator of the innate immune response and survival during experimental sepsis. *J Clin Invest*. 2006;116(4):984–995. doi:10.1172/JCI25790
- Kolac UK, Ustuner MC, Tekin N, Ustuner D, Colak E, Entok E. The anti-inflammatory and antioxidant effects of *Salvia officinalis* on lipopolysaccharide-induced inflammation in rats. *J Med Food*. 2017;20(12):1193–1200. doi:10.1089/jmf.2017.0035
- Epstein FH, Parrillo JE. Pathogenetic mechanisms of septic shock. *N Engl J Med*. 1993;328(20):1471–1477. doi:10.1056/NEJM199305203282008
- Opal SM. Endotoxins and other sepsis triggers. *Contrib Nephrol*. 2010;167:14–24. doi:10.1159/000315915
- Doi K. Role of kidney injury in sepsis. *J Intensive Care*. 2016;4(1):17. doi:10.1186/s40560-016-0146-3
- Kellum JA, Lameire N, for the KDIGO AKI Guideline Work Group. Diagnosis, evaluation, and management of acute kidney injury: A KDIGO summary (part 1). *Crit Care*. 2013;17(1):204. doi:10.1186/cc11454
- Gomez H, Ince C, De Backer D, et al. A unified theory of sepsis-induced acute kidney injury: Inflammation, microcirculatory dysfunction, bioenergetics, and the tubular cell adaptation to injury. *Shock*. 2014;41(1):3–11. doi:10.1097/SHK.0000000000000052
- Alberti C, Brun-Buisson C, Burchardi H, et al. Epidemiology of sepsis and infection in ICU patients from an international multicentre cohort study. *Intensive Care Med*. 2002;28(2):108–121. doi:10.1007/s00134-001-1143-z
- Ozduzger A, Cinelli, Koksel O, et al. The protective effect of N-acetylcysteine on apoptotic lung injury in cecal ligation and puncture-induced sepsis model. *Shock*. 2003;19(4):366–372. doi:10.1097/00024382-200304000-00012
- Cadirci E, Ugan RA, Dincer B, et al. Urotensin receptors as a new target for CLP induced septic lung injury in mice. *Naunyn-Schmiedeberg Arch Pharmacol*. 2019;392(2):135–145. doi:10.1007/s00210-018-1571-8
- Caroff M, Karibian D. Structure of bacterial lipopolysaccharides. *Carbohydr Res*. 2003;338(23):2431–2447. doi:10.1016/j.carres.2003.07.010
- Entok E, Ustuner MC, Ozbayer C, et al. Anti-inflammatory and antioxidant effects of *Nigella sativa* L.: 18FDG-PET imaging of inflammation. *Mol Biol Rep*. 2014;41(5):2827–2834. doi:10.1007/s11033-014-3137-2
- Schulte W, Bernhagen J, Bucala R. Cytokines in sepsis: Potent immunoregulators and potential therapeutic targets. An updated view. *Mediators Inflamm*. 2013;2013:165974. doi:10.1155/2013/165974
- Halliwell B, Gutteridge JMC. Oxygen toxicity, oxygen radicals, transition metals and disease. *Biochem J*. 1984;219(1):1–14. doi:10.1042/bj2190001
- Steven S, Dib M, Roohani S, Kashani F, Münzel T, Daiber A. Time response of oxidative/nitrosative stress and inflammation in LPS-induced endotoxaemia: A comparative study of mice and rats. *Int J Mol Sci*. 2017;18(10):2176. doi:10.3390/ijms18102176
- Devasagayam TPA, Tilak JC, Boloor KK, Sane KS, Ghaskadbi SS, Lele RD. Free radicals and antioxidants in human health: Current status and future prospects. *J Assoc Physicians India*. 2004;52:794–804. PMID:15909857.
- Lan KC, Chao SC, Wu HY, et al. Salidroside ameliorates sepsis-induced acute lung injury and mortality via downregulating NF- $\kappa$ B and HMGB1 pathways through the upregulation of SIRT1. *Sci Rep*. 2017;7(1):12026. doi:10.1038/s41598-017-12285-8

21. Wang H, Ward MF, Sama AE. Targeting HMGB1 in the treatment of sepsis. *Exp Opin Ther Targets*. 2014;18(3):257–268. doi:10.1517/14728222.2014.863876
22. Wang H, Bloom O, Zhang M, et al. HMG-1 as a late mediator of endotoxin lethality in mice. *Science*. 1999;285(5425):248–251. doi:10.1126/science.285.5425.248
23. Martinon F, Burns K, Tschopp J. The inflammasome. *Mol Cell*. 2002;10(2):417–426. doi:10.1016/S1097-2765(02)00599-3
24. Keller M, Rüegg A, Werner S, Beer HD. Active caspase-1 is a regulator of unconventional protein secretion. *Cell*. 2008;132(5):818–831. doi:10.1016/j.cell.2007.12.040
25. Hou L, Yang Z, Wang Z, et al. NLRP3/ASC-mediated alveolar macrophage pyroptosis enhances HMGB1 secretion in acute lung injury induced by cardiopulmonary bypass. *Lab Invest*. 2018;98(8):1052–1064. doi:10.1038/s41374-018-0073-0
26. Isik A, Soran A, Grasi A, Barry N, Sezgin E. Lymphedema after sentinel lymph node biopsy: Who is at risk? *Lymph Res Biol*. 2022;20(2):160–163. doi:10.1089/lrb.2020.0093
27. Brandt GEL, Schmidt MD, Prinsizano TE, Blagg BSJ. Gedunin, a novel Hsp90 inhibitor: Semisynthesis of derivatives and preliminary structure–activity relationships. *J Med Chem*. 2008;51(20):6495–6502. doi:10.1021/jm8007486
28. Wax S, Pieczyk M, Maritim B, Anderson P. Geldanamycin inhibits the production of inflammatory cytokines in activated macrophages by reducing the stability and translation of cytokine transcripts. *Arthritis Rheum*. 2003;48(2):541–550. doi:10.1002/art.10780
29. Madrigal-Matute J, López-Franco O, Blanco-Colio LM, et al. Heat shock protein 90 inhibitors attenuate inflammatory responses in atherosclerosis. *Cardiovasc Res*. 2010;86(2):330–337. doi:10.1093/cvr/cvq046
30. Ferraris FK, Moret KH, Figueiredo ABC, Penido C, Henriques MDGMO. Gedunin, a natural tetranortriterpenoid, modulates T lymphocyte responses and ameliorates allergic inflammation. *Int Immunopharmacol*. 2012;14(1):82–93. doi:10.1016/j.intimp.2012.06.002
31. Uddin SJ, Nahar L, Shilpi JA, et al. Gedunin, a limonoid from *Xylocarpus granatum*, inhibits the growth of CaCo-2 colon cancer cell line in vitro. *Phytother Res*. 2007;21(8):757–761. doi:10.1002/ptr.2159
32. Kamath SG, Chen N, Xiong Y, et al. Gedunin, a novel natural substance, inhibits ovarian cancer cell proliferation. *Int J Gynecol Cancer*. 2009;19(9):1564–1569. doi:10.1111/IGC.0b013e3181a83135
33. Conte F, Ferraris F, Costa T, et al. Effect of gedunin on acute articular inflammation and hypernociception in mice. *Molecules*. 2015;20(2):2636–2657. doi:10.3390/molecules20022636
34. Borges PV, Moret KH, Maya-Monteiro CM, et al. Gedunin binds to myeloid differentiation protein 2 and impairs lipopolysaccharide-induced Toll-like receptor 4 signaling in macrophages. *Mol Pharmacol*. 2015;88(5):949–961. doi:10.1124/mol.115.098970
35. Koc F, Tekeli MY, Kanbur M, Karayigit MÖ, Liman BC. The effects of chrysin on lipopolysaccharide-induced sepsis in rats. *J Food Biochem*. 2020;44(9). doi:10.1111/jfbc.13359
36. Basir S, Shailey S. Strengthening of antioxidant defense by *Azadirachta indica* in alloxan-diabetic rat tissues. *J Ayurveda Integr Med*. 2012;3(3):130. doi:10.4103/0975-9476.100174
37. Mazumdar S, Marar T, Devarajan S, Patki J. Functional relevance of gedunin as a bona fide ligand of NADPH oxidase 5 and ROS scavenger: An in silico and in vitro assessment in a hyperglycemic RBC model. *Biochem Biophys Rep*. 2021;25:100904. doi:10.1016/j.bbrep.2020.100904
38. Goetz F. Tumor necrosis factors. *Dev Comp Immunol*. 2004;28(5):487–497. doi:10.1016/j.dci.2003.09.008
39. Muller S. The double life of HMGB1 chromatin protein: Architectural factor and extracellular signal. *EMBO J*. 2001;20(16):4337–4340. doi:10.1093/emboj/20.16.4337
40. Sun J, Shi S, Wang Q, Yu K, Wang R. Continuous hemodiafiltration therapy reduces damage of multi-organs by ameliorating of HMGB1/TLR4/NFκB in a dog sepsis model. *Int J Clin Exp Pathol*. 2015;8(2):1555–1564. PMID:25973040.
41. McCauley MJ, Rueter EM, Rouzina I, Maher LJ, Williams MC. Single-molecule kinetics reveal microscopic mechanism by which high-mobility group B proteins alter DNA flexibility. *Nucl Acids Res*. 2013;41(1):167–181. doi:10.1093/nar/gks1031
42. Tergaonkar V. NFκB pathway: A good signaling paradigm and therapeutic target. *Int J Biochem Cell Biol*. 2006;38(10):1647–1653. doi:10.1016/j.biocel.2006.03.023
43. Ha T, Xia Y, Liu X, et al. Glucan phosphate attenuates myocardial HMGB1 translocation in severe sepsis through inhibiting NF-κB activation. *Am J Physiol Heart Circ Physiol*. 2011;301(3):H848–H855. doi:10.1152/ajpheart.01007.2010
44. Kaplan KA, Odabasoglu F, Halici Z, et al. Alpha-lipoic acid protects against indomethacin-induced gastric oxidative toxicity by modulating antioxidant system. *J Food Sci*. 2012;77(11):H224–H230. doi:10.1111/j.1750-3841.2012.02920.x
45. Jo EK, Kim JK, Shin DM, Sasakawa C. Molecular mechanisms regulating NLRP3 inflammasome activation. *Cell Mol Immunol*. 2016;13(2):148–159. doi:10.1038/cmi.2015.95
46. Yu R, Jiang S, Tao Y, Li P, Yin J, Zhou Q. Inhibition of HMGB1 improves necrotizing enterocolitis by inhibiting NLRP3 via TLR4 and NF-κB signaling pathways. *J Cell Physiol*. 2019;234(8):13431–13438. doi:10.1002/jcp.28022
47. Liu SF, Malik AB. NF-κB activation as a pathological mechanism of septic shock and inflammation. *Am J Physiol Heart Circ Physiol*. 2006;290(4):L622–L645. doi:10.1152/ajplung.00477.2005
48. Vogl T, Tenbrock K, Ludwig S, et al. Mrp8 and Mrp14 are endogenous activators of Toll-like receptor 4, promoting lethal, endotoxin-induced shock. *Nat Med*. 2007;13(9):1042–1049. doi:10.1038/nm1638

# Tumor suppressor miR-520a inhibits cell growth by negatively regulating PI3K/AKT signaling pathway in acute myeloid leukemia

\*Jing Xiao<sup>1,A–C,E,F</sup>, \*Fang Wan<sup>2,A,C,E,F</sup>, Lin Tian<sup>1,A,C–F</sup>, Yao Li<sup>1,A,C,F</sup>

<sup>1</sup> Department of Pathology, Renmin Hospital, Hubei University of Medicine, Shiyan, China

<sup>2</sup> Department of Pediatrics, Renmin Hospital, Hubei University of Medicine, Shiyan, China

A – research concept and design; B – collection and/or assembly of data; C – data analysis and interpretation; D – writing the article; E – critical revision of the article; F – final approval of the article

Advances in Clinical and Experimental Medicine, ISSN 1899–5276 (print), ISSN 2451–2680 (online)

*Adv Clin Exp Med.* 2024;33(7):729–738

## Address for correspondence

Yao Li

E-mail: leo9029@sina.com

## Funding sources

None declared

## Conflict of interest

None declared

\*Jing Xiao and Fang Wan contributed equally to this work.

Received on March 23, 2023

Reviewed on April 10, 2023

Accepted on August 16, 2023

Published online on October 19, 2023

## Abstract

**Background.** Short regulatory RNAs, called microRNAs (miRNAs), have been found to possess regulatory functions in cancer and, as such, have recently been evaluated for their therapeutic role against various human malignancies.

**Objectives.** The present work aimed to investigate whether miR-520a can play a therapeutic role in the treatment of human acute myeloid leukemia.

**Materials and methods.** Human myeloid leukemia cell lines (Kasumi-1, Kasumi-3, Kasumi-6, BDCM, and K562) and a normal myeloid cell line (NCI-H5N6) were used for the study. Cell lines were subjected to real-time quantitative polymerase chain reaction (RT-qPCR), evaluation of cell viability and proliferation by MTT assay and colony formation assays. Dual acridine orange (AO)/ethidium bromide (EB) staining was applied for transfected K562 cells with miR-negative control (NC) or miR-520a mimics, and annexin V-fluorescein isothiocyanate (FITC)/propidium iodide (PI) dual staining and flow cytometry were performed to analyze cancer cell apoptosis followed by western blot.

**Results.** Cancerous cell lines exhibited lower gene expression of miR-520a, and its overexpression significantly reduced ( $p < 0.05$ ) the proliferation and viability of cancer cells. Cancer cells demonstrated the induction of Bax/Bcl-2-mediated apoptosis following miR-520a overexpression. The miR-520a was shown to target the PI3K/AKT signaling pathway in human acute myeloid leukemia to exercise its regulatory role in cancer.

**Conclusions.** The study showed that miR-520a actively regulated cell proliferation in acute myeloid leukemia and illustrated the mechanism by which it exerts its regulatory role, emphasizing the possibility of targeting miR-520a as an efficient therapeutic strategy against human acute myeloid leukemia.

**Key words:** microRNA, cell proliferation, AO/EB staining, apoptosis, acute myeloid leukemia

## Cite as

Xiao J, Wan F, Tian L, Li Y. Tumor suppressor miR-520a inhibits cell growth by negatively regulating PI3K/AKT signaling pathway in acute myeloid leukemia. *Adv Clin Exp Med.* 2024;33(7):729–738. doi:10.17219/acem/171299

## DOI

10.17219/acem/171299

## Copyright

Copyright by Author(s)

This is an article distributed under the terms of the Creative Commons Attribution 3.0 Unported (CC BY 3.0) (<https://creativecommons.org/licenses/by/3.0/>)

## Background

There are many types of leukemia, but acute leukemia is one of the most common hematologic malignancies. It has been shown that acute leukemia occurs due to the abnormal proliferation of hematopoietic stem cells in the bone marrow and other hematopoietic tissues. Moreover, malignant cells have also been shown to accumulate in these tissues.<sup>1</sup> Acute myeloid leukemia results in impaired blood cell production and bone marrow failure.<sup>2</sup> If left untreated, patients with this disorder can die in a few weeks due to increased susceptibility to blood infections or uncontrolled blood loss caused by excessive bleeding.<sup>3</sup> Acute leukemia is generally classified as either acute lymphoblastic leukemia (ALL) or acute myeloid leukemia (AML), according to its distinctive morphology, prognosis and preferred treatment protocols to differentiate them.<sup>4</sup> Among hematopoietic disorders, AML is characterized by the presence of numerous cytogenetic and molecular abnormalities,<sup>5,6</sup> and there are high morbidity and mortality rates associated with AML when compared to other cancers. The main therapeutic strategies used in the treatment of AML are chemotherapy and allogeneic stem cell transplantation.<sup>7</sup> However, in general, the 5-year survival rate of patients with AML is still unsatisfactory.<sup>8</sup> Therefore, the etiology of the disease needs to be investigated, and new therapeutic strategies must be formulated.

Several studies have shown that microRNA (miR) has an important role to play in regulating the expression of genes by the regulation of post-translational expression. Furthermore, miRs may play a role in the progression of a significant number of diseases.<sup>9</sup> According to recent studies, miRNAs are involved in the regulation of leukemia progression, including both AML and chronic myeloid leukemia (CML).<sup>10</sup> The miR-520a controls the growth and progression of many human cancers.<sup>11</sup> A recent study has demonstrated that miR-520a suppresses the progression of non-small cell lung cancer by targeting the RRM2/Wnt pathway.<sup>12</sup> Based on investigations carried out in HCT116 and SW480 cells, silencing of ATAD2 modulates vascular endothelial growth factor A (VEGFA) and miR-520a in colorectal cancer.<sup>13</sup> Moreover, a study found that miR-520a regulates endoplasmic reticulum (ER) stress, proliferation, and the AKT1/NF- $\kappa$ B or PERK/eIF2 signaling pathways in Raji cells.<sup>14</sup> Another study showed that piperine significantly decreased analgesia in the rat model without compression of the lumbar disc herniation by specifically and directly targeting P65 with miR-520a to treat sciatica.

However, the regulatory function of miR-520a in AML is scarce, which prompted us to evaluate the potential underlying molecular mechanisms. Furthermore, in this study, we present the therapeutic benefits of miR-520a in activating the PI3K/AKT signaling pathway for AML and suggest that targeting miR-520a could be an effective anticancer strategy against this disease.

## Objectives

We aimed to investigate whether miR-520a can play a therapeutic role in the treatment of human AML by activating the PI3K/AKT signaling pathway.

## Materials and methods

### Tissue samples

Samples of blood from both AML patients (24 samples) and healthy controls (22 samples) were collected from Renmin Hospital (Hubei University of Medicine, Shiyang, China) between August 2019 and September 2020. The healthy control samples were collected from normal blood donors. There was no chemotherapy or radiation therapy administered to these patients prior to sample collection, and there was no evidence of infections or multiple cancers, indicating that there was no history of multiple cancers among these patients. Patient and healthy control demographics are outlined in Table 1. All patients signed an informed consent form before the procedure. The study was approved by the Ethics Committee of Renmin Hospital (protocol No. FPH-34/2341/22), and the experimental procedure was carried out in accordance with the principles of the Declaration of Helsinki.

### Cell lines

Human myeloid leukemia cell lines (Kasumi-1, Kasumi-3, Kasumi-6, BDCM, and K562) and a normal myeloid cell line (NCI-H5N6) were obtained as donations from the Department of Hematology of the Third Hospital of Shanxi Medical University (Taiyuan, China). Cell lines were cultured in RPMI-1640 medium (Invitrogen, Carlsbad, USA), containing 10% fetal bovine serum (FBS) in 5% CO<sub>2</sub> at 37°C. Plasma cells were isolated and cultured from peripheral blood smears according to previously published methods.<sup>15</sup> A colorimetric detection method (InvivoGen, San Diego, USA) was used to identify mycoplasma contamination in cell cultures, and the used cell cultures were free of mycoplasma contamination.

### Cell transfection

The cells were seeded in 6-well plates at a density of  $3 \times 10^5$  cells per well. According to our previous report, 5  $\mu$ L of miRNA (miR-negative control (NC) or miR-520a mimics, 50 nM; Thermo Fisher Scientific, Waltham, USA) were transfected into K562 cells during the logarithmic growth phase using HiPerFect Transfection Reagent (5  $\mu$ L in 300  $\mu$ L of Dulbecco's modified Eagle medium (DMEM); QIAGEN, Germantown, USA) without serum, and incubated at 37°C for 20 min following the manufacturer's instructions. The cells were cultured in a CO<sub>2</sub> incubator

**Table 1.** Demographics and clinical characteristics of patients and healthy blood donors

Variables	Characteristics											
	healthy volunteers (control or normal, n = 22)			AML patients (n = 24)			Mann–Whitney U			p-value		
	total (n = 22)	male (n = 15)	female (n = 7)	total (n = 24)	male (n = 18)	female (n = 6)	total	male	female	total	male	female
Age at diagnosis [years]												
Minimum	45.00	45.00	48.00	47.00	51.00	47.00	203	96	12	0.3655	0.2395	0.4293
Q1	48.75	48.00	49.00	54.50	55.00	48.00						
Median	55.50	56.00	53.00	57.00	57.00	49.00						
Q3	62.25	62.00	64.00	63.00	63.00	60.00						
Maximum	67.00	67.00	66.00	68.00	68.00	63.00						
Peripheral blasts [%]												
Minimum	–	–	–	37.00	37.00	40.10	–	–	–	–	–	–
Q1	–	–	–	40.93	41.50	40.65	–	–	–	–	–	–
Median	–	–	–	47.50	56.00	41.50	–	–	–	–	–	–
Q3	–	–	–	60.25	68.00	42.20	–	–	–	–	–	–
Maximum	–	–	–	78.00	78.00	42.30	–	–	–	–	–	–

AML – acute myeloid leukemia; Q1 – 1<sup>st</sup> quartile; Q3 – 3<sup>rd</sup> quartile. In healthy volunteers, there were usually no blast cells in the blood.

**Table 2.** Primers used in the study

Gene	Primers	Annealing temperature [°C]
miR-520a	forward: 5'-CCTAACAAACCCGTTGCCCTTCTTT-3' reverse: 3'-ACGTGACGGTGGCCAGGT-5'	53
U6	forward: 5'-CTGCCCTTGCCGAGCAAC-3' reverse: 5'-AAGCTCTTACGATAATTGCCT-3'	54
β-actin	forward: 5'-TGCCGAACCATTACCTACAA-3' reverse: 5'-ACCAGAGGATAACAGAGGGATG-3'	58

for 24 h at 37°C to determine whether the transgene was expressed in cells.

In this study, a control plasmid containing empty sequences was used as a control. All plasmids were obtained from Invitrogen.

### Real-time PCR

We used an Agilent High Sensitivity RNA Screen Tape (Agilent Technologies, Santa Clara, USA) as a tool to determine the quality of the RNA. The RNA was subjected to reverse transcription as soon as it was isolated from cells.<sup>16</sup>

Total RNA was extracted using TRIzol reagent to conduct RNA analysis in clinical samples and cell lines. This was done by following the manufacturer’s instructions. To quantify the level of miR-520a transcript, DNase I was used to remove any DNA contamination, and approx. 1 µg of purified RNA was used to produce complementary DNA (cDNA) using an iScript™ cDNA Synthesis Kit (Bio-Rad, Hercules, USA). Real-time polymerase chain reaction (PCR) was then performed using the SYBR Green Master mix (Thermo Fisher Scientific, Waltham, USA). Three replicates were used for each real-time reaction, and the relative expression levels were quantified using

the 2<sup>-ΔΔCt</sup> method. Human β-actin was used as an internal control for miR-520a expression. Primers (Table 2) were synthesized by Suzhou Ruibo Biotechnology Co., Ltd. (Guangzhou, China).

### MTT proliferation assay

The proliferation of K562 cancer cells, transfected with miR-NC or miR-520a mimics using Lipofectamine 2000 (Thermo Fisher Scientific), was estimated by the MTT assay. In brief, transfected K562 cancer cells (2×10<sup>5</sup> per well) were placed in a 96-well plate, then cultured in RPMI-1640 medium for 0, 12, 24, 48, or 96 h at 37°C. Each well had 10 µL of MTT reagent (dissolved in phosphate-buffered saline (PBS) (5 mg/mL)) added, followed by prolonged incubation for 4 h at 37°C. The culture medium was removed and dimethyl sulfoxide (DMSO) (150 µL) was added to each well. Then, the samples were processed for absorbance measurement at 570 nm to examine cell proliferation rates.<sup>16</sup>

### Colony-forming assay

Following its transfection with miR-NC or miR-520a mimics, each 6-well plate was filled with 100 µL

of homogeneous K562 cellular mix in RPMI-1640 medium. The plate was incubated for 10 days at 37°C. Subsequently, the cell cultures were harvested, rinsed 3 times with PBS, and then fixed and stained in ethanol (70%) with crystal violet (0.1%) (Abcam, Waltham, USA). The cells were examined under a microscope, and the relative colony number was presented as a percentage value. Two independent researchers (blind) counted colonies with >50 cells using a low-resolution bright field microscope (Olympus, Tokyo, Japan). A scan of each plate was also analyzed using colony counting software (ImageJ; National Institutes of Health, Bethesda, USA) to automatically detect colonies.<sup>16</sup>

### Acridine orange/ethidium bromide staining

The K562 cells ( $2 \times 10^5$  cells) with miR-NC or miR-520a mimics to stimulate miRNA expression were seeded in the 12-well plate. The cells were harvested after 24 h of culture at 37°C and washed twice with PBS. Then, they were fixed with methanol, and dual staining with acridine orange/ethidium bromide (AO/EB) (Cat No. E607308; Sangon Biotech Co., Ltd., Shanghai, China) was applied. A fluorescent microscope (Olympus Corp., Tokyo, Japan) was used to analyze their nuclear morphology.<sup>16</sup>

### Annexin V-FITC/PI dual staining and flow cytometry

Flow cytometry was performed to assess cell apoptosis. Briefly, miR-NC or miR-520a mimics were transfected and  $2 \times 10^6$  cells per well were cultured for 48 h in a 12-well plate. The K562 cells were incubated at 37°C for 2 h with 10  $\mu$ L of fluorescein isothiocyanate (FITC) and 5  $\mu$ L of propidium iodide (PI) (Beyotime, Nanjing, China). After centrifugation and washing with PBS, the cells were harvested and fixed in ethanol. Then, the apoptosis was detected by flow cytometry (BD Biosciences, San Diego, USA), following the manufacturer's instructions. Apoptotic subpopulations were differentiated as follows: early apoptosis (Annexin V+/PI-), late apoptosis (Annexin V+/PI+), or necrotic/dead (Annexin V-/PI+). A total of 10,000 cells were analyzed per replicate.<sup>16</sup>

### Western blot

The K562 cells transfected with miR-NC or miR-520a mimics were lysed with ice-cold radioimmunoprecipitation assay (RIPA) lysis buffer (Sigma-Aldrich, St. Louis, USA), and the total protein concentration was measured using a bicinchoninic acid (BCA) protein assay kit (Sigma-Aldrich). To analyze the protein of each sample, 30  $\mu$ g of protein from each sample was separated on a 10% sodium dodecyl-sulfate polyacrylamide gel electrophoresis (SDS-PAGE) gel (Bio-Rad Laboratories

Co., Ltd., Shanghai, China) before being transferred to polyvinylidene difluoride (PVDF) membranes (Millipore, Burlington, USA). Primary antibodies used are as follows: Bcl2 (Cat. No. MA5-11757, dilution 1:800; Thermo Fisher Scientific), Bax (Cat. No. MA5-14003, dilution 1:800; Thermo Fisher Scientific), PI3K (Cat. No. A27091, dilution 1:1000; Invitrogen), Phospho-PI3K (Cat. No. PA5-17387, dilution 1:1000; Invitrogen), AKT (Cat. No. A25810, dilution 1:1000; Antibodies, Cambridge, UK), and Phospho-AKT (Cat. No. A27292, dilution 1:800; Antibodies). The PVDF membranes were blocked with 10% fat-free milk in Tris-buffered saline/Tween-20 (TBST) and incubated with the primary antibodies for 3 h at room temperature. Then, a goat anti-rabbit horseradish peroxidase (HRP) conjugated secondary antibody (dilution 1:8000; Thermo Fisher Scientific) was incubated with the PVDF membranes for 2 h at room temperature. The bands were detected and photographed using a chemiluminescence analyzer (Biotech Co., Ltd., Beijing, China). A densitometric analysis of protein bands was performed using Quantity One software (Bio-Rad) with samples normalized to  $\beta$ -actin.<sup>16</sup>

### Statistical analyses

GraphPad Prism (v. 9.1; GraphPad Software, Boston, USA) was used to analyze the data, and a minimum of 3 or 5 independent replications were carried out for each experiment ( $n = 3-5$ ). The Mann-Whitney U test was performed with respect to age and sex distribution and peripheral blast (PB) count. The Shapiro-Wilk normality test and Kolmogorov-Smirnov test were performed to determine whether the data conformed to a normal distribution. We found that the data were non-normally distributed. Therefore, data are presented as a median with an interquartile range (Q1-Q3). The Mann-Whitney U test was employed to compare 2 groups, and the Kruskal-Wallis test, followed by Dunn's multiple comparison test were used for comparing multiple groups. A value of  $p < 0.05$  was considered statistically significant.

## Results

### The expression of miR-520a is negatively regulated in AML

Real-time PCR expression analysis was used to investigate the relative expression of miR-520a in tissue samples. We found that miR-520a displayed significantly reduced expression in cancerous tissues compared to normal bone marrow tissue specimens (Fig. 1A, Table 3;  $p < 0.0001$ ; Mann-Whitney test,  $U = 75.5$ ). Similarly, cancer cell lines showed a substantially lower expression of miR-520a transcripts compared to the normal myeloid cell line (Fig. 1B, Table 4;  $p = 0.0004$ ; Kruskal-Wallis test followed by Dunn's

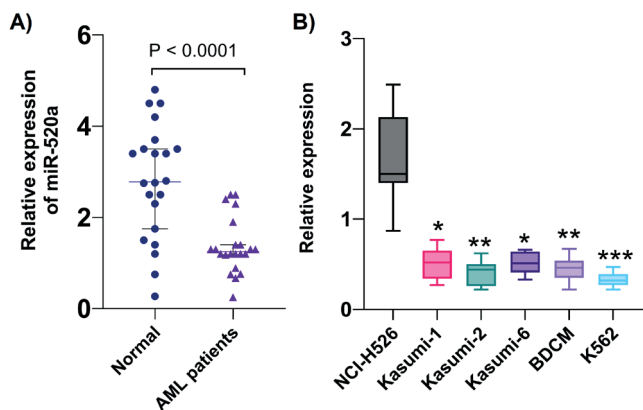


**Fig. 1.** MicroRNA (miR)-520a is downregulated in acute myeloid leukemia (AML). A. Real-time quantitative polymerase chain reaction (RT-qPCR) analysis of miR-520a in tissue specimens of AML patients and healthy volunteers. The data were not normally distributed and were tested by the Shapiro–Wilk test and Kolmogorov–Smirnov test with p-values for healthy control ( $p = 0.023$ ;  $p = 0.013$ ) and AML patients ( $p = 0.037$ ;  $p = 0.021$ ). The Mann–Whitney test was used to compare the 2 groups. The data are presented as a median with interquartile range (Q1–Q3); B. RT-qPCR analysis in normal myeloid cells (NCI-H5N6) and various myeloid cancerous cell lines. The data were not normally distributed and were tested by the Shapiro–Wilk test and Kolmogorov–Smirnov test with p-values for NCI-H526 ( $p = 0.032$ ;  $p = 0.0152$ ), Kasumi-1 ( $p = 0.027$ ;  $p = 0.021$ ), Kasumi-2 ( $p = 0.040$ ;  $p = 0.031$ ), Kasumi-6 ( $p = 0.015$ ;  $p = 0.041$ ), BDCM ( $p = 0.013$ ;  $p = 0.037$ ), and K562 ( $p = 0.01$ ;  $p = 0.026$ ). The Kruskal–Wallis test was used to compare multiple groups, followed by Dunn’s multiple comparison test. The data are presented as a median with an interquartile range (Q1–Q3). The upper and lower lines of each box indicate the 25<sup>th</sup> (Q1) and 75<sup>th</sup> (Q3) percentiles. The line inside each box indicates the median. The Kruskal–Wallis H test showed a significant difference in the mRNA expression levels of miR-520a between different groups ( $\chi^2(5) = 22.87$ ,  $p = 0.0004$ ; \* $p = 0.027$  for Kasumi-1; \* $p = 0.037$  for Kasumi-6; \*\* $p = 0.001$  for Kasumi-2; \*\* $p = 0.012$  for BDCM; \*\*\* $p = 0.0002$  for K652 cell lines compared to miR-negative control (NC);  $n = 3–5$ )

**Table 3.** Real-time quantitative polymerase chain reaction (RT-qPCR) analysis of microRNA (miR)-520a in tissue specimens of acute myeloid leukemia (AML) patients and healthy volunteers

Variables	Healthy volunteers (n = 22)	AML patients (n = 24)
Minimum	0.270	0.250
Q1	1.688	1.108
Median	2.780	1.250
Q3	3.550	1.525
Maximum	4.800	2.500
Mean ranks	30.07	14.93
Mann–Whitney U		75.5
p-value		<0.001*

\* $p < 0.001$  compared to miR-52a expression analysis in healthy volunteers; Q1 – 1<sup>st</sup> quartile; Q3 – 3<sup>rd</sup> quartile. The Mann–Whitney U test was used to compare the 2 groups.

multiple comparison tests;  $\chi^2(5) = 22.87$ ). The K562 cells possessed the lowest expression values ( $p = 0.0002$ ) among all cancer cell lines and were therefore selected for further characterization. Therefore, the results showed that miR-520a was negatively regulated in AML and may play a prognostic role in this malignancy.

## Overexpression of miR-520a decreases proliferation and viability

To examine the function of miR-520a in AML, miR-520a was overexpressed in K562 cells, and its overexpression was confirmed by real-time PCR (Fig. 2A, Table 5;  $p = 0.0006$ ; Mann–Whitney test,  $U = 0$ ). An MTT assay was used to investigate the proliferative impact of miR-520a impact on AML. The miR-520a-overexpressing K562 leukemia cells were found to exhibit significantly lower proliferation rates (Fig. 2B, Table 6;  $p = 0.031$ ; Mann–Whitney test,

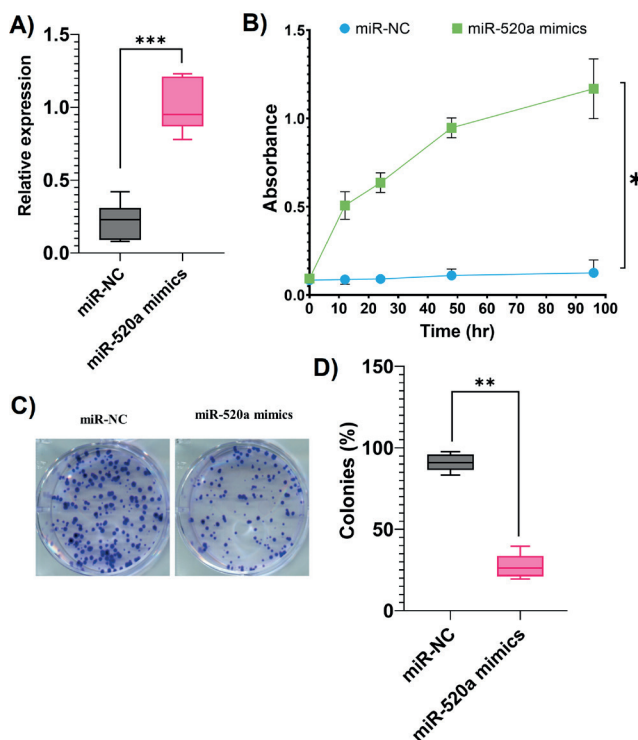


**Fig. 2.** Overexpression of microRNA (miR)-520a reduces leukemia cell proliferation and viability. A. Relative gene expression of miR-520a in miR-negative control (NC) or miR-520a mimics-transfected K562 cells. The data were not normally distributed and were tested by the Shapiro–Wilk test and Kolmogorov–Smirnov test with p-values for miR-NC ( $p = 0.013$ ;  $p = 0.021$ ) and miR-520a ( $p = 0.036$ ;  $p = 0.047$ ). The Mann–Whitney U test was used to compare the 2 groups. The data are presented as a median with an interquartile range (Q1–Q3). The upper and lower lines of each box indicate the 25<sup>th</sup> (Q1) and 75<sup>th</sup> (Q3) percentiles. The line inside each box indicates the median; B. MTT assay for proliferation analysis of miR-NC or miR-520a mimics-transfected K562 cells. The data were not normally distributed and were tested by the Shapiro–Wilk test and Kolmogorov–Smirnov test with p-values for miR-NC ( $p = 0.014$ ;  $p = 0.032$ ) and miR-520a ( $p = 0.034$ ;  $p = 0.027$ ), indicating significant difference at time intervals. The Mann–Whitney test was used to compare the 2 groups. The data are presented as a median with an interquartile range (Q1–Q3); C. Colony forming assay for viability analysis of miR-NC or miR-520a mimics-transfected K562 cells; D. Percentage number of colonies formed by miR-NC or miR-520a mimics-transfected K562 cells. The data were not normally distributed and were tested by the Shapiro–Wilk test and Kolmogorov–Smirnov test with p-values for miR-NC ( $p = 0.01$ ;  $p = 0.031$ ) and miR-520a ( $p = 0.015$ ;  $p = 0.025$ ). The upper and lower lines of each box indicate the 25<sup>th</sup> (Q1) and 75<sup>th</sup> (Q3) percentiles. The line inside each box indicates the median. The Mann–Whitney test was used to compare the 2 groups. The data are presented as a median with an interquartile range (Q1–Q3) ( $n = 3–5$ )

\*\*\* $p = 0.0006$ ; \* $p = 0.031$ ; \*\* $p = 0.002$  compared to miR-NC.

**Table 4.** Real-time quantitative polymerase chain reaction (RT-qPCR) analysis in normal myeloid cells (NCI-H5N6) and various myeloid cancerous cell lines

Variables	NCI-H526	Kasumi-1	Kasumi-2	Kasumi-6	BDCM	K562
Minimum	0.8700	0.2700	0.2200	0.3300	0.2200	0.2200
Q1	1.400	0.3400	0.2600	0.4100	0.3500	0.2700
Median	1.500	0.5200	0.4400	0.5100	0.4600	0.3200
Q3	2.130	0.6500	0.5000	0.6400	0.5400	0.3900
Maximum	2.490	0.7700	0.6200	0.6600	0.6700	0.4700
Mean ranks	39.00	23.14	15.71	22.43	19.14	9.571
Mean rank difference	–	15.86	23.29	16.57	19.86	29.43
Kruskal–Wallis statistic	$\chi^2(5) = 22.87; p = 0.0004$					
Dunn's multiple comparison test (p-value)	–	0.027*	0.001**	0.037*	0.012*	0.001***

\*p = 0.027 for Kasumi-1; \*p = 0.037 for Kasumi-6; \*\*p = 0.001 for Kasumi-2; \*\*p = 0.012 for BDCM; \*\*\*p = 0.0002 for K562 cell lines compared to NCI-H526; Q1 – 1<sup>st</sup> quartile; Q3 – 3<sup>rd</sup> quartile. The Kruskal–Wallis test was performed, followed by Dunn's multiple comparison test to compare the multiple groups.

**Table 5.** Relative gene expression of microRNA (miR)-520a in miR-negative control (NC) or miR-520a mimics-transfected K562 cells and the percentage number of colonies

Variables	Groups			
	A		B	
	miR-NC	miR-520a mimics	miR-NC (%)	miR-520a mimics (%)
Minimum	0.08000	0.7800	83.30	19.40
Q1	0.09000	0.8700	86.45	21.13
Median	0.2300	0.9500	90.95	26.20
Q3	0.3100	1.210	95.95	33.75
Maximum	0.4200	1.230	97.60	39.60
Mean ranks	4.000	11.00	9.500	3.500
Mann–Whitney U	0		0	
p-value	0.001***		0.002**	

A. Relative gene expression of miR-520a in miR-NC or miR-520a mimics-transfected K562 cells. The Mann–Whitney test was used to compared the 2 groups (n = 3–5); B. Percent number of colonies formed by miR-NC or miR-520a mimics-transfected K562 cells. The Mann–Whitney test was used to compare the 2 groups (n = 3–5); \*\*\*p = 0.001 (compared to miR-NC); Q1 – 1<sup>st</sup> quartile; Q3 – 3<sup>rd</sup> quartile.

U = 2). The viability of K562 cancer cells was negatively affected by miR-520a. Cancer cells transfected with miR-520a mimics showed markedly lower colony formation potential compared to normal cells transfected with miR-NC (Fig. 2C, Table 5; p = 0.002; Mann–Whitney test, U = 0). These findings demonstrate that miR-520a negatively regulates cancer cell proliferation in AML, indicating its anticancer therapeutic potential (Fig. 2D).

## Overexpression of miR-520a induces apoptosis in leukemia cells

Evaluation of the nuclear morphology of K562 leukemia cells using the AO/EB staining method showed that cancer cells exhibit a loss of nuclear viability when transfected with miR-520a mimics (Fig. 3A,B, Table 7; p = 0.002; Mann–Whitney test, U = 0). Consistent with these findings, Annexin V-FITC/PI dual staining revealed that K562 cells transfected with miR-520a mimics demonstrated apoptotic cell death (Fig. 3C,D, Table 7; p = 0.002; Mann–Whitney test, U = 0). Moreover, the expression of Bax

**Table 6.** MTT assay for proliferation analysis of microRNA-negative control (miR-NC) or miR-520a mimics-transfected K562 cells

Variables	miR-NC	miR-520a mimics
Minimum	0.084	0.091
Q1	0.086	0.295
Median	0.091	0.623
Q3	0.118	1.071
Maximum	0.126	1.181
Lower 95% CI	0.077	0.147
Upper 95% CI	0.122	1.195
Mann–Whitney U	2	
p-value	0.031*	

\*p = 0.0317 compared to miR-NC; Q1 – 1<sup>st</sup> quartile; Q3 – 3<sup>rd</sup> quartile; 95% CI – 95% confidence interval. The Mann–Whitney test was used to compare the 2 groups (n = 3–5 for both groups).

was found to increase, while Bcl-2 protein expression decreased due to the overexpression of miR-520a, which acts as a positive signal for the induction of apoptosis (Fig. 4A, Table 8; p = 0.002; Mann–Whitney test, U = 0). Together,



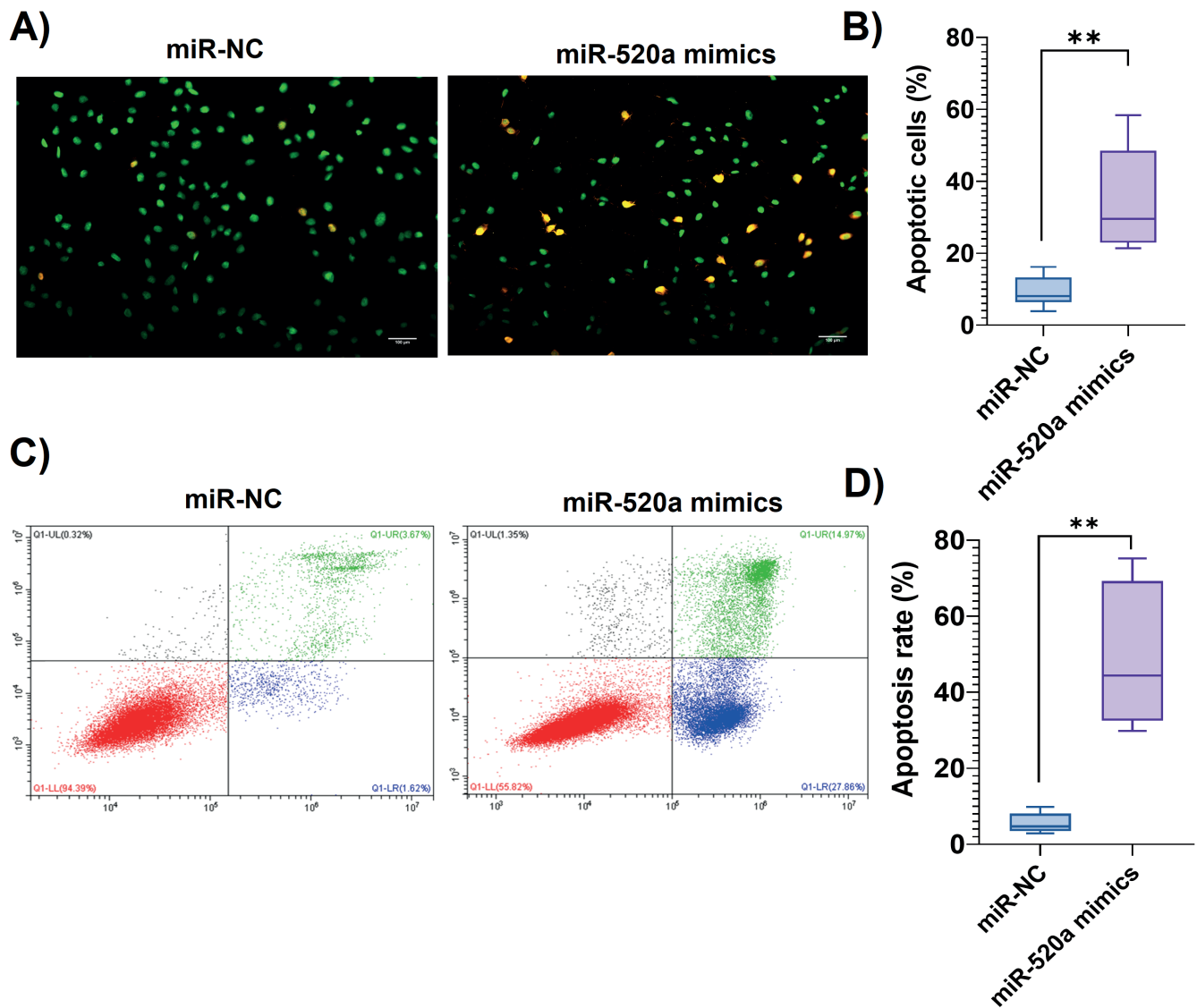


**Fig. 3.** Overexpression of microRNA (miR)-520a induces apoptosis in leukemia cells. **A.** Acridine orange/ethidium bromide (AO/EB) staining for the analysis of nuclear morphology of miR-negative control (NC) or miR-520a mimics-transfected K562 cells; **B.** Quantification of the percentage of apoptotic cells based on nuclear morphology in miR-NC and miR-520a mimics-transfected K562 cells. The data were not normally distributed and were tested by the Shapiro–Wilk test and Kolmogorov–Smirnov test with p-values for miR-NC ( $p = 0.011$ ;  $p = 0.021$ ) and miR-520a ( $p = 0.022$ ;  $p = 0.036$ ). The Mann–Whitney test was used to compare the 2 groups. The data are presented as a median with an interquartile range (Q1–Q3). The upper and lower lines of each box indicate the 25<sup>th</sup> (Q1) and 75<sup>th</sup> (Q3) percentiles. The line inside each box indicates the median; **C.** Flow cytometry-based analysis of apoptosis of miR-NC or miR-520a mimics-transfected K562 cells stained with Annexin V-fluorescein isothiocyanate (FITC)/propidium iodide (PI) dual staining mix; **D.** Quantification of the percentage rate of apoptosis of miR-NC or miR-520a mimics-transfected K562 cells based on flow cytometry analysis. The data were not normally distributed and were tested by the Shapiro–Wilk test and Kolmogorov–Smirnov test with p-values for miR-NC ( $p = 0.029$ ;  $p = 0.028$ ) and miR-520a ( $p = 0.034$ ;  $p = 0.017$ ). The Mann–Whitney test was used to compare the 2 groups. The data are presented as a median with an interquartile range (Q1–Q3). The upper and lower lines of each box indicate the 25<sup>th</sup> (Q1) and 75<sup>th</sup> (Q3) percentiles. The line inside each box indicates the median ( $n = 3–5$ )

\*\* $p = 0.002$  compared to miR-NC.

the findings support our hypothesis that miR-520a positively regulates cancer cell apoptosis in AML, further confirming its anticancer therapeutic potential against this disorder.

### miR-520a targets the PI/AKT signaling pathway in AML

To find a possible mechanism for the regulatory role of miR-520a in AML, we performed western blotting for

both AKT and PI3K proteins (non-phosphorylated and phosphorylated). The overexpression of miR-520a did not significantly affect non-phosphorylated PI3K and AKT protein levels. However, a substantial decrease in the expression levels of the phosphorylated AKT and PI3K (p-AKT and p-PI3K) was observed due to the overexpression of miR-520a (Fig. 4A–D, Table 8;  $p = 0.002$ ; Mann–Whitney test,  $U = 0$ ). This indicates that miR-520a targets and blocks the PI3K/AKT signaling pathway in AML to exert its anti-proliferative role.

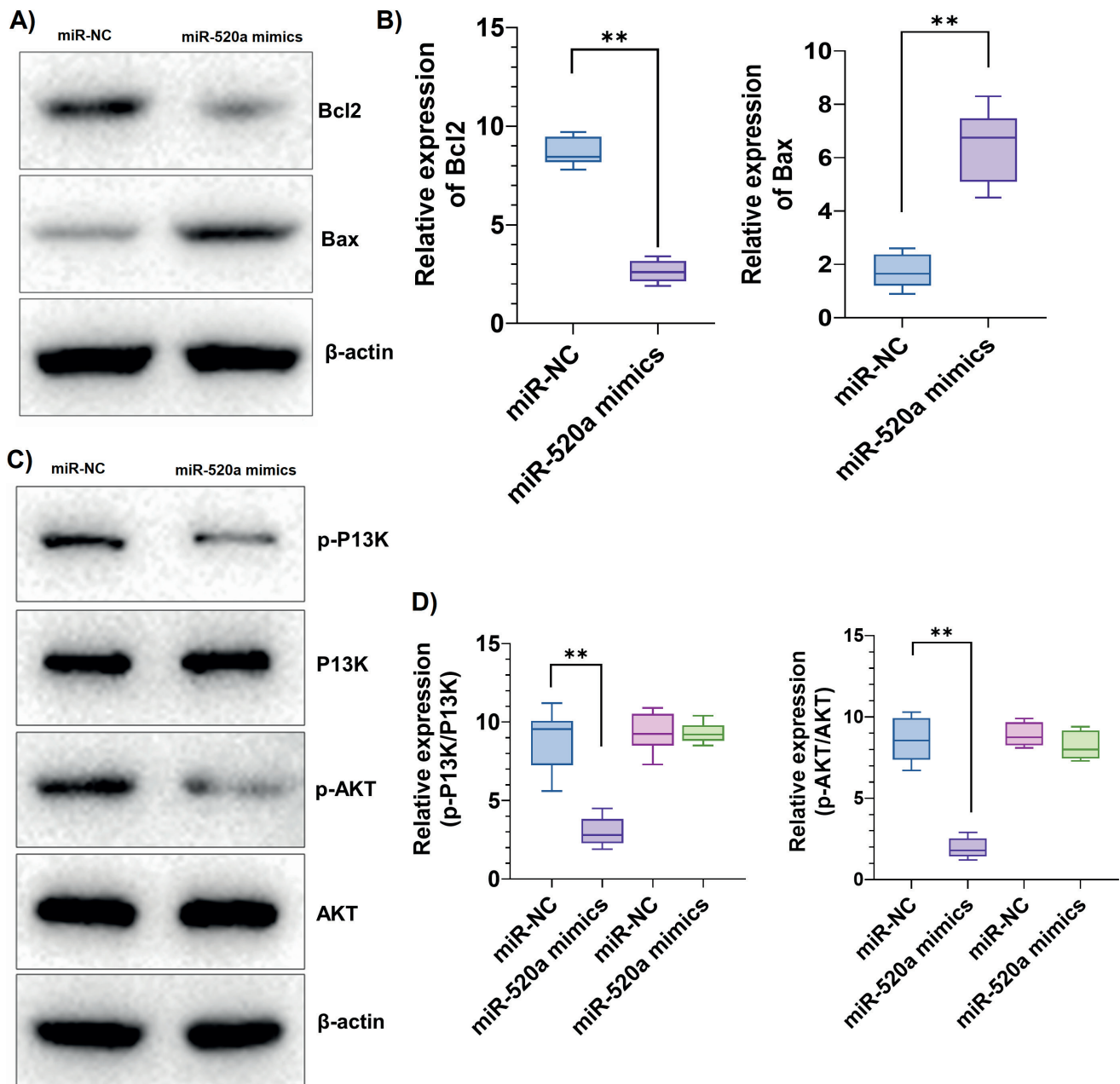


**Fig. 4.** MicroRNA (miR)-520a targets the PI3K/AKT signaling pathway in acute myeloid leukemia (AML). A. Western blotting of Bax and Bcl-2 proteins from miR-negative control (NC) or miR-520a mimics-transfected K562 cells using  $\beta$ -actin protein as an internal control; B. Relative protein expression levels of Bax and Bcl-2 proteins from miR-NC or miR-520a mimics-transfected K562 cells. The data were not normally distributed and were tested by the Shapiro–Wilk test and Kolmogorov–Smirnov test with p-values for miR-NC (Bax:  $p = 0.017$ ;  $p = 0.037$ , Bcl2:  $p = 0.047$ ;  $p = 0.021$ ) and miR-520a (Bax:  $p = 0.015$ ;  $p = 0.034$ , Bcl2:  $p = 0.019$ ;  $p = 0.042$ ). The Mann–Whitney test was used to compare the 2 groups. The data are presented as a median with an interquartile range (Q1–Q3). The upper and lower lines of each box indicate the 25<sup>th</sup> (Q1) and 75<sup>th</sup> (Q3) percentiles. The line inside each box indicates the median; C. Western blotting of phosphorylated (p)-PI3K, PI3K, p-AKT, and AKT proteins from miR-NC or miR-520a mimics-transfected K562 cells using  $\beta$ -actin protein as internal control; D. Relative protein expression levels of p-PI3K, PI3K, p-AKT, and AKT proteins from miR-NC or miR-520a mimics-transfected K562 cells. The data were not normally distributed and were tested by the Shapiro–Wilk test and Kolmogorov–Smirnov test with p-values for miR-NC (p-PI3K:  $p = 0.043$ ;  $p = 0.021$ , PI3K:  $p = 0.018$ ;  $p = 0.015$ , p-AKT:  $p = 0.037$ ;  $p = 0.027$ , AKT:  $p = 0.035$ ;  $p = 0.026$ ) and miR-520a (p-PI3K:  $p = 0.025$ ;  $p = 0.038$ , PI3K:  $p = 0.036$ ;  $p = 0.021$ , p-AKT:  $p = 0.016$ ;  $p = 0.014$ , AKT:  $p = 0.021$ ;  $p = 0.019$ ). The Mann–Whitney test was used to compare the 2 groups. The data are presented as a median with an interquartile range (Q1–Q3). The upper and lower lines of each box indicate the 25<sup>th</sup> (Q1) and 75<sup>th</sup> (Q3) percentiles. The line inside each box indicates the median ( $n = 3–5$ )

\*\* $p = 0.002$  compared to miR-NC.

## Discussion

Recently, miRs have been found to be crucial regulatory molecules in almost all eukaryotic organisms.<sup>17</sup> They are seen to influence many developmental and physiological

processes in humans,<sup>18</sup> such as proliferation, differentiation, programmed cell death, and apoptosis.<sup>19</sup> MicroRNAs exert their regulatory role through post-transcriptional silencing of target protein-coding genes.<sup>20</sup> Dysregulation of many miRs has been associated with various cancers, prompting

**Table 7.** Quantification of the percentage of apoptotic cells in microRNA-negative control (miR-NC) and miR-520a mimics-transfected K562 cells based on nuclear morphology and flow cytometry analysis

Variables	Groups			
	A		B	
	miR-NC	miR-520a mimics	miR-NC	miR-520a mimics
Minimum	3.900	21.40	2.900	29.80
Q1	6.450	22.90	3.500	32.50
Median	8.100	29.55	4.700	44.45
Q3	13.28	48.50	8.075	69.28
Maximum	16.20	58.40	9.800	75.20
Mann–Whitney U	0		0	
p-value	–	0.002**	–	0.002**

A. Quantification of the percentage of apoptotic cells based on nuclear morphology in miR-NC and miR-520a mimics-transfected K562 cells. The Mann–Whitney test was used to compare the 2 groups. The data are presented as median with interquartile range (Q1–Q3); B. Quantification of the percentage rate of apoptosis of miR-NC or miR-520a mimics-transfected K562 cells based on flow cytometry analysis. The Mann–Whitney test was used to compare the 2 groups; \*\*p = 0.002 compared to miR-NC; Q1 – 1<sup>st</sup> quartile; Q3 – 3<sup>rd</sup> quartile.

**Table 8.** MicroRNA (miR)-520a targets the PI3K/AKT signaling pathway in acute myeloid leukemia (AML) with protein expression levels of Bax and Bcl-2, phosphorylated (p)-PI3K, PI3K, p-AKT, and AKT

Variables	Groups											
	A. Bax		B. Bcl2		C. p-PI3K		D. PI3K		E. p-AKT		F. AKT	
	miR-NC	miR-520a mimics	miR-NC	miR-520a mimics	miR-NC	miR-520a mimics	miR-NC	miR-520a mimics	miR-NC	miR-520a mimics	miR-NC	miR-520a mimics
Minimum	0.9000	4.500	7.800	2.200	5.600	1.900	7.300	8.500	6.700	1.200	8.100	7.300
Q1	1.200	5.100	8.175	2.200	7.250	2.275	8.500	8.800	7.375	1.425	8.250	7.450
Median	1.650	6.750	8.450	2.600	9.550	2.800	9.250	9.200	8.550	1.800	8.750	8.000
Q3	2.375	7.475	9.475	3.175	10.08	3.825	10.53	9.800	9.925	2.525	9.675	9.175
Maximum	2.600	8.300	9.700	3.400	11.20	4.500	10.90	10.40	10.30	2.900	9.900	9.400
Mann–Whitney U	0		0		0		16.50		0		9	
p-value	0.002**		0.002**		0.002**		0.855		0.002**		0.179	

A,B. Relative protein expression levels of Bax and Bcl-2 proteins from miR-negative control (NC) or miR-520a mimics-transfected K562 cells. The Mann–Whitney test was used to compare the 2 groups (n = 6 for both groups); C–F. Relative protein expression levels of p-PI3K, PI3K, p-AKT, and AKT proteins from miR-NC or miR-520a mimics-transfected K562 cells (n = 3–5 for both groups); \*\*p = 0.002 compared to miR-NC; Q1 – 1<sup>st</sup> quartile; Q3 – 3<sup>rd</sup> quartile.

researchers to investigate their regulatory role in malignancy.<sup>21</sup> MicroRNAs are also important prognostic markers for human cancer.<sup>22</sup> Moreover, the dysregulation of miRs has been reported in AML.<sup>23</sup> In a recent report, miR-98 was highly expressed in AML, and the study findings were helpful in determining the prognostic importance of miR biomolecules.<sup>24</sup> The *miR-520a* is a tumor suppressor gene in many human cancers,<sup>25,19</sup> and its downregulation has been associated with human breast cancer.<sup>26</sup> In the present investigation, we found a similar dysregulation of miR-520a in AML. Previously, the upregulation of miR-520a was shown to negatively affect cancer cell proliferation,<sup>27</sup> which is supported by our results showing that the overexpression of miR-520a decreases AML cell proliferation.

Furthermore, we found that the reason behind the decrease in leukemia cell proliferation under miR-520a overexpression was the induction of apoptotic cell death in leukemia cells. Similar conclusions were drawn from previous research studies.<sup>11</sup> The PI3K/AKT signaling pathway has

shown involvement in the regulation of cell proliferation and apoptosis.<sup>28</sup> The abnormal activation of this pathway is coupled with increased cell proliferation and survival of cells in many human cancers.<sup>29</sup> Furthermore, it is important to highlight that phosphorylation of the PI3K and AKT proteins is responsible for stimulating the PI3K/AKT signaling pathway.<sup>28</sup>

Interestingly, the overexpression of miR-520a in leukemia cells considerably decreased the levels of phosphorylated AKT and PI3K proteins. This indicates that miR-520a inhibits the phosphorylation of these proteins and blocks the PI3K/AKT signaling cascade, leading to decreased proliferation of leukemia cells and the initiation of apoptosis. A similar mechanism of miR-520a has been reported previously.<sup>25</sup> In summary, the current study explored the possibility of using the drug-based targeting of miR-520a for its transcriptional enhancement, as an alternative anticancer approach that could be investigated in the future against human AML.

## Limitations

There were 3 limitations to this study. First, a limited number of cell lines were used in the present study to examine the effects of miR-520a. Second, inhibitors of miR-52a are not investigated in the present study. Third, other than PI3K/AKT, other significant signaling mechanisms are not explored in the current study.

## Conclusions

The results of the present research established the mechanism by which miR-520a regulates the progression of human AML. The study also revealed the tumor-suppressing role of miR-520a in AML, which can be amplified by activating the PI3K/AKT pathway that specifically targets regulatory molecules to prevent proliferation of human AML efficiently.

## Supplementary files

The Supplementary materials are available at <https://doi.org/10.5281/zenodo.8297073>. The package contains the following files:

Supplementary Fig. 1. Uncropped images of Western blots illustrated in Fig. 1.

## ORCID iDs

Jing Xiao  <https://orcid.org/0009-0001-1866-1638>  
 Fang Wan  <https://orcid.org/0009-0005-2874-5324>  
 Lin Tian  <https://orcid.org/0009-0002-7888-4857>  
 Yao Li  <https://orcid.org/0009-0009-5394-2441>

## References

- Gramatges MM, Rabin KR. The adolescent and young adult with cancer. State of the art: Acute leukemias. *Curr Oncol Rep.* 2013;15(4):317–324. doi:10.1007/s11912-013-0325-5
- Santini V, Lübbert M, Wierzbowska A, Ossenkoppele GJ. The clinical value of decitabine monotherapy in patients with acute myeloid leukemia. *Adv Ther.* 2022;39(4):1474–1488. doi:10.1007/s12325-021-01948-8
- Khadka S, Solanki D, Singh J, et al. Trends and outcomes of venous thromboembolism in adult hospitalizations with acute myeloid leukemia: Analysis of nationwide inpatient sample from 2010 to 2014. *Postgrad Med.* 2021;133(2):160–165. doi:10.1080/00325481.2020.1863717
- Guo S, Li B, Chen Y, et al. Hsa\_circ\_0012152 and Hsa\_circ\_0001857 accurately discriminate acute lymphoblastic leukemia from acute myeloid leukemia. *Front Oncol.* 2020;10:1655. doi:10.3389/fonc.2020.01655
- Guan J, Liu P, Wang A, Wang B. Long non-coding RNA ZEB2-AS1 affects cell proliferation and apoptosis via the miR-122-5p/PLK1 axis in acute myeloid leukemia. *Int J Mol Med.* 2020;46(4):1490–1500. doi:10.3892/ijmm.2020.4683
- Li ZJ, Cheng J, Song Y, Li HH, Zheng JF. LncRNA SNHG5 upregulation induced by YY1 contributes to angiogenesis via miR-26b/CTGF/VEGFA axis in acute myelogenous leukemia. *Lab Invest.* 2021;101(3):341–352. doi:10.1038/s41374-020-00519-9
- Koenig KL, Sahasrabudhe KD, Sigmund AM, Bhatnagar B. AML with myelodysplasia-related changes: Development, challenges and treatment advances. *Genes (Basel).* 2020;11(8):845. doi:10.3390/genes11080845
- Bernasconi P, Borsani O. Targeting leukemia stem cell-niche dynamics: A new challenge in AML treatment. *J Oncol.* 2019;2019:8323592. doi:10.1155/2019/8323592
- Wallace JA, O'Connell RM. MicroRNAs and acute myeloid leukemia: Therapeutic implications and emerging concepts. *Blood.* 2017;130(11):1290–1301. doi:10.1182/blood-2016-10-697698
- Wang L, Wang Y, Lin J. MiR-152-3p promotes the development of chronic myeloid leukemia by inhibiting p27. *Eur Rev Med Pharmacol Sci.* 2018;22(24):8789–8796. doi:10.26355/eurrev\_201812\_16646
- Yu J, Tan Q, Deng B, Fang C, Qi D, Wang R. The microRNA-520a-3p inhibits proliferation, apoptosis and metastasis by targeting MAP3K2 in non-small cell lung cancer. *Am J Cancer Res.* 2015;5(2):802–811. PMID:25973317. PMCID:PMC4396038.
- Xie Y, Xue C, Guo S, Yang L. MicroRNA-520a suppresses pathogenesis and progression of non-small-cell lung cancer through targeting the RRM2/Wnt axis. *Anal Cell Pathol (Amst).* 2021;2021:9652420. doi:10.1155/2021/9652420
- Hong S, Chen S, Wang X, et al. ATAD2 silencing decreases VEGFA secretion through targeting has-miR-520a to inhibit angiogenesis in colorectal cancer. *Biochem Cell Biol.* 2018;96(6):761–768. doi:10.1139/bcb-2018-0081
- Wang X, Wang P, Zhu Y, Zhang Z, Zhang J, Wang H. MicroRNA-520a attenuates proliferation of Raji cells through inhibition of AKT1/NF- $\kappa$ B and PERK/eIF2 $\alpha$  signaling pathway. *Oncol Rep.* 2016;36(3):1702–1708. doi:10.3892/or.2016.4975
- Holland M, Cunningham R, Seymour L, et al. Separation, banking, and quality control of peripheral blood mononuclear cells from whole blood of melanoma patients. *Cell Tissue Bank.* 2018;19(4):783–790. doi:10.1007/s10561-018-9734-x
- Chen XY, Qin XH, Xie XL, Liao CX, Liu DT, Li GW. Overexpression miR-520a-3p inhibits acute myeloid leukemia progression via targeting MUC1. *Transl Oncol.* 2022;22:101432. doi:10.1016/j.tranon.2022.101432
- He L, Hannon GJ. MicroRNAs: Small RNAs with a big role in gene regulation. *Nat Rev Genet.* 2004;5(7):522–531. doi:10.1038/nrg1379
- Chang TC, Mendell JT. microRNAs in vertebrate physiology and human disease. *Annu Rev Genom Hum Genet.* 2007;8(1):215–239. doi:10.1146/annurev.genom.8.080706.092351
- Su H, Ren F, Jiang H, Chen Y, Fan X. Upregulation of microRNA-520a-3p inhibits the proliferation, migration and invasion via spindle and kinetochore associated 2 in gastric cancer. *Oncol Lett.* 2019;18(3):3323–3330. doi:10.3892/ol.2019.10663
- Patil VS, Zhou R, Rana TM. Gene regulation by non-coding RNAs. *Crit Rev Biochem Mol Biol.* 2014;49(1):16–32. doi:10.3109/10409238.2013.844092
- Bhatti I, Lee A, Lund J, Larvin M. Small RNA: A large contributor to carcinogenesis? *J Gastrointest Surg.* 2009;13(7):1379–1388. doi:10.1007/s11605-009-0887-6
- Lan H, Lu H, Wang X, Jin H. MicroRNAs as potential biomarkers in cancer: Opportunities and challenges. *Biomed Res Int.* 2015;2015:125094. doi:10.1155/2015/125094
- Barrera-Ramirez J, Lavoie JR, Maganti HB, et al. Micro-RNA profiling of exosomes from marrow-derived mesenchymal stromal cells in patients with acute myeloid leukemia: Implications in leukemogenesis. *Stem Cell Rev Rep.* 2017;13(6):817–825. doi:10.1007/s12015-017-9762-0
- Hu N, Cheng Z, Pang Y, et al. High expression of MiR-98 is a good prognostic factor in acute myeloid leukemia patients treated with chemotherapy alone. *J Cancer.* 2019;10(1):178–185. doi:10.7150/jca.26391
- Lv X, Li CY, Han P, Xu XY. MicroRNA-520a-3p inhibits cell growth and metastasis of non-small cell lung cancer through PI3K/AKT/mTOR signaling pathway. *Eur Rev Med Pharmacol Sci.* 2018;22(8):2321–2327. doi:10.26355/eurrev\_201804\_14822
- Mu J, Ning S, Wang X, et al. The repressive effect of miR-520a on NF- $\kappa$ B/IL-6/STAT-3 signal involved in the glabridin-induced anti-angiogenesis in human breast cancer cells. *RSC Adv.* 2015;5(43):34257–34264. doi:10.1039/C4RA17062H
- Zhang R, Liu R, Liu C, et al. A novel role for MiR-520a-3p in regulating EGFR expression in colorectal cancer. *Cell Physiol Biochem.* 2017;42(4):1559–1574. doi:10.1159/000479397
- Chang F, Lee JT, Navolanic PM, et al. Involvement of PI3K/Akt pathway in cell cycle progression, apoptosis, and neoplastic transformation: A target for cancer chemotherapy. *Leukemia.* 2003;17(3):590–603. doi:10.1038/sj.leu.2402824
- Vara JÁF, Casado E, De Castro J, Cejas P, Belda-Iniesta C, González-Barón M. PI3K/Akt signalling pathway and cancer. *Cancer Treat Rev.* 2004;30(2):193–204. doi:10.1016/j.ctrv.2003.07.007

# MCT1 gene silencing enhances the immune effect of dendritic cells on cervical cancer cells

Xiaoxin Sui<sup>1,A–F</sup>, Xiaowei Xi<sup>2,B,C</sup>

<sup>1</sup> Department of Obstetrics and Gynecology, Shanghai Changzheng Hospital, Naval Medical University, Shanghai, China

<sup>2</sup> Department of Obstetrics and Gynecology, General Hospital, Shanghai Jiao Tong University School of Medicine, China

A – research concept and design; B – collection and/or assembly of data; C – data analysis and interpretation; D – writing the article; E – critical revision of the article; F – final approval of the article

Advances in Clinical and Experimental Medicine, ISSN 1899–5276 (print), ISSN 2451–2680 (online)

Adv Clin Exp Med. 2024;33(7):739–749

## Address for correspondence

Xiaoxin Sui

E-mail: suixiaoxinsjtu@126.com

## Funding sources

The study was funded by the National Natural Science Foundation of China (grant No. 81772767) and the Science and Technology Commission of Shanghai Municipality (grant No. 15411952300).

## Conflict of interest

None declared

Received on August 29, 2022

Reviewed on March 1, 2023

Accepted on August 21, 2023

Published online on January 5, 2024

## Abstract

**Background.** Dendritic cells (DCs) are a key class of immune cells that migrate to the draining lymph nodes and present processed antigenic peptides to lymphocytes after being activated by external stimuli, thereby establishing adaptive immunity. Moreover, DCs play an important role in tumor immunity.

**Objectives.** The aim of the study was to investigate whether *MCT1* gene silencing in DCs affects their ability to mount an immune response against cervical cancer cells.

**Materials and methods.** We silenced the expression of *MCT1* in DCs from mouse bone marrow (BM) by infection with adenovirus. The surface antigen profile of DCs was analyzed by flow cytometry and cytokine secretion was evaluated using enzyme-linked immunosorbent assay (ELISA) following sodium lactate (sLA) exposure and lipopolysaccharide (LPS) stimulation. Then, various groups of DC-induced cytotoxic T lymphocytes (CTLs) were prepared and their cytotoxicity against U14 was tested.

**Results.** Without sLA exposure, silencing *MCT1* did not affect the expression of CD1a, CD80, CD83, CD86, and major histocompatibility complex class II (MHCII) in DCs after LPS challenge. Similar results were found for interleukin (IL)-6, IL-12 p70 and tumor necrosis factor alpha (TNF- $\alpha$ ). After sLA exposure, silencing *MCT1* significantly decreased the expression of CD1a, CD80, CD83, CD86, and MHCII in DCs after the LPS challenge, as well as the secretion of IL-6, IL-12 p70 and TNF- $\alpha$ . In addition, sLA exposure significantly reduced the toxicity and inhibited the proliferation of DC-induced CTLs compared to U14 cells in vitro and in vivo. However, silencing *MCT1* significantly attenuated the changes caused by sLA exposure. At the same time, in the absence of sLA, silencing *MCT1* did not affect the toxicity nor inhibit the proliferation of DC-induced CTLs on U14 cells.

**Conclusions.** Lactate exposure reduces the immune effect of DCs on cervical cancer cells, but *MCT1* gene silencing attenuates these alterations.

**Key words:** dendritic cells, cervical cancer, immunity, *MCT1*

## Cite as

Sui X, Xi X. *MCT1* gene silencing enhances the immune effect of dendritic cells on cervical cancer cells. *Adv Clin Exp Med*. 2024;33(7):739–749. doi:10.17219/acem/171446

## DOI

10.17219/acem/171446

## Copyright

Copyright by Author(s)

This is an article distributed under the terms of the Creative Commons Attribution 3.0 Unported (CC BY 3.0) (<https://creativecommons.org/licenses/by/3.0/>)

## Background

Dendritic cells (DCs) represent a critical subset of immune cells that initiate adaptive immunity by migrating to the draining lymph nodes. These cells are activated by external stimuli and present processed antigenic peptides to lymphocytes.<sup>1,2</sup> Moreover, DCs play an essential role in tumor immunity by ingesting tumor antigens and maturing to express major histocompatibility complex (MHC) class I and II molecules, costimulatory factors, and adhesion factors.<sup>3,4</sup> In addition, DCs combined with T cells induce the killer cells to produce large quantities of interferon (IFN)- $\gamma$ , perforin and granzyme by secreting high concentrations of interleukin (IL)-12, thereby enhancing the lysis effect of target cells on cancer cells.<sup>3,4</sup> Simultaneously, DCs can induce the killing effect of CD8+ T cells, facilitating the clearance of antigen-specific tumor cells. Thus, DCs initiate the body's anti-tumor immunity and are the bridge between T cells and tumor cells.<sup>5,6</sup> Any alteration to the normal functioning of DCs can directly impact the body's anti-tumor immunity.

Tumor immunotherapy, especially chimeric antigen receptor (CAR)-T cell immunotherapy, has developed rapidly in recent years.<sup>7</sup> Despite significant clinical outcomes of immunotherapies in liquid tumors, their effectiveness in solid tumors is comparatively limited. The microenvironment of solid tumors has been identified as a key factor contributing to the significant difference in clinical responses to cell-based immunotherapy between these two forms of cancers.<sup>7,8</sup> The Warburg Effect is the most notable feature distinguishing tumor cells from normal cells, in which tumor cells preferentially choose to supply energy through glycolysis under anaerobic conditions, and lactate is the main by-product of glycolysis energy supply for tumor cells.<sup>9,10</sup> The Warburg Effect may provide tumor cells with an escape mechanism against the immune system, as high lactate concentrations have been reported to alter the phenotype of immune cells.<sup>11–13</sup> A recent study stated that lactate exposure attenuated DC maturation by downregulating CD80 and MHCII expression following lipopolysaccharide (LPS) stimulation.<sup>13</sup> Therefore, lactate is a barrier affecting the anti-tumor immunity of DCs.

Monocarboxylate transporters (MCTs) of the SLC16 solute carrier family are key proteins for intracellular and extracellular lactate exchange.<sup>14–16</sup> Under physiological conditions, MCTs prevent lactate accumulation within cells by eliminating its excess produced due to increased glycolytic activity. This process has potential implications for developing cancer therapeutics targeting lactate metabolism.<sup>16,17</sup> Dendritic cells express several MCTs, including MCT1, MCT2 and MCT4. The MCT1 and MCT2 are responsible for transporting extracellular lactate into the cell, while MCT4 is responsible for transporting intracellular lactate outside the cell.

Additionally, while MCT1 and MCT4 are regulated by lactate, MCT2 is not involved in lactate management.<sup>13,15,18</sup>

Therefore, we hypothesized that the expression level of MCT1 in DCs would have an impact on their phenotype under high lactate conditions, thereby affecting their anti-tumor immunity. In this study, we used adenovirus to silence MCT1 of mouse bone marrow (BM)-derived DCs to investigate their phenotypic changes and toxicity to cervical cancer cells in standard or high lactate environments.

## Objectives

This study aimed to examine the impact of DC-mediated immunity on cervical cancer cells following *MCT1* gene silencing.

## Materials and methods

### Ethics statement

This study was carried out following the National Institutes of Health Guide for the Care and Use of Laboratory Animals.<sup>19</sup> The protocol was approved by the Animal Ethics Committee of Shanghai Changzheng Hospital, Naval Medical University, China (approval No. 2017KY068).

### Cells and reagents

The U14 cells were purchased from American Type Culture Collection (Manassas, USA) and cultured in RPMI-1640 medium (A1049101; Gibco, Waltham, USA) with the addition of 10% fetal bovine serum (FBS) (10099141; Gibco) at 37°C with 5% CO<sub>2</sub>. Mouse SLC16A1 (*MCT1*) shRNA silencing adenovirus (Ad-sh*MCT1*) and its matched control shRNA adenovirus were purchased from Vector Biolabs (shADV-272089; Vector Biolabs, Malvern, USA). The anti-*MCT1* antibody was purchased from Abcam (ab156080; Cambridge, UK). Other used antibodies included FITC-conjugated CD1a antibody (ab27992; Abcam), CD80 antibody (ab18279; Abcam), CD83 antibody (MHCD8301; Thermo Fisher Scientific, Waltham, USA), CD86 antibody (MHCD8601; Thermo Fisher Scientific), and MHCII antibody (11-9956-42; eBioscience, San Diego, USA). The Cell Counting Kit-8 (CCK-8) (C0037), mouse IL-6 enzyme-linked immunosorbent assay (ELISA) kit (PI326) and mouse tumor necrosis factor alpha (TNF- $\alpha$ ) ELISA kit (PT512) were purchased from Beyotime Biotechnology (Shanghai, China). Finally, the mouse IL-12 p70 ELISA kit (EK0500) was purchased from Signalway Antibody (Greenbelt, USA).

### Adenovirus infection of BM-derived DCs

As previously described,<sup>20</sup> we prepared DCs from mouse BM. In brief, the mouse tibia was rinsed with phosphate-buffered saline (PBS), red blood cells were fully lysed, and

cells were collected by centrifugation. The cells from BM were cultured in RPMI-1640 medium supplemented with 10% FBS, 20 ng/mL rmGM-CSF (PMC2016; Thermo Fisher Scientific) and 20 ng/mL rmIL-4 (RMIL4I; Thermo Fisher Scientific) at 37°C with 5% CO<sub>2</sub> for 1 week. Subsequently, Ad-shCtrl or Ad-shMCT1 adenoviruses (MOI = 10:1) were added to BM-derived DCs for 12 h, cultured at 37°C with 5% CO<sub>2</sub>. Then, the medium was replaced with a fresh one to continue culturing.

## Immunoblot analysis

After 24 h of Ad-shCtrl or Ad-shMCT1 infection, DCs were harvested, and an appropriate amount of cell lysing solution was utilized to extract total cellular protein. Approximately 40 µg of cellular protein was analyzed using 10% sodium dodecyl-sulfate polyacrylamide gel electrophoresis (SDS-PAGE), followed by the transfer of protein molecules to a polyvinylidene difluoride (PVDF) membrane. Subsequently, the membrane was blocked with 5% non-fat milk powder at room temperature for 1 h and then incubated overnight at 4°C with the MCT1 antibody. After being washed 3 times with tris-buffered saline (TBS)+0.1% Tween-20 (TBST) buffer at room temperature, secondary antibodies were added to the membrane and it was incubated for 1 h at room temperature. Protein bands were developed using an ECL Chemiluminescence Kit (P0018FS; Beyotime), and the protein band grey value was analyzed using ImageJ v. 1.8.0 (<https://imagej.nih.gov/ij/index.html>).

## Dendritic cell phenotype analysis and cytokine assay

After 24 h of Ad-shCtrl or Ad-shMCT1 infection, 50 mM of sodium lactate (sLA) was added to the culture medium for 48 h (an equal amount of PBS was used as control) and then changed to a fresh medium supplemented with 1 µg/mL LPS (L2880; Sigma-Aldrich, St. Louis, USA), followed by culturing for another 24 h. Then, we collected DCs and analyzed their phenotype using a flow cytometer. The cell culture medium was collected and investigated for cytokine content (IL-6, IL-12 p70 and TNF-α), in accordance with the manufacturer's instructions.

## Cytotoxicity assay

Dendritic cells were co-cultured with mouse splenic T cells for 1 week at a ratio of 1:10 after adenovirus infection, sLA exposure (PBS as control) and LPS challenge. Then, we collected the T cells after 7 days, defining them as cytotoxic T lymphocytes (CTLs). Using a CCK-8 kit, the *in vitro* cytotoxicity of DC-induced CTLs was assayed by culturing the CTLs with target U14 cells for 24 h at effector:target (E:T) ratios of 90:1, 30:1 and 10:1.

## Cell clone formation test

The DC-induced CTLs and U14 cells were mixed and cultured (1:10), and after 24 h of culture, they were digested with trypsin. The cells were resuspended as a single-cell suspension, and 1000 cells were seeded into a 6-centimeter culture dish and incubated in a culture medium at 37°C with 5% CO<sub>2</sub> for 14 days. Then, the cells were stained with crystal violet and the number of clones was counted.

## Nude mouse U14 cell xenograft

After a week of adaptive feeding, 42 nude mice (6–8 weeks old, 18–22 g) were randomly divided into 6 groups. The U14 cells in the ratio of 2×10<sup>6</sup> cells/100 µL were injected subcutaneously into the back of the mice. After 10 days, 2×10<sup>6</sup> cells/200 µL of DC-induced CTLs were injected into U14 xenografts for treatment once a week for a period of 30 days. Subsequently, mice were euthanized, and the U14 xenografts were isolated and compared for tumor tissue weight.

## Statistical analyses

The SPSS v. 20.0 (IBM Corp., Armonk, USA) and GraphPad Prism (v. 5.0; GraphPad Software, Boston, USA) were used to analyze data. The measurement data were expressed as mean ± standard deviation. We used the Shapiro–Wilk test to assess whether the measured data conform to the normal distribution in SPSS. The *p*-value was calculated using analysis of variance (ANOVA) followed by Tukey's multiple comparison test between multiple groups in GraphPad Prism. Student's *t*-test was used to compare the differences between 2 groups. A value of *p* < 0.05 was considered statistically significant.

## Results

### Analysis of silencing MCT1 in DCs

Immunoblotting was used to detect the expression of MCT1 protein in DCs in order to analyze the *MCT1* gene silencing effect of Ad-shMCT1 adenovirus. Results showed that Ad-shMCT1 adenovirus significantly decreased the expression of MCT1 protein in DCs compared to the control group (*p* < 0.05, honestly significant difference (HSD) test following ANOVA, Fig. 1 and Table 1).

### MCT1 silencing alters the phenotype of mature DCs following sLA exposure

In the absence of sLA, MCT1 silencing did not affect the percentage of DCs expressing CD1a, CD80, CD83, CD86, and MHCII. Upon sLA exposure and MCT1

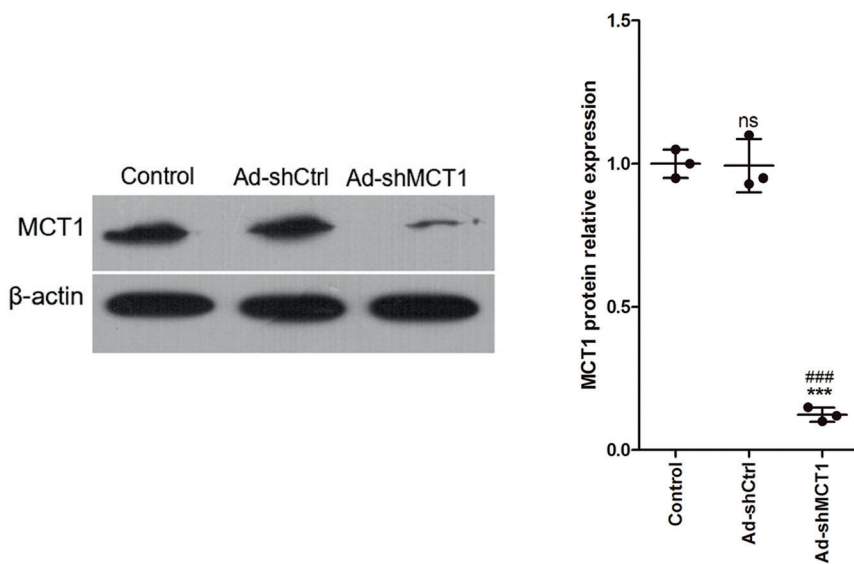


**Fig. 1.** Analysis of MCT1 inhibition in dendritic cells (DCs). We used immunoblotting to analyze the inhibition efficacy of mouse SLC16A1 (MCT1) shRNA silencing adenovirus (Ad-shMCT1) on the expression of MCT1 in DCs, and ImageJ software was used to analyze the relative MCT1 expression. The column height represents the average value, and the error bar represents the standard deviation. The p-value was calculated by Tukey's honestly significant difference (HSD) test following the analysis of variance (ANOVA). We performed 3 independent replicates for MCT1 protein detection in each group

<sup>ns</sup>  $p > 0.05$ , <sup>###</sup>  $p < 0.001$  compared to the control group; <sup>\*\*\*</sup>  $p < 0.001$  compared to the Ad-shCtrl group.

**Table 1.** Statistics for Fig. 1

Variable		Minimal	Q1	Median	Q3	Maximal	Mean	SD
MCT1	control (n = 3)	0.95	0.95	1.00	1.05	1.05	1.00	0.05
	Ad-shCtrl (n = 3)	0.93	0.93	0.95	1.10	1.10	0.99	0.09
	Ad-shMCT1 (n = 3)	0.10	0.10	0.12	0.15	0.15	0.12	0.025

SD – standard deviation; Q1 – 1<sup>st</sup> quartile; Q3 – 3<sup>rd</sup> quartile; Ad-shMCT1 – mouse SLC16A1 (MCT1) shRNA silencing adenovirus.

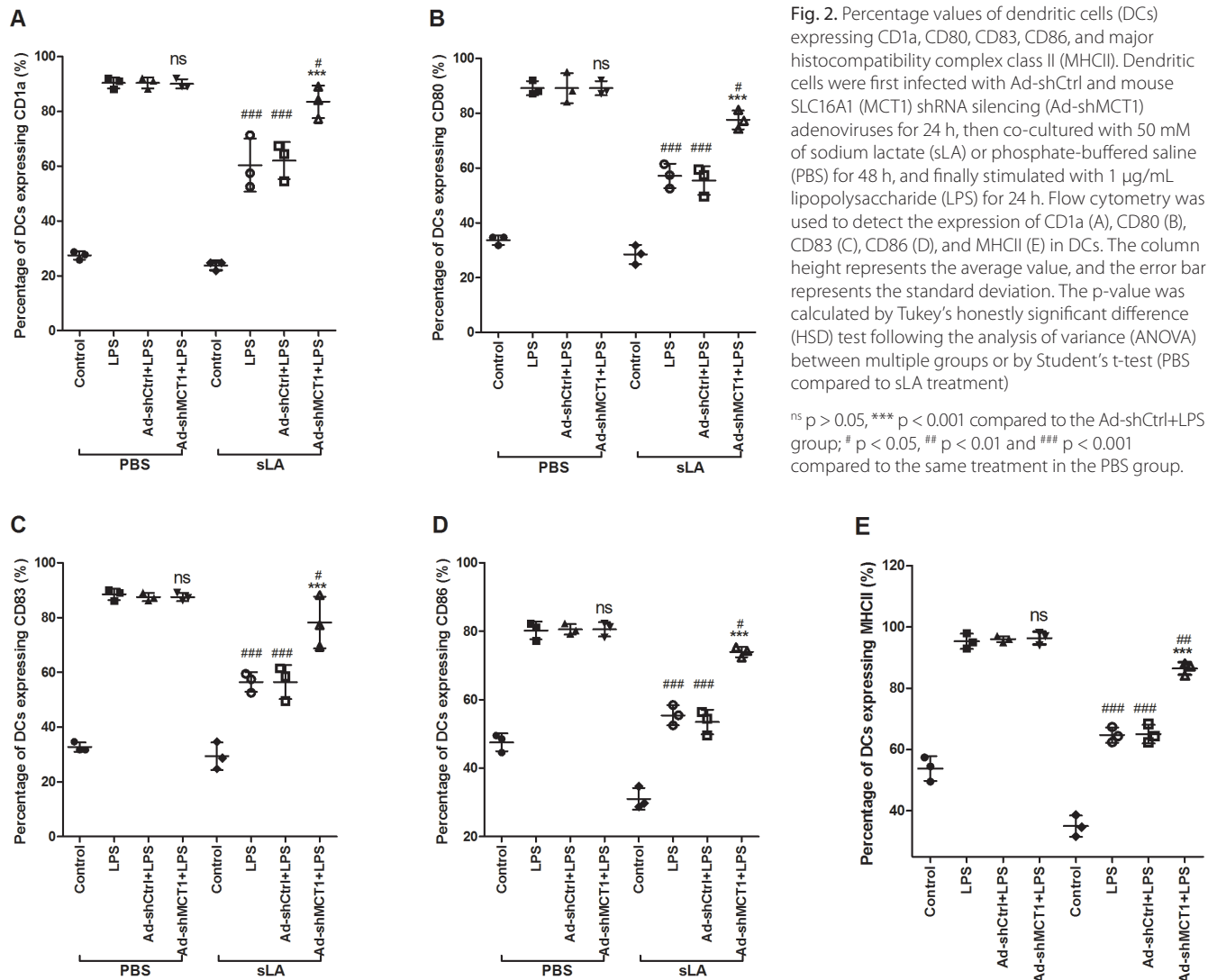


**Fig. 2.** Percentage values of dendritic cells (DCs) expressing CD1a, CD80, CD83, CD86, and major histocompatibility complex class II (MHCII). Dendritic cells were first infected with Ad-shCtrl and mouse SLC16A1 (MCT1) shRNA silencing (Ad-shMCT1) adenoviruses for 24 h, then co-cultured with 50 mM of sodium lactate (sLA) or phosphate-buffered saline (PBS) for 48 h, and finally stimulated with 1  $\mu$ g/mL lipopolysaccharide (LPS) for 24 h. Flow cytometry was used to detect the expression of CD1a (A), CD80 (B), CD83 (C), CD86 (D), and MHCII (E) in DCs. The column height represents the average value, and the error bar represents the standard deviation. The p-value was calculated by Tukey's honestly significant difference (HSD) test following the analysis of variance (ANOVA) between multiple groups or by Student's t-test (PBS compared to sLA treatment)

<sup>ns</sup>  $p > 0.05$ , <sup>\*\*\*</sup>  $p < 0.001$  compared to the Ad-shCtrl+LPS group; <sup>#</sup>  $p < 0.05$ , <sup>##</sup>  $p < 0.01$  and <sup>###</sup>  $p < 0.001$  compared to the same treatment in the PBS group.



silencing, the percentage of DCs significantly increased ( $p < 0.05$ , HSD test following ANOVA, Fig. 2 and Table 2). However, after sLA exposure and LPS stimulation, the rate of DCs significantly decreased, without a concomitant change in DC viability (Supplementary Fig. 1, Supplementary Table 1).

### MCT1 silencing alters the secretion of cytokine from DCs after sLA exposure

The MCT1 silencing significantly increased the DC levels of IL-6, IL-12 p70 and TNF- $\alpha$  after sLA exposure ( $p < 0.05$ , HSD test following ANOVA, Fig. 3 and Table 3).

Table 2. Statistics for Fig. 2 (n = 3)

Variable		Minimal	Q1	Median	Q3	Maximal	Mean	SD
PBS-CD1a	control	25.74	25.74	27.72	28.71	28.71	27.39	1.51
	LPS	88.12	88.12	91.09	92.08	92.08	90.43	2.06
	Ad-shCtrl+LPS	88.12	88.12	91.09	92.08	92.08	90.43	2.06
	Ad-shMCT1+LPS	89.11	89.11	89.11	92.08	92.08	90.1	1.72
sLA-CD1a	control	21.78	21.78	24.75	24.75	24.75	23.76	1.72
	LPS	52.48	52.48	57.43	71.29	71.29	60.40	9.75
	Ad-shCtrl+LPS	54.46	54.46	64.36	67.33	67.33	62.05	6.74
	Ad-shMCT1+LPS	77.23	77.23	84.16	89.11	89.11	83.50	5.97
PBS-CD80	control	31.68	31.68	34.65	34.65	34.65	33.66	1.72
	LPS	87.13	87.13	88.12	92.08	92.08	89.11	2.62
	Ad-shCtrl+LPS	84.16	84.16	88.12	95.05	95.05	89.11	5.51
	Ad-shMCT1+LPS	87.13	87.13	88.12	92.08	92.08	89.11	2.62
sLA-CD80	control	24.75	24.75	28.71	31.68	31.68	28.38	3.48
	LPS	52.48	52.48	57.43	61.39	61.39	57.1	4.46
	Ad-shCtrl+LPS	49.50	49.5	57.43	59.41	59.41	55.45	5.24
	Ad-shMCT1+LPS	74.26	74.26	77.23	81.19	81.19	77.56	3.48
PBS-CD83	control	31.68	31.68	31.68	34.65	34.65	32.67	1.72
	LPS	86.14	86.14	89.11	90.10	90.10	88.45	2.06
	Ad-shCtrl+LPS	86.14	86.14	87.13	89.11	89.11	87.46	1.51
	Ad-shMCT1+LPS	86.14	86.14	87.13	89.11	89.11	87.46	1.51
sLA-CD83	control	24.75	24.75	28.71	34.65	34.65	29.37	4.98
	LPS	52.48	52.48	57.43	59.41	59.41	56.44	3.57
	Ad-shCtrl+LPS	49.50	49.50	58.42	61.39	61.39	56.44	6.19
	Ad-shMCT1+LPS	69.31	69.31	77.23	88.12	88.12	78.22	9.44
PBS-CD86	control	44.55	44.55	48.51	49.50	49.50	47.52	2.62
	LPS	77.23	77.23	81.19	82.18	82.18	80.20	2.62
	Ad-shCtrl+LPS	79.21	79.21	80.20	82.18	82.18	80.53	1.51
	Ad-shMCT1+LPS	78.22	78.22	81.19	82.18	82.18	80.53	2.06
sLA-CD86	control	28.71	28.71	29.70	34.65	34.65	31.02	3.18
	LPS	52.48	52.48	55.45	58.42	58.42	55.45	2.97
	Ad-shCtrl+LPS	49.50	49.50	54.46	56.44	56.44	53.47	3.58
	Ad-shMCT1+LPS	72.28	72.28	74.26	75.25	75.25	73.93	1.51
PBS-MHCII	control	49.50	49.50	54.46	57.43	57.43	53.80	4.01
	LPS	93.07	93.07	95.05	98.02	98.02	95.38	2.49
	Ad-shCtrl+LPS	95.05	95.05	96.04	97.03	97.03	96.04	0.99
	Ad-shMCT1+LPS	94.06	94.06	97.03	98.02	98.02	96.37	2.06
sLA-MHCII	control	31.68	31.68	34.65	38.61	38.61	34.98	3.48
	LPS	62.38	62.38	64.36	67.33	67.33	64.69	2.49
	Ad-shCtrl+LPS	62.38	62.38	64.36	68.32	68.32	65.02	3.02
	Ad-shMCT1+LPS	84.16	84.16	87.13	88.12	88.12	86.47	2.06

SD – standard deviation; Q1 – 1<sup>st</sup> quartile; Q3 – 3<sup>rd</sup> quartile; LPS – lipopolysaccharide; sLA – sodium lactate; MHCII – major histocompatibility complex class II; Ad-shMCT1 – mouse SLC16A1 (MCT1) shRNA silencing adenovirus; PBS – phosphate-buffered saline.

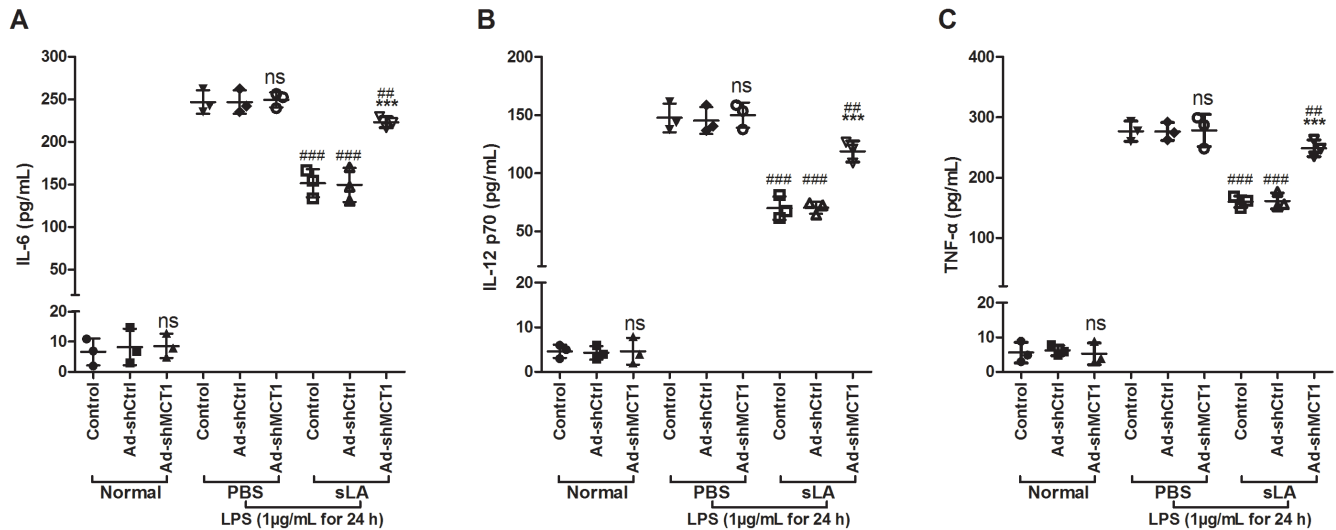


**Fig. 3.** Secretion of cytokine from dendritic cells (DCs). Dendritic cells were first infected with Ad-shCtrl and mouse SLC16A1 (MCT1) shRNA silencing (Ad-shMCT1) adenoviruses for 24 h, then co-cultured with 50 mM of sodium lactate (sLA) or phosphate-buffered saline (PBS) for 48 h, and finally stimulated with 1  $\mu$ g/mL lipopolysaccharide (LPS) for 24 h. The content of interleukin (IL)-6, IL-12 p70 and tumor necrosis factor alpha (TNF- $\alpha$ ) in the DC culture medium was detected by enzyme-linked immunosorbent assay (ELISA) kit. The column height represents the average value, and the error bar represents the standard deviation. The p-value was calculated by Tukey's honestly significant difference (HSD) test following the analysis of variance (ANOVA) testing between multiple groups or by Student's t-test (PBS compared to sLA treatment)

ns  $p > 0.05$ , \*\*\*  $p < 0.001$  compared to the Ad-shCtrl+LPS group; #  $p < 0.05$ , ##  $p < 0.01$  and ###  $p < 0.001$  compared to the same treatment in the PBS group.

**Table 3.** Statistics for Fig. 3 (n = 3)

Variable		Minimal	Q1	Median	Q3	Maximal	Mean	SD
Normal IL-6	control	1.98	1.98	6.93	10.89	10.89	6.60	4.46
	Ad-shCtrl	2.97	2.97	6.93	14.85	14.85	8.25	6.05
	Ad-shMCT1	4.95	4.95	7.92	12.87	12.87	8.58	4.00
PBS IL-6	control	235.60	235.60	242.60	262.40	262.40	246.90	13.88
	Ad-shCtrl	235.60	235.60	242.60	262.40	262.40	246.90	13.88
	Ad-shMCT1	239.60	239.60	252.50	256.40	256.40	249.50	8.81
sLA IL-6	control	133.70	133.70	154.50	166.30	166.30	151.50	16.54
	Ad-shCtrl	130.70	130.70	147.50	170.30	170.30	149.50	19.88
	Ad-shMCT1	216.80	216.80	222.80	229.70	229.70	223.10	6.44
Normal IL-12 p70	control	2.97	2.97	4.95	5.94	5.94	4.62	1.51
	Ad-shCtrl	2.97	2.97	3.96	5.94	5.94	4.29	1.51
	Ad-shMCT1	1.98	1.98	3.96	7.92	7.92	4.62	3.03
PBS IL-12 p70	control	137.60	137.60	143.60	161.40	161.40	147.50	12.37
	Ad-shCtrl	136.60	136.60	140.60	158.40	158.40	145.20	11.61
	Ad-shMCT1	137.60	137.60	153.50	158.40	158.40	149.80	10.87
sLA IL-12 p70	control	61.39	61.39	67.33	81.19	81.19	69.97	10.16
	Ad-shCtrl	64.36	64.36	72.28	74.26	74.26	70.30	5.24
	Ad-shMCT1	108.90	108.90	120.80	126.70	126.70	118.80	9.07
Normal TNF- $\alpha$	control	2.94	2.94	4.90	8.82	8.82	5.55	2.99
	Ad-shCtrl	4.90	4.90	5.88	7.84	7.84	6.21	1.50
	Ad-shMCT1	2.94	2.94	3.92	8.82	8.82	5.23	3.15
PBS TNF- $\alpha$	control	259.80	259.80	277.50	293.10	293.10	276.80	16.68
	Ad-shCtrl	262.80	262.80	274.50	292.20	292.20	276.50	14.80
	Ad-shMCT1	248.00	248.00	287.30	299.00	299.00	278.10	26.69
sLA TNF- $\alpha$	control	150.00	150.00	161.80	168.60	168.60	160.10	9.42
	Ad-shCtrl	152.00	152.00	155.90	176.50	176.50	161.40	13.17
	Ad-shMCT1	235.30	235.30	248.00	262.80	262.80	248.70	13.74

SD – standard deviation; Q1 – 1<sup>st</sup> quartile; Q3 – 3<sup>rd</sup> quartile; sLA – sodium lactate; IL – interleukin; TNF- $\alpha$  – tumor necrosis factor alpha; Ad-shMCT1 – mouse SLC16A1 (MCT1) shRNA silencing adenovirus; PBS – phosphate-buffered saline.

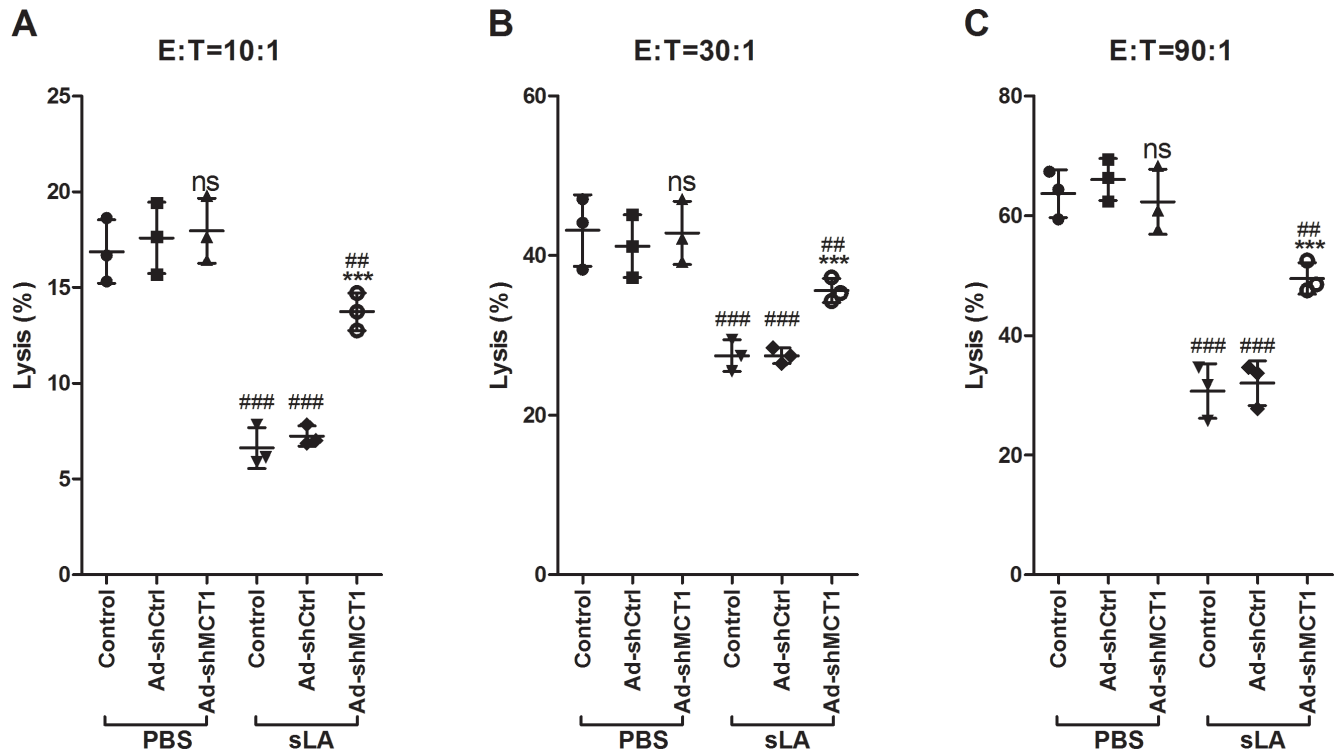


**Fig. 4.** Lysis rate of U14 cells by dendritic cell (DC)-induced cytotoxic T lymphocytes (CTLs). Different CTLs were co-cultured with U14 at different seeding ratios of 10:1 (A), 30:1 (B) and 90:1 (C) for 72 h, and then the cell viability was detected using a Cell Counting Kit-8 (CCK-8). Control conditions were the activity of U14 cells cultured alone. The column height represents the average value, and the error bar represents the standard deviation. The p-value was calculated by Tukey's honestly significant difference (HSD) test following the analysis of variance (ANOVA) between multiple groups or by Student's t-test (phosphate-buffered saline (PBS) compared to sodium lactate (sLA) treatment)

E – effector (DC-induced CTLs); T – target (U14 cells); ns  $p > 0.05$ , \*\*\*  $p < 0.001$  compared to the Ad-shCtrl group; #  $p < 0.05$ , ##  $p < 0.01$  and ###  $p < 0.001$  compared to the same treatment in the PBS group.

**Table 4.** Statistics for Fig. 4 (n = 3)

Variable		Minimal	Q1	Median	Q3	Maximal	Mean	SD
10:1 PBS	control	15.32	15.32	16.67	18.63	18.63	16.87	1.66
	Ad-shCtrl	15.69	15.69	17.65	19.41	19.41	17.58	1.86
	Ad-shMCT1	16.44	16.44	17.65	19.79	19.79	17.96	1.70
10:1 sLA	control	5.88	5.88	6.13	7.84	7.84	6.62	1.07
	Ad-shCtrl	6.86	6.86	7.02	7.84	7.84	7.24	0.53
	Ad-shMCT1	12.75	12.75	13.73	14.71	14.71	13.73	0.98
30:1 PBS	control	38.24	38.24	44.12	47.06	47.06	43.14	4.49
	Ad-shCtrl	37.25	37.25	41.18	45.10	45.10	41.18	3.93
	Ad-shMCT1	39.22	39.22	42.16	47.06	47.06	42.81	3.96
30:1 sLA	control	25.49	25.49	27.45	29.41	29.41	27.45	1.96
	Ad-shCtrl	26.47	26.47	27.45	28.43	28.43	27.45	0.98
	Ad-shMCT1	34.31	34.31	35.29	37.25	37.25	35.62	1.50
90:1 PBS	control	59.41	59.41	64.36	67.33	67.33	63.70	4.00
	Ad-shCtrl	62.38	62.38	66.34	69.37	69.37	66.03	3.51
	Ad-shMCT1	57.72	57.72	60.89	68.32	68.32	62.31	5.44
90:1 sLA	control	25.74	25.74	31.68	34.65	34.65	30.69	4.54
	Ad-shCtrl	27.72	27.72	33.66	34.65	34.65	32.01	3.75
	Ad-shMCT1	47.52	47.52	48.51	52.48	52.48	49.50	2.63

SD – standard deviation; Q1 – 1<sup>st</sup> quartile; Q3 – 3<sup>rd</sup> quartile; sLA – sodium lactate; Ad-shMCT1 – mouse SLC16A1 (MCT1) shRNA silencing adenovirus; PBS – phosphate-buffered saline.

In the absence of sLA exposure, MCT1 silencing did not affect the secretion of IL-6, IL-12 p70 and TNF- $\alpha$  from DCs. However, the exposure of DCs to sLA and LPS decreased the levels of these cytokines.

### Impact of *MCT1* gene silencing on the immune effect of DCs

To analyze the toxicity effect of DC-induced CTLs on cervical cancer cells, we generated CTLs (defined as DC-induced CTLs) by co-culturing DCs and T cells for 1 week, and then co-culturing the obtained CTLs with U14 cells. In DC-induced CTLs without sLA exposure, the lysis rate of U14 cells was independent of whether MCT1 was silenced ( $p < 0.05$ , HSD test following ANOVA, Fig. 4 and Table 4). However, DC-induced CTLs with sLA exposure and MCT1 silencing significantly increased the lysis rate of U14 cells ( $p < 0.05$ , HSD test following ANOVA testing,

Fig. 4 and Table 4). Simultaneously, in a DC-induced CTL and U14 cell co-culture system, the MCT1 silencing without sLA exposure did not affect the number of U14 clones, but it decreased the U14 cell clone number ( $p < 0.05$ , HSD test following ANOVA testing, Fig. 5 and Table 5). Consistently, in vivo, MCT1 silencing without sLA exposure did not affect the weight of U14 xenograft, while xenografts demonstrated significantly decreased weight with MCT1 silencing and sLA exposure ( $p < 0.05$ , HSD test following ANOVA testing, Fig. 6 and Table 6).

## Discussion

For decades, lactate was considered a metabolic waste product. However, in recent years, it has been reported that the output of lactic acid from the glycolysis of tumor cells can promote the proliferation of tumor cells in the tumor

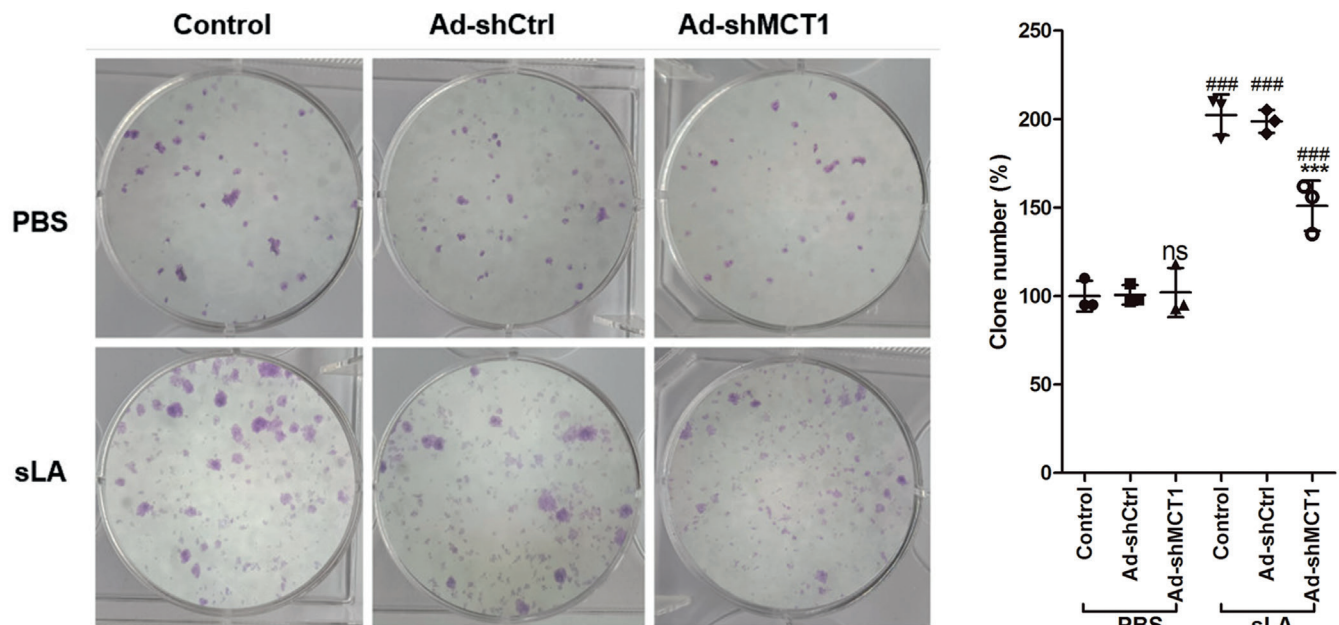


**Fig. 5.** Effects of dendritic cell (DC)-induced cytotoxic T lymphocytes (CTLs) on the proliferation of U14 cells in vitro. Different CTLs were co-cultured with U14 cells at 30:1 effector:target (E:T) ratio for 2 weeks, and then the colony numbers were counted for comparison. The column height represents the average value, and the error bar is the standard deviation. The p-value was calculated by Tukey's honestly significant difference (HSD) test following the analysis of variance (ANOVA) between multiple groups or by Student's t-test (phosphate-buffered saline (PBS) compared to sodium lactate (sLA) treatment)

<sup>ns</sup>  $p > 0.05$ , <sup>\*\*\*</sup>  $p < 0.001$  compared to the Ad-shCtrl group; <sup>###</sup>  $p < 0.001$  compared to the same treatment in the PBS group; Ad-shMCT1 – mouse SLC16A1 (MCT1) shRNA silencing adenovirus.

**Table 5.** Statistics for Fig. 5 (n = 3)

	Variable	Minimal	Q1	Median	Q3	Maximal	Mean	SD
PBS	control	95	95	95	110	110	100	8.66
	Ad-shCtrl	97	97	98	107	107	100.7	5.508
	Ad-shMCT1	93	93	95	118	118	102	13.89
sLA	control	189	189	208	210	210	202.3	11.59
	Ad-shCtrl	192	192	199	205	205	198.7	6.506
	Ad-shMCT1	135	135	156	162	162	151	14.18

SD – standard deviation; Q1 – 1<sup>st</sup> quartile; Q3 – 3<sup>rd</sup> quartile; sLA – sodium lactate; Ad-shMCT1 – mouse SLC16A1 (MCT1) shRNA silencing adenovirus; PBS – phosphate-buffered saline.

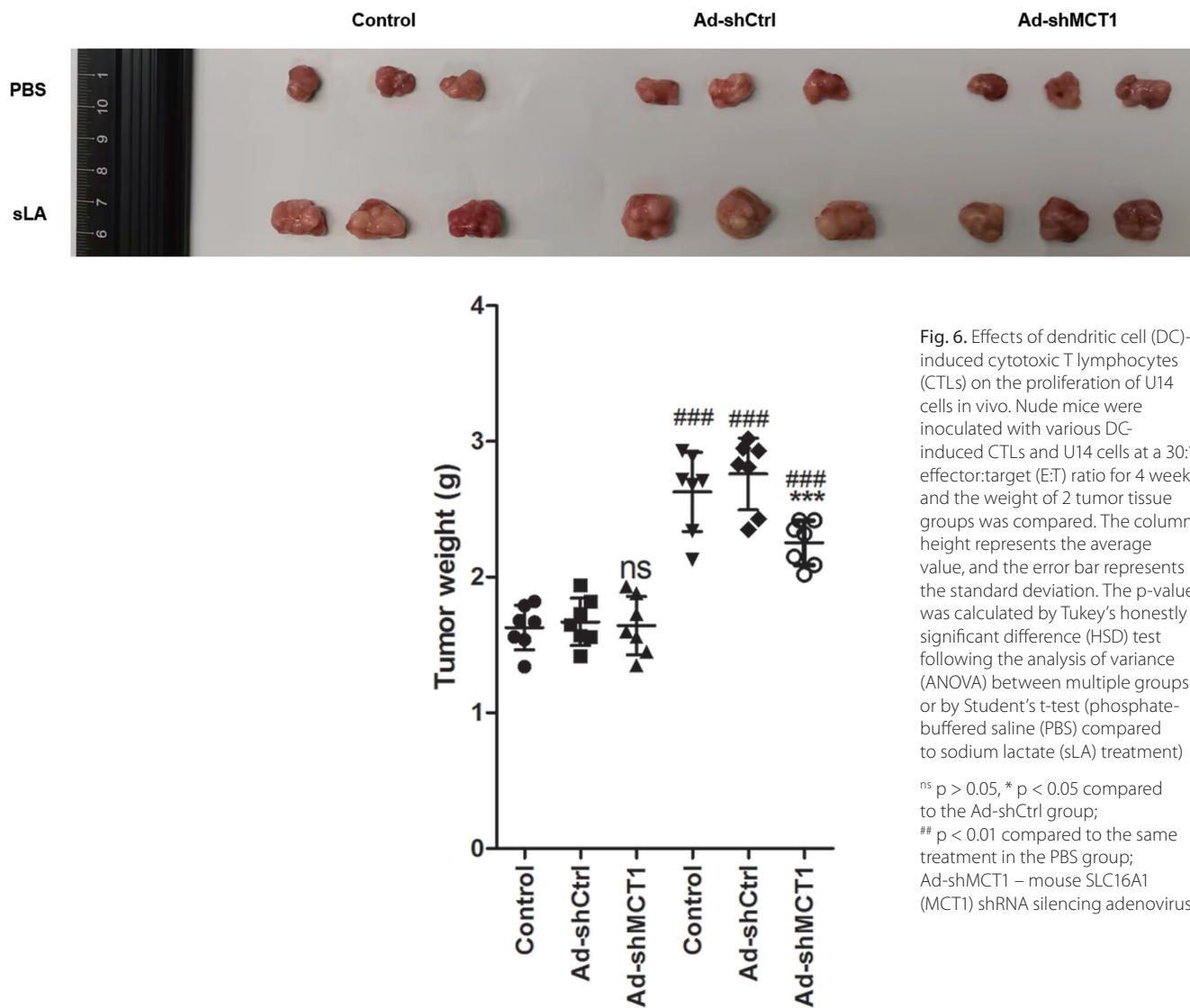


**Fig. 6.** Effects of dendritic cell (DC)-induced cytotoxic T lymphocytes (CTLs) on the proliferation of U14 cells in vivo. Nude mice were inoculated with various DC-induced CTLs and U14 cells at a 30:1 effector:target (E:T) ratio for 4 weeks, and the weight of 2 tumor tissue groups was compared. The column height represents the average value, and the error bar represents the standard deviation. The p-value was calculated by Tukey's honestly significant difference (HSD) test following the analysis of variance (ANOVA) between multiple groups or by Student's t-test (phosphate-buffered saline (PBS) compared to sodium lactate (sLA) treatment)

<sup>ns</sup> p > 0.05, \* p < 0.05 compared to the Ad-shCtrl group;  
<sup>##</sup> p < 0.01 compared to the same treatment in the PBS group;  
 Ad-shMCT1 – mouse SLC16A1 (MCT1) shRNA silencing adenovirus.

**Table 6.** Statistics for Fig. 6 (n = 3)

Variable		Minimal	Q1	Median	Q3	Maximal	Mean	SD
PBS	control	1.34	1.54	1.67	1.79	1.82	1.63	0.16
	Ad-shCtrl	1.42	1.56	1.65	1.82	1.94	1.67	0.18
	Ad-shMCT1	1.35	1.45	1.60	1.88	1.93	1.64	0.22
sLA	control	2.13	2.34	2.71	2.89	2.93	2.63	0.29
	Ad-shCtrl	2.35	2.43	2.83	2.95	3.02	2.76	0.26
	Ad-shMCT1	2.02	2.09	2.32	2.42	2.42	2.25	0.16

SD – standard deviation; Q1 – 1<sup>st</sup> quartile; Q3 – 3<sup>rd</sup> quartile; sLA – sodium lactate; Ad-shMCT1 – mouse SLC16A1 (MCT1) shRNA silencing adenovirus; PBS – phosphate-buffered saline.

microenvironment. Moreover, it aids in immune tolerance and helps tumor cells escape detection by immune cells.<sup>21–23</sup> The Warburg Effect of cancer cells makes them more inclined to use glycolysis for energy, and the accompanying lactic acid is a product of their metabolism. Importantly, lactate exported by cancer cells into the tumor microenvironment promotes tumor cell proliferation, metastasis, angiogenesis, and immune tolerance.<sup>9,10</sup> It has been reported that lactate is a potent inhibitor of T cell and

NK cell survival and function, modulating the phenotype of DCs and macrophages.<sup>11–13</sup> A recent study reported that AZD3965, an MCT1 inhibitor, could reverse the immunosuppressive micro-environment of solid tumors, thereby improving the safety and anti-tumor efficacy of cancer immunotherapy.<sup>24</sup> Hence, the inhibition of MCT1 can be viewed as a new strategy for tumor immunotherapy.

In this study, we silenced the MCT1 expression in BM-derived DCs by adenovirus infection and found that MCT1

silencing affected the phenotype and cytokine secretion of BM-derived DCs, although only when also exposed to sLA. Specifically, *MCT1* silencing upregulated the expression of CD1a, CD80, CD83, CD86, and MHCII, and the secretion of IL-6, IL-12 p70 and TNF- $\alpha$  in BM-derived DCs after sLA exposure and LPS challenge. The *MCT1* is a member of the monocarboxylate transporter family, which plays an essential regulatory role in glycolysis by mediating the transmembrane transport of lactate.<sup>25,26</sup> It has been reported that *MCT1* is upregulated in cervical cancer tissues and contributes to disease progression by promoting the proliferation, migration and angiogenesis of cervical cancer cells. Its mechanism is thought to be related to the regulation of lactate metabolism in the tumor microenvironment.<sup>27–29</sup>

Furthermore, lactate that is accumulated in the tumor microenvironment is transported from extracellular to intracellular microenvironment via *MCT1* to regulate its phenotypic changes, ultimately resulting in immunosuppression.<sup>13,18</sup> This is considered an essential measure of immune evasion of tumor cells. Sangsuwan et al. revealed that lactate exposure reduces the expression of CD11c, CD80, CD86, and MCHII, and results in a decreased secretion of IL-12 in DCs, which is consistent with the results of the present study.<sup>13</sup> More importantly, our study found that silencing *MCT1* attenuated these changes induced by lactate exposure in DCs, providing a new strategy for tumor immunotherapy.

A robust immune response against tumors depends on several factors, such as the degree of maturation and activation of DCs, their ability to capture, process and present exogenous antigens, as well as their transport to secondary lymphoid organs and the tissue types from which they arise.<sup>30,31</sup> Dendritic cells are critical for initiating anti-tumor immunity, as they activate various immune cells, including T cells, to establish anti-tumor resistant barriers. In this study, we demonstrated that we could induce CTLs by co-culturing DCs and splenic T cells. Our findings showed that CTLs derived from sLA-exposed DCs were less effective against U14 cells than those derived from DCs not exposed to sLA. However, *MCT1* silencing significantly increased the toxicity of sLA-exposed DC-derived CTLs to U14 cells both in vivo and in vitro. The results suggest that lactate exposure reduced the antigen-presenting capacity of DCs, but *MCT1* silencing could attenuate the effects of lactate exposure. Under physiological conditions, DCs often exhibit an immature phenotype in vivo, characterized by low surface levels of MHCII and costimulatory molecules, and induce suboptimal T cell priming, often resulting in T cell anergy or tolerance.<sup>32–34</sup> Dendritic cells matured and activated by antigens were found to highly express MHCII and costimulatory molecules (CD80, CD83 and CD86), which induced potent T cell activation and effector differentiation.<sup>35,36</sup> However, lactate-mediated signaling has been shown to hinder the maturation, activation and antigen presentation of DCs, resulting in widespread

immunosuppression.<sup>37</sup> The *MCT1* is a crucial protein involved in the signaling pathways of lactate in DCs, and conversely, lactate has been shown to regulate the expression of *MCT1*. Therefore, silencing of *MCT1* could theoretically attenuate the functional and phenotypic changes of DCs induced by lactate exposure. Our findings provide evidence to support this hypothesis.

## Limitations

The present study demonstrated that *MCT1* gene silencing attenuated lactate exposure and decreased dendritic cell immunity against cervical cancer cells both in vitro and in vivo. However, this study did not further investigate the specific molecular mechanism of the changes caused by *MCT1* silencing.

## Conclusions

Lactate exposure reduces the immunological effect of DCs on cervical cancer cells. However, this effect can be mitigated by *MCT1* gene silencing, thereby reducing the impact of lactate exposure on DCs.

## Data availability

The dataset used and/or analyzed during the current study is available from the corresponding author upon reasonable request.

## Supplementary data

The supplementary materials are available at <https://doi.org/10.5281/zenodo.8281170>. The package contains the following files:

Supplementary Table 1. Statistics for Fig. 1.

Supplementary Table 2. Statistics for Fig. 2.

Supplementary Table 3. Statistics for Fig. 3.

Supplementary Table 4. Statistics for Fig. 4.

Supplementary Table 5. Statistics for Fig. 5.

Supplementary Table 6. Statistics for Fig. 6.

Supplementary Table 7. Statistics for Supplementary Fig. 1.

Supplementary Fig. 1. Cube maps for the levels of DC marker expression after sLA exposure and LPS challenge. Dendritic cells were first infected with Ad-shCtrl and Ad-shMCT1 adenoviruses for 24 h, then co-cultured with 50 mM of sLA or PBS for 48 h, and finally stimulated with 1  $\mu$ g/mL LPS for 24 h. Flow cytometry was used to detect the expression of CD1a (A), CD80 (B), CD83 (C), CD86 (D), and MHCII (E) in DCs. The column height represents the average value, and the bar of the column is the standard deviation. The p-value was calculated by Tukey's honestly significant difference (HSD) test following analysis of variance (ANOVA) between multiple groups or by Student's t-test (PBS compared to sLA treatment).

## ORCID iDs

Xiaoxin Sui  <https://orcid.org/0009-0009-4863-0945>

Xiaowei Xi  <https://orcid.org/0000-0001-7306-3254>

## References

- Gardner A, De Mingo Pulido Á, Ruffell B. Dendritic cells and their role in immunotherapy. *Front Immunol.* 2020;11:924. doi:10.3389/fimmu.2020.00924
- Collin M, Bigley V. Human dendritic cell subsets: An update. *Immunology.* 2018;154(1):3–20. doi:10.1111/imm.12888
- Lee YS, Radford KJ. The role of dendritic cells in cancer. *Int Rev Cell Mol Biol.* 2019;348:123–178. doi:10.1016/bs.ircmb.2019.07.006
- Patente TA, Pinho MP, Oliveira AA, Evangelista GCM, Bergami-Santos PC, Barbuto JAM. Human dendritic cells: Their heterogeneity and clinical application potential in cancer immunotherapy. *Front Immunol.* 2019;9:3176. doi:10.3389/fimmu.2018.03176
- Enamorado M, Khouili SC, Iborra S, Sancho D. Genealogy, dendritic cell priming, and differentiation of tissue-resident memory CD8<sup>+</sup> T cells. *Front Immunol.* 2018;9:1751. doi:10.3389/fimmu.2018.01751
- Fu C, Jiang A. Dendritic cells and CD8 T cell immunity in tumor microenvironment. *Front Immunol.* 2018;9:3059. doi:10.3389/fimmu.2018.03059
- Hou B, Tang Y, Li W, Zeng Q, Chang D. Efficiency of CAR-T therapy for treatment of solid tumor in clinical trials: A meta-analysis. *Dis Markers.* 2019;2019:3425291. doi:10.1155/2019/3425291
- Akhoundi M, Mohammadi M, Sahraei SS, Sheykhasan M, Fayazi N. CAR T cell therapy as a promising approach in cancer immunotherapy: Challenges and opportunities. *Cell Oncol.* 2021;44(3):495–523. doi:10.1007/s13402-021-00593-1
- Vaupel P, Schmidberger H, Mayer A. The Warburg Effect: Essential part of metabolic reprogramming and central contributor to cancer progression. *Int J Radiat Biol.* 2019;95(7):912–919. doi:10.1080/09553002.2019.1589653
- San-Millán I, Brooks GA. Reexamining cancer metabolism: Lactate production for carcinogenesis could be the purpose and explanation of the Warburg Effect. *Carcinogenesis.* 2016;38(2):119–133. doi:10.1093/carcin/bgw127
- Brand A, Singer K, Koehl GE, et al. LDHA-associated lactic acid production blunts tumor immunosurveillance by T and NK cells. *Cell Metab.* 2016;24(5):657–671. doi:10.1016/j.cmet.2016.08.011
- Fischer K, Hoffmann P, Voelkl S, et al. Inhibitory effect of tumor cell-derived lactic acid on human T cells. *Blood.* 2007;109(9):3812–3819. doi:10.1182/blood-2006-07-035972
- Sangsuwan R, Thuamsang B, Pacifici N, et al. Lactate exposure promotes immunosuppressive phenotypes in innate immune cells. *Cel Mol Bioeng.* 2020;13(5):541–557. doi:10.1007/s12195-020-00652-x
- Halestrap AP. The SLC16 gene family: Structure, role and regulation in health and disease. *Mol Aspects Med.* 2013;34(2–3):337–349. doi:10.1016/j.mam.2012.05.003
- Sun X, Wang M, Wang M, et al. Role of proton-coupled monocarboxylate transporters in cancer: From metabolic crosstalk to therapeutic potential. *Front Cell Dev Biol.* 2020;8:651. doi:10.3389/fcell.2020.00651
- Fiaschi T, Marini A, Giannoni E, et al. Reciprocal metabolic reprogramming through lactate shuttle coordinately influences tumor–stroma interplay. *Cancer Res.* 2012;72(19):5130–5140. doi:10.1158/0008-5472.CAN-12-1949
- Doherty JR, Cleveland JL. Targeting lactate metabolism for cancer therapeutics. *J Clin Invest.* 2013;123(9):3685–3692. doi:10.1172/JCI69741
- Manoharan I, Prasad PD, Thangaraju M, Manicassamy S. Lactate-dependent regulation of immune responses by dendritic cells and macrophages. *Front Immunol.* 2021;12:691134. doi:10.3389/fimmu.2021.691134
- National Research Council (U.S.), Institute for Laboratory Animal Research (U.S.), National Academies Press (U.S.), eds. *Guide for the Care and Use of Laboratory Animals.* 8<sup>th</sup> ed. Washington, D.C, USA: National Academies Press; 2011. ISBN:978-0-309-15400-0/978-0-309-15401-7.
- Zhu Y, Zheng Y, Mei L, et al. Enhanced immunotherapeutic effect of modified HPV16 E7-pulsed dendritic cell vaccine by an adeno-shRNA-SOCS1 virus. *Int J Oncol.* 2013;43(4):1151–1159. doi:10.3892/ijo.2013.2027
- Abbaszadeh Z, Çeşmeli S, Biray Avcı Ç. Crucial players in glycolysis: Cancer progress. *Gene.* 2020;726:144158. doi:10.1016/j.gene.2019.144158
- Chen AN, Luo Y, Yang YH, et al. Lactylation, a novel metabolic reprogramming code: Current status and prospects. *Front Immunol.* 2021;12:688910. doi:10.3389/fimmu.2021.688910
- Brown TP, Ganapathy V. Lactate/GPR81 signaling and proton motive force in cancer: Role in angiogenesis, immune escape, nutrition, and Warburg phenomenon. *Pharmacol Ther.* 2020;206:107451. doi:10.1016/j.pharmthera.2019.107451
- Huang T, Feng Q, Wang Z, et al. Tumor-targeted inhibition of monocarboxylate transporter 1 improves T-cell immunotherapy of solid tumors. *Adv Healthcare Mater.* 2021;10(4):2000549. doi:10.1002/adhm.202000549
- Payen VL, Mina E, Van Hée VF, Porporato PE, Sonveaux P. Monocarboxylate transporters in cancer. *Mol Metab.* 2020;33:48–66. doi:10.1016/j.molmet.2019.07.006
- Zhao Y, Li M, Yao X, et al. HCAR1/MCT1 regulates tumor ferroptosis through the lactate-mediated AMPK-SCD1 activity and its therapeutic implications. *Cell Rep.* 2020;33(10):108487. doi:10.1016/j.celrep.2020.108487
- Pinheiro C, Garcia EA, Morais-Santos F, et al. Reprogramming energy metabolism and inducing angiogenesis: Co-expression of monocarboxylate transporters with VEGF family members in cervical adenocarcinomas. *BMC Cancer.* 2015;15(1):835. doi:10.1186/s12885-015-1842-4
- Silva LS, Gonçalves LG, Silva F, et al. STAT3/FOXM1 and MCT1 drive uterine cervix carcinoma fitness to a lactate-rich microenvironment. *Tumor Biol.* 2016;37(4):5385–5395. doi:10.1007/s13277-015-4385-z
- Payen VL, Hsu MY, Rädercke KS, et al. Monocarboxylate transporter MCT1 promotes tumor metastasis independently of its activity as a lactate transporter. *Cancer Res.* 2017;77(20):5591–5601. doi:10.1158/0008-5472.CAN-17-0764
- Wculek SK, Cueto FJ, Mujal AM, Melero I, Krummel MF, Sancho D. Dendritic cells in cancer immunology and immunotherapy. *Nat Rev Immunol.* 2020;20(1):7–24. doi:10.1038/s41577-019-0210-z
- Nava S, Lisini D, Frigerio S, Bersano A. Dendritic cells and cancer immunotherapy: The adjuvant effect. *Int J Mol Sci.* 2021;22(22):12339. doi:10.3390/ijms222212339
- Jang JE, Hajdu CH, Liot C, Miller G, Dustin ML, Bar-Sagi D. Crosstalk between regulatory T cells and tumor-associated dendritic cells negates anti-tumor immunity in pancreatic cancer. *Cell Rep.* 2017;20(3):558–571. doi:10.1016/j.celrep.2017.06.062
- Davison GM. Dendritic cells, T-cells and their possible role in the treatment of leukaemia and lymphoma. *Transfus Apher Sci.* 2010;42(2):189–192. doi:10.1016/j.transci.2010.01.018
- Garris CS, Luke JJ. Dendritic cells, the T-cell-inflamed tumor microenvironment, and immunotherapy treatment response. *Clin Cancer Res.* 2020;26(15):3901–3907. doi:10.1158/1078-0432.CCR-19-1321
- Shevchenko J, Khristin A, Kurilin V, et al. Autologous dendritic cells and activated cytotoxic T-cells as combination therapy for breast cancer. *Oncol Rep.* 2019;43(2):671–680. doi:10.3892/or.2019.7435
- Gajewski TF, Schreiber H, Fu YX. Innate and adaptive immune cells in the tumor microenvironment. *Nat Immunol.* 2013;14(10):1014–1022. doi:10.1038/ni.2703
- Srinivasan S, Babensee J. Dendritic cells support a proliferative antigen-specific T-cell response in the presence of poly(lactic-co-glycolic acid). *J Biomed Mater Res.* 2021;109(11):2269–2279. doi:10.1002/jbm.a.37211





# Anoikis-related gene signatures can aid prognosis of lung adenocarcinoma

Guiyan Mo<sup>1,A,B,D,F</sup>, Xuan Long<sup>2,A,C,D,F</sup>, Zan Hu<sup>3,A,B,E,F</sup>, Yuling Tang<sup>1,B,C,E,F</sup>, Zhiguo Zhou<sup>1,A,E,F</sup>

<sup>1</sup> Department of Respiratory and Critical Care Medicine, The First Hospital of Changsha, China

<sup>2</sup> Department of Respiratory and Critical Care Medicine, Shanghai Tenth People's Hospital, Tongji University School of Medicine, China

<sup>3</sup> Department of Respiratory and Critical Care Medicine, The Affiliated Changsha Central Hospital, Hengyang Medical School, University of South China, China

A – research concept and design; B – collection and/or assembly of data; C – data analysis and interpretation;

D – writing the article; E – critical revision of the article; F – final approval of the article

Advances in Clinical and Experimental Medicine, ISSN 1899–5276 (print), ISSN 2451–2680 (online)

*Adv Clin Exp Med.* 2024;33(7):751–761

## Address for correspondence

Zan Hu

E-mail: huzan1982@126.com

## Funding sources

None declared

## Conflict of interest

None declared

Received on December 19, 2022

Reviewed on May 22, 2023

Accepted on August 23, 2023

Published online on September 28, 2023

## Abstract

**Background.** Lung adenocarcinoma (LUAD) is the most common subtype of lung cancer, and while advancements in diagnosis, surgery, radiotherapy, and molecular therapy have improved clinical prognosis, the long-term survival rate and quality of life of patients remain unsatisfactory. Therefore, identifying new prognostic biomarkers and potential therapeutic targets is crucial.

**Objectives.** This study aimed to analyze the role of anoikis-related gene characteristics in LUAD.

**Materials and methods.** The anoikis-related genes were obtained from the GeneCards database. Genetic expression data and clinical characteristic information were collected from The Cancer Genome Atlas (TCGA)-LUAD, and the Gene Expression Omnibus (GEO) GSE31210, GSE37745, and GSE68465 datasets. Random survival forest and least absolute shrinkage and selection operator (LASSO) models were applied to construct the risk model. An analysis of immune cell infiltration and function was performed with the scores.

**Results.** Four prognosis-related genes (*TLE1*, *GLI2*, *PLK1*, and *BAK1*) were obtained and used to construct the anoikis score. We found that the patient survival rate was higher in the low-anoikis score (LAS) group. Moreover, both the stromal and immune scores were negatively correlated with the anoikis score. With the increase of the anoikis score, the levels of natural killer cells, regulatory T cells, CD4<sup>+</sup> T cells, CD8<sup>+</sup> T cells, B cells, and macrophages decreased. The anoikis score had a negative regulatory relationship with the immune response, natural killer cell activation and T cell activation. The TP53 mutation was significant in LUAD patients and was present in 56% of the high-anoikis score (HAS) group and in 40% of the LAS group.

**Conclusions.** The anoikis score was associated with poor prognosis in LUAD patients. Anoikis-related genes were associated with tumor immune dysregulation and TP53 mutation in LUAD. This study opens a new perspective for LUAD therapy.

**Key words:** prognosis, immune, mutation, lung adenocarcinoma (LUAD), anoikis

## Cite as

Mo G, Long X, Hu Z, Tang Y, Zhou Z. Anoikis-related gene signatures can aid prognosis of lung adenocarcinoma.

*Adv Clin Exp Med.* 2024;33(7):751–761.

doi:10.17219/acem/171482

## DOI

10.17219/acem/171482

## Copyright

Copyright by Author(s)

This is an article distributed under the terms of the Creative Commons Attribution 3.0 Unported (CC BY 3.0)

(<https://creativecommons.org/licenses/by/3.0/>)

## Background

Lung cancer remains one of the leading causes of cancer-related deaths worldwide<sup>1</sup> and its incidence continues to increase.<sup>2</sup> The most common subtype of lung cancer is lung adenocarcinoma (LUAD), which accounts for approx. 40% of cases.<sup>3</sup> While progress in diagnosis, surgery, radiotherapy, and molecular therapy has resulted in improved clinical outcomes for LUAD patients,<sup>4</sup> the overall quality of life and long-term survival rates remain unsatisfactory.<sup>5–7</sup> Therefore, there is a need to identify new prognostic biomarkers and potential therapeutic targets.

Anoikis refers to the type of cell death that is triggered when a cell loses its connection to both surrounding cells and the extracellular matrix (ECM).<sup>8</sup> This type of cell death plays a crucial role in maintaining tissue homeostasis and regulating normal development.<sup>9</sup> Anoikis is primarily triggered by the interaction between mitochondrial interference and cell surface death receptor activation.<sup>10,11</sup> However, during tumorigenesis and development, cells can develop resistance to anoikis, which is believed to be a key factor in promoting cancer cell metastasis<sup>12</sup> and survival under unfavorable conditions.<sup>13</sup> Several studies have demonstrated the prognostic significance of anoikis in various diseases, such as glioblastoma (GBM),<sup>14</sup> head and neck squamous cell carcinoma (HNSCC)<sup>15</sup> and clear cell renal cell carcinoma (ccRCC).<sup>16</sup> Additionally, the management of anoikis resistance is a critical factor in cancer development.<sup>17,18</sup> To gain more insight into the role of anoikis in LUAD, we analyzed the genetic signatures related to this biological process.

The rapid advancement of publicly available biological databases has facilitated easy access to vast amounts of bioinformatics data samples related to lung cancer. This makes bioinformatics results with large sample sizes more representative. In addition, with the widespread application of databases and network tools, and the integration of bioinformatics methods, medical research is trending towards utilizing these advancements.<sup>19</sup> The least absolute shrinkage and selection operator (LASSO) model is a common machine learning analysis method that has been widely used to select genetic features, due to its ability to effectively select important feature values with non-zero coefficients.<sup>20</sup> Multiple studies have utilized bioinformatics analysis, including LASSO analysis, to predict the prognostic value of various genes in a wide array of diseases.<sup>21–23</sup> These studies pave the way for further data mining and validation of related biomolecular targets.

## Objectives

Survival curves, immunity and mutation analysis were used to identify the role of anoikis-related genes in LUAD and their potential as prognostic markers.

## Materials and methods

### Data acquisition

We collected 337 genes related to anoikis from the GenCards database and standardized them based on a relevance score greater than 1.<sup>24</sup> Data related to genetic expression associated with anoikis and clinical characteristics were obtained from The Cancer Genome Atlas (TCGA)-LUAD dataset (502 cases) and the Gene Expression Omnibus (GEO) datasets, including GSE31210 (226 cases), GSE37745 (106 cases) and GSE68465 (442 cases). The TCGA-LUAD data were used as a training set, while the GSE31210, GSE37745 and GSE68465 data served as the test set.

### Construction of the risk model

The study involved conducting a univariate analysis between the anoikis genes and TCGA datasets. Afterwards, the anoikis genes were subjected to a random survival forest analysis to identify prognosis-related genes. Further analysis using the LASSO model was performed to construct the prognosis score, also known as the anoikis score (Equation 1):

$$\begin{aligned} \text{anoikis score} = & \\ = 1.6411 \times TLE1 + 0.6449 \times GLI2 + & \quad (1) \\ + 0.9709 \times PLK1 + 0.569 \times BAK1 & \end{aligned}$$

A diagrammatic representation of the study workflow is shown in Fig. 1. The LASSO regression minimized the loss function to obtain coefficient estimates for each explanatory variable. Then, the number of non-zero coefficients was observed to determine the number of variables selected for the risk model.

### Immune cell infiltration and function analysis

The infiltrating immune cells in LUAD patients were assessed using multiple algorithms, including Estimation of STromal and Immune cells in Malignant Tumours using Expression data (ESTIMATE), Microenvironment Cell Populations-counter (MCPcounter), single sample Gene Set Enrichment Analysis (ssGSEA), and Tumor Immune Estimation Resource (TIMER), to determine the prognostic index. Based on anoikis scoring, the tumor infiltration of the immune cell subpopulations and the expression levels of immune checkpoints in LUAD patients were evaluated using Pearson's correlation analysis. To gain further insight into the influence of the anoikis score on functional pathways in LUAD, the Gene Ontology (GO) enrichment analysis was performed using GSEA with the clusterProfiler.

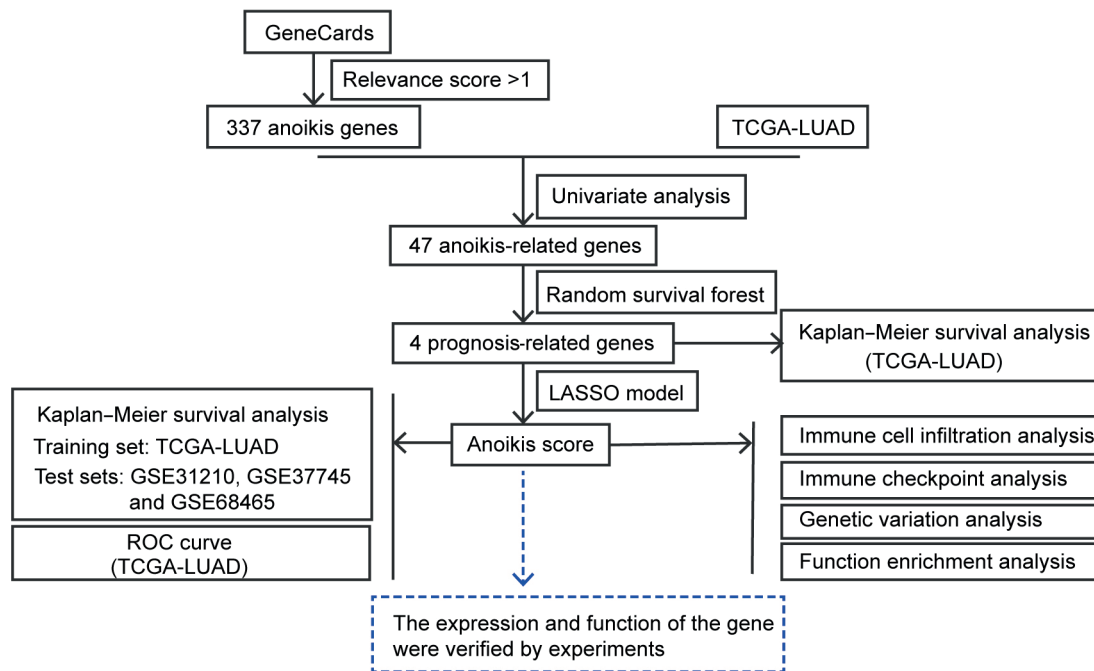


**Fig. 1.** The workflow diagram of the study. Prognosis-related anoikis gene signatures were defined and analyzed in lung adenocarcinoma (LUAD). The black solid lines represent the executed analysis or obtained results, while the blue dashed lines represent future research plans

TCGA – The Cancer Genome Atlas; ROC – receiver operating characteristic.

## Mutation and CNV analysis

The mutation and copy number variation (CNV) analyses were conducted using data from TCGA. The R package *maftools* were used for mutation analysis. The CNV landscape and the copy number gains or losses at the peaks were evaluated using the GISTIC 2.0 (<https://gatk.broadinstitute.org>).

## Statistical analyses

Data were visualized using the R package “*ggplot2*”. The patient survival curve was generated using the Kaplan–Meier method. The receiver operating characteristic (ROC) curve was estimated using the R package “*pROC*”. The likelihood ratio test (univariate analysis), the log-rank test (Kaplan–Meier survival analysis), Pearson’s correlation test (Pearson’s correlation analysis), and Fisher’s exact test ( $\chi^2$  test) were also performed. For Pearson’s correlation test, the *t*-statistic was calculated based on the Pearson’s correlation coefficient (*cor*) transformation in order to determine the *p*-value according to the degrees of freedom (*df*) and the level of significance. The Benjamini–Hochberg (BH) method was performed to correct *p*-values. The value of  $p < 0.05$  was considered statistically significant.

## Results

### Construction of the anoikis score in LUAD

Anoikis is a type of programmed cell death that occurs when cells are detached from their ECM. Using data from the GeneCards database with a relevance score  $>1$ , 337 genes associated with anoikis were identified.

A univariate analysis was performed on gene expression data from the TCGA-LUAD dataset, resulting in the identification of 47 anoikis-related genes (Fig. 2A and Supplementary Table 1). Among these genes, 42 were classified as high-risk genes (hazard ratio (HR)  $> 1$ ), including *FADD*, *TLE1*, *PPP2R1A*, *SHC1*, *ITGB1*, and *RELA*, and 5 genes (*LMO3*, *HGF*, *DAPK2*, *PPP1R13B*, and *PIK3CG*) were classified as low-risk genes (HR  $< 1$ ). Further analysis using the random survival forest algorithm revealed 4 prognosis-related genes, including *TLE1*, *GLI2*, *PLK1*, and *BAK1* (Fig. 2B). Together, these genes were used to construct an anoikis score with the LASSO model, which assigned weights to each gene based on its predictive value. The anoikis score is displayed in Fig. 2C.

### Survival analysis

We categorized patients into 2 subgroups based on their high or low anoikis score, and the survival of LUAD patients was analyzed by comparing high-anoikis score (HAS) and low-anoikis score (LAS) groups. Based on the TCGA-LUAD training dataset, the Kaplan–Meier survival plots were created, revealing that patients in the LAS group had higher survival rate than those in the HAS group ( $p < 0.001$ , cut-off point = 2.29 and log-rank test = 13.56) (Fig. 3A). Similar results were obtained from the validation dataset GSE31210 ( $p = 0.004$ , cut-off point = 1.68 and log-rank test = 8.23), GSE37745 ( $p = 0.021$ , cut-off point = 1.17 and log-rank test = 5.30) and GSE68465 ( $p = 0.002$ , cut-off point = 1.90 and log-rank test = 9.30) (Fig. 3B–D and Supplementary Fig. 1). The effectiveness of the model was assessed using a ROC curve (Fig. 3E). The 1-year area under the ROC curve (AUC) was 0.727, the 3-year AUC was 0.707 and

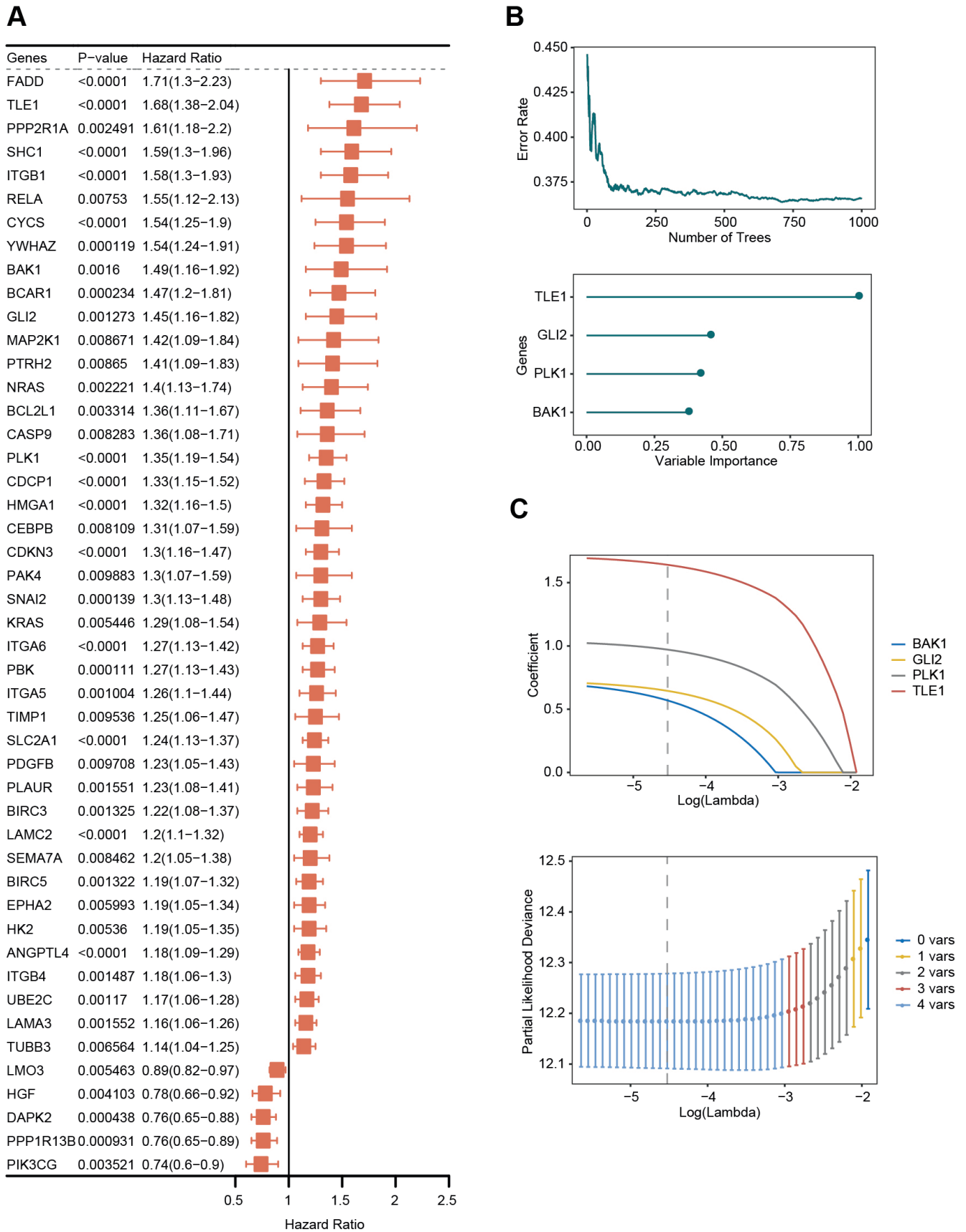
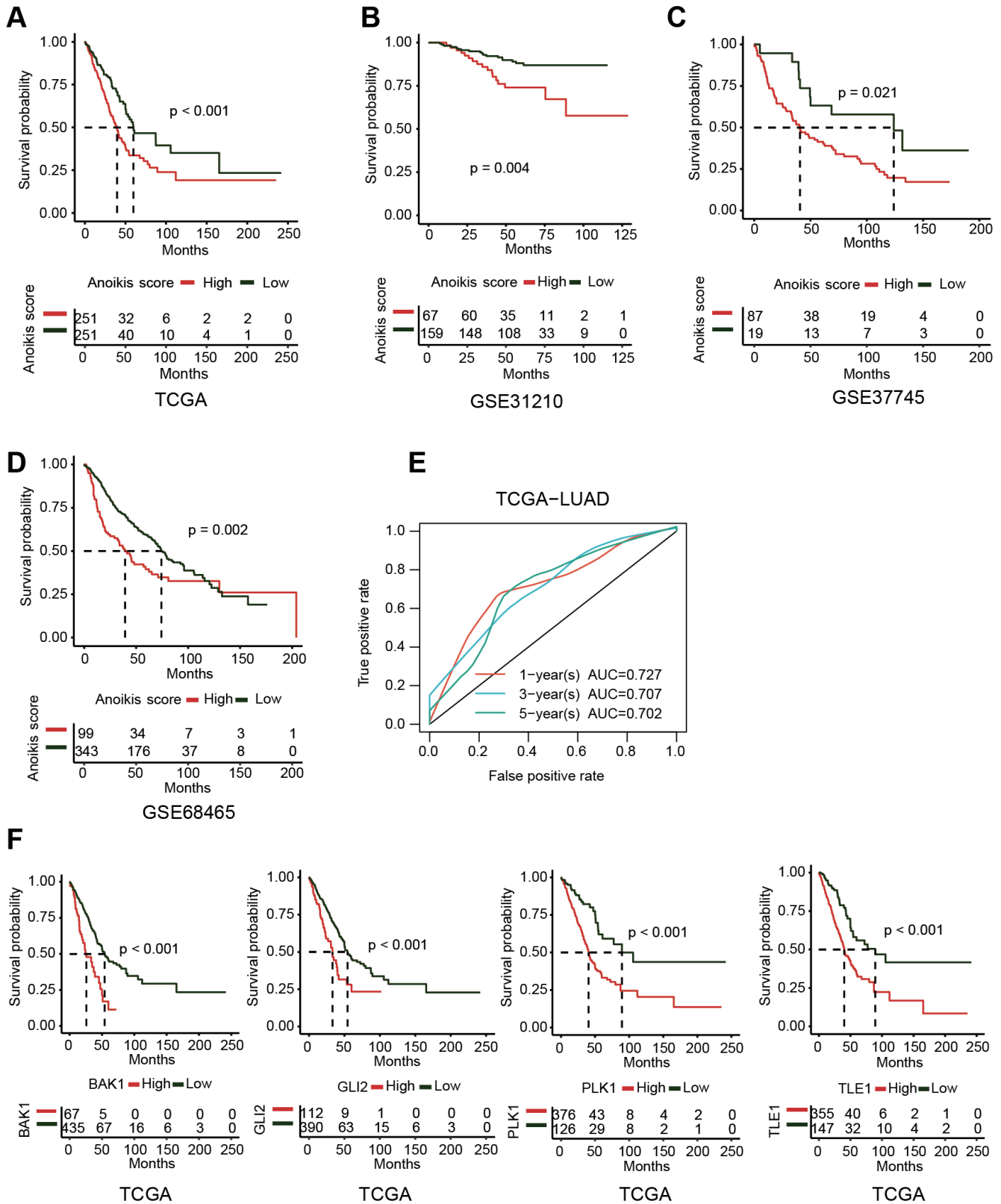


Fig. 2. Screening of anoikis-related genes and construction of the anoikis score. A. Anoikis-related genes ( $n = 47$ ) were visualized. Hazard ratio (HR)  $> 1$  predicted the gene to be a high-risk gene, and HR  $< 1$  indicated a low-risk gene; B. Four prognosis-related genes (*TLE1*, *GLI2*, *PLK1*, and *BAK1*) were obtained using the random survival forest analysis; C. Least absolute shrinkage and selection operator (LASSO) coefficient values of the 4 prognosis-related genes (*TLE1*, *GLI2*, *PLK1*, and *BAK1*)



**Fig. 3.** Prediction of patient outcomes. A–D. Patient survival analysis in the The Cancer Genome Atlas (TCGA)-lung adenocarcinoma (LUAD) ( $p < 0.001$ , cut-off point = 2.29 and log-rank test = 13.56), GSE31210 ( $p = 0.004$ , cut-off point = 1.68 and log-rank test = 8.23), GSE37745 ( $p = 0.021$ , cut-off point = 1.17 and log-rank test = 5.30), and GSE68465 ( $p = 0.002$ , cut-off point = 1.90 and log-rank test = 9.30). The Kaplan–Meier method was used for survival analysis; E. Receiver operating characteristic (ROC) curve (1-, 3- and 5-year) was performed to evaluate the predictive effectiveness of the model in the TCGA-LUAD; F. Patient survival analysis in the TCGA-LUAD based on the *TLE1* ( $p < 0.001$ , cut-off point = 3.90 and log-rank test = 22.15), *GLI2* ( $p < 0.001$ , cut-off point = 1.40 and log-rank test = 13.35), *PLK1* ( $p < 0.001$ , cut-off point = 2.85 and log-rank test = 20.93), and *BAK1* ( $p < 0.001$ , cut-off point = 5.33 and log-rank test = 24.78) expression. The Kaplan–Meier method was used for survival analysis

AUC – area under the ROC curve.

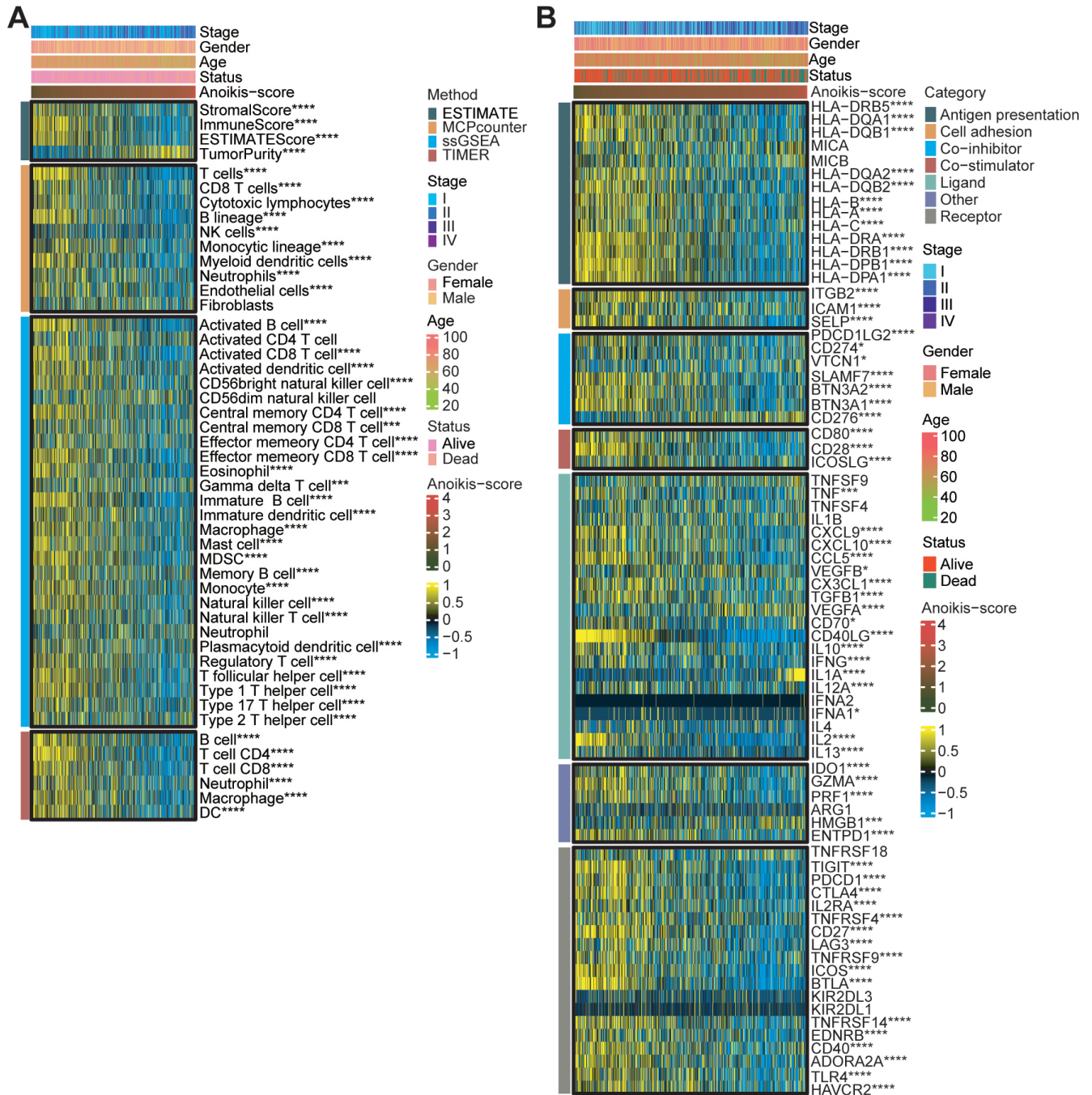


Fig. 4. Immune cell infiltration and checkpoint analysis. The infiltrating immune cells (A) and immune checkpoint levels (B) were appraised with the anoikis score and prognostic index (stage, gender, age, and status)

\*  $p < 0.05$ ; \*\*\*  $p < 0.001$ ; \*\*\*\*  $p < 0.0001$  (all Pearson's correlation).

the 5-year AUC was 0.702. Patients with high expression of the 4 prognosis-related genes: *TLE1* ( $p < 0.001$ , cut-off point = 3.90 and log-rank test = 22.15), *GLI2* ( $p < 0.001$ , cut-off point = 1.40 and log-rank test = 13.35), *PLK1* ( $p < 0.001$ , cut-off point = 2.85 and log-rank test = 20.93), and *BAK1* ( $p < 0.001$ , cut-off point = 5.33 and log-rank test = 24.78) had lower survival rates than those with low expression of the above genes (Fig. 3F). These findings suggested that a high anoikis score predicts poor outcomes in LUAD patients.

## Immune cell infiltration and immune checkpoint analysis

The anoikis score was correlated with immune cell infiltration using ESTIMATE, MCPcounter, ssGSEA, and TIMER algorithms (Fig. 4A and Supplementary Table 2). Our results showed a negative correlation between the anoikis score and stromal score ( $p < 0.001$ , Pearson's correlation) and immune score ( $p < 0.001$ , Pearson's

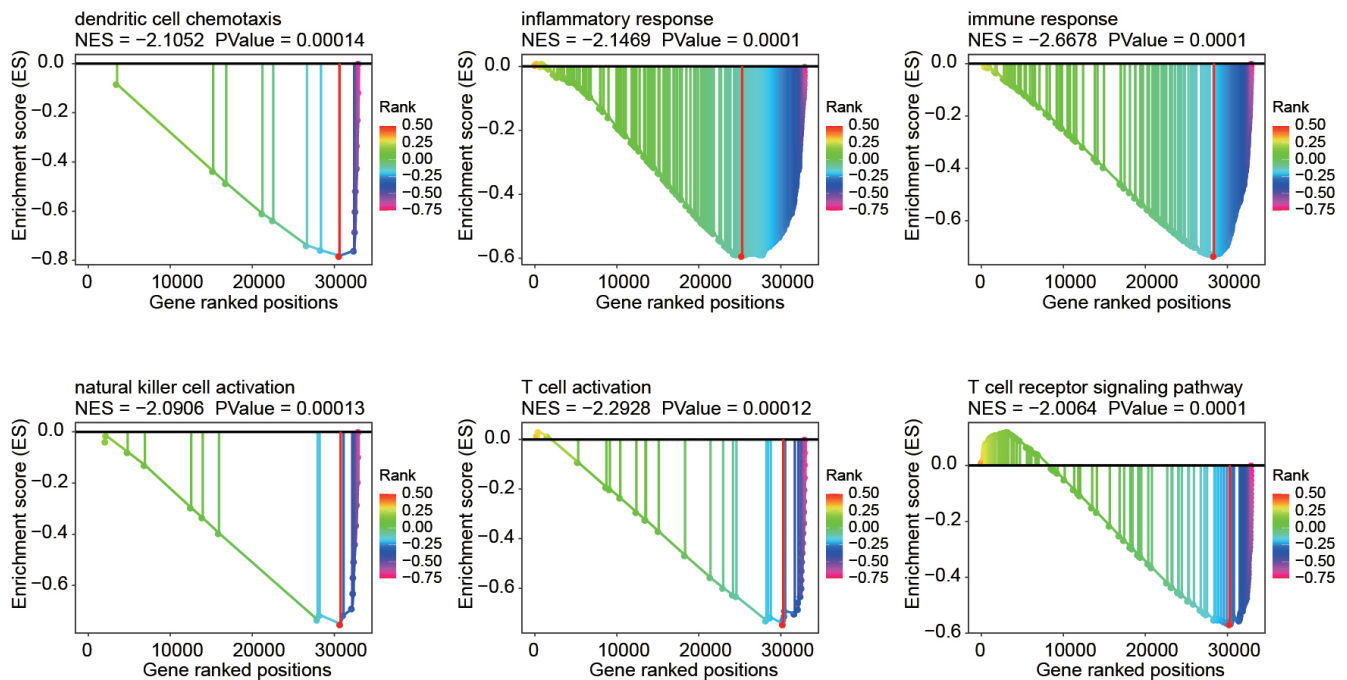


Fig. 5. Functional analysis. Gene Set Enrichment Analysis (GSEA) was performed to analyze the functional pathways associated with the anoikis score in lung adenocarcinoma (LUAD). Normalized enrichment score (NES) < 0 implies negative control of this signaling pathway

correlation). As the anoikis score increased, there was a significant decrease in the infiltration levels of eosinophils, immature B cells, mast cells, monocytes, natural killer cells, regulatory T cells, CD4<sup>+</sup> T cells, CD8<sup>+</sup> T cells, B cells, and macrophages.

In addition, we analyzed the expression of immune checkpoints for the anoikis score (Fig. 4B and Supplementary Table 3). We found that the levels of the checkpoint for antigen presentation (*HLA-DQA1* and *HLA-DPB1*), cell adhesion (*ITGB2* and *SELP*), co-inhibitor (*SLAMF7* and *BTN3A2*), co-stimulator *CD28*, ligand (*CXCL9*, *CCL5*, *CD40LG*, and *IL2*), and receptor (*TIGIT*, *PDCD1*, *CTLA4*, *CD27*, and *TLR4*) were negatively correlated with the anoikis score. However, co-inhibitor *CD276* and ligands (*VEGFA* and *IL1A*) were positively correlated with the anoikis score.

## Functional enrichment analysis by GSEA

After analyzing the immune cell infiltration and immune checkpoints, we examined the functional pathways associated with the anoikis score through GSEA. We found that several functional pathways were negatively correlated with the anoikis score (Fig. 5). Specifically, these pathways included the dendritic cell chemotaxis (normalized enrichment score (NES) = -2.1052,  $p < 0.001$ ), inflammatory response (NES = -2.1469,  $p < 0.001$ ), immune response (NES = -2.6678,  $p < 0.001$ ), natural killer cell activation (NES = -2.0906,  $p < 0.001$ ), T cell activation (NES = -2.2928,  $p < 0.001$ ), and T cell receptor signaling pathway (NES = -2.0064,  $p < 0.001$ ).

## Genetic variation analysis

Data presented in Fig. 6A visualizes the top 20 mutated genes in LUAD patients. Our analysis revealed that a mutation in one of these genes was present in 97.58% of patients in the HAS group compared to 85.48% in the LAS group. In addition, *TP53* mutations were found in 56% of the patients in the HAS group and in 40% of the patients in the LAS group. The frequency of gene mutants was analyzed to further compare the number of patients with mutations between the 2 groups. Genes that showed a higher frequency of mutations in the HAS group compared to the LAS group ( $p < 0.001$ ,  $\chi^2$  test) included *TTN* (HAS:  $n = 138$ ; LAS:  $n = 87$ ), *ENPP2* (HAS:  $n = 18$ ; LAS:  $n = 1$ ), *MUC16* (HAS:  $n = 117$ ; LAS:  $n = 78$ ), *LRP1B* (HAS:  $n = 98$ ; LAS:  $n = 61$ ), *TP53* (HAS:  $n = 138$ ; LAS:  $n = 99$ ), *NCOR2* (HAS:  $n = 19$ ; LAS:  $n = 3$ ), *CNTN5* (HAS:  $n = 26$ ; LAS:  $n = 7$ ), and *CSMD2* (HAS:  $n = 47$ ; LAS:  $n = 21$ ) (Fig. 6B and Supplementary Table 4). Moreover, the CNV frequency was found to be different between the 2 groups, as illustrated in Fig. 6C. Our findings indicated a significant association between the anoikis score, gene mutation and CNV in LUAD patients.

## Discussion

Anoikis plays a significant role in the metastatic characteristics of tumors.<sup>25</sup> Our research has identified anoikis-associated prognostic features for LUAD. The constructed genetic feature, known as the anoikis score, has been shown

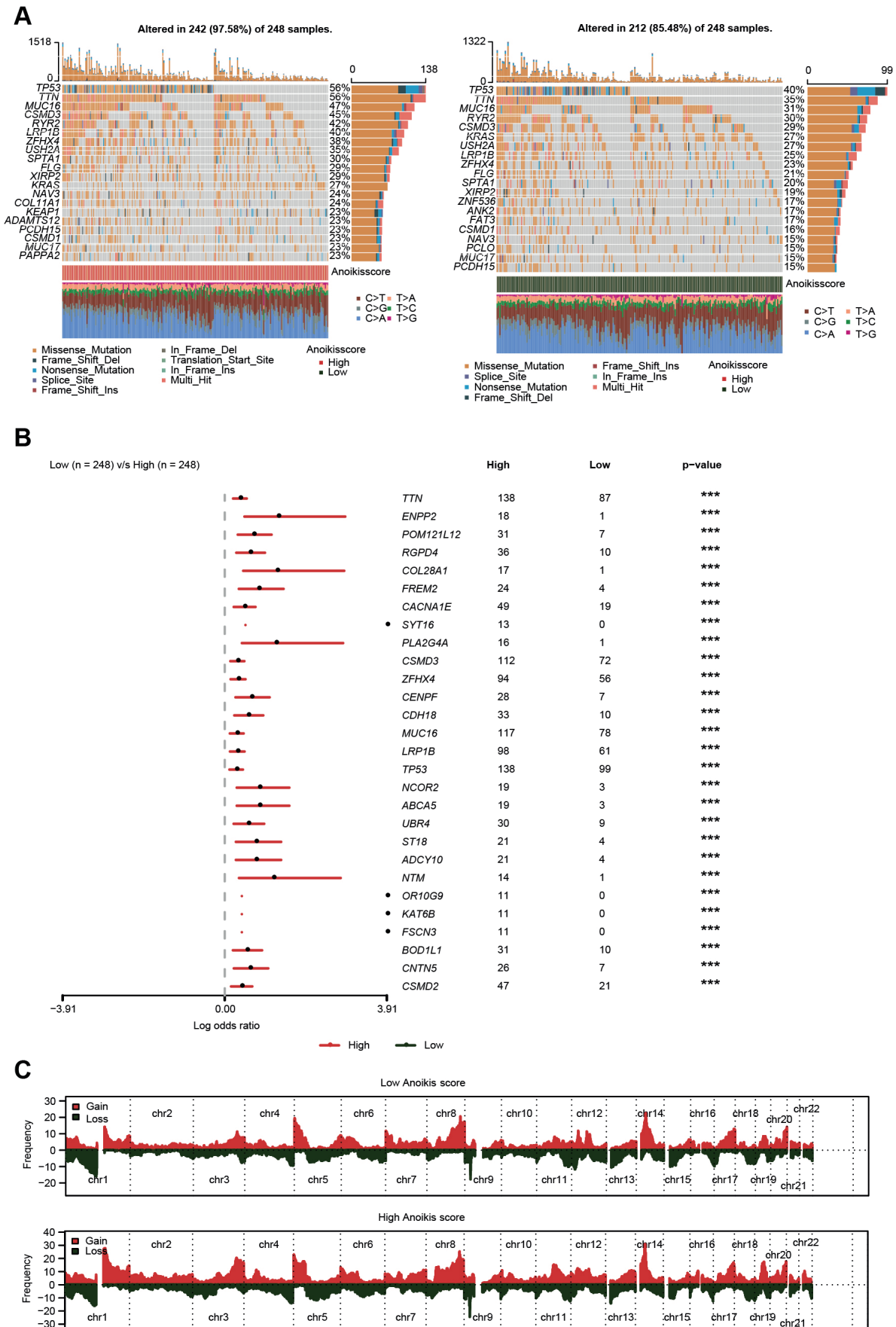


**Fig. 6.** Mutation and copy number variation (CNV) analysis. A. Visualization of the top 20 mutated genes; B. Comparison of the number of patients with mutations per mutated gene between the 2 groups. Log odds ratio >0 represented that the gene was more likely to be mutated in the high- than in the low-anoikis score group (\*\*\*  $p < 0.001$ ,  $\chi^2$  test); C. CNV frequency



to predict patient prognosis, and it outperformed multiple other prognostic models for LUAD.<sup>26,27</sup> The anoikis score encompasses the *TLE1*, *GLI2* and *PLK1* genes, among other factors, which play a crucial role in LUAD prognosis. Specifically, *TLE1*, a transcriptional repressor protein, is involved in cell growth and anti-apoptotic processes.<sup>28,29</sup> The *TLE1* hinders Bit1-mediated anoikis by reducing the formation of the pro-apoptotic Bit1-Amino-terminal Enhancer of Split (AES) complex in the nucleus<sup>30,31</sup> and inhibits E-cadherin expression, promoting epithelial–mesenchymal transition.<sup>32</sup> In our study, high levels of *TLE1* were a prognostic risk factor for LUAD,<sup>33</sup> and we demonstrated that patients in the high-*TLE1* group had a lower survival rate. Similarly, the transcription factor *GLI2* is positively correlated with the human epidermal growth factor receptor 2 (HER2)<sup>34,35</sup> and increases the resistance to anoikis in HER2-overexpressing breast cancer cells.<sup>35</sup> The *PLK1*, as a mitotic master Ser/Thr kinase, is involved in cell cycle regulation and cell proliferation.<sup>36</sup> It regulates the  $\beta$ -catenin protein level, which in turn protects cancer cells from anoikis by inhibiting ubiquitination and degradation of  $\beta$ -catenin protein.<sup>37</sup> Therefore, high levels of *GLI2* and *PLK1* in LUAD could lead to poor prognosis as they enhance anti-apoptosis and migration ability, contributing to anoikis resistance. Overall, our findings illustrated the vital role of *TLE1*, *GLI2* and *PLK1* in the prognosis of LUAD and their relationship with anoikis resistance.

In both HAS and LAS groups, *TTN*- and *TP53*-mutated genes were altered, and a high anoikis score predicted a higher likelihood of *TTN* and *TP53* mutations. These gene mutations have been shown to affect the chemotherapy response in patients with LUAD.<sup>38</sup> The *TP53* mutation is one of the most common mutations in early LUAD, observed in about 50% of patients.<sup>39</sup> Additionally, the presence of both *TP53* and *PLK1* mutations in primary breast tumors has been linked to a worse prognosis.<sup>40</sup> Tumors with *TP53* deletion and high *PLK1* expression may potentially benefit from *PLK1* inhibitors, although the available data are controversial.<sup>36</sup> Meanwhile, *TP53* mutant cancers have been associated with higher levels of anti-tumor immunity markers, suggesting a possible relationship between *TP53* mutation and the immune response.<sup>41</sup>

Following our analysis, it became evident that the increase in anoikis score led to a decrease in the levels of natural killer cells, CD4<sup>+</sup> T cells, CD8<sup>+</sup> T cells, B cells, and macrophages. The Hedgehog (Hh) protein, which is a signaling molecule present between cells, plays a crucial role in cancer tissue homeostasis and repair. The transcription factor *GLI2*, which responds to Hh, attenuates T-cell activation and proliferation by driving gene transcription.<sup>42</sup> However, knocking out *GLI2* can exclude immunosuppressive bone marrow cells and inhibit tumor growth by recruiting natural killer cells.<sup>43</sup> The expression of *GLI2* is negatively correlated with T cell activation and natural killer cells. Our analysis concluded that the anoikis-related gene *GLI2* might participate in immune cell infiltration

in LUAD. Meanwhile, the transcriptional activity of *GLI2* can regulate cytokine communication in the tumor micro-environment, promote immunoglobulin secretion and increase interleukin (IL)-6 expression.<sup>44</sup> By regulating *GLI2*, the expression of tumor growth factor (TGF)- $\beta$ 1 in human CD4<sup>+</sup> T cells can be reversed.<sup>45</sup> These findings are consistent with our functional analysis, which indicates that the anoikis score has a negative regulatory relationship with the immune response, natural killer cell activation and T cell activation in the context of LUAD.

Ultimately, our results suggested that *TLE1*, *GLI2* and *PLK1* genes may be associated with cancer cell progression, gene mutations and immune cell infiltration in LUAD. Further in vitro and in vivo experiments are necessary to elucidate the mechanisms underlying these genes and to identify potential therapeutic strategies.

## Limitations

Due to limited funds, expression verification and functional analysis of anoikis-related genes were not further examined in this study. These topics will be our next research direction.

## Conclusions

Our study identified a group of anoikis-related prognostic features in LUAD. High scores on these features were found to be highly predictive of poor patient outcomes. Moreover, we found a strong correlation between the anoikis score, *TP53* mutation and immune cell infiltration. These findings suggest that targeting anoikis-related genes could be a promising approach for the treatment of LUAD.

## Supplementary data

The supplementary materials are available at <https://doi.org/10.5281/zenodo.8271767>. The package contains the following files:

Supplementary Fig. 1. Patient survival analysis in the GSE31210 dataset.

Supplementary Table 1. Forty-seven anoikis-related genes were obtained by univariate analysis.

Supplementary Table 2. Correlation analysis between immune cells and anoikis score.

Supplementary Table 3. Correlation analysis between immune checkpoints and anoikis score.


Supplementary Table 4. Comparison of gene mutation frequencies.

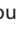
## ORCID iDs

Guiyan Mo  <https://orcid.org/0009-0002-1836-1800>

Xuan Long  <https://orcid.org/0000-0001-8669-5381>

Zan Hu  <https://orcid.org/0009-0005-3098-4842>

Yuling Tang  <https://orcid.org/0009-0002-3966-0543>

Zhiguo Zhou  <https://orcid.org/0000-0002-7621-7156>

## References

- Lu T, Yang X, Huang Y, et al. Trends in the incidence, treatment, and survival of patients with lung cancer in the last four decades. *Cancer Manag Res.* 2019;11:943–953. doi:10.2147/CMAR.S187317
- Bade BC, Dela Cruz CS. Lung cancer 2020: Epidemiology, etiology, and prevention. *Clin Chest Med.* 2020;41(1):1–24. doi:10.1016/j.ccm.2019.10.001
- Denisenko TV, Budkevich IN, Zhivotovsky B. Cell death-based treatment of lung adenocarcinoma. *Cell Death Dis.* 2018;9(2):117. doi:10.1038/s41419-017-0063-y
- Juriscic V, Vukovic V, Obradovic J, Gulyaeva LF, Kushlinskii NE, Djordjević N. EGFR polymorphism and survival of NSCLC patients treated with TKIs: A systematic review and meta-analysis. *J Oncol.* 2020;2020:1973241. doi:10.1155/2020/1973241
- Travis WD, Brambilla E, Noguchi M, et al. International Association for the Study of Lung Cancer/American Thoracic Society/European Respiratory Society International Multidisciplinary Classification of Lung Adenocarcinoma. *J Thorac Oncol.* 2011;6(2):244–285. doi:10.1097/JTO.0b013e318206a221
- Vijayvergia N, Shah PC, Denlinger CS. Survivorship in non-small cell lung cancer: Challenges faced and steps forward. *J Natl Compr Canc Netw.* 2015;13(9):1151–1161. doi:10.6004/jnccn.2015.0140
- Hubbard MO, Fu P, Margevicius S, Dowlati A, Linden PA. Five-year survival does not equal cure in non-small cell lung cancer: A Surveillance, Epidemiology, and End Results-based analysis of variables affecting 10- to 18-year survival. *J Thorac Cardiovasc Surg.* 2012;143(6):1307–1313. doi:10.1016/j.jtcvs.2012.01.078
- Han HJ, Sung JY, Kim SH, et al. Fibronectin regulates anoikis resistance via cell aggregate formation. *Cancer Lett.* 2021;508:59–72. doi:10.1016/j.canlet.2021.03.011
- Kakavandi E, Shahbahrami R, Goudarzi H, Eslami G, Faghihloo E. Anoikis resistance and oncoviruses. *J Cell Biochem.* 2018;119(3):2484–2491. doi:10.1002/jcb.26363
- Amoedo ND, Rodrigues MF, Rumjanek FD. Are mitochondria accessory to metastasis? *Int J Biochem Cell Biol.* 2014;51:53–57. doi:10.1016/j.biocel.2014.03.009
- Zhong X, Rescorla FJ. Cell surface adhesion molecules and adhesion-initiated signaling: Understanding of anoikis resistance mechanisms and therapeutic opportunities. *Cell Signal.* 2012;24(2):393–401. doi:10.1016/j.cellsig.2011.10.005
- Malagobadan S, San Ho C, Hasima Nagoor N. MicroRNA-6744-5p promotes anoikis in breast cancer and directly targets NAT1 enzyme. *Cancer Biol Med.* 2020;17(1):101–111. doi:10.20892/j.issn.2095-3941.2019.0010
- Adeshakin FO, Adeshakin AO, Afolabi LO, Yan D, Zhang G, Wan X. Mechanisms for modulating anoikis resistance in cancer and the relevance of metabolic reprogramming. *Front Oncol.* 2021;11:626577. doi:10.3389/fonc.2021.626577
- Sun Z, Zhao Y, Wei Y, Ding X, Tan C, Wang C. Identification and validation of an anoikis-associated gene signature to predict clinical character, stemness, IDH mutation, and immune infiltration in glioblastoma. *Front Immunol.* 2022;13:939523. doi:10.3389/fimmu.2022.939523
- Chi H, Jiang P, Xu K, et al. A novel anoikis-related gene signature predicts prognosis in patients with head and neck squamous cell carcinoma and reveals immune infiltration. *Front Genet.* 2022;13:984273. doi:10.3389/fgene.2022.984273
- Chen Z, Liu X, Zhu Z, et al. A novel anoikis-related prognostic signature associated with prognosis and immune infiltration landscape in clear cell renal cell carcinoma. *Front Genet.* 2022;13:1039465. doi:10.3389/fgene.2022.1039465
- Song J, Liu Y, Liu F, et al. The 14-3-3σ protein promotes HCC anoikis resistance by inhibiting EGFR degradation and thereby activating the EGFR-dependent ERK1/2 signaling pathway. *Theranostics.* 2021;11(3):996–1015. doi:10.7150/thno.51646
- Ye G, Yang Q, Lei X, et al. Nuclear MYH9-induced CTNBN1 transcription, targeted by staurosporin, promotes gastric cancer cell anoikis resistance and metastasis. *Theranostics.* 2020;10(17):7545–7560. doi:10.7150/thno.46001
- Anashkina AA, Leberfarb EY, Orlov YL. Recent trends in cancer genomics and bioinformatics tools development. *Int J Mol Sci.* 2021;22(22):12146. doi:10.3390/ijms222212146
- Xue F, Yang L, Dai B, et al. Bioinformatics profiling identifies seven immune-related risk signatures for hepatocellular carcinoma. *PeerJ.* 2020;8:e8301. doi:10.7717/peerj.8301
- Chen DL, Cai JH, Wang CCN. Identification of key prognostic genes of triple negative breast cancer by LASSO-based machine learning and bioinformatics analysis. *Genes.* 2022;13(5):902. doi:10.3390/genes13050902
- Lei T, Qian H, Lei P, Hu Y. Ferroptosis-related gene signature associates with immunity and predicts prognosis accurately in patients with osteosarcoma. *Cancer Sci.* 2021;112(11):4785–4798. doi:10.1111/cas.15131
- Lu H, Wu J, Liang L, Wang X, Cai H. Identifying a novel defined pyroptosis-associated long noncoding RNA signature contributes to predicting prognosis and tumor microenvironment of bladder cancer. *Front Immunol.* 2022;13:803355. doi:10.3389/fimmu.2022.803355
- Chen S, Gu J, Zhang Q, Hu Y, Ge Y. Development of biomarker signatures associated with anoikis to predict prognosis in endometrial carcinoma patients. *J Oncol.* 2021;2021:3375297. doi:10.1155/2021/3375297
- Yu Y, Song Y, Cheng L, et al. CircCEMIP promotes anoikis-resistance by enhancing protective autophagy in prostate cancer cells. *J Exp Clin Cancer Res.* 2022;41(1):188. doi:10.1186/s13046-022-02381-7
- Cao K, Ling X, Jiang X, Ma J, Zhu J. Pan-cancer analysis of UBE2T with a focus on prognostic and immunological roles in lung adenocarcinoma. *Respir Res.* 2022;23(1):306. doi:10.1186/s12931-022-02226-z
- Lu L, Liu LP, Zhao QQ, Gui R, Zhao QY. Identification of a ferroptosis-related lncRNA signature as a novel prognosis model for lung adenocarcinoma. *Front Oncol.* 2021;11:675545. doi:10.3389/fonc.2021.675545
- Zhang X, Chen HM, Jaramillo E, Wang L, D’Mello SR. Histone deacetylase-related protein inhibits AES-mediated neuronal cell death by direct interaction. *J Neurosci Res.* 2008;86(11):2423–2431. doi:10.1002/jnr.21680
- Sonderegger CK, Vogt PK. Binding of the corepressor TLE1 to Qin enhances Qin-mediated transformation of chicken embryo fibroblasts. *Oncogene.* 2003;22(12):1749–1757. doi:10.1038/sj.onc.1206308
- Yao X, Jennings S, Ireland SK, et al. The anoikis effector Bit1 displays tumor suppressive function in lung cancer cells. *PLoS One.* 2014;9(7):e101564. doi:10.1371/journal.pone.0101564
- Brunquell C, Biliran H, Jennings S, Ireland SK, Chen R, Ruoslahti E. TLE1 is an anoikis regulator and is downregulated by Bit1 in breast cancer cells. *Mol Cancer Res.* 2012;10(11):1482–1495. doi:10.1158/1541-7786.MCR-12-0144
- Yao X, Ireland SK, Pham T, et al. TLE1 promotes EMT in A549 lung cancer cells through suppression of E-cadherin. *Biochem Biophys Res Commun.* 2014;455(3–4):277–284. doi:10.1016/j.bbrc.2014.11.007
- Ma Q, Xiao F, Hao Y, et al. The prognostic role of the transducin-like enhancer of split protein family in lung adenocarcinoma. *Transl Lung Cancer Res.* 2021;10(7):3251–3263. doi:10.21037/tlcr-21-582
- Javelaud D, Alexaki VI, Dennler S, Mohammad KS, Guise TA, Mauviel A. TGF-β/SMAD/GLI2 signaling axis in cancer progression and metastasis. *Cancer Res.* 2011;71(17):5606–5610. doi:10.1158/0008-5472.CAN-11-1194
- Gupta P, Gupta N, Fofaria NM, Ranjan A, Srivastava SK. HER2-mediated GLI2 stabilization promotes anoikis resistance and metastasis of breast cancer cells. *Cancer Lett.* 2019;442:68–81. doi:10.1016/j.canlet.2018.10.021
- Yim H, Erikson RL. Plk1-targeted therapies in TP53- or RAS-mutated cancer. *Mutat Res Rev Mutat Res.* 2014;761:31–39. doi:10.1016/j.mrrev.2014.02.005
- Lin DC, Zhang Y, Pan QJ, et al. PLK1 is transcriptionally activated by NF-κB during cell detachment and enhances anoikis resistance through inhibiting β-catenin degradation in esophageal squamous cell carcinoma. *Clin Cancer Res.* 2011;17(13):4285–4295. doi:10.1158/1078-0432.CCR-10-3236
- Xue D, Lin H, Lin L, Wei Q, Yang S, Chen X. TTN/TP53 mutation might act as the predictor for chemotherapy response in lung adenocarcinoma and lung squamous carcinoma patients. *Transl Cancer Res.* 2021;10(3):1284–1294. doi:10.21037/tcr-20-2568
- Wu C, Rao X, Lin W. Immune landscape and a promising immune prognostic model associated with TP53 in early-stage lung adenocarcinoma. *Cancer Med.* 2021;10(3):806–823. doi:10.1002/cam4.3655

40. King SI, Purdie CA, Bray SE, et al. Immunohistochemical detection of Polo-like kinase-1 (PLK1) in primary breast cancer is associated with TP53 mutation and poor clinical outcome. *Breast Cancer Res.* 2012;14(2):R40. doi:10.1186/bcr3136
41. Li L, Li M, Wang X. Cancer type-dependent correlations between TP53 mutations and antitumor immunity. *DNA Repair.* 2020;88:102785. doi:10.1016/j.dnarep.2020.102785
42. Furmanski AL, Barbarulo A, Solanki A, et al. The transcriptional activator Gli2 modulates T-cell receptor signalling through attenuation of AP-1 and NFκB activity. *J Cell Sci.* 2015;128(11):2085–2095. doi:10.1242/jcs.165803
43. Scales MK, Velez-Delgado A, Steele NG, et al. Combinatorial Gli activity directs immune infiltration and tumor growth in pancreatic cancer. *PLoS Genet.* 2022;18(7):e1010315. doi:10.1371/journal.pgen.1010315
44. ElSawa SF, Almada LL, Ziesmer SC, et al. GLI2 transcription factor mediates cytokine cross-talk in the tumor microenvironment. *J Biol Chem.* 2011;286(24):21524–21534. doi:10.1074/jbc.M111.234146
45. Furler RL, Uittenbogaart CH. GLI2 regulates TGF-β1 in human CD4<sup>+</sup> T cells: Implications in cancer and HIV pathogenesis. *PLoS One.* 2012;7(7):e40874. doi:10.1371/journal.pone.0040874

